THE EFFECT OF LINER DESIGN UPON CHARGE MOTION IN A ROTARY MILL

M.S. Powell

September 1988

Submitted to the University of Cape Town
in fulfilment for the degree of
Master of Science in Applied Science.

I, M.S. Powell, submit this thesis in fulfilment of the requirements for the degree of Master of Science in Applied Science. I claim that this is my original work and has not been submitted in this or in a similar form for a degree at any University.

ACKNOWLEDGEMENTS

Thanks are due to the Council for Mineral Technology (Mintek), the support of which has been essential to this work. The assistance of and suggestions from Dr L.A. Vermeulen, Mr F.S. Cornelius, and Mr R. Visser are acknowledged with gratitude.

ABSTRACT

Rotary mills are used extensively to reduce the coarse rocks of mined ores down to a product fine enough to facilitate the extraction of the valuable minerals. On the South African gold mines alone about 110 million tons of ore is mined annually, at a power cost of about R90 million, and a liner material cost of about R30 million.

The charge motion in mills has been studied both theoretically and experimentally since the beginning of the century. However, a lot of the work has been purely empirical, and some of it ill-conceived, resulting in there still being a poor understanding of the topic. The influence of lifter-bars upon charge motion has only been considered in the past few decades, and mostly to a very limited extent. This state of affairs has left the field wide open to further research.

The charge motion of an isolated rod or ball, and how it is influenced by a flat-faced lifter-bar of any face-angle and of any height, was modelled theoretically. The charge motion of rods in a glass-ended mill was filmed with a high-speed camera. The mill was fitted with a variety of lifter-bars with different face-angles and heights, and was run at a wide range of speeds. The filmed trajectories of the rods were then tracked. The coefficients of friction between the rods and lifter-bar material were measured under vibrating conditions as are found in the mill. The power draw of the mill was also measured at a wide range of mill speeds, and with lifter-bars of different heights in the mill.

A good correlation between the theoretical predictions and experimental results was found over a wide range of conditions. The impact point, at which the grinding element strikes the mill shell, was considered to be of primary importance in the analysis. It was found that the height of the lifter-bar has a strong influence on charge trajectories, as the height increases

from zero up to just greater than one charge radius. Thereafter the lift increases until a critical lifter-bar height is reached, beyond which the grinding element is projected off the lifter prior to reaching the tip, the height of the impact point increasing slightly and then decreasing to a constant height. However, the change in the height of the impact point is very small, so in practical terms an increase in lifter-bar height, once it is higher than the radius of the grinding element, has a very small effect upon the charge trajectories.

An increase in the angle of the lifter-bars was found to have a strong influence upon the height of the charge trajectories. A linear relationship between the mill speed and the impact angle was dicovered, and changes in the mill speed strongly influence the charge trajectories. It was also found that the power draw of a mill depends on the liner configuration, with power draw decreasing as the lifter-bar height is increased.

Some new and surprising effects of lifter-bar geometry upon the charge trajectories, which are of great practical importance, have been discovered. The theoretical model is an advance upon all previous models, and agrees well with experimental results over a wide range of conditions.

CONTENTS

LIST OF TABLES

LIST OF ILLUSTRATIONS

NOMENCLATURE

General variables

a	Rod radius
α	Angular acceleration of rod
c_1, c_2	Dummy variables used in solution of differential equation
δ	$\sin\alpha(R-h) - a \equiv$ a constant
f	Frictional force between lifter face and rod
F	Resultant force on the rod
g	Gravitational acceleration (9.8 $m.s^{-2}$)
h	Radial height of lifter bar
h'	Perpendicular height of lifter
h''	Perpendicular distance from mill shell to top of lifter
I	Moment of inertia of rod
m	Mass of rod
m_1, m_2	Dummy variables used in solution of differential equation
N	Normal force exerted by lifter on rod
R	Internal radius of mill
r	Distance from mill centre to rod centre
$\vec{r}$	Vector directed from mill centre to rod centre
r_0	R - a
S, s	r.cosß
$\vec{s}$	Vector parallel to lifter face, directed from tip to base
$\dot{s}$	Linear velocity of rod up lifter face
$\ddot{s}$	linear acceleration of rod up lifter face
t	time
Γ	Torque
μ_s	Static coefficient of friction between rod and lifter
μ_K	Kinetic coefficient of friction between rod and lifter
v	Net velocity of the rod, in cartesian coordinate system
Ω	Angular velocity of mill
x	Horizontal cartesian coordinate of rod centre
y	Vertical cartesian coordinate of rod centre
y	Half width of lifter bar base
$\perp$	Perpendicular
$\parallel$	Parallel

Angles

α	Between lifter face and a radial line passing through the tip of the lifter
β	Between radius vector to rod, and lifter face
ϵ	Between radius vector to base of lifter face, and lifter face
γ	Subtended by $\vec{s}$ and x axis
ϕ	Subtended by $\vec{r}$ and $\vec{x}$
ψ	Subtended at centre, between lifter centre and lifter tip
ρ	Between lifter face and lifter base
σ	To horizontal of rods velocity vector
θ	Subtended at centre, between lifter tip and x axis
ξ	Subtended at centre between lifter tip and $\vec{r}$

Subscripts

$_0$	Point of equilibrium
$_L$	Tip of lifter
$_{cm}$	About centre of mass of rod
$_m$	Maximum
$_I$	Point of transition from rolling to sliding
$_P$	Point of contact between rod and lifter face
$_x$	In X direction
$_y$	In Y direction
$_E$	Point at which rod strikes mill shell
$_{//}$	Parallel to
$_r$	Radial component
$_\perp$	Perpendicular to

Superscripts

^{0}	Angular degrees

GLOSSARY

Critical speed The speed at which the gravitational and cetrifugal forces acting on a point at the top of the mill just balance, so a small particle would theoretically centrifuge at that speed.

Liner The thick lining that covers the inside of the mill shell. It consists of blocks, having the same curvature as the mill, that are bolted to the shell.

Ring : A circumferential line of blocks, there are usually 4 to 8 down the length of a mill.

Row : A line of blocks running the length of the mill, there are asually 20 to 32 rows in a mill.

Minus 75μm Particles smaller than 75 microns in size

RoM mills Run-of-mine mills

Shoulder of charge The uppermost section of the bulk charge, from which the charge is then projected into flight, or tumbles down upon itself.

Toe of charge The lowest section of bulk charge, against the downward moving side of the mill.

CHAPTER ONE

INTRODUCTION

This work investigates theoretically and experimentally the influence of varying the design of shell liners, on the performance of rotary mills. Mills on gold mines were used as the basis of this study, however the same basic principles apply to all forms of milling. A general understanding of rotary mills and the function of their shell liners is necessary prior to analysing liner design in detail.

All gold ore has to be reduced to a fine particle size, to enable the efficient extraction of the gold, this size reduction process is referred to as comminution. On the South African gold mines comminution is carried out principally by primary crushers followed by rotary mills. The mills are basically hollow cylinders that rotate horizontally about their central axes. The mills used on the gold mines generally have a length of about twice their diameter. The crushers reduce the rocks to a coarse sand, this is then diluted with water to form a pulp that is fed to the mills. This pulp enters a mill via a chute leading into the feed end. The ore and grinding media within a mill is known as the 'charge'. The rotary motion of the mill causes the charge to be lifted up the side of the mill, the charge then tumbles down upon itself under the influence of gravity. This motion abrades and crushes the ore particles. The ore continuously flows in through the inlet end and out through the discharge end of the mill. The desired final product from a milling circuit is generally about 80 per cent smaller than 75μm particles.

If a mill has a circulating load then the discharge pulp is classified into undersize, ore that is fine enough to continue to the next stage of processing, and oversize that returns to the feed end of the mill to be reground. This circulating load is generally one to two times the quantity of the fresh feed. This separating is almost exculsively carried out by a hydrocyclone classifier. Over 70 per cent of all ore is initially crushed in

the crusher circuit, then fed to a set of primary mills which carry out the major part of the grinding. These usually each feed two secondary mills that reduce the ore to its final size. To assist in the grinding of the ore a grinding media is used in the mills, the mills are classified according to this.

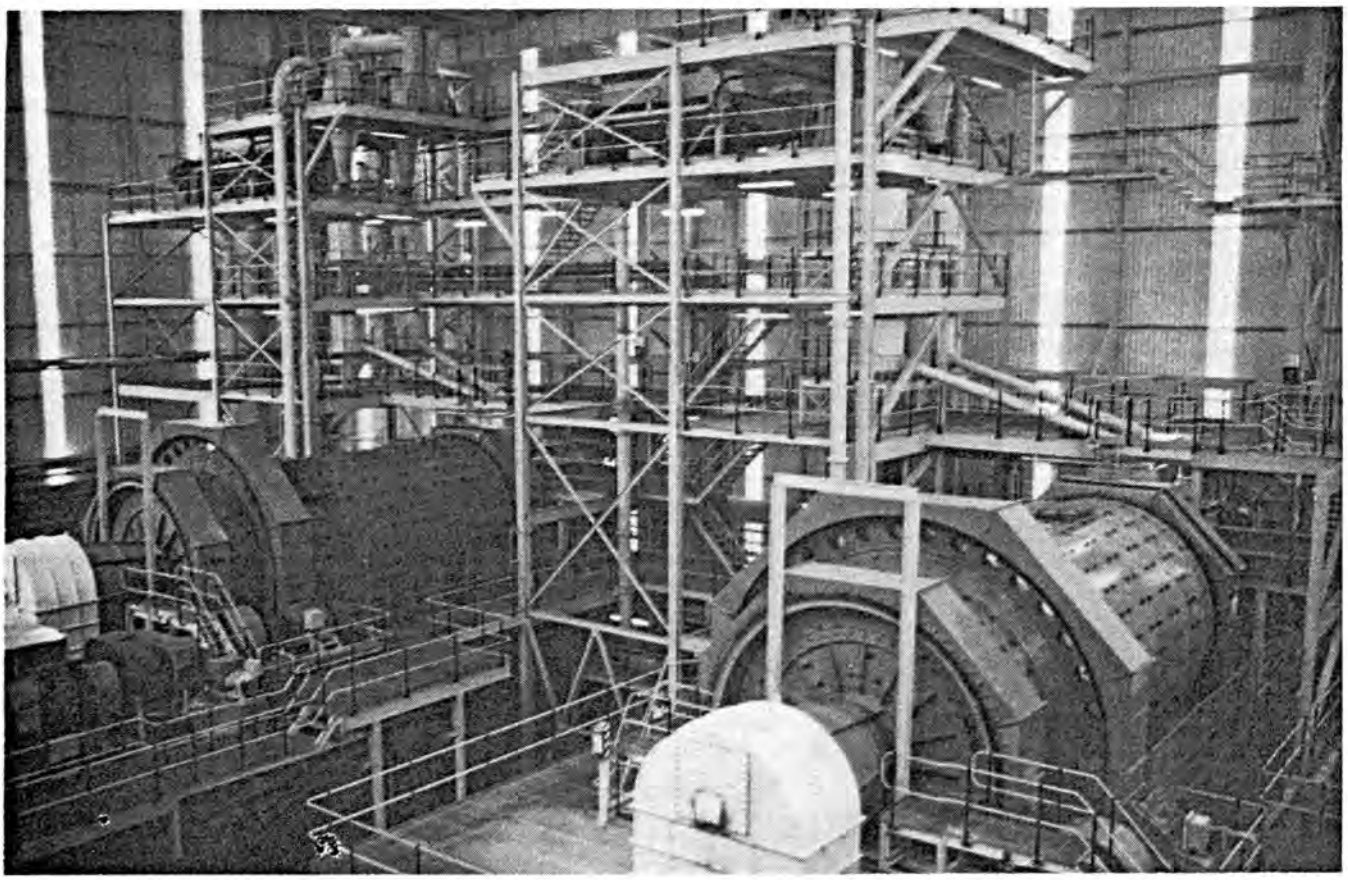

FIGURE 1. Twin 4,9 by 10,8m run-of-mine mills at Harmony Gold Mine, number four shaft

Rod mills are charged with steel rods that run the length of the mill, and tumble horizontally with the rotary motion of the mill. These are used exclusively for primary grinding, and do not have a circulating load. Ball mills are filled to about 45 per cent of their volume with balls. These are principally used for primary grinding, and most do have a circulating load. Pebble mills use a selected size fraction of rocks from the mined ore, as their grinding media. These are generally used as secondary mills for

fine grinding of the ore. Composite mills have a mixed charge of balls and pebbles, and generally carry out secondary grinding. Run-of-mine (RoM) mills are large, single-stage mills that are fed directly with the ore from underground, possibly crushed to a top size of 150mm. These use the large rocks and usually a 5 to 10 per cent ball charge to grind the ore to final size. These run-of-mine mills are a relatively new introduction, and due to their lower capital and running costs are replacing the conventional milling circuits. The 28 per cent[17] of ore that does not follow the conventional crusher plant, primary and secondary mills, grinding route is accounted for by thr RoM mills.

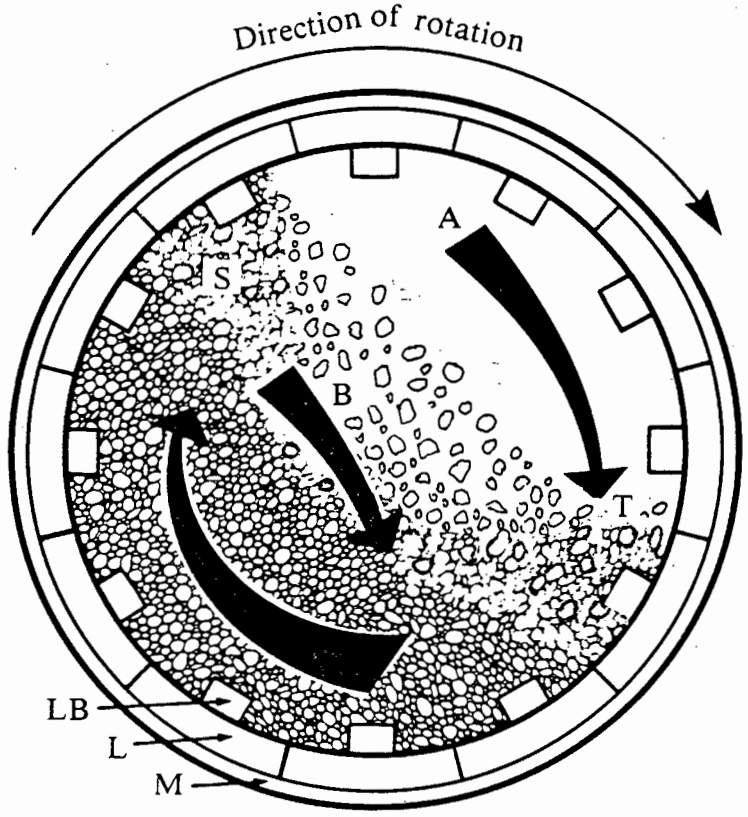

M Mill shell
S Shoulder of charge
T Toe of charge
A Cataracting charge
B Cascading charge
L Liner block
LB Lifter bar

FIGURE 2. Cross-section of a rotary mill

The mill liner consists of thick blocks that are fastened to the inside of the mill shell. These sacraficially protect the mill shell from wear caused by the abrasive action of the ore within the mill, and are the means by which the rotary motion of the

mill is transferred to the charge. When it is worn out the liner is removed and replaced with a new one, and the material left over from the old liner is scrapped. This whole procedure is referred to as relining. There are two distinct portions of liner, the shell liner that covers the cylindrical section of the mill, and the end liners that cover the flat inlet and outlet ends of the mill. Due to the long barrel-like shape of the South African gold mills the end liners play a small part in the overall performance of the mill, so only the shell liners are dealt with in this study.

The relining process is expensive not only due to the cost of materials, but also because the mill has to be shut down for the duration of this process. These expenses can be greatly reduced, as shown in practical trials carried out by DD Howat on rod mills[15], and by changing the liner configuration on RoM mills[16]. Tonnage throughput is the primary factor that must be maintained, as it is imperative that all ore mined is processed, so downtime must be kept to a minimum. Relining generally imposes a downtime of about 5 per cent upon the running time of a mill, therefore it is important that a liner should last as long as possible.

To maximise the mill throughput a liner is needed that produces the most favourable charge motion for rapid reduction of the ore. If the throughput can be increased then the size or number of mills planned for a reduction plant can be reduced, at a considerable saving of capital expenditure. Due to the lowering grades of ore that are being mined, the plants have to treat increasing quantities of ore to maintain their output of gold. This has resulted in many reduction plants working above their rated capacity. The resultant increased mill feed has a trade-off of coarser grind. As the per centage extraction of gold is dependent upon the fineness of grind, this coarser grind results in an increased fraction of the gold being lost on the dumps, at a substantial loss of revenue to the mine. Therefore for plants already in production it is important that the mill should run at its maximum efficiency to produce the optimal fineness of grind. It is of interest to note here that whereas the optimal

percentage of minus 75μm material in the product is quoted at around 80 per cent, the overall average on all the gold mines is 72 per cent.

Because of the high cost of electrical energy the liner should transfer energy as efficiently as possible to the charge. It has been proposed[19] that a practical method for determining the efficiency of the milling process is to compare the energy requirement to that required for slow, free crushing of the ore. This was tested for typical Witwatersrand quartzite gold bearing ore[18]. It was found that about 14 kW.h of energy was required per ton of ore crushed from crusher-run size to 72 per cent finer than 75μm size. It is found that the overall average energy requirement for grinding, excluding crushing, on the gold mines is 20,2 kW.h/t for that average fineness of grind[17]. Thus on average the mills require 40 per cent more energy than the practical minimum required to grind the ore, and there is therefore a wide margin available for improvement.

The following figures help emphasise the relevance of reducing the power consumption and downtime, and increasing the throughput of mills. On the South African gold mines 2400 million kW.h of energy are used annually for the reduction of 108 million tons of ore. At an electricity cost of 3,7c/kW.h this totals to R89 million, about 11 per cent of the total power cost of the gold mines. So a 5 per cent saving in power consumption is effectively a saving of R4,4 million per annum. The cost of mill down-time is dependent upon the mine production and the number of mills in a reduction plant, it is generally estimated by plant personnel to cost many thousands of rand for a few hours down-time on a single mill, due to lost production. When one considers that mill down time is about 8 hours to change two rings, out of a total of six to eight rings, this could add up to a considerable cost. However it is the author's opinion, based on crude calculations estimating the actual decrease in extracted gold, that this cost may actually be considerably lower than that generally quoted by the mining community. Therefore the cost of down-time will not be included as an important factor.

The liner can weigh up to 80 tons and cost R120 000 for a large mill. When it is considered that the liners on large RoM mills tend to last less than 90 days, and experiments with new liner designs have yielded lives four times as long[16,20], it can be seen that considerable savings can be afforded through improved liner design. In addition to these savings one should take into account the possible savings in labour costs. Thus it is clear that by minimising liner wear and power consumption the mines can affect substantial monetary savings. In addition improved liner design can improve the milling efficiency and consequently increase the production of the mills.

It can be seen therefore that a shell liner must satisfy three main criteria, it must have a long life, optimise charge motion, and efficiently transfer energy to the charge. For long life the best material must be chosen and the profile design should minimise the effects of wear. These two factors are strongly interdependent as different materials are resistant to different types of abrasive motion. For example white iron has good sliding abrasion resistance, but poor impact resistance, whereas rubber can withstand large perpendicular impacts but is susceptable to wear by sliding abrasion and low-angle impacts. To optimise charge motion the liner must impart the correct degree of lift to the charge. The correct balance between cascading (tumbling down over the bulk of the charge), and cataracting (being projected into flight and impacting onto the toe of the charge) must be obtained. Finally, to transfer the maximum available energy from the mill to the charge the liner must prevent slip of the charge relative to it, and again optimise charge motion so as to minimise the energy used per ton of ore milled to the desired size fraction.

Consensus has not been reached on what the optimum charge motion is, despite the large quantity of experimental work that has been carried out on milling. Indeed it is no doubt dependent upon the type and hardness of the ore, and the degree of reduction that is required. It is simple enough to prevent slip by designing a liner that has a strong keying-in action, however this must be

balanced against producing the desired charge motion. Thus it can be seen that liner design is not a straight forward matter, especially when one considers that it is exceedingly difficult to monitor the motion and conditions within a mill. At present liner design is rather more empirically, based on past experience, than scientifically guided.

When investigating milling one must take account of the difficulties encountered in attempting to monitor the very aggresive conditions within a mill. It is also difficult to experiment on production mills as mines don't like to risk excessive downtime or lost production arising from trials or failed experiments. There are more opportunities for investigating RoM mills as mines are converting to this comminution route so they are more willing to experiment at present, so as to optimise the operating conditions prior to comissioning their full complement of RoM mills.

As a consequence of the expense and difficulties encountered in full-scale investigations, it is imperative to establish both a sound theoretical basis and an experimental back-up on model mills. On a model mill conditions can be varied and monitored far more easily, and ideas given a fair trial. With successful results on a model mill, one can more confidently carry out trials on a production mill. The problem still encountered is deciding just how closely the model simulates the motion inside a real mill, where the interparticle forces and stresses are much greater, thus resulting in different milling conditions for similar charge motions.

Upon considering the complexity and scope of the problem of liner design, and the work that had previously been carried out by other investigators, it was decided to concentrate primarily upon 'the effect of liner design upon charge motion'. This is a fundamental aspect of milling that is not well understood, yet is important in understanding the effect of liner design on comminution. From a basic theoretical and experimental understanding of charge motion, its effect upon comminution can

then be better understood. In addition the liner can be better designed to withstand the harsh abrasive conditions within the mill.

From an analysis of previous work and results in this field, it was decided that the best form in which to study liner design was lifter-bars mounted onto flat profile backing blocks. The full analysis of the advantages of lifter-bars is reported in reference 16, 'The use of lifter bars in rotary mills'. The objectives of the work were then laid out as follows. To develop a theoretical model of charge motion, as affected by lifter-bar height and geometry. To film the charge motion in a glass-ended model mill, with lifter-bars of varying heights and geometry. To then try and correlate the theoretical predictions and experimental observations. Once a reasonable correlation had been established, the influence of lifter-bar height, lifter-bar face-angle, and mill speed upon the motion of the charge could be analysed to provide information on their combined influence upon the motion within the mill. To also measure the power consumption of the mill for a variety of lifter-bar geometries, and then try to correlate this with the observed charge motions. This would therefore form a comprehensive study of the effect of liner design upon the charge motion within a rotary mill.

CHAPTER TWO

LITERATURE SURVEY

In this survey only papers on charge motion, techniques of investigating it, and the effect of liner design on charge motion, have been considered. From the few that actually cover this topic, out of the many papers collected on milling (about 200), it can be seen that this fundamental aspect of milling invites further investigation. The papers are discussed in chronological order so as to highlight the development of this study over the years. A brief resumé of each paper is given then a critical analysis of its usefulness is made.

2.1. The theory of the Tube Mill[1]
by H.A. White (1905)

White based his work on the premise that in a tube mill the balls generally keep to the same layers, thus the motion was that of rows of balls within each other. His experimental work was carried out on tubes of up to 9 inches in diameter with glass plates on the ends and a hole through which water could be to added or extracted.

A "circle of reference" representing the path followed by the centres of the outermost balls is used. The balls travel up this circle until the gravitational and centrifugal forces acting upon them balance. They are then projected into free flight and follow a parabolic path until the circle is intersected at the opposite side of the mill, whereupon this circular path is resumed. The curve that defines the surface of departure for different layers of balls forms a semi-circle, and the curve that defines the surface of impact is found to be a limacon and trisectrix. The optimum conditions for maximum impact are derived from the trajectory that yields the maximum height of fall, which is in fact the one that passes through the centre of the circle.

The cycle time of each layer, according to its radius, is worked out, this is then integrated over all layers to yield the average cycle time and time in flight of the charge as a whole. The average fall of a ball, allowing for the relative number of balls in each layer, can then be derived. Inserting an approximate average ball size relative to the mill diameter, the optimum speed for greatest average fall is found.

(1) As White always had to use higher speeds than theoretically predicted to produce a given charge motion he concluded "It is clear that a sufficient quantity of balls must be present or friction between them and the rim will be insufficient and there will be relative slip. Here may also be observed one of the factors causing undue wear of the liners and wasted energy".

White proposed that the outer layer of balls be maintained in a state of centrifuging so as to protect the liner against wear, and the load be held at 66 per cent of the internal mill volume to allow an efficient falling distance. For crushing to be effective the water level should be maintained below the depth of charge at the bottom of the tube mill, otherwise falling balls waste their energy in passing through the water. He proposed a much lower speed and load if attrition grinding was concluded to be of greater importance than crushing, in wet milling. The relative importance of each mode of reduction was rather controversial, so he could not make a firm proposal. He also advised that a practical method of determining the best speed at which to run a mill would be to find that speed at which the highest power per revolution is absorbed.

A supporting comment in the discussion of the paper was that at Glen Deep mine the mills ran most efficiently when charged with a minimum of water.

This is the first mathematical study of charge motion that has been found. It is certainly a thorough and useful piece of work. He assumes perfect keying-in of material within the body of the charge, but acknowledges slip on the liner as being important.

His observations of fairly short-length model mills loaded with balls all of the same diameter lead White to the conclusion that "... balls keep to their own layer". However, when looking at such a mill one is observing the motion of the end row, that is firmly packed against the glass. These balls would be neatly stacked upon one another in concentric circles so are likely to retain their rows. Within the body of a real mill there is a wide range of ball sizes which will be unevenly packed so the formation of neat, well defined rows that are maintained with the cyclic motion of the charge is improbable.

Although an idealized model the analysis and its conclusions are generally valid. It helps considerably in the understanding of and improving of the milling operation, and as the predicted trends are based upon the fundamental laws of physics they are most likely correct. In his own words White claimed that "The true use of theoretical considerations is to shape the course of practical trials". He acknowledged his work as a guide to rather than the solution of milling practice.

2.2. Fine crushing in Ball Mills[2]

by E.W. Davis (1919)

From the large volume of available data on milling almost any theory of charge motion can be "proved" by careful selection of data. So "... a consideration which is entirely theoretical and devoid of any personal element would seem to be desirable and instructive."[2]. This led Davis to carry out the second, but seemingly quite independent of White's work, mathematical study of the mechanics of the ball mill, upon which most other work on the subject is based.

He analysed ball motion under the same conditions as White, but carried out his derivations slightly differently. He obtained the following charge profile and ball paths, that are identical to those derived by White, and are illustrated in Figure 3.

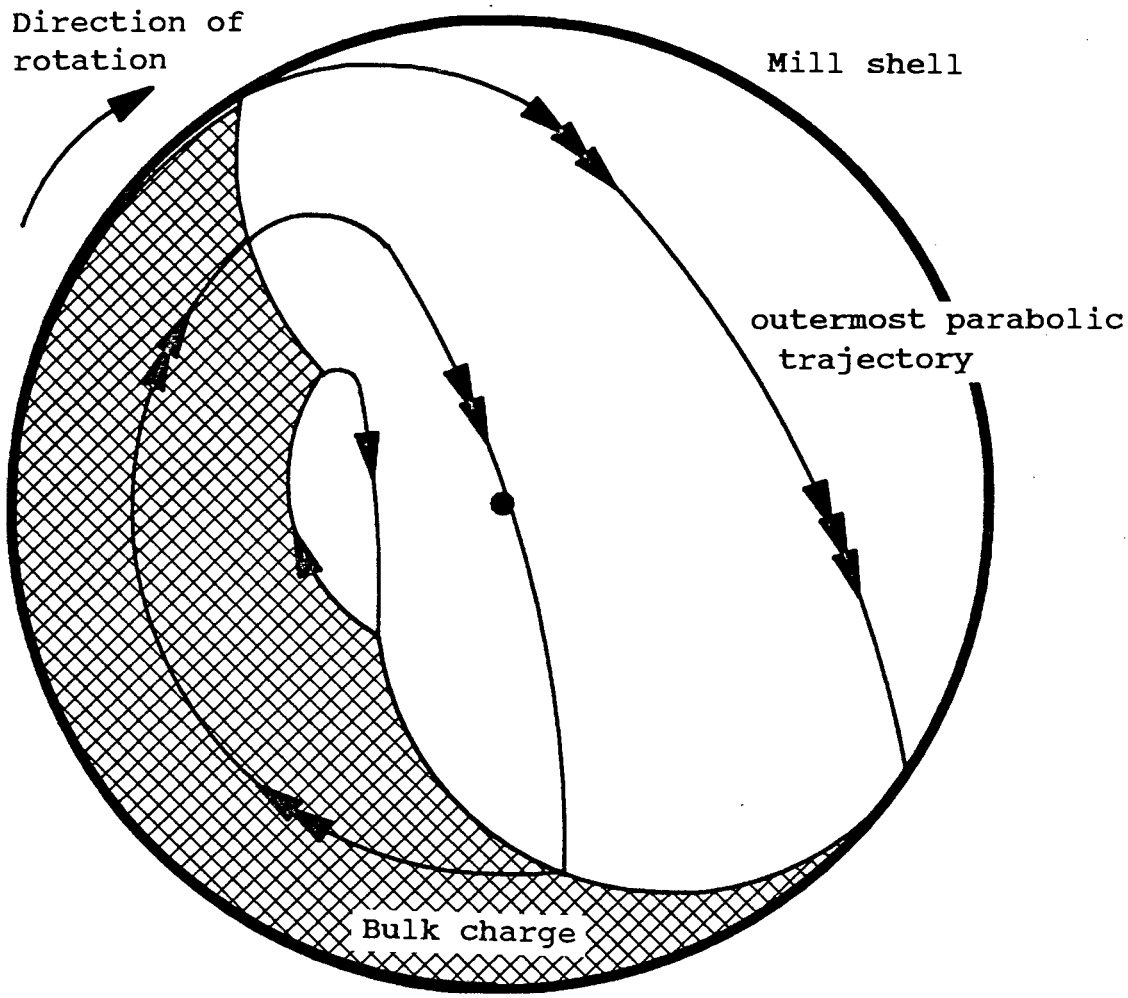

FIGURE 3. Ball paths in a cylindrical mill (after Davis[2])

In carrying out impact grinding the most effective blow struck by a falling ball is found by determining the ball's velocity relative to the lining, or another layer of balls, and maximizing it for given conditions. This was found to be for a departure angle (measured to the point at which the ball is projected off the shoulder of the charge and into flight) of 54^0 from the vertical. But as the angle of departure varies with radius from the mill centre the radius of gyration of the charge is used to work out the optimum conditions for the charge as a whole. From this is derived the relationship between the inner and outer radii of the charge, on its circular path, for optimum operating conditions of the mill. The correlation between these radii and the charge volume then have to be determined. The sum of a ball's

circular and parabolic path times, taken at the radius of gyration, are deemed to be the charge's cycle time. There are found to be 1,44 cycles per mill revolution, so 56% of the ball's time is spent in the circular path resulting in that same percentage of total charge being in this region. This gives the correlation between the inner and outer radii and the charge volume.

Davis claimed that by use of his equations one can determine the charge profile, velocity of ball strike, number of ball strikes, and the relation between speed, diameter and charge volume for best theoretical efficiency.

He then tested his theories by comparing them with the charge motion observed in a small (76 by 51mm) mill loaded with fine sand. He claimed a good correlation, with differences due to interference between particles. This, he argued, arose because the initial velocity vectors of two adjacent particles at their points of departure intersected when extrapolated a short distance. He also pointed out that his calculated best speed was for impact crushing, not attrition grinding.

A mathematical treatment does not entirely eliminate the personal factor Davis referred to, due to the simplifications and assumptions that are of necessity introduced. He has assumed that no slip takes place against the liner or within the body of the charge, this may be a fair approximation for coarse particles within the main body of the charge, but extensive slip surely occurs at the upper end of the circular path. This is important, as the velocity of departure determines the subsequent trajectory of the particle. There does not appear to be any sound basis for assuming that particles land at the same radius as they are projected from, as there must be extensive interference at the toe of the charge, where they land.

Davis warned that any theory can be "proved" by data selection, but he appears to have fallen into this trap by making his observations fit his data. He had already shown that his derived

parabolic paths do not intersect, then he claimed that the intersection of the paths of the particles causes interference which results in the differences between his observed and calculated paths. Thus to substantiate his calculations he introduced a self-contradiction.

In a discussion of the paper H.A. White pointed out that the inner layers of balls have a far shorter cyclic time than the outer layers so that an estimation of this time using the centre of gyration is too inaccurate, it should in fact be calculated by summing over all radii. He also raised the point that maximum efficiency and capacity appear to occur at different mill speeds, for on Witwatersrand mills the maximum capacity is found at a higher speed than that predicted.

Davis' derivations appear to be flawed by over-simplifications, but the basic approach is useful, being founded on the fundamental laws of motion. Thus his theories can be used as a basis upon which further work can be developed.

2.3. Ball Paths in Tube Mills[3]

by H.E.T. Haultain and F.C. Dyer (1922)

This work was inspired by Davis' theories, however it claimed Davis' theory of ball motion to be incorrect. The study was experimental with purely qualitative conclusions.

Two glass-ended mills each half an inch long, one 24 and the other 6 inches in diameter, were used in the experimental work. These were loaded with brass discs, seeds, or crushed marble, in both wet and dry mixtures. The discs had four projections on either side to prevent sticking to the glass when used wet. By recording the charge motion with still photographs and high speed film (120 frames per second) it was clearly observed that extensive slippage, or adjustment of position, took place between the discs and lining and layers of discs. Black radial lines on the ends of the discs clearly showed the rotation of the discs relative to each other as this adjusting of position took place.

This slip resulted in Davis' theoretical paths of motion not being attained. In addition segregation of the charge into small discs in the centre and large at the periphery at low speeds, and the reverse at high speeds in the cataracting regime, was observed. This led the authors to conclude that a speed just below cataracting would be optimum for even mixing, thus avoiding a central section of underutilized large balls.

The authors admit that these mills do not reflect real conditions but rather are a guide, or indication of the motion in a real mill.

Upon receiving this paper Davis requested the experiments to be carried out with the addition of a quartz charge. This did reduce the slip against the shell dramatically, even to zero for the main part of the circular path. The observed paths still did not fully correlate with those predicted by Davis, although the correlation was certainly far better than previously. Davis claimed this remaining non-correlation to be entirely due to slip near the top of the circular path of the particles. Haultain, however, maintained his standpoint that there were significant differences between Davis' theory and observation, with slip being the important unaccounted for factor in his calculations, especially as the effect of slurries was unknown.

This work serves well to illustrate the importance of slip in charge motion, both against the mill shell and within the charge. It thus demonstrates the incompleteness of Davis' theory, showing that his basic assumption of no slip is invalid. An important point as suggested by Davis is the large effect of slip just near the top of the circular path, which is most likely due to a loss in charge pressure (see Vermeulen's paper[8]). The end effects in this mill were acknowledged to decrease the effect of slip and therefore would have tended to work against, rather that than for, the authors claims.

2.4. A Laboratory Investigation of Ball Milling[4]

by A.M. Gow, A.B. Campbell, W.H. Coghill (1929)

Experimental work was carried out on a laboratory mill of 3 foot diameter and 6 inches long, firstly with grids then with glass screens at either end. According to their observations the balls were thrown further than predicted by the parabolic path theory. This they concluded was because the balls do not act independently when they leave the shell but continue in contact, pushing those ahead until they pass the apex of their flight. Due to their intimate contact this stream of balls can't lose velocity thus they have a horizontal speed at their apex equal to their peripheral speed against the shell.

Segregation of large and small balls was also observed, with the large balls near the outside for slow speeds and in the middle for high speeds. This was determined to be purely a function of size as the same result was obtained for wooden balls. It was concluded that small balls have their centre of mass closer to the mill shell therefore they cataract further thus tending to migrate to the outside of the mill at speeds high enough for cataracting to occur. No explanation was given for the opposite occurring at low speeds.

As a result of the longer path length they had observed it was concluded that slower mill speeds than previously predicted as optimum should be used. Speeds of 50 to 65 per cent instead of 75 per cent of the critical speed were recommended. The grinding tests carried out to substantiate these claims were also carried out on 6 inch diameter mills. They stated that a short mill was used so as to reduce slippage of the charge.

In a discussion of the paper Davis mentioned that due to end grid effects it was entirely possible for the 1" grids being only 6" apart to hold the 1.25" balls locked effectively between them thus carrying the balls much further than they would otherwise travel. He also mentioned that photographs by Haultain and Dyer were nearer his results, in fact indicating less lift than

predicted by his theories and therefore indicating the presence of some slip, a factor of about 9 per cent fitting his predictions.

The end effect mentioned by Davis is undoubtedly the major shortcoming of this work. This is substantiated by White who pointed out that the grinding characteristics obtained were quite different to those of real mills. In addition if one considers the range of ball sizes and their random packing it is highly improbable, except possibly for brief bursts, that the balls could form neat integral rows that remain intact during the upward part of the flight of the balls. It seems reasonable to therefore discount this explanation, and others similar to it. The real value of this paper is that it shows the importance of realistic experimental designs.

2.5. Ball Mill Studies[5]

by A.W. Fahrenwald and H.E. Lee (1931)

The ball path analysis is based on the work of Davis with some slight modifications and additions. The influence of ball size on mill efficiency was appreciated and a formula for optimizing it was derived, assuming a single sized ball. For mills of different size, but maintaining the same angles of departure of the outer layer, the theory predicts identical charge motion. So it was concluded that all mills should run at the same optimum percentage of critical speed. From their consideration of the outer layer of balls the authors decided that when extrapolating to a full charge the effects must be modified, but that presumably the trends in behaviour accompanying changes in the variables remain the same.

The 'new theories' of Gow, Campbell, and Coghill[4] were found to predict paths that extended too far, with the parabolic theory giving closer correlation. It was noted that the work of Gow *et al.* was based on the abnormal conditions that promoted jamming of the charge between the mill ends, so those observations and consequent formulae should not be accepted as representing true

paths of balls in a normal mill.

In the words of the authors "The large number of variables prevailing in this study prevent a complete statement of the conditions in mathematical form". So they felt the trends could be predicted but the optimum points had to be found experimentally. Knowing the optimum conditions for one mill they may be approximately calculated for any other mill.

In the experimental study power was monitored for variations in mill speed, ball size, and load. It was found that the power draw of a mill peaked at a definite combination of these variables. This was concluded to occur when the charge consumed the most energy, and the mill was thus operating at its maximum efficiency. A factor of slip between the charge and the lining was indicated, this was assumed to impart a rolling action to the balls that resulted in a radial component of force which led to them departing from the liner sooner than expected. A formula for the modified velocity was derived.

The coefficient of friction for different size quartz at varying moisture was found by dragging balls across a wrought-iron surface with a layer of slurry on it. A decrease in the coefficient of sliding friction from dry to wet was found, which greatly out-weighed any increase in viscosity. As the frictional factor dropped a higher pressure, and therefore load, would be required to maintain the same charge motion.

Conclusions on the effect of balls rolling due to slip on the liner do not consider the retarding effect of the surrounding charge which will most probably prevent any such independent rolling. The observations and comments in this work are useful, however most of the conclusions are not sufficiently backed-up or well considered to be taken as fact, but rather as suggestions. Comments on the effect of slurries are useful as very few papers mention the influence of slurry addition on charge motion. This is also the first paper that considers the importance and effect of varying coefficients of friction, on the charge motion.

2.6. Technical Design of Autogenous Mills[6]

by R.C. Meaders and A.R. MacPherson (1964)

Experimental work was carried out with a model mill running in closed circuit, and the parameters that were considered to be primarily responsible for determining the operating efficiency of the mill were varied. These are the height and spacing of lifter-bars, the method of product discharge, and the length and speed of the mill. After each variable had been optimized, the tests were repeated to ensure that the set of conditions for maximum efficiency had not changed the optimum settings that had been previously established for the individual parameters. The energy used to produce one unit of new surface area was used as the basis for comparison of the results.

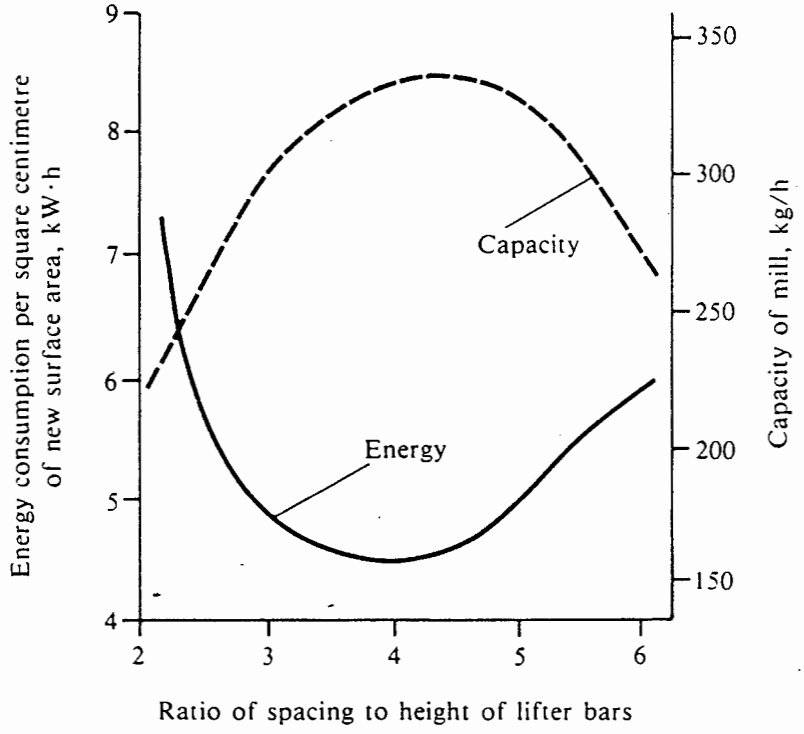

FIGURE 4. The ratio of spacing to height of lifter-bars, and its effect on the performance of a mill (after Meaders and MacPherson[6])

Variations in the ratio of spacing to height of the lifter-bars were found to have a marked influence on the operation of the

mill. Figure 4 shows that a distinct peak in mill capacity and a minimum in the energy per unit of surface area produced was obtained at a ratio of spacing to height of between 4,0 and 4,5.

It was also found that the optimum height of the lifter-bars depends on the speed of the mill. A mill with a smooth lining has to be operated at over 90 per cent of the critical speed, whereas at slower speeds the height of the lifters has to be increased to maintain optimum conditions. However, the best overall operation was obtained at a speed of around 77 per cent of the critical speed, with a ratio of mill diameter to lifter-bar height of 17,6.

This is a well-planned and carefully executed piece of experimental work, and confidence can be placed in the authors' findings. The important conclusions that can be drawn from this work are that the overall efficiency of a mill can be optimized at a certain speed with lifter-bars of the correct height, and that, for a given speed, there is an optimum height for the lifter-bars. These heights must also then be related to the spacing between the lifter-bars.

2.7. Contribution to a Study of Dry Quasi-autogenous milling[7]

by B. Marechal (1968)

Third part: Internal Mechanics of the Aerofall Mill

The three theories on trajectories of solids within a mill upon which this paper was based where those of E.W. Davis (1905)[2], R. von Steiger (1929) and A. Joissel (1951). The simple theory of Davis, of particles following circular paths then being projected into parabolic trajectories, was chosen. Although the transcendent trajectories and conservation of volume theories of Von Steiger and Joissel were considered to each be slightly more accurate this difference was considered too slight to warrant the extra complications introduced into the subsequent analysis. The main results of Davis' theory that were used being: solids move perpendicular to the mill axis; there is no slip on the mill shell; air resistance can be neglected.

It was assumed that slippage takes place only at the free surface of the charge, claiming this can be verified for slippage against the mill shell being negligible. From this the curve of equilibrium of the charge surface is calculated. It is found that mill speed and degree of filling has little effect on the equilibrium slope but that coefficient of friction of the charge has a large effect. It was concluded that this surface does not represent the free surface of the charge but rather the surface below which solids rotate without slipping and above which they fall or roll in cascade.

The role of lifter-bars is then considered. In calculating the lift of a lifter-bar the following assumptions and approximations are made: the lifter is of negligible height relative to the mill radius; the sides of the lifter are parallel to the radius vector; the particles are released into free parabolic motion at the moment they begin to slip. Based on these assumptions it is calculated that the lifter-bars promote only a slight increase in lift relative to a smooth non-slip liner, so particles lying in the spaces between lifters are lifted slightly higher than the rest of the charge. However, the greater the diameter of the mill the less effect this has on the general motion within the body of the charge. It is thus considered that the only effect of lifter-bars is to produce a zone of higher peripheral trajectories of particles that lie between the lifter-bars, the motion of the rest of the charge being that produced by a non-slipping mill liner.

The assumption of no slip between the charge and liner appears to be justified as sound by assuming the use of low lifter-bars, the lifters being considered as perfect keying-in agents. This is most likely valid for the circular path below the main bulk of the charge but is an inadequate assumption for the last part of the path where charge pressure is too low to key-in the charge effectively, this region being critical in determining the subsequent trajectory of the particles. If it is assumed that there is no slip between a smooth liner and the charge then no doubt it can be shown that there is no slip within the body of

the charge, but again this is surely not so at the upper end of the circular path just prior to particles projecting or rolling away from the bulk of the charge. The equilibrium surface that is derived is most likely the zone passing through the kidney in the centre of the charge.

The calculations of the charge motion and of the equilibrium surface are based upon the spiral-circular path predicted by Davis' theory, but not observed in practice.

In the analysis of the effect of lifter-bars they must be just high enough to hold a particle as it is assumed that the particle is set into free flight the moment it begins to slip. In actual fact a particle will slip or roll down the face of a lifter until it reaches the tip of the lifter, only then being projected into flight. This is due to the lifter-bar maintaining a constant radial velocity and therefore remaining in contact with the particle until it reaches the tip of the lifter-bar (L.A. Vermeulen, 1984[10]). Also according to Vermeulen it is invalid to assume that the sides of the lifters are parallel to the radius vector as this is an important factor influencing the charge motion.

The statement that lifters have little effect on the general charge motion, especially as the mill gets larger, is one to be taken note of. The extent to which they key-in the charge is important but their actual profile may have little effect on the bulk motion of the charge. The existence of a surface of equilibrium within the charge body is also of interest.

This work is based almost exactly on that of Rose and Sullivan[13], and reaches the same conclusions. However the book contains many errors in its analyses, so although it is on the topic it is not analysed.

2.8. Fluctuations in the Slip of the Grinding Charge in Rotary Mills with Smooth Liners[8]

by L.A. Vermeulen and D.D. Howat (1984)

In this study, the motion of grinding elements in contact with the smooth liner of an experimental mill was investigated. A model mill with transparent ends was loaded with rods to a charge level of over 40% of capacity. The motion of the rods during operation of the mill was filmed, and the velocities of the rods were calculated from measurements made on successive frames of the film. Although the mill was run at a constant speed, large fluctuations in the velocities of the rods occurred, varying from less than 50 to almost 100 per cent of the peripheral speed of the mill, with an average velocity in the region of 60 per cent of the velocity of the mill shell.

It was found that surging of the charge consisted of alternating phases of cataracting, as the charge reached its maximum angle of repose, and of cascading, as the charge slipped back. From this observation it was concluded that when cataracting takes place, with at least 20 per cent of the rods in flight, the charge pressure decreases which leads to slip of the charge, then with the resumption of cascading the charge pressure increases so the charge keys-in again to the motion of the mill thus increasing the charge's angle of repose until cataracting again takes place.

An expression for the slip is given, which along with an estimate for charge pressure at the mill shell is used to test the postulate that fluctuations in mean speed, and therefore slip, are proportional to fluctuations in dynamic pressure. This is achieved by calculating rod speeds and comparing these to those observed in the model mill. An excellent correlation, within 5 per cent, is found, which provides good evidence in support of the postulate.

Therefore, in the case of a smooth lining, there is a minimum pressure of charge required for an adequate keying-in action of the rods on the shell and at any lower pressure extensive slip

takes place. This slip represents a large loss of energy, since the motion of the mill is not transferred effectively to the charge. In addition, extensive wear of the lining results from the intense sliding motion of the charge across the surface of the lining, a conclusion that is corroborated by the circumferential grooving that is observed on smooth linings in ball mills.

2.9. Effects of speed and liner configuration on ball mill performance[9]

by R.E. McIvor (1983)

This investigation of the effect of liners upon the power consumption of mills is based on the analysis of previous experimental work and on theoretical modelling.

Initially some general facts about grinding are presented, including the observations that a large circulating load decreases overgrinding, and that large balls are preferable for coarse grinding, while small balls favour fine grinding. Impact breakage is defined as the action of a particle being smashed between balls or ball and lining, or slow compression fracturing or crushing. Attrition grinding is defined as either abrasion, the surface removal of grains by rubbing action, or chipping, where pieces are removed by forces that fail to break the whole particle.

The author states that "The outer row of balls being acted upon directly by the mill shell is prominent in determining the motion of the entire charge. Besides dissipating a significant fraction of the total energy consumed by the mill, the outer row is the only portion of the charge in direct contact with the shell and so forms the key link for energy transmission to the remainder of the charge."

The downfall of previous experiments (Gow, *et al.*[4], Farenwald and Lee[5]) due to interference or wedging of balls between the end liners of short-length laboratory mills was also mentioned, thus

throwing doubt on the validity of their refinements to earlier theories.

To avoid similar experimental pitfalls and since he found no analysis of the effects of lifters on charge motion he carried out a theoretical analysis of particle motion in a mill. This consisted of considering a flat bar at some angle to the liner. The particle take-off point is determined to occur at the moment the gravitational, centrifugal, and frictional forces balance out. The particle is then assumed to follow an unobstructed free fall. From these computations it is found that the trajectory of a particle is independent of the size of a mill. From this it was concluded that the percentage of critical speed should be constant for any size of mill. It is also apparent that particle trajectories are highly sensitive to the lifter-bar leading face angle. Although not directly revealed by the computations, it is concluded that power draw will vary with different original liner designs and vary throughout the liner-wear life as the profile of the liner changes.

The author decided that extension of the theory to the entire charge is too complex, however the following general observations are noted: the ball charge level has a significant effect on overall charge motion; transverse segregation of ball sizes exist as observed by previous workers; increased lifter height or decreased ball diameter results in higher trajectories of the outer row of balls; if the ball diameter is approximately equal to the lifter height then the trajectories of the outer row of balls are relatively unaffected by subsequent rows due to their lack of direct lift on the outer row and lower percentage critical speed at the reduced diameter of the inner rows.

In conclusion it is stated that due to the complexity of milling, past experience and empirical relationships are important, but that they do not promote understanding of the fundamental processes so are of little help in promoting basic improvements. Thus "While investigations of grinding mechanisms and charge motion require further refinement, they can provide basic

knowledge useful for improving the design and operating performance of grinding circuits."[9].

This investigation illustrates the important effect of the profile of the liner on the motion of the charge and on the power usage of a mill. The outer layer of the charge consumes a significant proportion of the total input of power to the mill, and is responsible for the transfer of energy to the bulk of the charge. The motion of the outer layer of the charge also has a significant effect on the motion of the bulk of the charge.

This is one of the first proper analyses of the effect of lifter-bars on charge motion. Its main drawback is that the height of the lifter-bars is not taken into account, despite the experimental observation that the height has a significant effect on the lifting action. Although incomplete the analysis forms a useful basis upon which to develop further work, and it gives some good guidelines upon which to base liner design.

2.10. <u>The lifting action of lifter bars in rotary mills</u>[10]
by L.A. Vermeulen (1984)

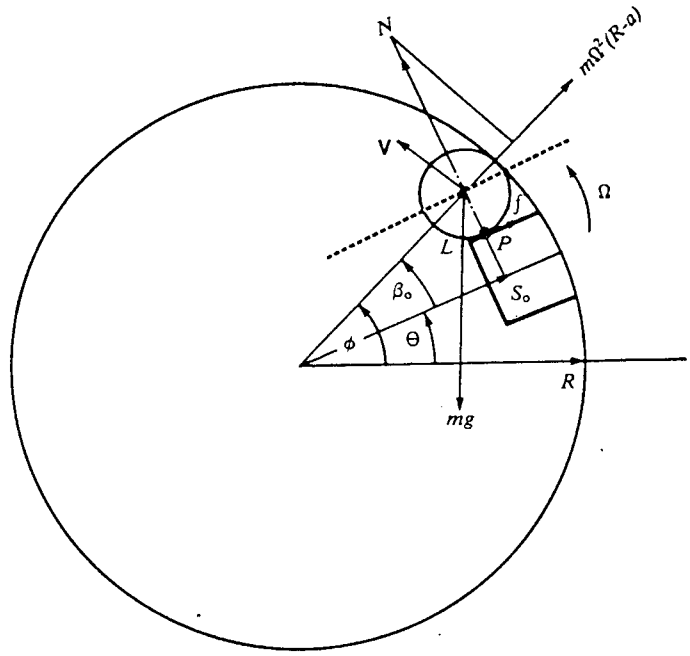

FIGURE 5. Diagram basic to the motion analysis[10]

A standard rectangular cross-section lifter-bar was considered. By exaggerating the scale of the bar and grinding element (in this case a rod is chosen) some previously unappreciated factors are made clear, see figure 5. Due to the width of the bar its leading edge is not perpendicular to the mill shell, thus the normal reaction of the bar has a radial component. It is also noted that the rod could not be free of the bar once the equilibrium conditions are reached, as they start with the same initial velocity and the rod can only experience a decrease in tangential velocity due to the force of gravity, once in flight. Therefore the bar remains in contact with the rod, causing it to roll or slide down the lifter face. This factor is determined to have a significant added effect on the computed lift and to introduce a substantial radial component to the rod's initial velocity once it is projected into flight.

The lift is defined as the final angle of departure from the lifter minus the departure angle from a smooth non-slip liner. The analysis involves finding the angle at which the gravitational, normal, and centrifugal forces balance, then considering the rod sliding down a plane of constantly changing inclination. The calculations are thorough and errorless with only one assumption introduced in the theoretical derivations, that the final rolling/sliding interaction at the tip of the lifter is sufficiently small to be ignored as it introduces only a slight error in the velocity and position of the rod as it leaves the lifter.

A filmed study was made of rod motion in an experimental mill fitted with various height lifters. Images of the cine' film strips were projected onto graph paper and the positions of rods in successive frames were plotted, thus tracing their paths of motion. These are compared with the calculated trajectories, the two being found to correlate very well for the coefficient of friction being chosen as zero. The motion of the rod down the lifter is concluded to be sliding as opposed to rolling, which produces more lift than that experimentally found. It is pointed out that the coefficient of friction must be finite and thus

produce some rolling action but that this factor would, according to the correlation found, be small. The relationship between spin-frequency of the rods, as they leave the lifter, and the coefficient of friction are determined so the latter can be derived by measuring the former. It is also pointed out that as the lifter-bar wears the angle of its leading edge is reduced, thus reducing the lift.

This is by far the most thorough and correct analysis of charge motion encountered. There is a minor approximation, in ignoring the interaction at the tip of the lifter, the effect of which is pointed out. The coefficient of friction was not measured, but used as an adjustable variable to fit the predicted to the observed results. This can cast some doubt upon the exact correlation between the theory and the measured results. The sound mathematics make this study an ideal one upon which to base further work. Important points, such as the effect of lifter height and leading face angle, are shown for the first time in this paper. It is fairly certain that the presence of ore will have a significant effect on the coefficient of friction, thus producing greater lift in real mills, but once this factor is experimentally determined it can be accounted for in the calculations.

2.11. Physical information from the inside of a rotary mill[11]

by L.A. Vermeulen, M.J. Ohlson de Fine, and F. Shakowski, (1984)

The bolts used to clamp the mill liners to the shell of an industrial pebble mill, were instrumented to continuously relay information about internal conditions of the mill to external receivers. The impact bolt consisted of a piezo-electric sensor inserted into the end of a hole drilled up most of the length of the bolt. The conduction bolt was drilled right through its length and an electrically insulated electrode inserted, this experienced enhanced conduction when immersed in the mineral pulp. Periodic and largely reproducable signals were obtained

from each of the bolts.

The structure of each piezo-electric signal indicates the presence of five distinct impact zones of material onto the shell of the mill. Theoretical impact points were calculated based on the assumptions of: spherical pebbles; keying of the charge into the rotary motion of the mill; no pebble interactions in the neighbourhood of departure; the body of the charge consisting of concentric rows of pebbles. A complete mismatch was found between these calculated and piezo-indicated impact points, the calculated ones yielding less lift and far shorter paths for the trajectories.

The possible action of the lifter-bars is considered. These can lift the smaller pebbles up to 30° further, but can only act on two or possibly three layers. These cannot account for the five impact zones spread over an angular range of 60°. The interaction of pebbles can only occasionally be sufficiently large to produce the required extra lift, thus not explaining the ever-present structure within the peaks.

The action of the pulp in providing a possible weak adhesion sufficient to carry the pebbles much further was then considered. Supposing that the adhesive force was proportional to the centrifugal force, a relationship between the radius of a row of charge and the effect of adhesion was developed. Inserting values for the arbitrary constant and average pebble radius, required to solve the relationship, reasonable predictions of the indicated impact positions were obtained.

The conduction signal indicates the angles of entry to and departure from the charge. There is considerable noise in the signal before the point of entry due to material impacting onto the liner. The entry and exit points are considered to give an indication of the charge repose angle and the mill load.

This work introduces a novel method of analysing charge motion within a real mill. It has shown the possible effect of the

adhesive action of the pulp in producing higher flight paths than predicted by the simple theories of charge motion that are generally used. There is no conclusive indication, however, that this is the correct explanation of the observed impact points. The work emphasises the importance of studying charge motion under realistic conditions. An indication is also given of the information that may be deduced from measurements with these instrumented bolts. The experimental techniques presented here should certainly be used to their fullest in any work on charge motion.

2.12. Estimation of milling parameters by use of a conductivity bolt[12]

by L.A. Vermeulen (1985)

All the information that could be deduced from conductivity bolt measurements was worked out, based on the existence of an equilibrium surface within the charge. This BHF (Barth-Hinsley-Fobelets) surface is considered to separate the *en masse* material keyed-into the rotary motion of the mill, and the loose material cascading and rolling down over this. By considering a mass in equilibrium under the action of gravitational and centrifugal forces with a friction term along the tangent of this surface, the form of the BHF surface is derived. The volume between the mill shell and this surface can then also be worked out. From measurements of the angle of entry and departure of a bolt into and out of the charge and knowing the mill speed, the two constants in the equations can be determined. Estimates of the dynamic angle of repose of the load and of the mill power were then made, based on the profile of the BHF surface.

The correlation between calculated and measured values was then investigated, on both experimental and real mills. Although the measured values were not the same as the calculated values of mill charge volume, there was found to be a linear relationship. The larger calculated values are thought to be due to expansion of the charge when in motion. Power calculations are about 20 per cent high, thought also to result from using the static

instead of dynamic charge density.

The BHF surface is considered to be well defined from the kidney to where the material departs from the charge, but ill-defined towards the toe of the charge were impacting and cascading result in many more than the three basic forces considered, being present. It was concluded that the most information that can be deduced from conductivity bolt measurements are estimates of mill load and power; dynamic angle of charge repose; and dynamic density of the charge.

It is somewhat doubtful that the BHF surface exists in the form proposed, the calculated surface being unlikely to coincide with the equilibrium surface reportedly observed to pass through the kidney of a rotating charge. The major reason being that the forces exerted by the material tumbling down over this surface are not taken into account. This notion is backed up by the BHF surface giving over-estimates of charge volume when in fact there is generally about 20 per cent of the charge in-flight in mills rotating at the speeds that were considered. However, from the linear relationship between calculated and actual values it is apparent that consideration of this surface is useful. This paper also gives a good idea of the scope of application of a conductivity bolt as an investigative tool.

2.13. General discussion of the papers reviewed

The papers considered present a variety of ideas upon which to base both experimental and theoretical work. That simplifications have to be made is quite apparent, but the shortcomings of unrealistic simplifications and assumptions are also clear. The work of Vermeulen is clearly the most advanced and mathematically thorough, and therefore the best upon which to base any theoretical derivations. It can be seen that there is a great deal of scope for improvement of the present theories of charge motion, thus making a study of this nature a valid and useful pursuit.

CHAPTER THREE

THEORY

The following is a theoretical study of the effect that lifter-bars of varying face angle and height have upon the charge motion within a rotary mill.

The simplest case of an isolated rod keyed-in to the mill motion is considered. Rods, as opposed to balls, are studied as they are the more favourable medium to use in the study of charge motion in a model mill.

A rod resting on a lifter and against the shell of a rotating mill, reaches a point of equilibrium where the sum of the forces acting on it is zero. Here the net forces on the rod, parallel ($\parallel$) to and radially perpendicular ($\perp$) to the motion of the rod are zero. The rod will then start to roll or slip down the face of the lifter[10].

3.1. Point of equilibrium

Refer to Figures I-1 and I-2.
The forces acting on the rod are:

Gravitational acceleration, acting vertically downwards, mg.
Centrifugal force directed radially outwards towards the mill shell, $m\Omega^2 r$.
Normal force of the lifter-bar, N.
Frictional force between the rod and lifter-bar. This is parallel to the face, and directed towards the base of, the lifter-bar, f.

For the purposes of this analysis the forces are resolved into components parallel and perpendicular to the lifter-bar leading face, and in the plane of rotation of the mill. The frame of

reference is the rotating polar coordinates following the rotary motion of the mill.

The nomenclature used is listed at the beginning of this thesis.

Forces $\parallel$ to lifter face.

$$m\Omega^2 r_0.\cos\beta_0 + \mu_s N - mg.\sin\gamma_0 = 0 \qquad (1)$$

Forces $\perp$ to lifter face.

$$N - mg.\cos\gamma_0 - m\Omega^2 r_0.\sin\beta_0 = 0 \qquad (2)$$

Substituting for N (from equation (2)) into equation (1), and dividing by m:

$$\Omega^2 r_0(\cos\beta_0 - \mu_s.\sin\beta_0) + g(\mu_s.\cos\gamma_0 - \sin\gamma_0) = 0$$

$$\rightarrow \sin\gamma_0 - \mu_s'.\cos\gamma_0 = \frac{1}{g}.\Omega^2 r_0(\cos\beta_0 - \mu_s.\sin\beta_0) \qquad (3)$$

By Appendix II

$$\mathrm{Sin}\beta_0 = \frac{\delta}{r_0}$$

where $\delta = (R-h).\sin\alpha - a \equiv$ constant. (4)

Now $\cos^2\beta_0 + \sin^2\beta_0 = 1$

$$\rightarrow \cos\beta_0 = \sqrt{1 - \left(\frac{\delta}{r_0}\right)^2}$$

Plug in values for γ_0 till residual = 0 then have equil pt.

So:

$$\sin\gamma_0 - \mu_s'.\cos\gamma_0 = \frac{\Omega^2}{g'}\left(r_0'\sqrt{1 - \left(\frac{\delta}{r_0}\right)^2} - \mu_s'\delta\right) \qquad (5)$$

This has to be solved by numerical methods.

For $\hat{s}$ the unit vector parallel to the lifter face and directed outwards, We have at the point of equilibrium:

$S = S_0$ and $\beta = \beta_0$ where:

$$S_0 = r_0.\cos\beta_0 \tag{6}$$

$$\beta_0 = \arcsin\left(\frac{\delta}{r_0}\right) \tag{7}$$

Using equations (5) , (6) and (7) the rod's location at the point of equilibrium can be fully determined.

The distance S_L and angle β_L when the rod is at the tip of the lifter can be calculated, as seen in figure I-3.
From Δ OLO', we get

$$S_L = (r-h).\cos\alpha \tag{8}$$

$$\beta_L = \arctan\left(\frac{\delta}{S_L}\right) \tag{9}$$

Between the point of equilibrium and the tip of the lifter the rod rolls and slides down the face of the lifter. It is not projected into free flight from the point of equilibrium because its tangential velocity is reduced due to the retarding force of gravity, whereas the lifter maintains a constant tangential velocity. Thus the lifter continues to exert a normal force on the rod as it travels down the face of the lifter.

The situation can arise though where the face of the lifter slopes forward of vertical, ie. γ exceeds 90^0, while the rod is still in contact with the lifter. In such a case the rod will fall away from the lifter once the normal force N is negative, ie. $m\Omega^2 r.\sin\beta + mg.\cos\gamma < 0$. This case is dealt with separately later, so the following derivations apply to the case where N is positive and the rod remains in contact with the face of the lifter until it reaches the tip of the lifter. It should be noted that in forming the equations the rod is in theory constrained to move on the face of the lifter-bar.

If the static coefficient of friction is greater than zero, the rod will start by undergoing pure rolling due to the torque

applied by f (figure I-2), where:

$$f \leq \mu_s N$$

3.2. Rod rolling down the face of the lifter bar

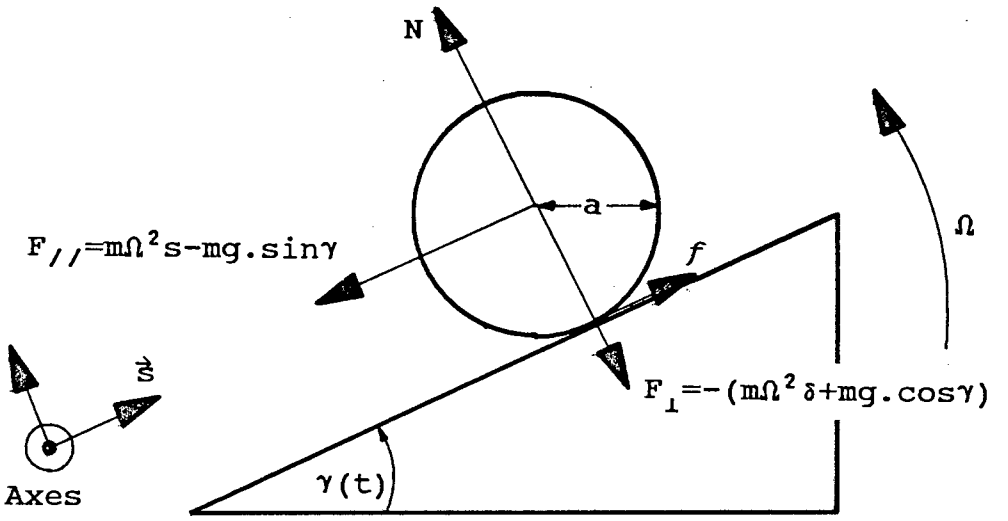

FIGURE 6. Cylinder rolling down a slope of changing incline, $\gamma(t)$

Considering the forces acting on the cylinder as it rolls down a slope that is subjected to a constant angular acceleration, the following equations can be derived, with the aid of figure 6.

Normal to incline : $N - mg.\cos\gamma - m\Omega^2\delta = 0$ (10)

In plane of incline : $m\Omega^2 s - mg.\sin\gamma + f = m\ddot{s}$ (11)

Torque about centre of mass (cm) $\Gamma_{cm} = I_{cm}\alpha$ (12)

α = angular acceleration of the rod about its centre.

Only f acts at a distance from cm, so:

$$f.a = I_{cm}\alpha \qquad \rightarrow f = \frac{I_{cm}.\alpha}{a}$$

For a cylinder $I_{cm} = \frac{1}{2}ma^2$

This moment of inertia about the centre of mass is the only factor that differentiates between the motion of a cylinder and a

sphere when rolling down a plane.
(For a sphere $I_{cm} = {}^2/_5 ma^2$)

Now the angular acceleration is directly related to the linear acceleration, while the rod doesn't slip, by.

$$\alpha = -\frac{\ddot{s}}{a} \qquad (13)$$

($\ddot{s}$ is negative for positive α, due to the orientation of the axes)

$$\rightarrow f = -\frac{m\ddot{s}}{2} \qquad (14)$$

$$\left(f = -\frac{2m\ddot{s}}{5} \quad \text{for a sphere} \right)$$

Substituting into equation (11) yields:

$$m\Omega^2 s - mg.\sin\gamma - \frac{m\ddot{s}}{2} = m\ddot{s}$$

$$\ddot{s} = \frac{2}{3}(\Omega^2 s - g.\sin\gamma)$$

$$\ddot{s} - \frac{2}{3}\Omega^2 s = -\frac{2}{3} g.\sin\gamma \qquad (15)$$

$$\left(\ddot{s} - \frac{5}{7}\Omega^2 s = -\frac{5}{7} g.\sin\gamma \quad \text{for a sphere} \right)$$

where:
$\gamma = \gamma_0 + \Omega t$ i.e. $\gamma = \gamma(t)$

This is a linear non-homogenous second order differential equation.

By Appendix III, the solution consistent with the boundary conditions of :

$S(0) = S_0$, which is known

$\left(\frac{ds}{dt}\right)_{t=0} = 0$; as the rod has not yet started rolling.

$$S(t) = \left(S_0 - \frac{2g}{5\Omega^2}.\sin\gamma_0\right).\cosh\sqrt{\frac{2}{3}}.\Omega t - \frac{\sqrt{6}g}{5\Omega^2}.\cos\gamma_0.\sinh\sqrt{\frac{2}{3}}.\Omega t + \frac{2g}{5\Omega^2}.\sin(\gamma_0 + \Omega t) \qquad (16)$$

$$\frac{ds}{dt} = \sqrt{\frac{2}{3}}\,\Omega\left(S_0 - \frac{2g}{5\Omega^2}.\sin\gamma_0\right).\sinh\sqrt{\frac{2}{3}}.\Omega t - \frac{2g}{5\Omega}.\left(\cos\gamma_0.\cosh\sqrt{\frac{2}{3}}.\Omega t - \cos(\gamma_0 + \Omega t)\right) \qquad (17)$$

Equations 16 and 17 describe the position and velocity of the rod for pure rolling down the face of a lifter. The solutions for a sphere are given in appendix III.

3.3. Maximum angle for pure rolling

There is a limit on the force f given by $\mu_s N$, so for a given static coefficient of friction (μ_s) and mill parameters, there is a maximum angle γ_m up to which pure rolling will occur. Beyond that angle the linear acceleration is too high for equation (13) to hold, thus the surface of the cylinder must begin to slip across the face of the lifter-bar. The theoretical maximum angle for pure rolling can be calculated from the equations that express the forces on the rolling cylinder and give its acceleration.

Substituting equation (15) into equation (11) yields:

$$m\Omega^2 s - mg.\sin\gamma + f = \frac{2}{3}m\Omega^2 s - \frac{2}{3}mg.\sin\gamma$$

$$f = \frac{m}{3}(g.\sin\gamma - \Omega^2 s) \qquad (18)$$

$f \leq \mu_s N$: so from equations (10) and (18)

$$\mu_s(mg.\cos\gamma + m\Omega^2\delta) \geq \frac{m}{3}(g.\sin\gamma - \Omega^2 s)$$

$$\rightarrow \quad 3\mu_s g.\cos\gamma + 3\mu_s\Omega^2\delta \geq g.\sin\gamma - \Omega^2 s$$

$$g.\sin\gamma - 3\mu_s g.\cos\gamma \leq 3\mu_s\Omega^2\delta + \Omega^2 s$$

$$\sin\gamma - 3\mu_s.\cos\gamma \leq \frac{\Omega^2}{g}(3\delta\mu_s + s) \qquad (19)$$

at the limit:

$$\sin\gamma_m - 3\mu_s.\cos\gamma_m = \frac{\Omega^2}{g}(3\delta\mu_s + s) \qquad (20)$$

$$\left(\sin\gamma_m - \frac{7}{2}\cos\gamma_m = \frac{\Omega^2}{g}\left(\frac{7}{2}\delta\mu_s + s\right) \quad \text{for a sphere}\right)$$

However, $s = s(t)$ so this cannot be directly solved. Equation (20) can be solved numerically for $s = s_L$ to yield $\gamma_m(\min)$, the minimum possible value of γ_m. Equation (16) can then also be numerically solved for $s = s_L$. However, if $\gamma_L > \gamma_m(\min)$ then there must be a transition from pure rolling to rolling and slipping.

3.4. Transition from pure rolling to rolling and sliding

To calculate this transition point, the equations for γ_m and $s(t)$ must be solved simultaneously. $S(t)$, from equation (16), can be substituted into equation (19) to yield the limit for pure rolling.

$$\rightarrow \quad \sin\gamma - 3\mu_s.\cos\gamma \leq \frac{\Omega^2}{g}\left[3\delta\mu_s + \left(s_0 - \frac{2g}{5\Omega^2}\sin\gamma_0\right).\cosh\sqrt{\frac{2}{3}}.\Omega t - \sqrt{6}\frac{g}{5\Omega^2}.\cos\gamma_0.\sinh\sqrt{\frac{2}{3}}.\Omega t + \frac{2g}{5\Omega^2}\sin\gamma\right]$$

$$\rightarrow \sin\gamma - 3\mu_s.\cos\gamma \leq \frac{3\Omega^2\delta\mu_s}{g} + \left(\frac{s_0\Omega^2}{g} - 0{,}4\ \sin\gamma_0\right).\cosh\sqrt{\frac{2}{3}}.\Omega t - \frac{\sqrt{6}}{5}.\cos\gamma_0.\sinh\sqrt{\frac{2}{3}}.\Omega t + 0{,}4\ \sin(\gamma_0 + \Omega t)$$

$$\boxed{0{,}6\ \sin(\gamma_0 + \Omega t) - 3\mu_s.\cos(\gamma_0 + \Omega t) \leq \frac{3\Omega^2\delta\mu_s}{g} + \left(\frac{s_0\Omega^2}{g} - 0{,}4\ \sin\gamma_0\right)\cosh\sqrt{\frac{2}{3}}.\Omega t - \frac{\sqrt{6}}{5}.\cos\gamma_0.\sinh\sqrt{\frac{2}{3}}.\Omega t} \qquad (21)$$

$$\left\{\frac{7}{12}\sin(\gamma_0 + \Omega t) - \frac{7\mu_s}{2}.\cos(\gamma_0 + \Omega t) \leq \frac{7\Omega^2\delta\mu_s}{2g} + \left(\frac{s_0\Omega^2}{g} - \frac{5}{12}\sin\gamma_0\right)\cosh\sqrt{\frac{5}{7}}.\Omega t - \frac{5\sqrt{3}}{12}.\cos\gamma_0.\sinh\sqrt{\frac{5}{7}}.\Omega t\right\}$$

for a sphere

This can be solved numerically for t_I at the equality, where t_I is the time at which the transition from rolling to sliding takes place.

Using equations (16) and (17) the location and velocity of the rod can be calculated at this transition point.

$$S(t_I) = S_I \quad \text{and} \quad \left(\frac{ds}{dt}\right)_{t_I} = v_I$$

3.5. Rolling and sliding

A combination of rolling and sliding yields a linear motion that is equivalent to pure sliding. The equation of motion is given by:

$$m\Omega^2 r.\cos\beta - mg.\sin\gamma + \mu_k N = m\ddot{s}$$

As there is a torque about the centre of mass there must be an angular acceleration of the rod, but this doesn't contribute to or affect the linear motion. Some of the energy loss due to friction is converted to rotational motion.

The angular acceleration is independent of the coefficient of friction, so once the rod starts sliding its angular acceleration continues as for pure rolling.

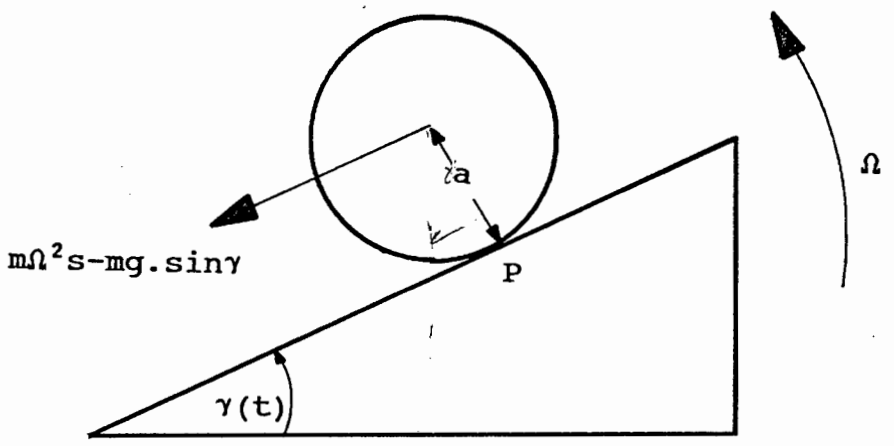

FIGURE 7. Cylinder sliding down a slope

Considering the forces illustrated in figure 7, and calculating the torque about the contact point, p, one finds:

$$\Gamma_p = I_p.\alpha \qquad \alpha = \frac{\Gamma_p}{I_p}$$

$$\Gamma_p = (m\Omega^2 s - mg.\sin\gamma)a \qquad \text{About point p.}$$

$I_p = \frac{3}{2}ma^2$ By parallel axis theorem.

($I_p = \frac{7}{5}ma^2$ for a sphere)

Therefore: $\alpha = \frac{2}{3a}(\Omega^2 s - g.\sin\gamma)$ (22)

($\alpha = \frac{5}{7a}(\Omega^2 s - g.\sin\gamma)$ for a sphere)

This yields the constant angular acceleration of the rod once it starts sliding.

3.6. Sliding after rolling

Considering pure sliding down the face of the lifter.
Using Force = mass x acceleration, referring to figure I-2, and considering the forces resolved parallel and perpendicular to the face of the lifter, we have:

$\parallel$ to lifter face:

$$m\Omega^2 r.\cos\beta + \mu_k N - mg.\sin\gamma = m.\frac{d^2s}{dt^2} \quad (23)$$

$\perp$ to lifter face:

$$N - mg.\cos\gamma - m\Omega^2 r.\sin\beta = 0 \quad (24)$$

Substituting for N from equation (24) into equation (23) yields the linear acceleration.

$$\Omega^2 r(\cos\beta + \mu_k.\sin\beta) + g(\mu_k.\cos\gamma - \sin\gamma) = \frac{d^2s}{dt^2}$$

Now : $s = r.\cos\beta$

and $\delta = r.\sin\beta \equiv$ constant (by Appendix II)

$$\ddot{s} - \Omega^2 s = g[\mu_k.\cos(\gamma_0 + \Omega t) - \sin(\gamma_0 + \Omega t)] + \Omega^2 \mu_k \delta \quad (25)$$

The boundary conditions at t = 0 are

$$s(o) = s_I \quad \text{and} \quad \left(\frac{ds}{dt}\right)_{t=0} = V_I$$

Equation (25) is a linear non-homogeneous second order differential equation. By Appendix IV, it is found that the

solution consistent with these boundary conditions is:

$$s(t) = \left[S_I + \mu_k \delta + \frac{g}{2\Omega^2}(\mu_k.\cos\gamma_I - \sin\gamma_I) \right] \cosh \Omega t + \left[\frac{v_I}{\Omega} - \frac{g}{2\Omega^2}(\mu_k.\sin\gamma_I + \cos\gamma_I) \right] \sinh \Omega t - \frac{g}{2\Omega^2} \left[\mu_k.\cos(\gamma_I + \Omega t) - \sin(\gamma_I + \Omega t) \right] - \mu_k \delta \quad (26)$$

$$\frac{ds}{dt} = \Omega \left[s_I + \mu_k \delta + \frac{g}{2\Omega^2}(\mu_k.\cos\gamma_I - \sin\delta_I) \right] \sinh \Omega t + \left[v_I - \frac{g}{2\Omega}(\mu_k.\sin\gamma_I + \cos\gamma_I) \right] \cosh \Omega t - \frac{g}{2\Omega} \left[-\mu_k.\sin(\gamma_I + \Omega t) - \cos(\gamma_I + \Omega t) \right] \quad (27)$$

Equation (26) is solved numerically for $s(t) = s_L$, to yield t, which in turn yields the velocity and position ,γ, for the rod at the tip of the lifter-bar. The t now used starts at zero at the transition point between rolling and sliding, so the total time moving along the lifter-bar is $t + t_I$.

3.7. Special case of N negative

When γ exceeds 90^0 the force of gravity acts away from the lifter face. Once the normal component of gravitational force exceeds the normal component of centrifugal force, the rod accelerates away from the lifter face. Thus in all stages of calculation the condition of:

$$mg.\cos\gamma + m\Omega^2 r.\sin\beta < 0$$

ie

$$g.\cos\gamma + \Omega^2 \delta < 0 \quad (28)$$

must be checked for continuously. If this condition is satisfied the rod goes into free flight at that point. This also overcomes

the conditions imposed by the equations of motion, of the rod being constrained to move on the face of the lifter-bar. Therefore no physically false conditions arise.

3.8. Free flight trajectory

At the tip of the lifter the rod is immediately projected into free flight, there being no further significant interaction with the tip of the lifter, due to the radial velocity of the rod, and the curve of its surface. Here a sharp edge is assumed, if the lifter is worn or rounded at the tip, this may not be the case. This is also not strictly true for a very low lifter-bar, the same or only slightly greater in height than the radius of the rod, as the rod does not have sufficient radial velocity to escape from the lifter-bar without some slight interaction at the tip. This is likely to be only a small effect, so is not studied in detail here. The condition for the lifter-bar having a smaller height than the radius of a rod is analysed in section 3.11.

The free flight trajectory is illustated in figure 8. At the tip of the lifter the following are known:

$$V_L,\ S_L,\ \theta_L,\ \beta_L,\ \gamma_L$$

$$\left.\begin{aligned} r_L &= \frac{s_L}{\cos\beta_L} \\ \phi_L &= \gamma_L - \beta_L \end{aligned}\right\} \qquad (29)$$

This gives the radial coordinates of the rod; $(r_L;\ \phi_L)$

For determining the free-flight trajectory it is convenient to change the reference frame to static cartesian coordinates, with the origin at the centre of the mill, and the Y axis directed vertically upwards.
The cartesian coordinates are:

$$(x_L,\ y_L) = (r_L.\cos\phi_L,\ r_L.\sin\phi_L) \qquad (30)$$

V_L is the velocity of the rod along the face of the lifter, to

this must be added the velocity due to the rotation of the mill, arising from the change of reference frames. This velocity component is tangential and equals $r_L\Omega$.

$$(v_{xL} \; ; \; v_{yL}) = (v_L.\cos\gamma_L - \Omega r_L.\sin\phi_L \; ; \; V_L.\sin\gamma_L + \Omega r_L.\cos\phi_L) \quad (31)$$

The net velocity is $v_L = \sqrt{v_{xL}^2 + v_{yL}^2}$ (32)

The angle of departure is $\sigma_L = \arctan\left(-\frac{v_{yL}}{v_{xL}}\right)$ to the horizontal (33)

Once in free flight the rod follows a parabolic path given by:

$$x = x_L + v_{xL}t \quad (34)$$

$$y = y_L + v_{yL}t - \tfrac{1}{2}gt^2 \quad (35)$$

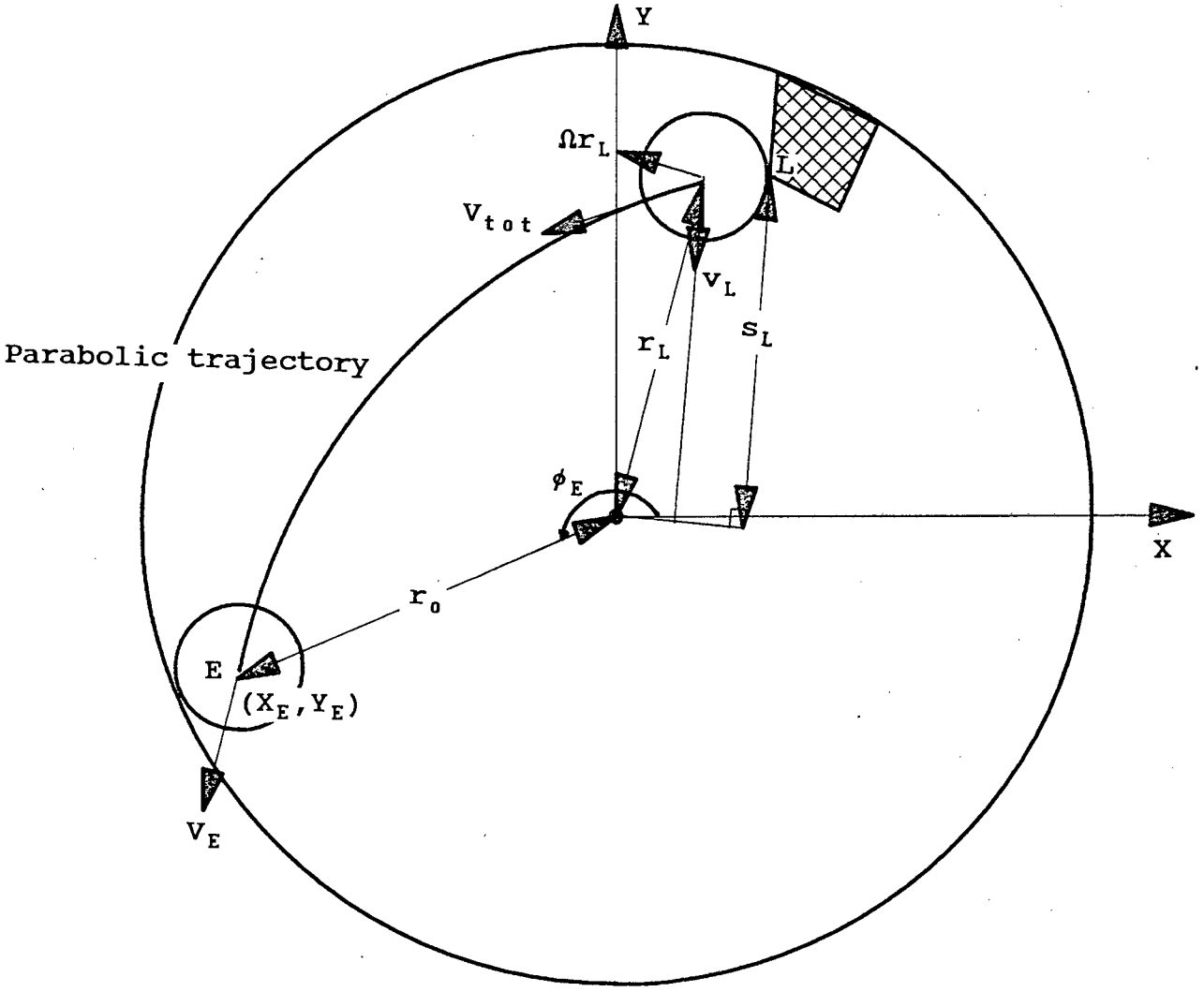

FIGURE 8. Parabolic trajectory of the rod from its point of departure from the lifter-bar

The point at which the rod strikes the mill shell, assuming no interaction with the charge mass en route, is satisfied by the condition:

$$x_E^2 + y_E^2 = r_0^2 \tag{36}$$

The velocity components are given by:

$$\left.\begin{aligned} v_{xE} &= v_{xL} \\ v_{yE} &= v_{yL} - gt \end{aligned}\right\} \tag{37}$$

so the velocity of impact with the mill shell is:

$$v_E = \sqrt{v_{yE}^2 + v_{xE}^2} \tag{38}$$

at an angle σ_E to the horizontal.

$$\sigma_E = \arctan\left(\frac{v_{yE}}{v_{xE}}\right) \tag{39}$$

The full path of the rod in flight, and its conditions of impact with the shell have thus been derived.

3.9. A special case for the lifter face parallel to the rod radius vector $\vec{r}$

For this condition to hold $\beta_0 = 0$

So : $\sin \beta_0 = \dfrac{\sin\alpha(R-h) - a}{r_0} = 0$ (by Appendix II)

$$\rightarrow \quad 0 = \sin\alpha(R-h) - a$$

$$\rightarrow \quad \frac{a}{(R-h)} = \sin \alpha$$

$$\boxed{\alpha_{//} = \arcsin\left(\frac{a}{R-h}\right)} \tag{40}$$

This $\alpha_{//}$ is the face-angle of a lifter-bar that yields zero-lift, relative to a smooth liner with perfect keying-in. For zero-lift to actually occur the rod would have to rest on the tip of the lifter, i.e. the lifter would be one rod radius high.

For $\alpha < \alpha_{//}$ one gets positive lift,

For $\alpha > \alpha_{//}$ one gets negative lift,

provided the lifter is of minimum height.
This points out the interesting, and practically important for high speed mills, possibility of installing lifters that promote good keying-in of the charge, while providing no extra lift.

For a smooth liner and perfect keying-in of the charge, we have at the point of departure:

$$F_r = m\Omega^2 r_0 - mg.\sin\phi = 0$$

$$\sin\phi = \frac{r_0\Omega^2}{g}$$

$$\phi = \arcsin\left(\frac{r_0\Omega^2}{g}\right) \qquad (41)$$

The rod would theoretically depart from the same angle, ϕ , as a lifter of face angle $\alpha_{//}$ and of minimum height.

3.10. Rod resting upon another rod

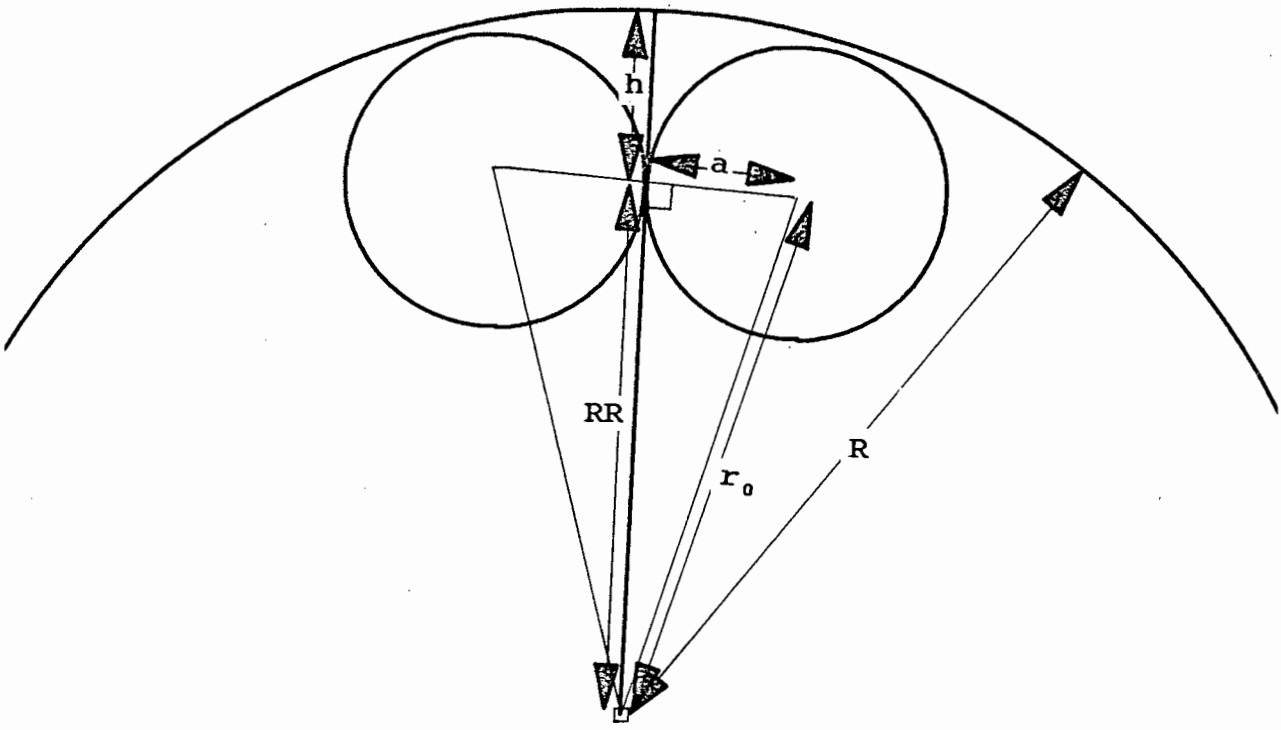

FIGURE 9. Rod resting upon another rod

This situation is equivalent to a rod resting upon a radial lifter-bar of height h_{rod}, as illustated in figure 9.

$$h_{rod} = R - \sqrt{r_0^2 - a^2} \qquad (42)$$

If it is assumed that there is no further interaction between the rods after the point of equilibrium is reached, then this can be treated in the same manner as the lifter-bar calculations.

3.11. Lifter-bar lower than a rod radius

A different set of conditions apply if the lifter-bar is lower than the radius of a rod, as the rod rests on the tip of the lifter-bar, as illustrated in figure 10.

For the rod resting on the tip of a lifter-bar of height h, we have, by the cosine rule in triangle OLA,

$$\eta = \arccos\left(\frac{a^2 + (R - h_r)^2 - r_0^2}{2a(R-h_r)}\right)$$

$$\lambda = 180^0 - \eta - \alpha$$

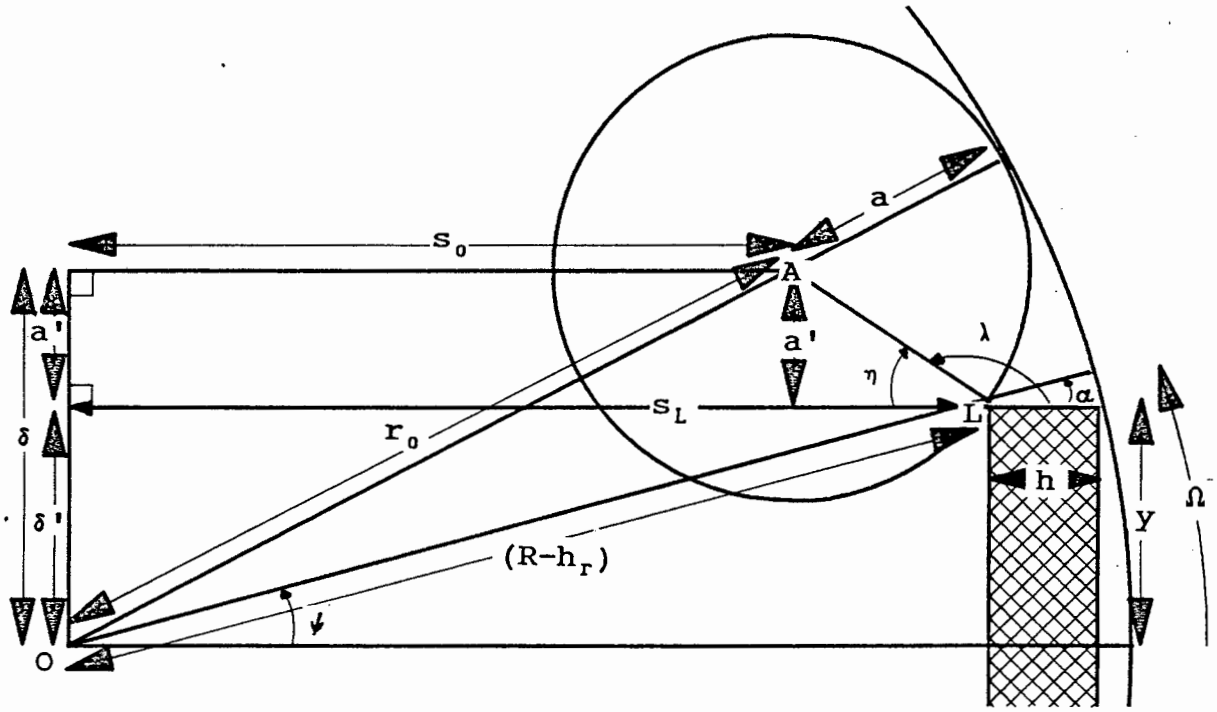

FIGURE 10. Rod resting on the tip of a low lifter-bar

If λ is greater than 90^0 this indicates that the rod is resting upon the tip of a lower lifter-bar, so this parameter can be used as a check in calculations

Referring to figure 11 the following equations of force can be derived.

$$F_{//} = m\Omega^2 r_0.\cos\beta_0 - \mu_s N.\cos(180^0-\lambda) - mg.\sin\gamma_0 \quad (45)$$

$$F_{\perp} = N.\sin(180^0-\lambda) - mg.\cos\gamma_0 - m\Omega^2 r_0.\sin\beta_0 \quad (46)$$

Equations (45) and (46) are both $\equiv 0$ at the point of equilibrium. With this condition, equation (46) implies that:

$$N = \frac{mg.\cos\gamma_0 + m\Omega^2 r_0.\sin\beta_0}{\sin(180^0-\lambda)} \quad (47)$$

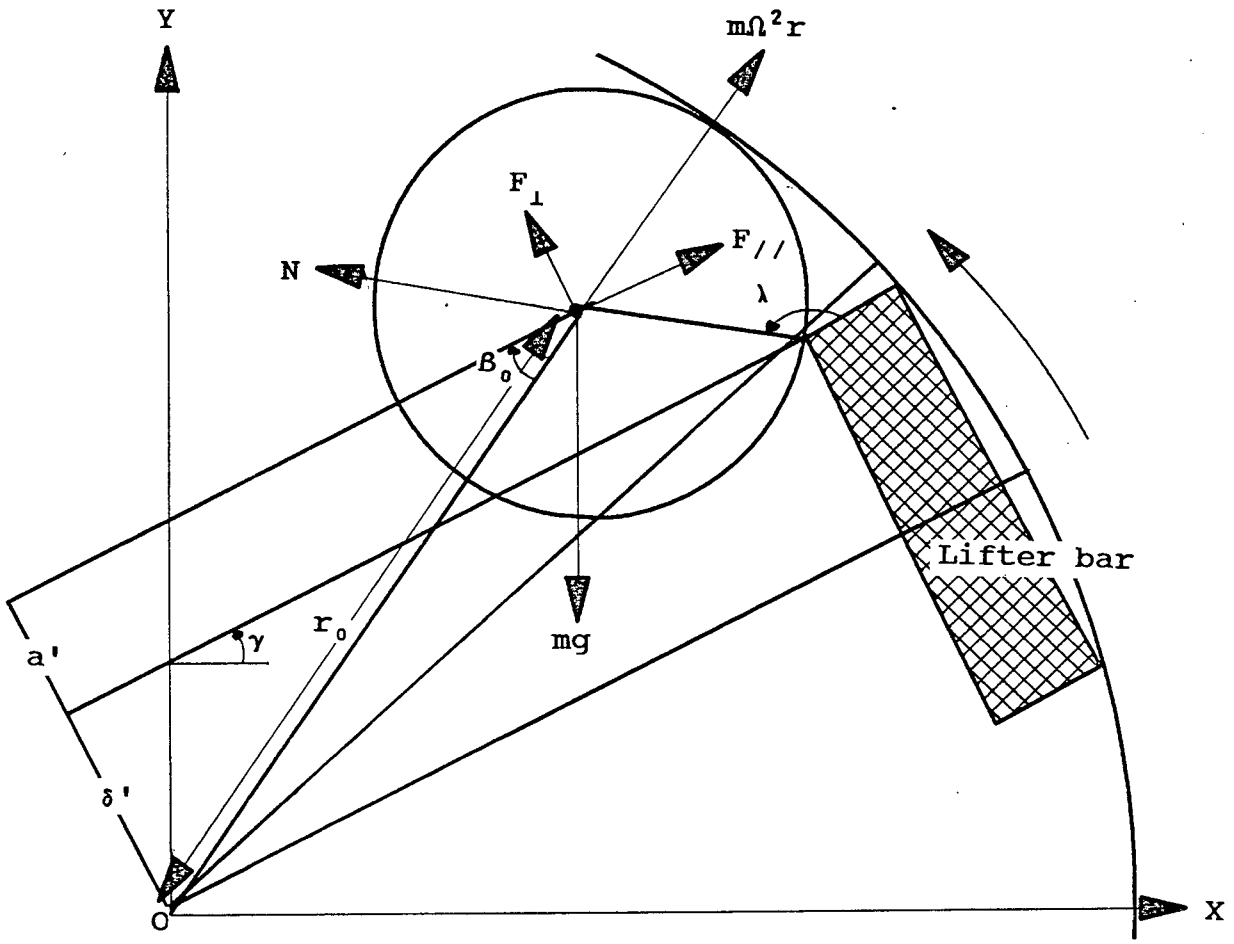

FIGURE 11. Forces acting on a rod that is resting upon the tip of a lifter-bar

Substituting equation (47) into equation (45) and dividing by m yields:

$$\Omega^2 r_0.\cos\beta_0 - \mu_s.\cos(180^0-\lambda)\left(\frac{g.\cos\gamma_0 + \Omega^2 r_0.\sin\beta_0}{\sin(180^0-\lambda)}\right) - g.\sin\gamma_0 = 0 \qquad (48)$$

Now; $\sin\beta_0 = \frac{\delta}{r_0}$

$$\rightarrow \quad \cos\beta_0 = \sqrt{1 - \left(\frac{\delta}{r_0}\right)^2}$$

and we have $\tan(180^0-\lambda) = -\tan\lambda$

Expanding equation (48) yields:

$$\Omega^2 r_0 \sqrt{1 - \left(\frac{\delta}{r_0}\right)^2} + \mu_s \Omega^2 \delta.\tan\lambda = -\mu_s g.\tan\lambda.\cos\gamma_0 + g.\sin\gamma_0 \qquad (49)$$

$$\rightarrow \quad \sin\gamma_0 - \mu_s.\tan\lambda.\cos\gamma_0 = \frac{\Omega^2}{g}\left(r_0 \sqrt{1-\left(\frac{\delta}{r_0}\right)^2} + \mu_s \delta.\tan\lambda \right) \qquad (50)$$

This equation has to be solved by numerical methods

If the static coefficient of friction is zero, ie. $\mu_s = 0$, then the equation (50) simplifies to:

$$\sin\gamma_0 = \frac{\Omega^2}{g} r_0 \sqrt{1-\left(\frac{\delta}{r_0}\right)^2} \qquad (51)$$

The solution to equation (50) or (51) yields the point of equilibrium of the rod, from this point the rod is assumed to go into flight with no further interaction with the lifter-bar.

3.12. Summary

This completes the analysis of the motion of an isolated rod in a rotary mill with flat-faced lifter-bars of any face angle and of any height.

An outline of the procedure required to carry out a full calculation of a rod's motion in a rotary mill is given in appendix VI.

CHAPTER FOUR

EXPERIMENTAL

A series of experiments against which the theory could be tested were carried out. These were also intended to provide visual representations of charge motion, so that a study of bulk charge motion, rod interactions, and the effect of changing mill parameters could be carried out. The principal work involved filming the motion of the charge in a glass-ended model mill, in which the configuration of the lining was varied. The motion of individual rods could then be traced. The coefficient of friction, the only unknown in the theory, was measured. When it was realised that the vibration of the mill is important, the principal frequency of vibration of the lifter-bars was measured. The effect of this on the static and kinetic coefficients of friction was then measured. Thus all the information required to test the theory was acquired. In addition the power draw of the mill, for varying speeds and lifter configurations, was measured. This was to seek some correlation between charge motion and energy usage.

4.1. Filming of Charge Motion

4.1.1. Aims

To provide directly measurable data on the flight paths of individual rods in a mill. To install lifter-bars in a mill, and record their influence on the charge motion. To vary the heights and face-angles of the lifter-bars, the mill speed, and charge filling, for the purpose of monitoring the influence of all these factors upon the motion of the charge.

4.1.2. Apparatus

A glass-ended model mill running on rubber wheels formed the basis of the work. The ends of the mill were removable, so that it could be loaded with rods and the lifters could be changed. Initially the rig was driven by an electric motor with a variable

power supply. As this tended to allow the mill speed to fluctuate, the drive system was changed to a constant speed electric motor connected to a continuously variable mechanical gearbox.

A variable-speed 16 mm camera was used to film the charge motion. Photographic floodlights, each of 2000W power were used to illuminate the inside of the mill. High speed daylight colour film was used for the filming.

A wooden information board was mounted in front of, and surrounding the mill. This held an interchangeable information chart giving the details of each run, a constant speed motor (functioning as a clock), and a digital watch. Horizontal and vertical lines, and later crosshairs, were centred about the centre axis of the mill. The constant speed asynchronous motor, running at 200 r.p.m., had a pointer mounted on its shaft, and in front of a dial face. This acted as a back-up clock. A photodiode, connected to a digital frequency counter, was used to set the strobe accurately. The strobe was used to check the asynchronous motor speed, and to set the speed of the mill.

Bars machined from rectangular mild steel bar, and tapped to receive screws passing through the mill shell, formed the lifter-bars. Rods 12 mm in diameter were cut into 295 mm lengths to act as the charge. These were rounded at both ends and a small hole drilled in one end, to act as a centre marker. Some rods also had a radial line cut into the end, so as to enable any rotational motion of the rods to be observed.

The apparatus layout, the mill, and the profiles of the experimental lifter-bars are illustrated in figures 12 to 14.

A detailed list of all the apparatus is given in appendix VII.

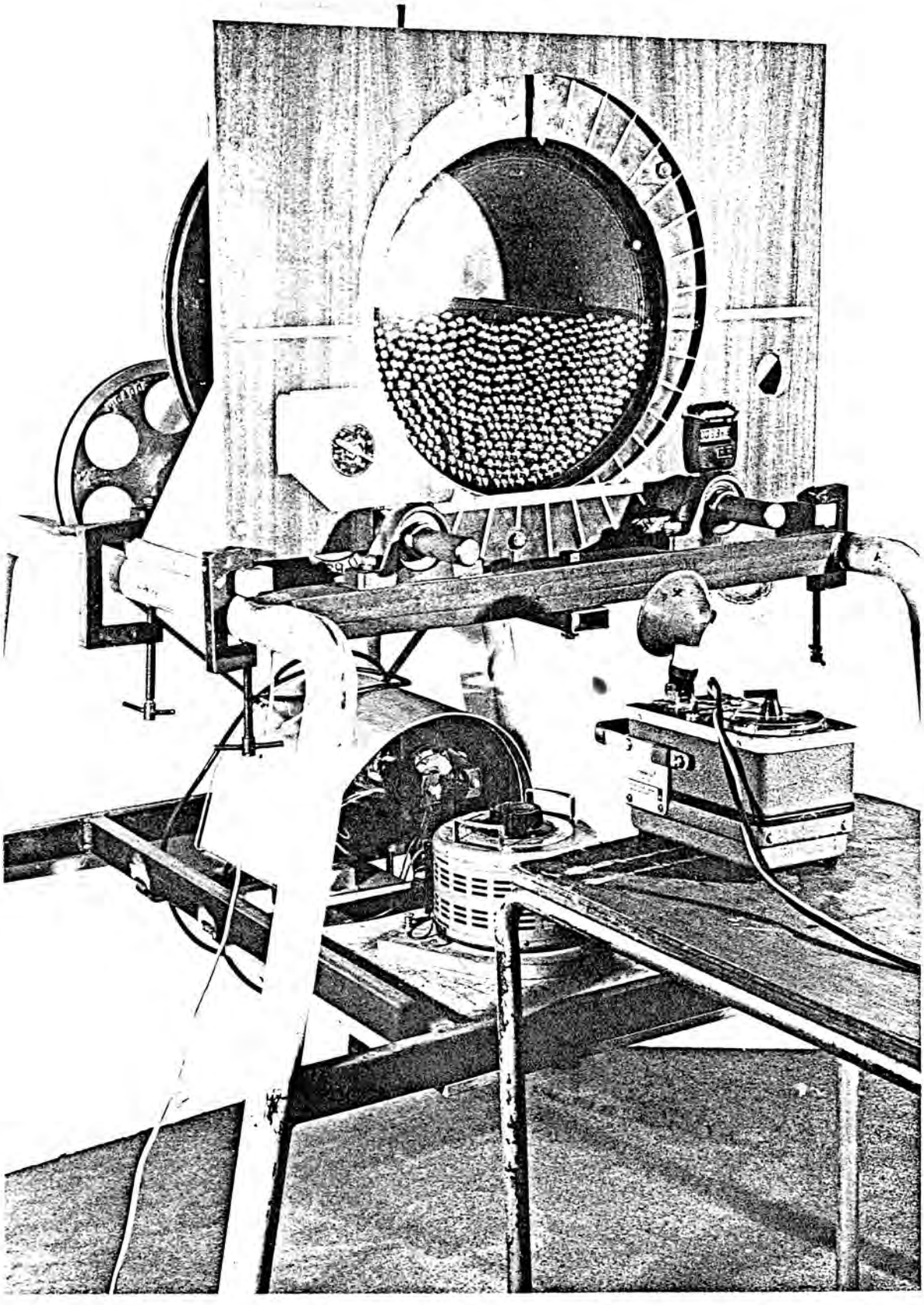

FIGURE 12. The initial experimental apparatus

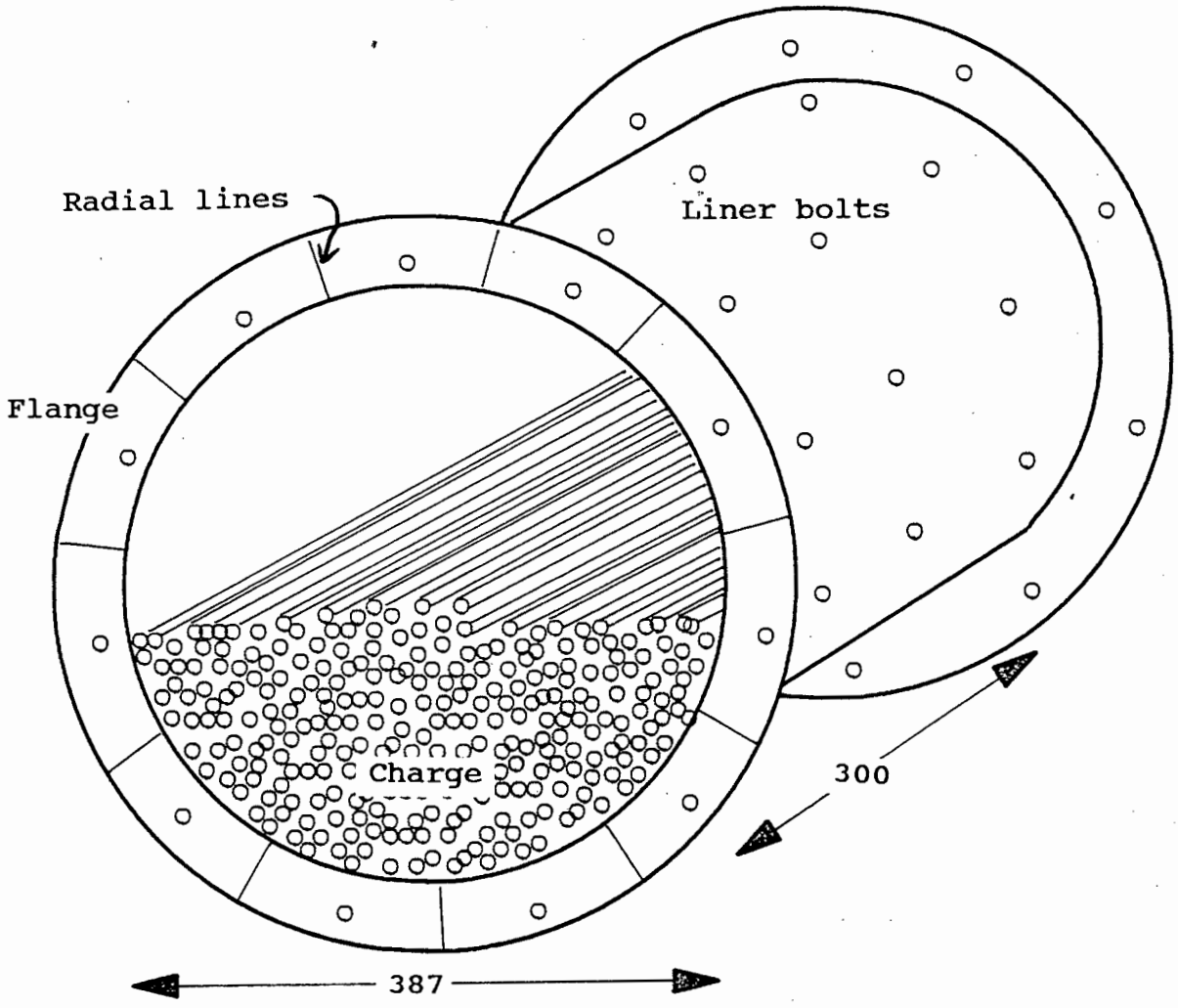

FIGURE 13. Schematic diagram of the mill

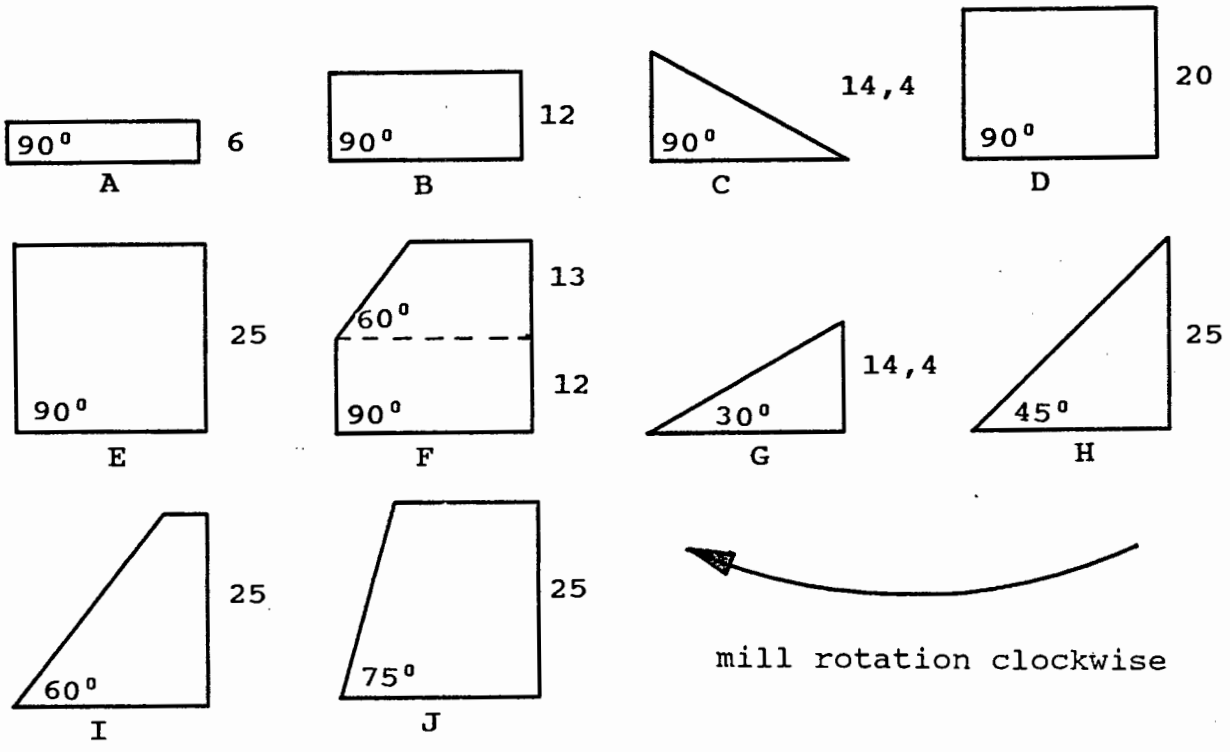

FIGURE 14. Profiles of the lifter-bars

4.1.3. Preparation and precautions

All rods were washed and their ends were smoothed off with emery paper. Initially some of the centre holes and all radial lines were pinted white. Some of the ends were also darkened with a permanent marker pen. Upon experimentation between sets of filming, it was decided to colour the ends of most of the rods red. This reduced the glare of the spotlights, and the remaining blue or silver ended rods could be picked out for tracking through the bulk of the charge. In addition all the centre holes were painted white, so that they could be more accurately located when analysing the film.

It is important for the analysis of the films of charge motion to have a reference time on the film, from which the filming speed and mill speed can be accurately determined. Initially a large-faced l.e.d. digital stop watch was used, but it was found that the figures did not show up on the film. Thereafter only the back-up clock was used. This was constructed from an asynchronous motor, mounted behind a dial, and with a pointer affixed to the output shaft of the motor. The speed of this was checked to be accurate and constant by testing under a strobe, and observing that the apparent position of the needle did not vary over a five minute period. The strobe frequency was calibrated against a digital frequency counter, by fastening a photodiode to the reflector and linking this diode to the counter.

A wooden information board was constructed, to be mounted in front of and surrounding the mill. This allowed the clocks and information to be mounted close to the mill in the corners of the filming frame, with the mill still filling the full height of each film frame. Horizontal and vertical lines crossing the central axis of the mill were marked on the board. These provided a reference according to which the image of the mill could be centrally located when analysing the film. This board was clamped onto the mill rig, and carefully located about the centre of the mill. All writing and dials were darkened considerably, to compensate for the very bright lighting

conditions required during filming.

The camera was set up 2,1 m from the face of the mill. Great care was taken in setting the lens of the camera perpendicular to, and in line with, the centre of the face of the mill. This was to ensure that there was no distortion of the image of the mill on the film. This was also to prevent the centre of the information board from being moved out of alignment on the film by an error of parallax. To achieve this the mill centre and camera lens were positioned the same distance from a straight wall, and the same height above a horizontal floor. The mill axis was set parallel to the wall, then by centralising the mill image in the crosshairs of the camera's through-lens viewfinder, the camera was correctly positioned. This position was clearly marked, as the camera is easily moved while loading the film. The camera was focussed at 2,1m (7ft), then checked visually with the special focussing lens. The focussing prism was then removed and the filming prism replaced. The camera speed was set at about 300 frames per second. The film was loaded under the cover of a thick black cloth, so as to provide well subdued lighting conditions. Once loaded it was run through for a couple of seconds, so as to ensure that the exposed leader was reeled beyond the lens.

The spot lights were located on either side of the mill, and about a metre in front of it, and set slightly above it. They were then directed to shine across the centre of the mill and slightly downwards, so as to minimise the glare reflecting off the mill window onto the camera. This is important as a strong glare can completely obscure the filmed image. Because of their high power rating, the lamps and mill motor were plugged into isolated power supplies.

The rear window of the mill was initially blocked off with an exterior sheet of black paper, but later a thin steel sheet was clamped on the inner face of the window. This served the dual purpose of both obscuring the background, and protecting the glass of the rear window. The front window was thoroughly

polished with silvo or brasso to clean it and clear the smaller scratches. The lifter-bars were installed, ensuring that the machined faces were on the leading edges. A set square was used to set them perpendicular to the mill face, and they were securely bolted on to prevent them from shaking loose.

On the front flange of the mill 36 Radial lines had been painted. Using the strobe set to 36 times the desired rotational speed of the mill, the speed of the mill was set. Filming could then commence. The Spot lights were switched to full power and the camera started up. For each run 2 seconds were allowed for the camera to reach full speed then 5 seconds for filming. Up to 11 runs could be taken with one reel of film. Considerable difficulty was experienced in setting the correct camera exposure, as there was no direct method or internal light meter by which to set it. In a trial film an exposure of 2.0 was found to be correct, but the final set of films were under-exposed at this setting. This was possibly due to all the rod ends being coloured after the trial film was taken.

4.1.4. Procedure

In the first batch of filming two loads were used, 15 per cent and 45 per cent filling by volume, two speeds were used, 75% and 90% of the critical speed, and 8 types of liners were tested.

The number of rods required to give the desired filling were calculated for each liner configuration as given in equation 52. This was based on 8 lifters being covered by the charge for a 45% filling, and 4 for a 15% filling.

$$\% \text{ filling} = \frac{(\text{No.of rods})(12)^2\sqrt{3}/_2(\text{Cross-sectional area of lifters})}{\pi.(193,5)^2} \qquad (52)$$

TABLE 1

Mill filling for various liner configurations

Type of lifter	Number of rods	
	15% filling	45% filling
Smooth	142	425
B 90°, 12 mm	132	405
E 90°, 25 mm	121	384
F 90° & 60°	123	388
G 30°	136	413
H 45°	131	404
I 60°	127	396
J 75°	124	390

The mill speed in revolutions per minute (rpm) for a given critical speed is calculated as follows:

$$\text{rpm} = \frac{42{,}3 \;.\; \%\ \text{critical}}{\sqrt{D} \;.\; 100} \qquad (53)$$

where D is the internal mill diameter in metres.

All the eight liner types were, where possible, run at both speeds, and with both fillings for each speed.

In the second batch of filming, only 365 rods, giving about a 40% filling, were used. A range of seven speeds, and five lifter heights for 90° lifters were filmed. In addition the range of speeds were tested for 25mm, 45° lifters.

TABLE 2

Mill speed in rpm for a range of percentage critical speeds

% Critical	60	70	75	80	85	90	100
Rpm	40,8	47,6	51,0	54,4	57,8	61,2	68,0

The lifter heights were smooth, 6mm, 12mm, 15mm, 20mm, and alternating rows of 20 and 12 mm lifters.

4.2. Analysis of films

4.2.1. Aims

The primary aim of the film analysis was to plot the trajectories of individual rods in such a manner that the predictions of the theoretical model could be compared with these trajectories, and to form a visual record of the charge motion. The second aim was to establish the effect of varying the lifter height, lifter face angle, and mill speed upon the charge motion. The third aim was to establish some idea of the effect of group interactions upon the trajectory of an individual rod. The fourth aim was to obtain an overview of the bulk charge motion.

4.2.2. Apparatus

The film analysis was carried out by projecting the film frame-by-frame onto a graphics tablet. The rod positions were then recorded directly from the tablet by using a mouse, and then stored on a floppy disk.

A standard 16 mm projector was used. The graphics tablet was linked to a personal computer and a four-function flat mouse was used. This has a circular,transparent, magnifying locator with cross-hairs marking the centre. A circle with the same radius as the images of the rods was drawn on the locator, to help centralise it on the image of the rods. Software was written to drive the mouse, and control the assimilation, storage, manipulation, and printing of readings. Details of this programme are given in appendix IX.

4.2.3. Preparation and precautions

The apparatus is set up as illustrated in figure 15. A wide angle lens was used on the projector so that it could be placed close to the graphics tablet, (f= 1,5 and 25mm lens). The tablet was held vertically against the wall by an elastic band extending beyond the edges of the tablet, so that it could be slid back and forth to centralise the image. It is important that the projector is placed perpendicular to the screen, so that a true circular image is attained. To achieve this one side of the table was

placed against the wall and the projector aligned with the other side. It was also ensured that the centre of the lens was the same distance from both the edge and surface of the table as the centre of the graphics tablet.

FIGURE 15. Film analysis equipment

A circle, filling the full area of the graphics tablet, was drawn on as a template upon which to project and locate the image of the mill. The centre and radius of this circle were carefully located in the tablet coordinates, as this is essential for accurate readings to be obtained. Horizontal and vertical lines located about the centre point were marked on the edge of the circle. This allowed the image to be accurately located by the similar lines on the information board. With the film in focus the projector was located so that the inner surface of the shell of the mill coincided with the template circle.

The film was fed through the projector in such a manner as to by-pass the driving wheels. Then with the projector on frame hold the film could be fed through manually and held at any frame. The vertical position of the image was set by careful adjustment

of the frame position.

Transparent plastic sheet was taped onto the tablet so that progressive positions of the rods being traced could be marked. In general only every second frame of the film was analysed. the rod positions were marked each five readings so as to prevent the rod that was being traced from being mistaken for a nearby one.

4.2.4. Procedure

The software allowed 6 rods to be followed for up to 200 frames. In general the tip of a lifter-bar, and the 4 rods in front of it were followed, as illustrated in figure 16 below.

The rods were traced from a point at which rod 5 had almost reached equilibrium and was about to move off the shell. All four rods and the tip of the lifter-bar were then followed until rod 2 struck the opposite side of the mill or landed on the charge. The recorded positions were saved directly as cartesian coordinates scaled to the mill dimensions. Where possible an isolated rod was followed as this condition is directly applicable to the theory.

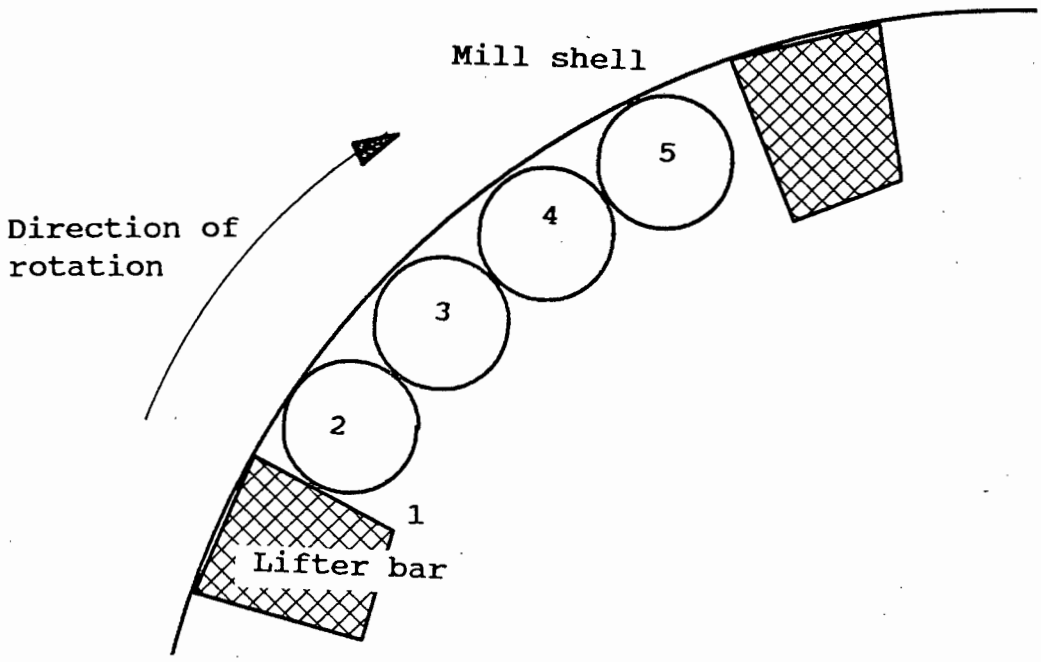

FIGURE 16. The rod formation that was tracked

The mill and camera speeds also had to be checked for each run. It was ensured that each set of trackings was started well into the run, so that the camera had reached full speed. The mill speed was found by marking the position of the clock's pointer, and the position of a radial mark on the mill flange. The number of frames were then counted till the mill had executed a full revolution. The number of clock revolutions were counted, noting the number of film frames for each revolution. This yielded both the total time for one mill revolution and the film speed.

Every filmed run was analysed. Some were analysed twice to check the reproducibility of results and the regularity of the trajectories of different rods.

4.3. Lifter-bar Vibration

4.3.1. Aim

The mill vibrated extensively while it rotated, and it was realised that this would have a large effect on the coefficient of friction between the lifter-bar and a rod resting on it. It was therefore decided to measure the principal frequency at which a lifter-bar vibrated. The coefficients of friction could then be measured under these vibrating conditions.

4.3.2. Apparatus

An accelerometer was screwed directly into a lifter-bar, as illustrated in figure 17. A cable was taken from this through a bolt hole in the flange and taped to the centre of the mill window. This long cable was then twisted to accomodate many revolutions of the mill. The cable was then connected to a charge amplifier, which was linked to a storage oscilloscope.

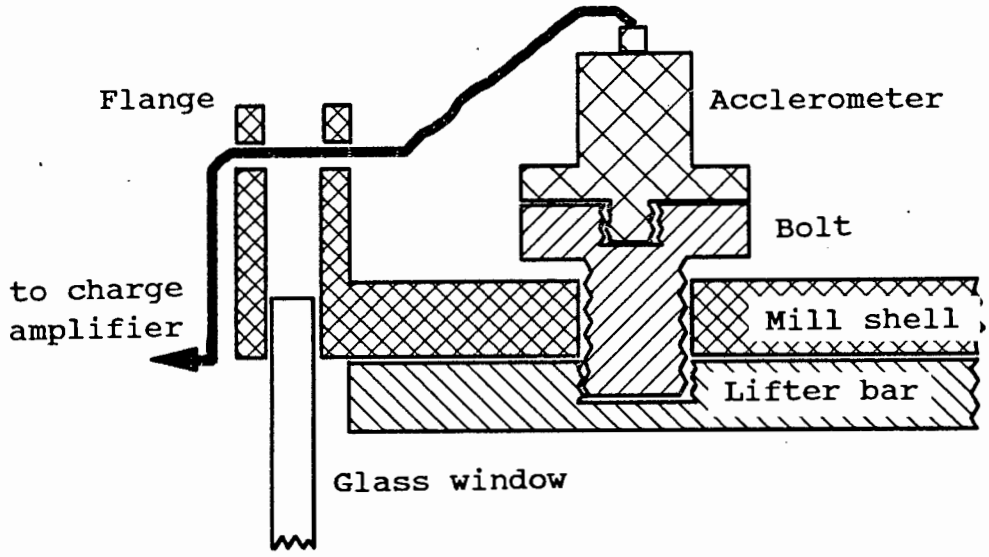

FIGURE 17. Layout of the accelerometer

4.3.3. Procedure and precautions

It was ensured that the screw into which the accelerometer was attached, did not touch the mill shell, so that only the vibration of the lifter-bar was detected.

The mill was run with a standard 40 per cent charge, and a signal was triggered on the oscilloscope in the storage mode. Data was accumulated over a full revolution of the mill. The principal frequency of vibration was sought across the frequency spectrum. The period was then measured directly off the screen, and checked for reproducibility. The signal was also photographed as a permanent record of the spectrum.

4.4. Measurement of the coefficients of friction

4.4.1. Aims

The static and kinetic coefficients of friction, between the rod and the lifter, are central to the proposed theory of rod motion. It was therefore important to measure these, under the same conditions and with the same materials as in the mill. It was decided to carry out a simple experiment of a sample sliding down an inclined plane.

4.4.2. Apparatus

A 1m long mild steel sheet was machined in the same manner as the

lifter-bars. This was mounted onto a rack which allowed the angle of the sheet to be varied from 0° through to 45°. A rod was cut into four pieces which were then welded together to form a square that could act as the sliding sample. The sliding surfaces thus formed the same contacting pair of materials as present in the rod / lifter-bar interface. The apparatus was placed onto thick foam sheets, and the end of the rack left overhanging. A vibrator was screwed onto the end of the rack, and firmly supported at the correct height for the weight of the rack to half depress the vibrating head. The sliding sheet was clamped onto the rack, to prevent it from bouncing off with the vibration. A large protractor was made and its zero line set to horizontal, the angle of the sliding sheet could then be read directly off it. A graduated strip was fastened to the side of the sheet, from which the position of the sliding sample could be read. This apparatus is illustrated in figure 18.

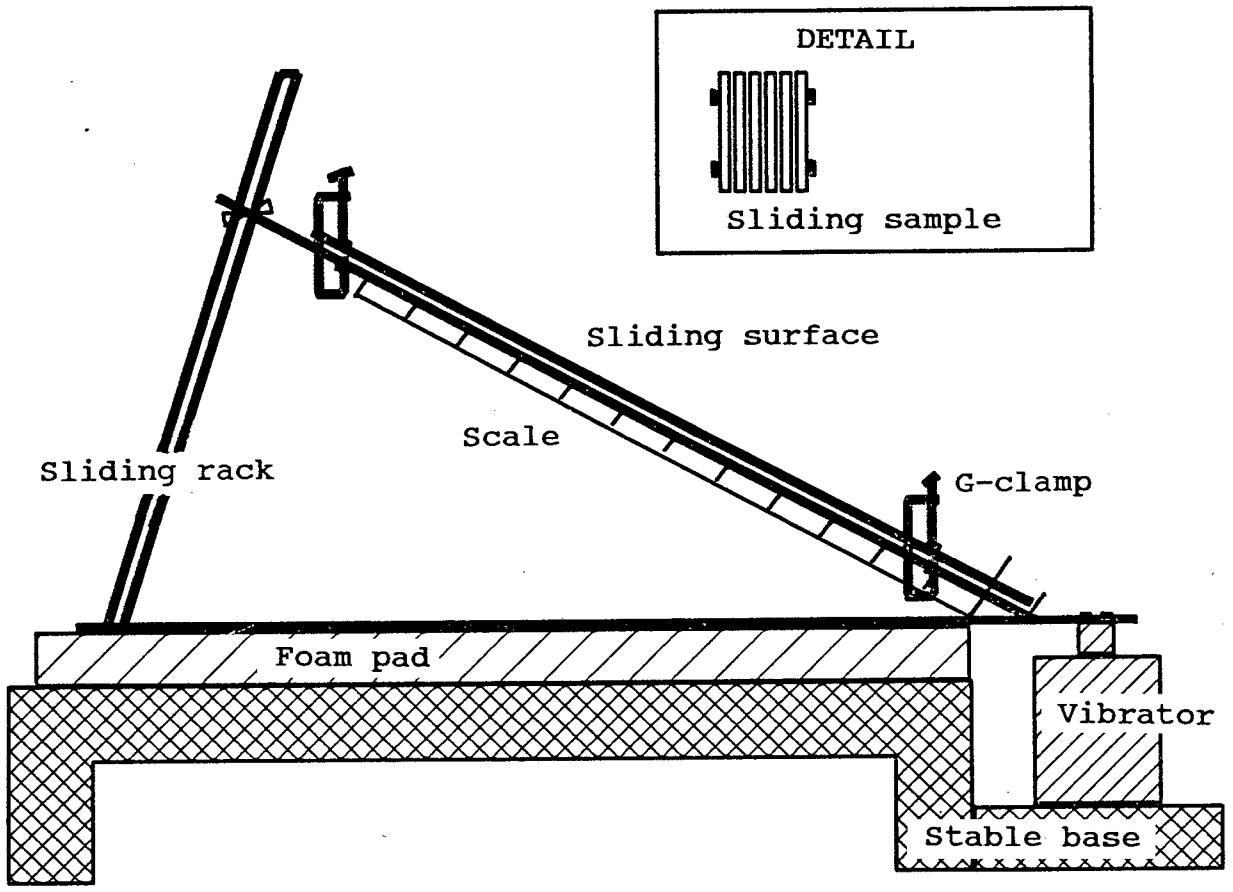

FIGURE 18. Sliding friction apparatus

A standard video camera was used to film the motion of the sliding sample. Specialised video editing equipment was initially used for the film analysis, subsequently a more standard video recorder with a special frame-by-frame advancing facility was used.

4.4.3. Preparation and precautions

The protractor was mounted above the pivot point, and flush with the face of the sliding surface. The zero of the protractor was set horizontal with a spirit level.

Initially a stop watch was used for timing the sliding time of the test piece, but this time was found to vary considerably. It was therefore decided to record the motion on video and then analyse this. Accordingly the video was set up close to the apparatus, central and perpendicular to it. The apparatus was well lit and a plain white sheet placed behind it.

To measure the static coefficient of friction the sliding piece was placed on the surface, and the surface gradually lifted until the angle at which the sample just began to slip was reached. This was repeated a few times so as to accurately check the angle. The sliding piece was placed with the rod sections perpendicular to the direction of motion, as is the case under real conditions in the mill.

The kinetic coefficient of friction was determined from the sliding time of the sample, from the moment of release at the top to a fixed point near the base. A line was marked at the base point, and vertical markers placed on either side of it, so that it would be clearly visible on the video recording. The slope was tilted to an angle that allowed the sample to slide freely. The sample was then lightly held by two finger tips at the top line, then released as quickly as possible. This made the release time clearly distinguishable on video.

4.4.4. Procedure

Static and kinetic coefficients of friction were measured at the

following frequencies: Stationary, 10Hz, 100Hz, 300Hz, 600Hz, and 1000Hz. Two amplitudes of vibration were tested for each frequency. 1000Hz was the limit of response of this heavy rig to the vibrator. Six runs were filmed for each set of conditions, all at a slope of 18^0 for the sliding friction measurements.

4.4.5. Analysis of the video

Each run was analysed, and the average time of a set for a particular condition was used as the sliding time. The video speed is 25 frames per second and there are two fields per frame, Therefore a time interval of 0,02s was obtainable. The video was gradually advanced in the frame by frame mode until a blurring of the fingers, that held the sample, was noted. The counter was zero'd from there and the video advanced until the sample just reached or crossed the line. The exact number of fields was counted to ensure an accuracy to within 0,02s.

4.5. Power draw of the mill

4.5.1. Aim

The object of this set of experiments was to plot the power draw of the mill as a function of lifter height and mill speed, for a fixed mill load.

4.5.2. Procedure

The mill was run as it was normally run for all the filming. An ammeter was connected into the live wire of the supply line to measure the current drawn. To prevent the ammeter from being overloaded upon start-up of the mill, it was placed in parallel to a switch. The switch was opened once the mill was running, so that the full current passed through the ammeter. As the phase-lag between voltage and current changes with the power draw, this phase-lag was also measured as a function of power draw. This was achieved by connecting an oscilloscope with two separate inputs for voltage and current. The two signals were displayed simultaneously and the phase lag could be measured directly from the peak-to-peak distance on the time scale of the oscilloscope.

The experimental set-up is illustrated in figure 19.

A range of 13 speeds, from 60 to 120 per cent of the critical speed, and six liner configurations were tested.

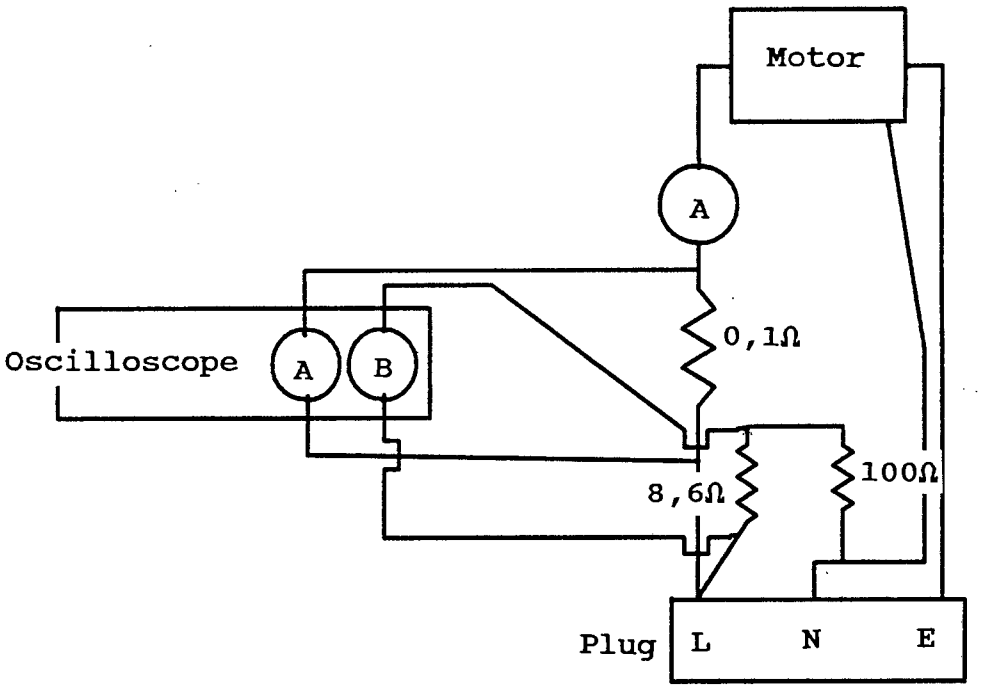

FIGURE 19. Phase-lag measurement apparatus

CHAPTER FIVE

RESULTS

5.1. Films of charge motion

A total of seven reels of film were taken during the two sets of experimental work. The first set of films were overexposed, and the second set underexposed, despite taking a trial film at different exposures. A detailed list of the 65 sets of conditions that were filmed is given in table VIII-1.

It was hoped that with the 15 per cent mill filling a number of isolated rods could be located for each run, however this was not the case, as the rods still tended to pack together in groups between the lifter bars. The rod paths were visible on all the films, but because of exposure problems it was sometimes difficult to accurately locate the centres of the rods that were being traced.

The different size and shaped lifter-bars yielded clearly discernable differences in the motion of the charge, both in the outer layers and in the bulk of the charge.

5.2. Analysis of the films

A plot of each of the filmed conditions was made. The analyses were of the trajectories of the outermost, isolated rods resting on the lifter-bars. This was to provide experimental results against which the theoretical predictions could be tested.

These paths were successfully traced and plotted out. Once the experimental procedure had been well established and practiced, the resulting flight paths were adequately smooth and continuous. Sample trajectories are illustrated in figures 20 and 21. The comparative plots in figure 21 are of two different rods in the same run, and illustrate the variability in observed flight

paths. The erratic paths at the end of the trajectories are due to the rods bouncing off the bulk of the charge. Further plots, that are discussed at a later stage, are presented in figures I-4 to I-6, and 27 to 37.

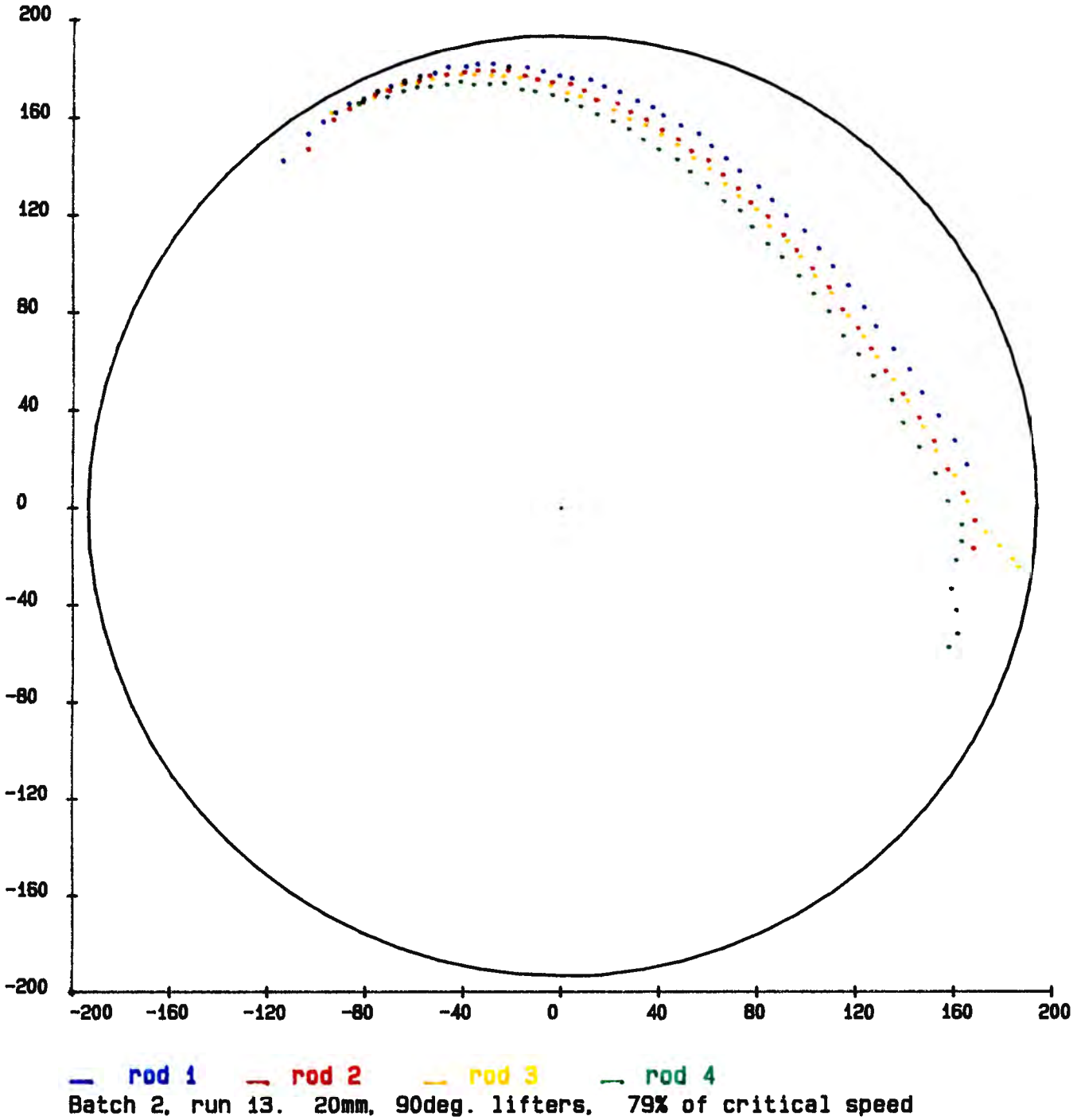

FIGURE 20. The flight paths of a group of four rods

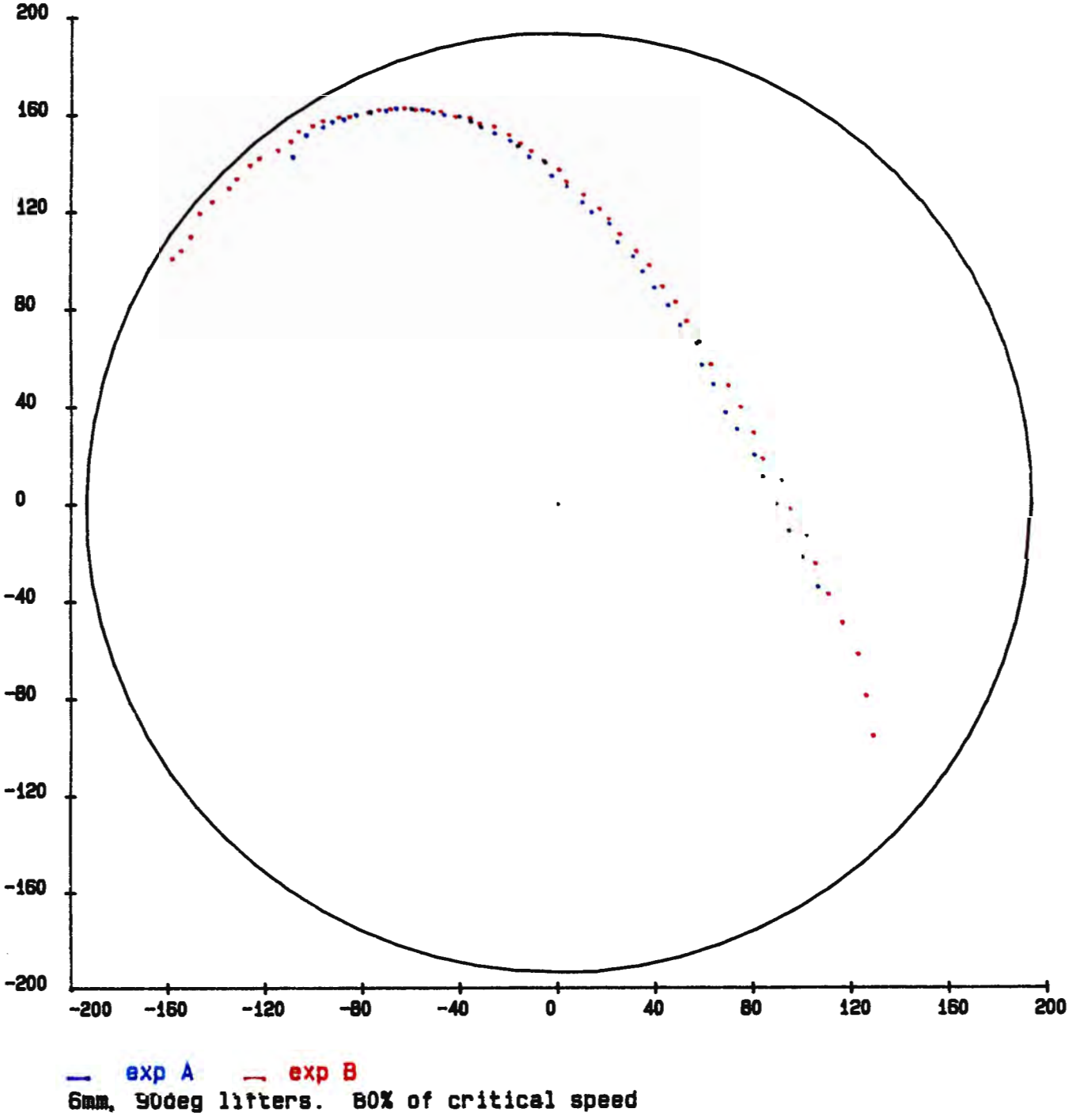

FIGURE 21. Comparative plots of the same run

5.3. Lifter-bar vibration

A good set of reproducible traces of the response of the accelerometer were obtained on the oscillascope trace.

When the mill was rotated manually a major set of peaks having a 70μs period were observed. When running the mill continuously for about a minute, a 70μs period peak was again obtained. This indicates that the lifter-bar has a principle frequency of vibration of 14,3kHz.

5.4. The coefficients of friction

5.4.1. Static coefficient of friction

In the static condition the sliding sample was found to just start sliding at an angle of 13^0, this yields a static coefficient of friction of 0,23.

A list of the variation in the apparent static coefficient of friction under a range of vibrating conditions, is given in table VIII-2. It was somewhat difficult to judge the exact angle at which the sample began to slide, however the observed variation was not great, and was estimated to be within 1^0. Although the results only extend up to 1kHz it is clear that the apparent coefficient of friction is tending to zero, and will be approximately 0 when the sample is resting upon the surface of a lifter-bar that is vibrating with a frequency of 14kHz.

5.4.2. Kinetic coefficient of friction

Recording the sliding of the sample on a video allowed sufficiently accurate and reproducable readings of the sliding times to be taken. The frame-by-frame analysis of the video yielded clearly discernable release times and finish times, of the sliding motion. A full summary of the results is given in table VIII-3.

The kinetic coefficient of friction is calculated according to

the following equation,

$$\mu_k = \frac{\sin\gamma - 2d/gt^2}{\cos\gamma} \qquad (54)$$

This equation is derived in appendix X.

The kinetic coefficient of friction stabalises at 0,19 , for frequencies from 0,3kHz to 1kHz. Although the vibrator could not drive the sliding surface at a frequency of above 1kHz, it is reasonable to assume that there shall not be a sudden change in the coefficient of friction above that frequency.

5.5. Power draw of the mill

A full range of readings for the current draw of the mill were obtained. As the current fluctuated considerably with the rotation of the mill, a high and low value were noted and the average taken to be a representative current. The full set of readings are given in table VIII-4, for 90° lifter bars of various heights, and at a range of mill speeds.

At a range of current draws the phase lag, between current and voltage, was measured. A detailed list of these measurements is given in table VIII-5.

CHAPTER SIX

ERROR AND REPRODUCIBILITY ANALYSIS

The variations arising from possible inaccuracies in reading figures, tracing rod paths, and variations in experimental procedure, are classed as experimental errors. Variations in results arising from limitations in apparatus, natural vibrations, and other uncontrollable factors, are taken as being inherent to the experiment. Both of these variations are analysed as they jointly contribute to limitations in the accuracy and reproducability of results.

6.1. Filming of the charge motion

Great pains were taken to ensure that the camera was aligned perpendicular to and centrally relative to the face of the mill, so as to avoid distorting the circularity of the image and to minimise the error of parallax between the information board and mill face. Any errors in the projected image that may have arisen from misalignment of the camera were too small to be measured, so are treated as negligible.

Vibrating and shaking of the mill, and slight fluctuations in the speed of the mill appear to give rise to some non-reproducibility of the rod trajectories. This is seen in figure 21, which is a plot of the paths of two different rods in the same run, and thus illustrates the expected reproducibility of rod trajectories. The lifter-bars were machined to within better than 1mm in height and 1^0 in face-angle relative to the specifications, variations within these limits will also contribute to the slight fluctuations in rod trajectories.

6.2. Analysis of films

6.2.1. Location of rod image

The image of the mill was very carefully aligned with the circle

drawn on the graphics tablet, although the dark image of the inner shell made it difficult to set the image size exactly, it could be set to within 1mm around the entire circumference of the mill. With the edge of the mill being set to within 1mm on a 284mm diameter image, a 0,4% uncertainty in the position of the rod images is introduced.

The location of the centre of the rod becomes difficult when the image is overexposed or there is a glare on the glass face of the mill. This problem is especially prevalent with the first batch of three films. In general the major problem is the slightly blurred nature of the images, when viewed from close up. This blurring is also contributed to by the rounded nature of the ends of the rods. It is estimated that the images could be located to within 1mm of their actual positions. When adding the 1mm uncertainty in centering the mill image, a total uncertainty of 2mm is obtained. This translates to a 1mm uncertainty in the final plots that are produced. In figure 21 it can be seen that this error is within the reproducability of the trajectories of the rods. A good indication of the accuracy of the image analysis is seen in figure 20, upon analysing the scatter in the experimental points about the smooth curve that it is expected should join them.

6.2.2. Mill speed

The speed of the clock was checked with a calibrated oscillascope, and found to appear constant over a one minute period. If it is taken that one can judge the location of the needle within 3^0 of its original location, then after 200 revolutions of the clock an accuracy of 2^0 in 360^0x200 ie. 0,003% can be derived. This is negligibly small relative to the other errors.

In checking the speed of the mill, the number of revolutions of the clock corresponding to one revolution of the mill are counted. The image of the needle can be located to within One hundredth of a revolution, at either end of the count. So the

uncertainty is: $\pm\frac{2\times300}{100}$ms = ±6ms

This is over a period of about 1 second, so the uncertainty is ±0,6%. Taking average mill speeds of 54 rpm, 80% of critical, an uncertainty of ±0,3rpm or ±0,5% in critical speed is obtained.

6.3. Lifter-bar vibration

The major peak found, that had a 70μs period, had an amplitude of at least 10 times that of the subsidiary frequencies, so was distinctly the principal frequency of vibration of the accelerometer. To check that this was the frequency of vibration of the lifter-bar and not of the bolt, a degree of magnitude calculation is given below.

We have $v = \nu.\lambda$

where $v \equiv$ velocity of wave propogation

$\nu \equiv$ frequency of the wave

$\lambda \equiv$ wave length

For metal, v is in the range $(3 \rightarrow 6)\times10^{3}m.s^{-1}$, so on average is about $4,5\times10^{3}m.s^{-1}$.

For a lifter-bar 0,3m long, the principal frequency of vibration should be:

$$\nu \simeq \frac{4,5\times10^{3}m.s^{-1}}{0,3m} = 1,5\times10^{4}Hz$$

ie. $\nu \simeq$ 15kHz

For a 6mm screw, the maximum possible wavelenth is 12mm, so:

$$\nu_{max} \simeq \frac{4,5\times10^{3}m.s^{-1}}{0,12m} \simeq 400kHz$$

So the measured frequency of vibration is that expected of the lifter-bar.

The errors in the measurement of the period and derived frequency of 14,3kHz are irrelevant in this work, when considering that the vibrator used to excite the sliding-plane only responded up to 1kHZ.

6.4. Coefficients of friction

6.4.1. Static coefficient

The angle of the sliding-plane could be set to within about one degree, when determining the angle at which the sliding sample just began to slip. So at 13° the error is about ±8%, and at 3° it is about ±30%. So for the range of derived coefficients of friction the uncertainty is approximately constant, at ±0,015 .

Figure 22 and table VIII-2 show that there is a wide variation in the derived coefficient of friction, dependent upon the magnitude of the vibration. However as the frequency increases the width of this band decreases, so is expected to be very narrow at high frequencies. The coefficient of friction is a strongly decreasing function of frequency, as shown by the curve that indicates the general trend in figure 22. As it is neccesary to extrapolate so far out of the measurement range, the assumption of $\mu_s \rightarrow 0$ cannot be properly justified, but is reasonable when one considers that the curve is a monotonically decreasing function.

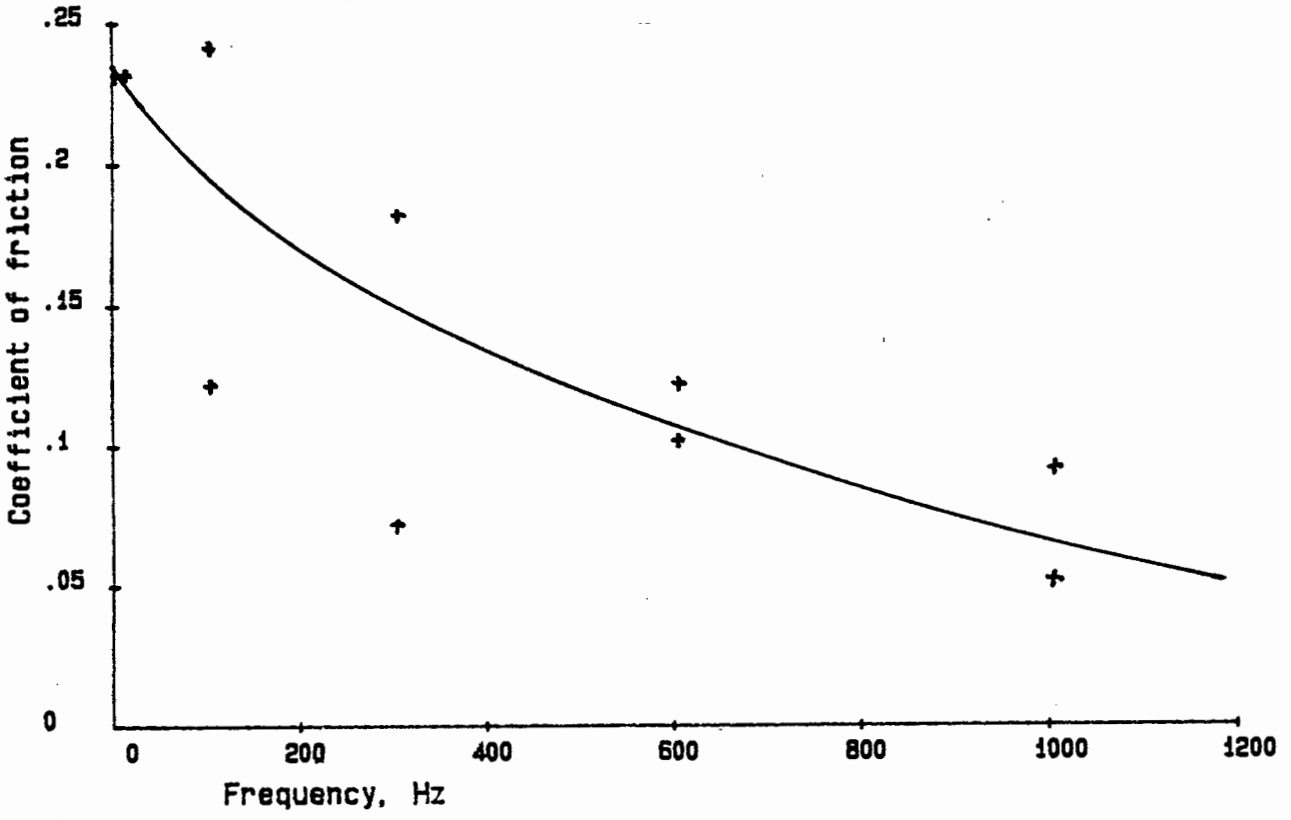

FIGURE 22. Apparent static coefficient of friction

6.4.2. Kinetic coefficient

The accuracy of analysis of the video is within one frame at either end of the sliding period. The total accuracy is within 2 x ½frame = 0,02s. Over an average sliding period of 1,14s, this gives an uncertainty of approximately ±2%. So $\mu_k \equiv 0,19 \pm 0,003$, ie. μ_k is accurate to two decimal places.

Again extensive extrapolation beyond the 1kHz range, to 14kHz is required, due to limitations in the experimental equipment. Although it is assumed that the kinetic coefficient of friction stabalises at 0,19 , it is possible that it may decrease slightly as the frequency is increased to 14kHz. As it is not feasible to extrapolate from the small range of readings, it is considered most reasonable to take μ_k as 0,19 .

If the sliding time, t, decreases by 0,06s (which from an inspection of the figures given in table VIII-3 appears likely), then the error in t is 5,4%. As μ_k is a function of t^2, the error in μ_k is about 11%. So it is estimated that μ_k has a high probability of being in the range 0,19 to 0,17. It is possible that the sliding time could decrease by as much as 0,3s, if the slope of the curve fitted to the times does not flatten out substantially, in which case μ_k could be as low as 0,10 . This is considered to be the lowest possible value of μ_k.

6.4.3. Effect of varying the coefficients of friction

As μ_s and μ_k are central to the theory it is informative to illustrate the influence of the uncertainty in these quantities on the theoretically predicted rod trajectories. Figure 23 shows the influence on the trajectories, of varying the static coefficient of friction from 0 to 0,05.

The change in the trajectory of rods with 90° lifter-bars is negligible. With 60° lifter-bars in the mill, the change in trajectory is slightly greater, but well within the experimental uncertainties. The experimental evidence indicating that the static coefficient of friction is approximately zero is sufficiently strong, and the variation in trajectories with μ_s is

sufficiently small, to consider any error arising out of the uncertainty in the static coefficient of friction as negligibly small in this analysis.

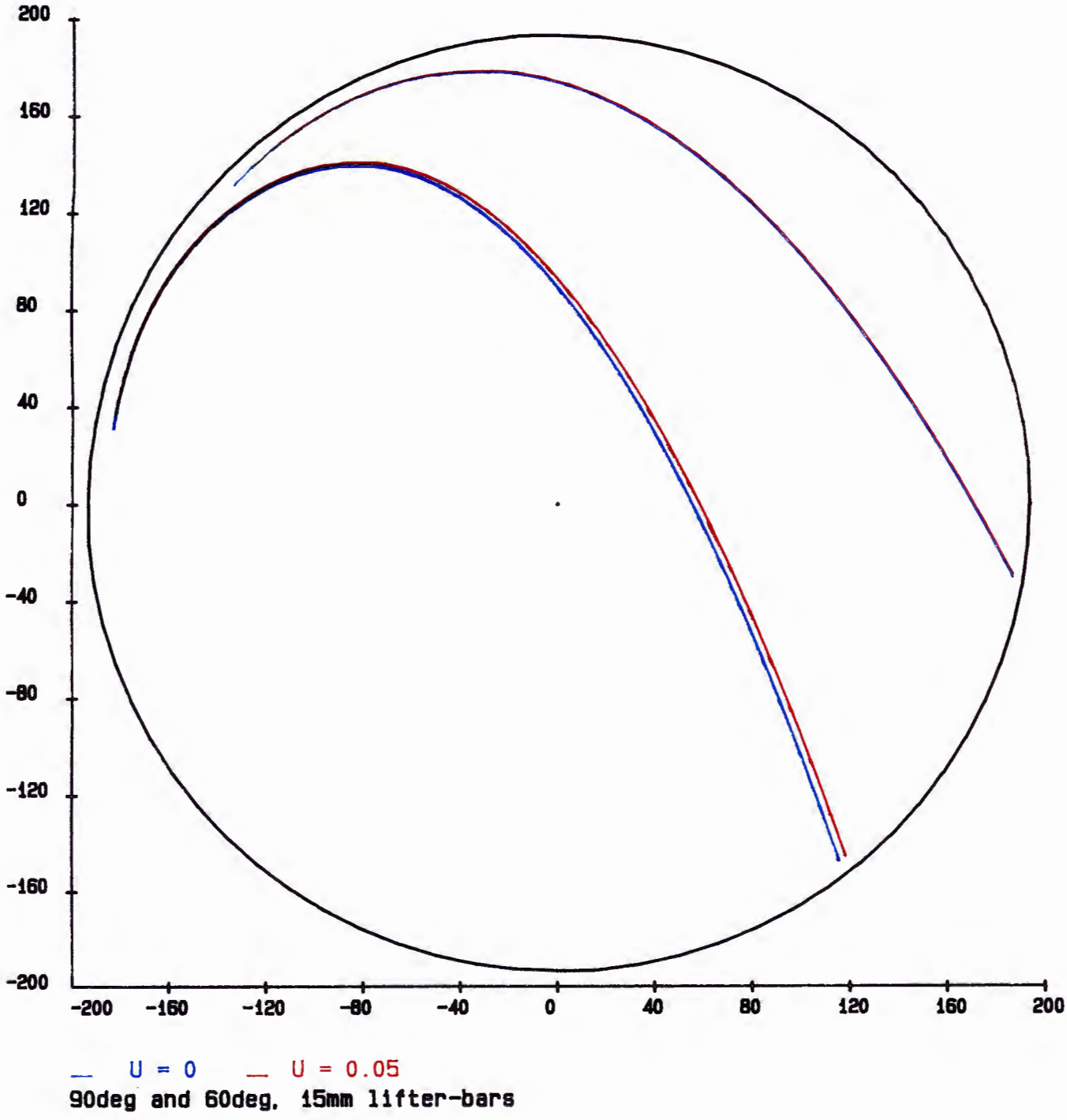

FIGURE 23. Influence upon the rod trajectory of varying μ_s

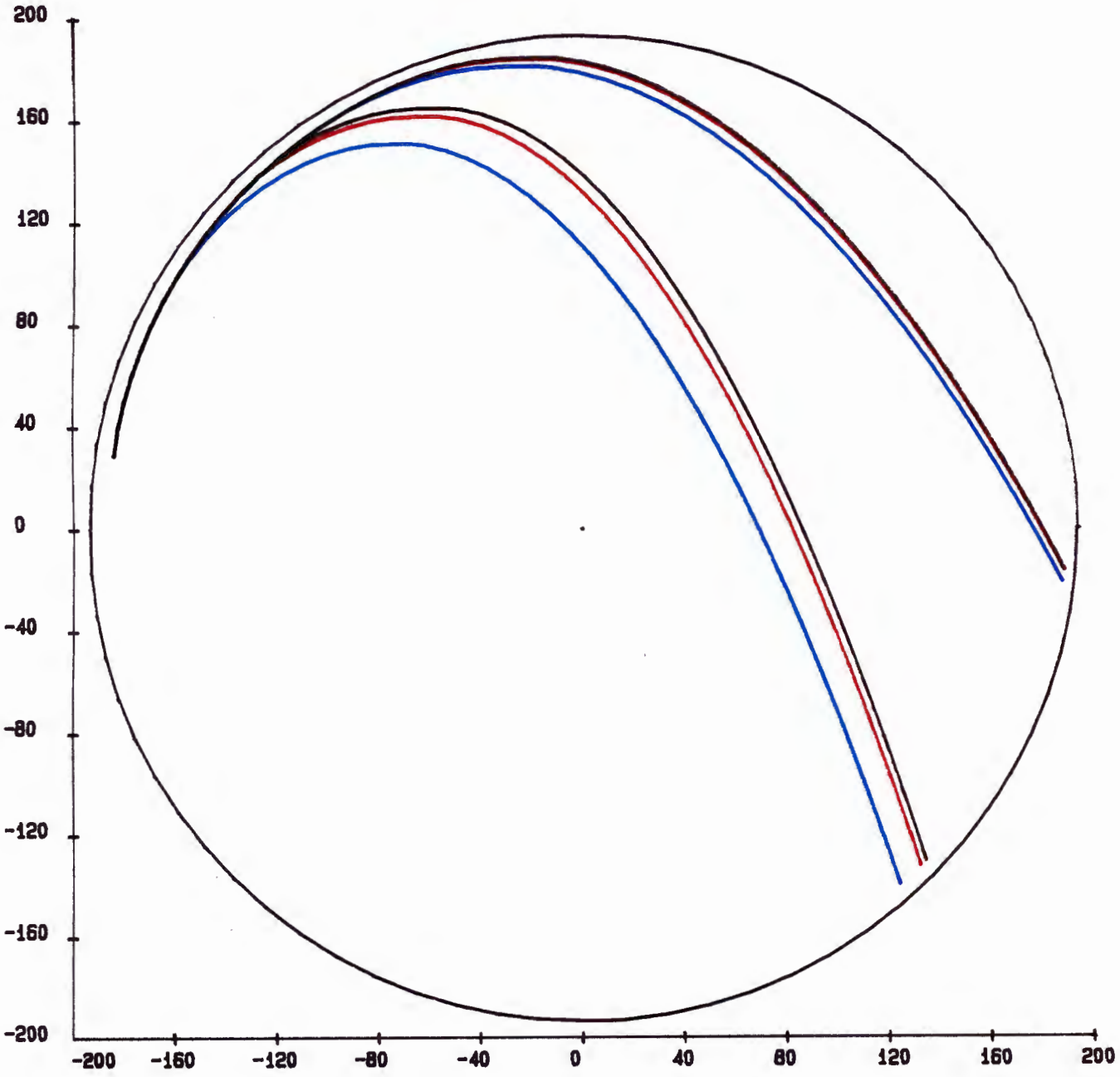

FIGURE 24. Influence upon the rod trajectories of reducing μ_k

Figure 24 illustrates the effect of reducing the kinetic coefficient of friction, upon the resultant rod trajectories. With 90° lifter-bars the influence upon the trajectories of reducing μ_k from 0,19 to 0,17 is almost indescernable. Even reducing it to 0,10 has only a small effect. However with 60°

lifter-bars the change in rod trajectories is significant, even with a 0,02 reduction in μ_k. Reducing μ_k to 0,10 has a large influence upon the predicted rod trajectories.
In summary these plots indicate that the uncertainties in the coefficients of friction will have little effect upon the predicted trajectories for perpendicular lifter-bars, but could introduce a significant error in the predicted trajectories for sloping-faced lifter-bars.

6.5. Power draw of the mill

The current draw could be read to within 0,01 Amps, however the current drawn by the mill fluctuated by around 0,1 Amps, which is a real effect noted in production mills. The error in current measurement therefore arises from taking the average of the highest and lowest observed readings. So it is estimated that this error is half the average fluctuation, ie. ±0,5 Amps. The measured range is around 5 Amps, yielding an uncertainty of ±1%. ≈10%

In determining the phase-lag, the phase differences could be measured to within about 0,1ms. Taken over the average phase difference of 3,5ms, this yields an error of about ±3%. Considering the phase-lag graph, given in figure 25, the horizontal error bars are given as the minimum and maximum readings taken for a particular current reading. The vertical error bars are given by 3% of the average figure of 0,4 , which is approximately 0,01. The fit of a straight line to this data yields a coefficient of correlation of 0,992 , which indicates a reasonable fit. This line falls outside the area of uncertainty for only one of the readings, thus corroborating the validity of the fit.

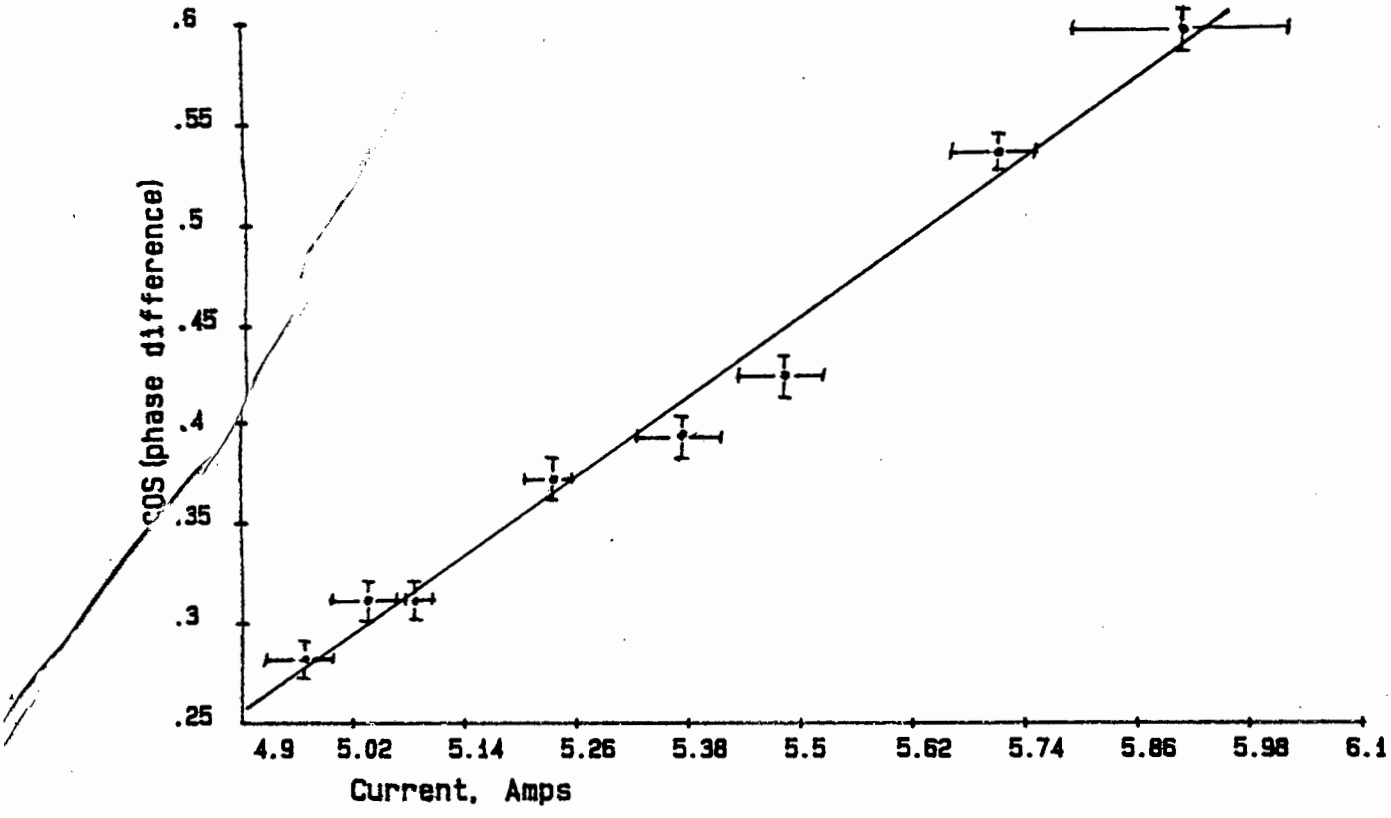

FIGURE 25. Phase-lag between current and voltage

Now as the power is proportional to aI^3+bI^2 (equation 58, section 7.4.), and the error in current measurement is about 1%, and the error in the constant a is about 3%, the total uncertainty in the power figures is 3% + 3x1% = 6%. This accuracy is sufficient to facilitate a qualitative discussion of the derived power draw curves.

CHAPTER SEVEN

DISCUSSION

During the course of the discussion particular points in the trajectories of the rods shall be repeatedly referred to, so these are illustrated in figure 26.

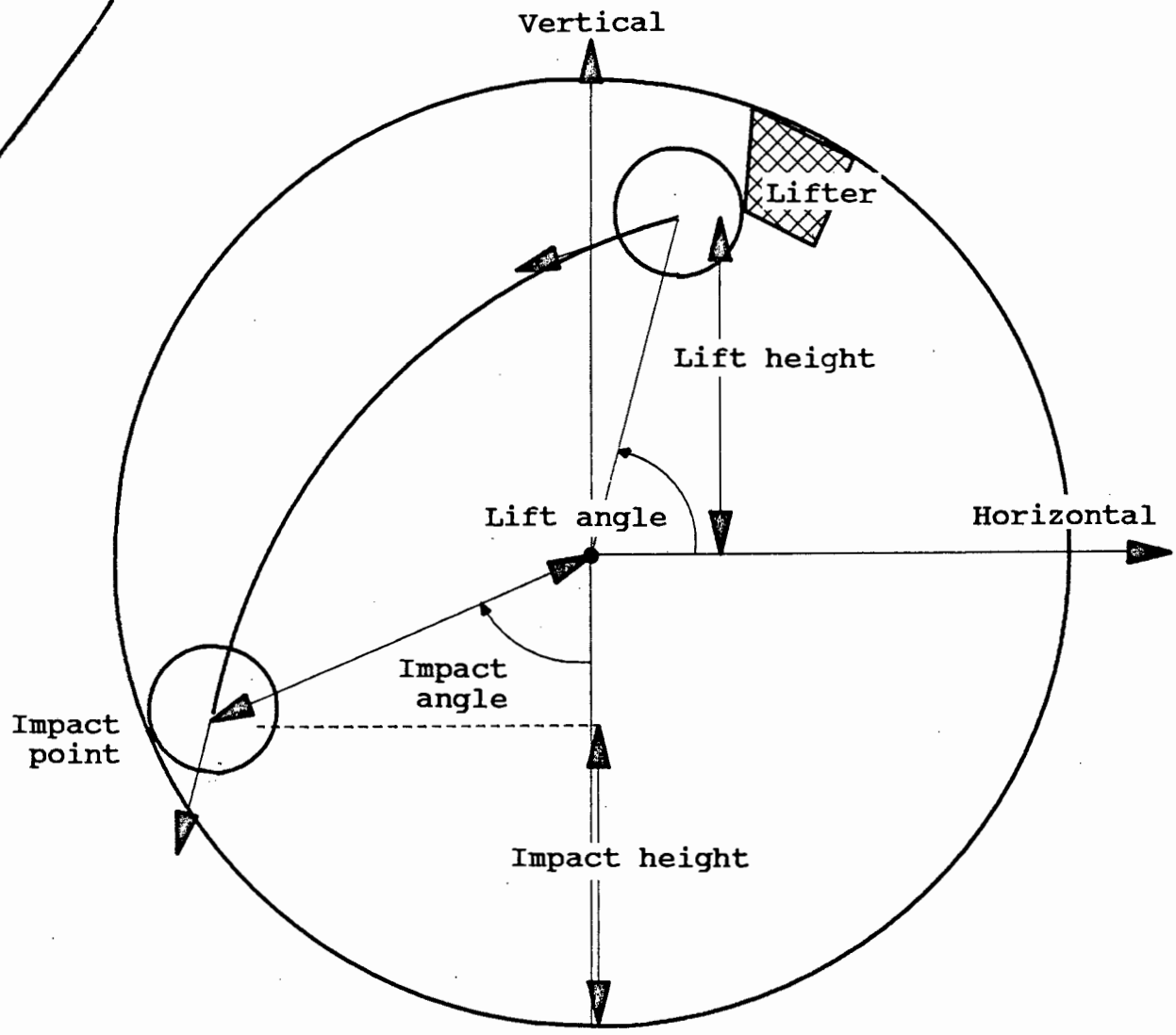

FIGURE 26. The lift and impact point of a rod

7.1. Charge motion

The range of experimental conditions studied provides a good background from which general conclusions on the influence of lifter-bar height, lifter-bar face-angle, and mill speed upon the charge motion can be drawn. In this study the motion of the outer layer of charge is concentrated upon, as this defines the outermost envelope within which the bulk of the charge motion takes place, and this is the section of charge most strongly influenced by the liner configuration.

Figure 27 is a plot of the motion of three consecutive layers of charge at the base of the mill, having a smooth lining and a 45 per cent filling. The outer line is the trace of a reference point on the edge of the mill shell. This figure illustrates the extensive slip that takes place against a smooth shell. While the shell rotates through an angle of 113,5°, layer 1 only rotates through 91,5°, and layers 2 and 3 through 77°. Therefore Layer 1 experiences a 20% slip relative to the mill shell, and layer 2 experiences a 16% slip relative to layer 1, while layer 3 experiences no slip relative to layer 2. This demonstrates the importance of the keying-in action of the lifter-bars on the bulk of the charge. One can consider that there is a 20% loss, due to the slip of the outer layer, in the useful lifting work carried out by the mill. The degree of slip would undoubtedly be reduced for a production mill with a high charge pressure, and with an ore slurry assisting the charge to key into the motion of the mill. The importance of the charge pressure in keying the charge into the rotary motion of the mill was clearly shown by the fact that there was too much slip for any tumbling of the charge to occur, when only a 15% mill filling was used (Table VIII-1, Batch 1, runs 3 and 4). The importance of the charge pressure in keying-in the charge is studied in detail in work by Vermeulen[8].

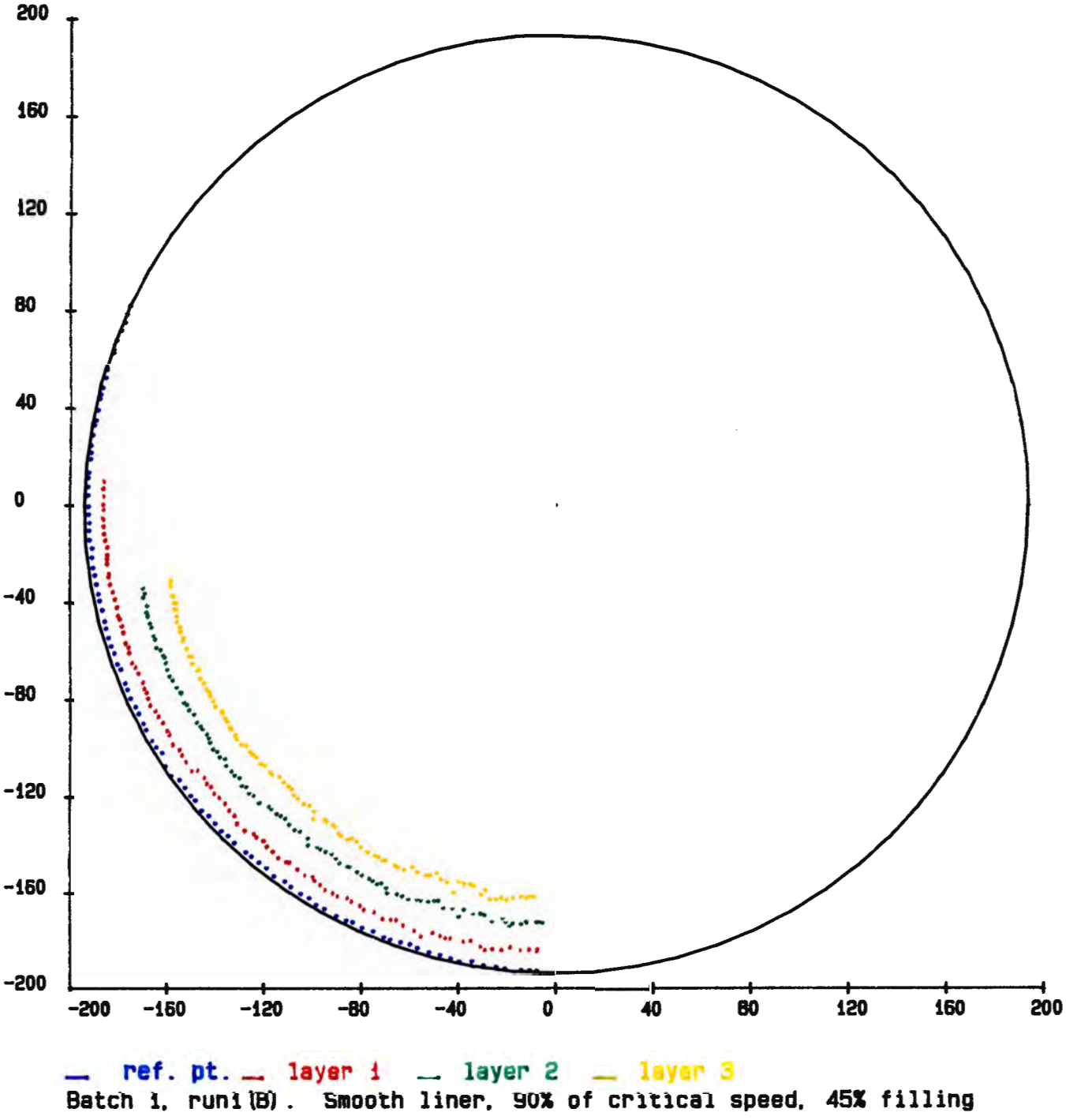

FIGURE 27. Slip of the charge in a smooth-lined mill

The lift and projection of four consecutive layers of charge in a smooth-lined mill, are illustrated in figure 28. Even at 90% of the critical speed the rods are barely projected into flight. They follow short parabolic trajectories and drop back onto the bulk of the charge near the shoulder.

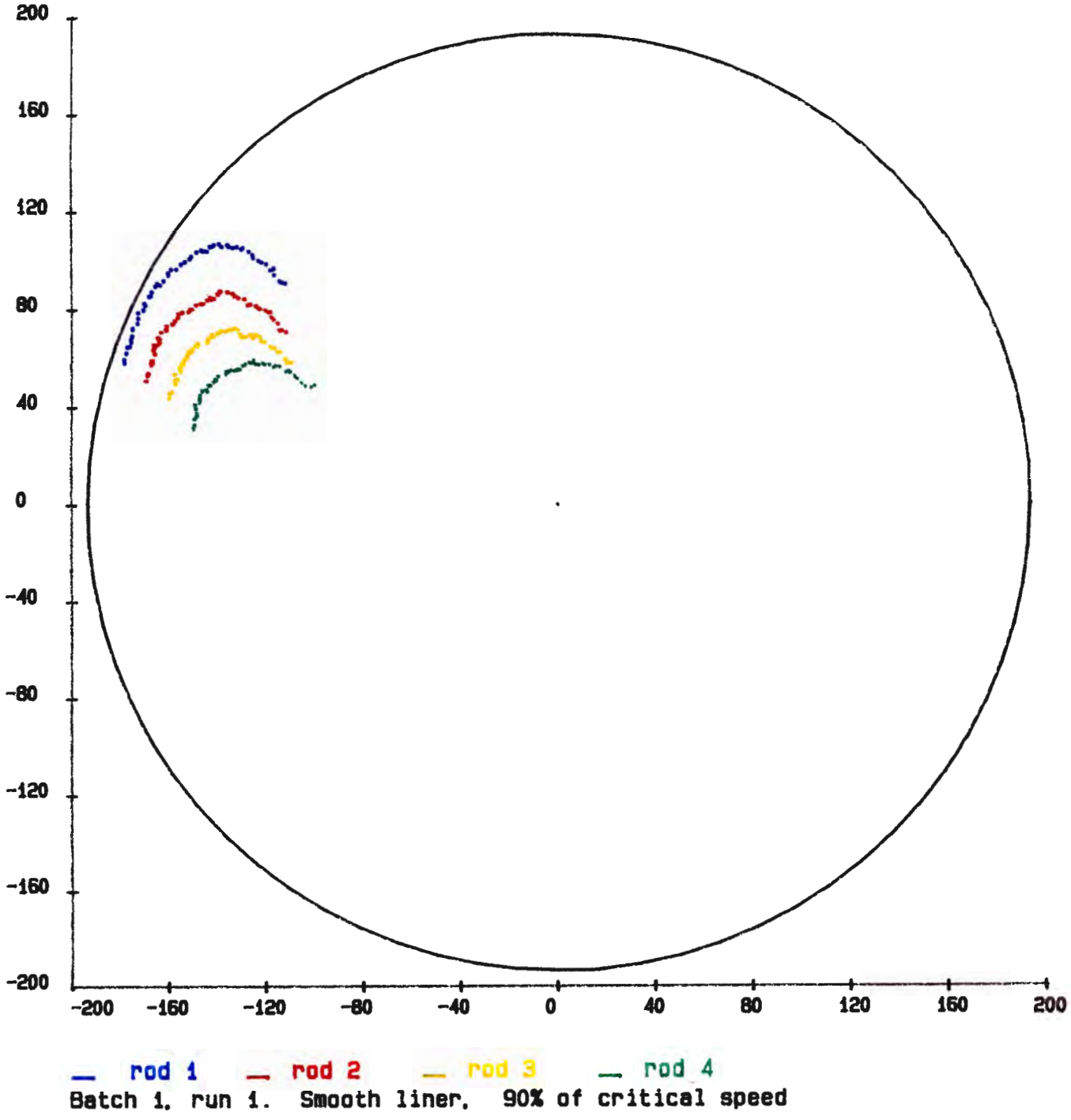

FIGURE 28. The lift of rods in a smooth-lined mill

The fluctuating nature of the charge motion in a smooth-lined mill is demonstrated by the higher parabolic trajectory at a lower critical speed, of 75%, in figure 29. This is brought about by the alternate surging and slipping phases of the bulk charge. This phenomena is discussed in detail by Vermeulen[8].

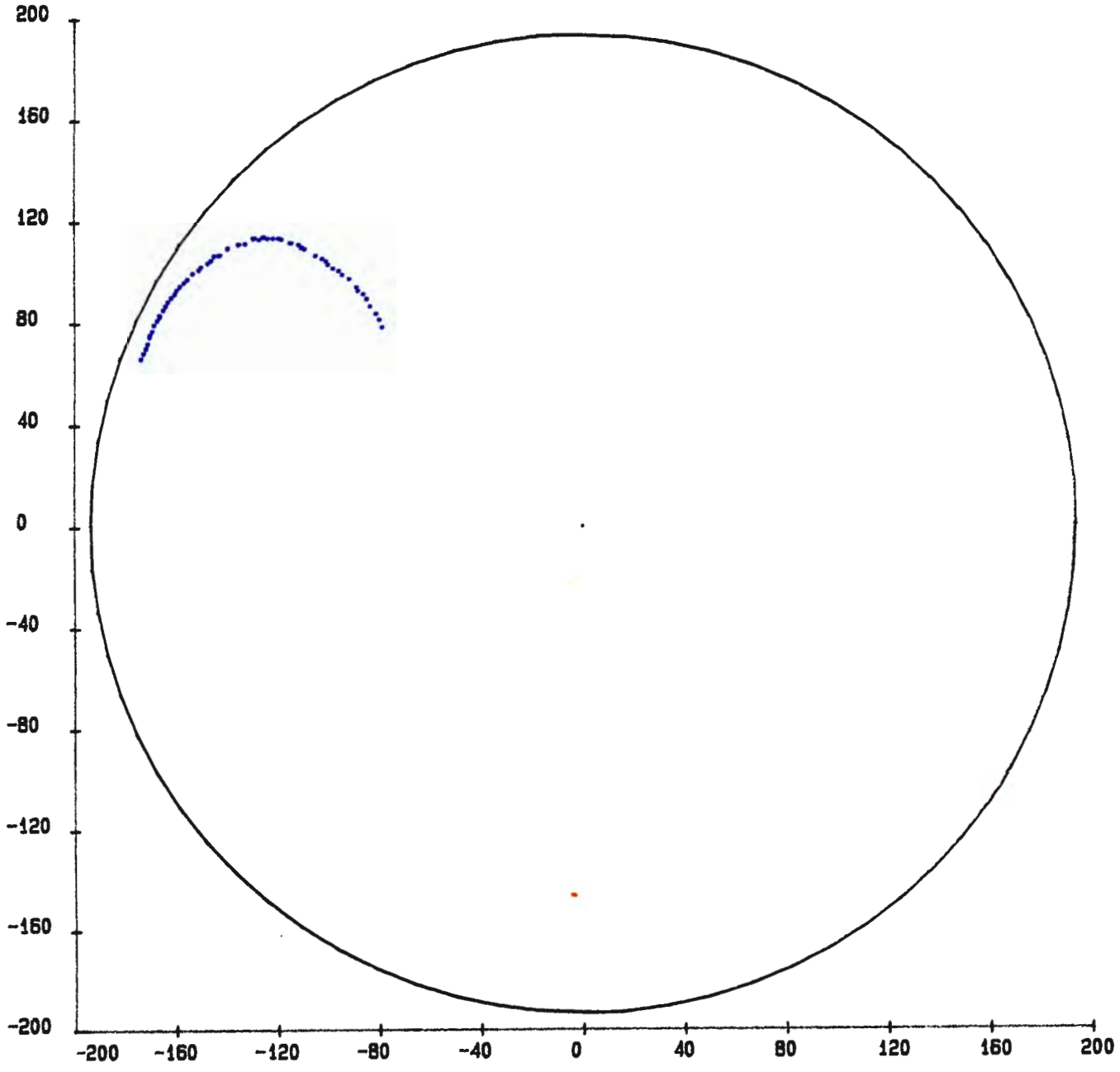

FIGURE 29. The lift of a rod in a slow-speed smooth-lined mill

Figure 30 illustrates the motion of four stacked rods, the formation of which is illustrated in figure 16. Note here however that the numbering of the rods is different, as the lifter-bar is not included the number of each rod is decreased by one. It can be seen that the rod resting against the lifter-bar is lifted and projected far further than the other three rods, each of which rested upon another rod.

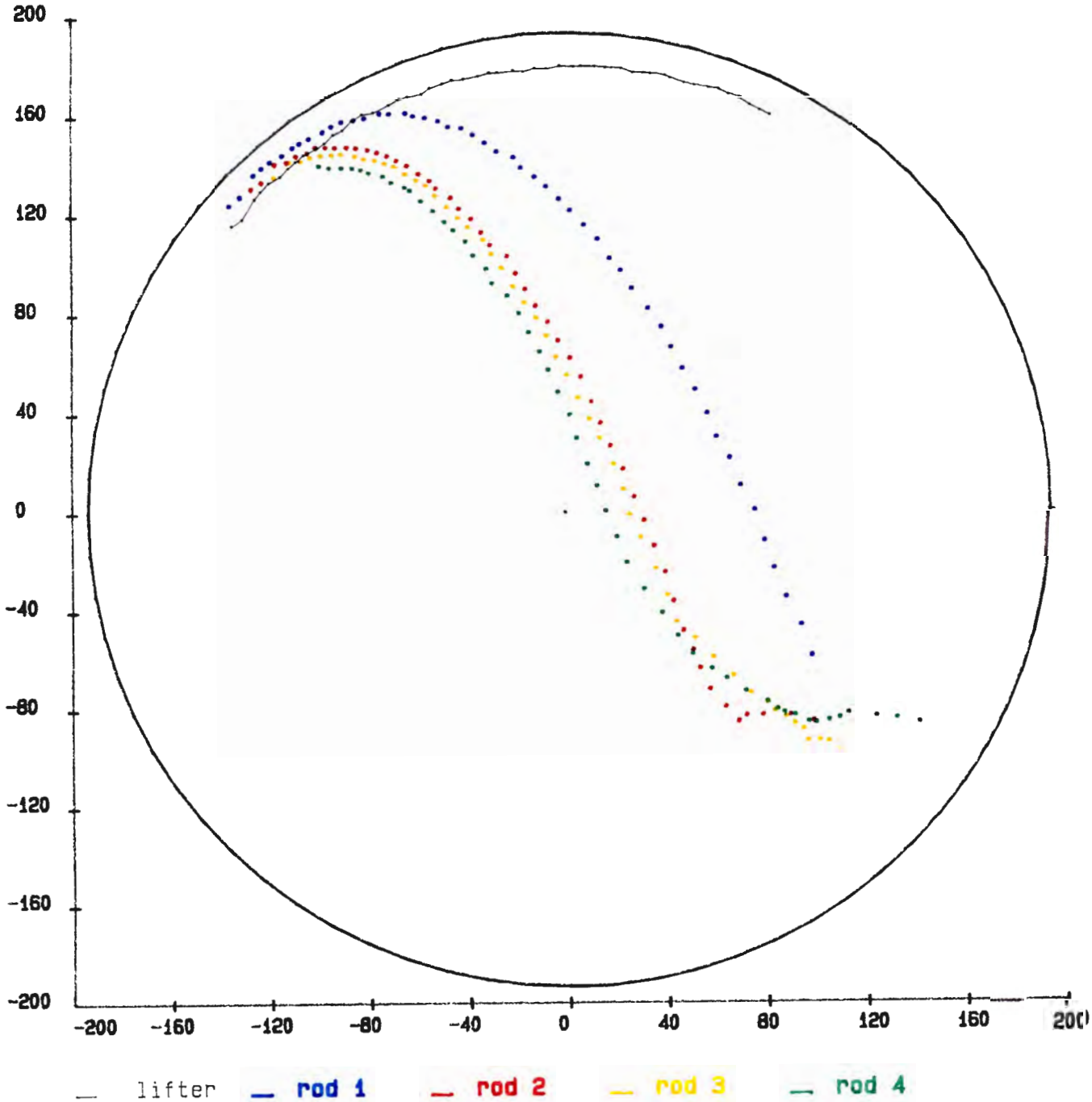

FIGURE 30. The effective lifting action of a lifter-bar

The rods are projected to well within the toe of the charge at this low speed, even with these substantial lifter-bars. This plot also shows that the second rod is clear of the lifter-bar before the first rod slides down the face of the lifter-bar.

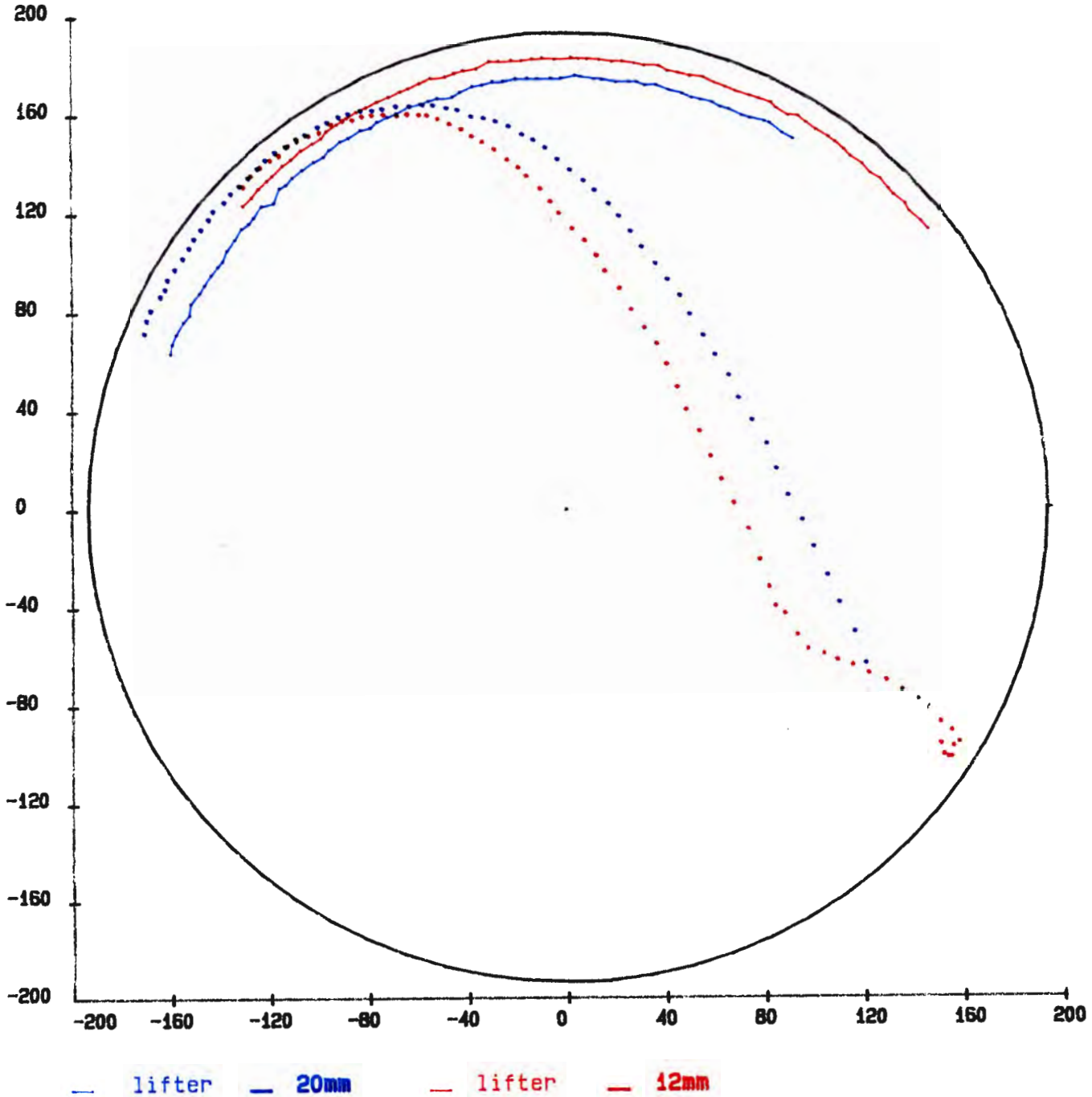

FIGURE 31. Rod trajectories for alternate rows of 20 and 12mm lifter-bars

The difference in rod trajectories for different height lifter-bars is shown in figure 31, which is a plot from the run in which alternate rows of 12 and 20mm lifter-bars were installed in the mill. The trajectories are not substantially different, despite the one lifter-bar being considerably higher than the other.

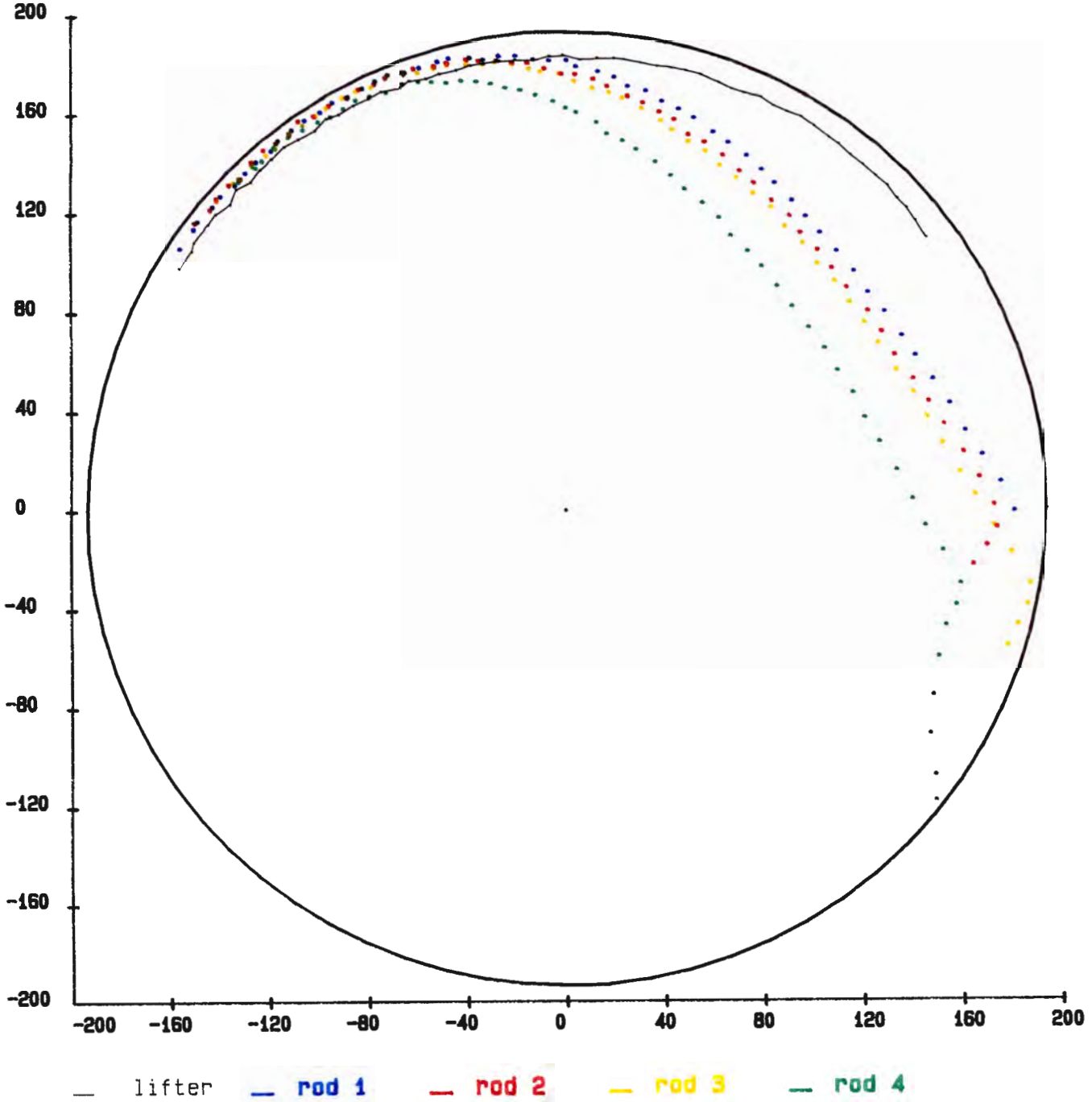

FIGURE 32. The rod interaction at 80% of critical speed

The influence of mill speed is clearly illustrated by a comparison of figures 30 and 32, in which the mill speed is

increased from 60% to 80% of the critical speed. In the faster mill the outer charge is projected to about the horizontal line, above the toe of the charge. In addition the trajectories of rods 2 and 3 are far closer to that of rod 1, while the outermost rod 4 has a noticeably lower lift than the other three. This implies that the outermost rod was supporting the adjacent rod it was resting upon, which was subsequently projected further than expected. With the slower speed mill this does not appear to be the case.

The motion of the outer layer of charge in a mill running at 100% of the critical speed is plotted in figure 33. It can be seen that the three rods that don't rest on the lifter-bar definitely drop away from the shell of the mill. Rod 1 remains in contact with the mill shell but accelerates down it, away from the face of the lifter-bar. So even with this substantial lifter-bar the charge does not truely centrifuge at 100% of the critical speed.

As noted in batch 2 of table VIII-1, only the outer or fully keyed-in layers of charge centrifuged at 100% of the critical speed. It should be pointed out that the percentage of critical speed is calculated for the inner surface of the mill shell. Now the percentage of critical speed is proportional to the square root of the radius of rotation:

$$\% \text{ critical speed} = \frac{\text{rpm}.\sqrt{r}.100}{29,9} \qquad (55)$$

Thus as the distance of the centre of the rod from the centre of the mill decreases, so its percentage of critical speed decreases for a fixed rate of rotation, ie. speed in rpm is constant. Therefore when the mill is rotating at 100% of the critical speed, even the outer layer of charge does not quite centrifuge as the radius of its path of rotation is one rod radii less than the mill radius. Because of the larger effective radius of rotation of smaller grinding elements, when held against the mill shell, it is evident that they will centrifuge at slightly lower mill rotation speeds than larger elements. This points out the interesting possibility that at mill speeds close to 100%

critical, the smaller particles will have a greater tendency to centrifuge than the large ones, and will thus tend to migrate to the periphery of the mill. This has infact been found to be the case, as discussed in work by Nityanand *et al.*[22].

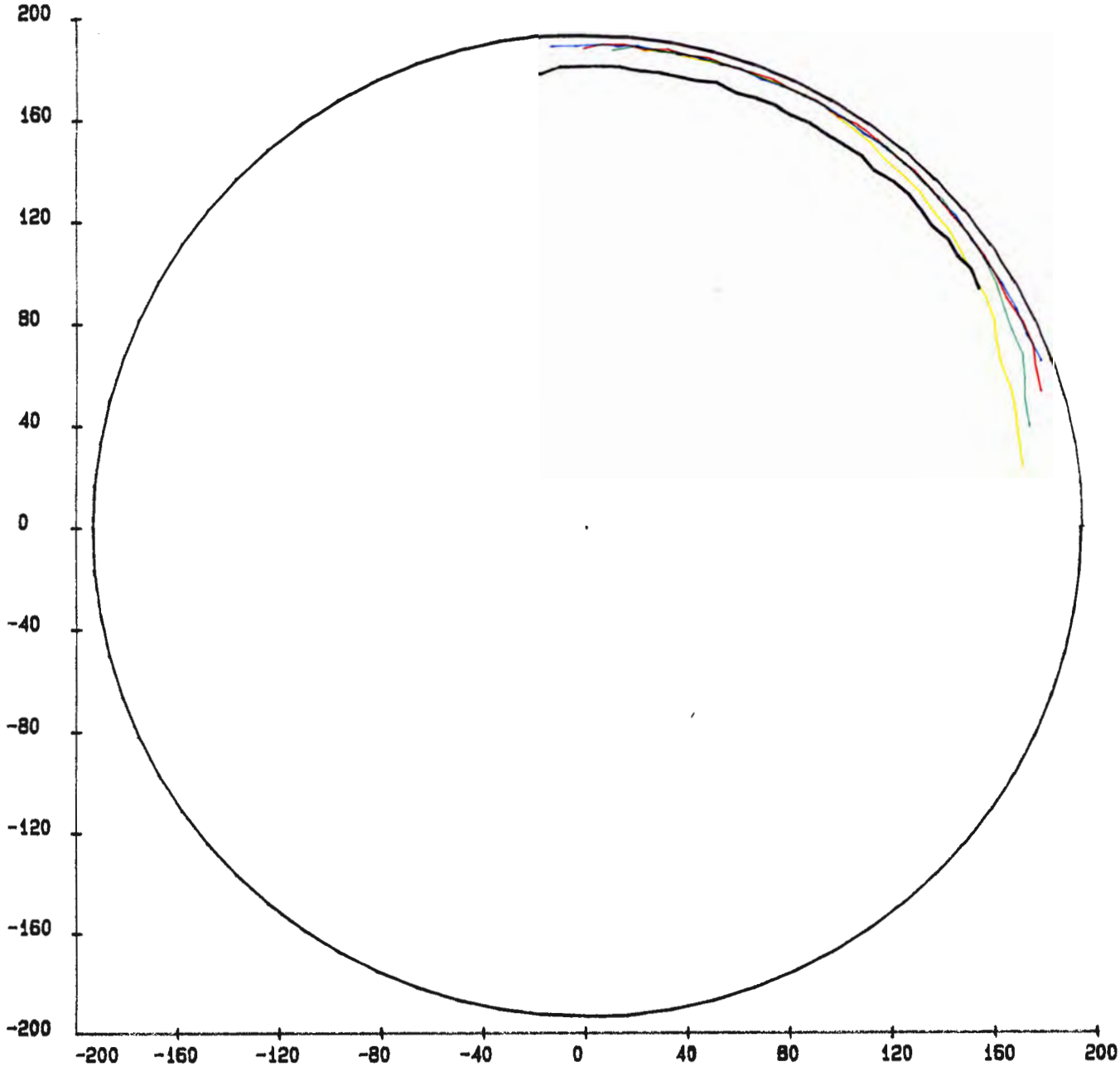

FIGURE 33. Acceleration of the outer rods at 100% of the critical mill speed.

Further illustrations highlighting the effects of changing mill speed upon the motion of the rods are given in figures I-4 to I-6 A composite plot of the rod motion from five different runs is illustrated in figure 34, the rod resting against the lifter-bar is used throughout. The effect of changing the mill speed, for all other conditions remaining constant, can easily be seen. It is clear that the increasing speed has a substantial effect on

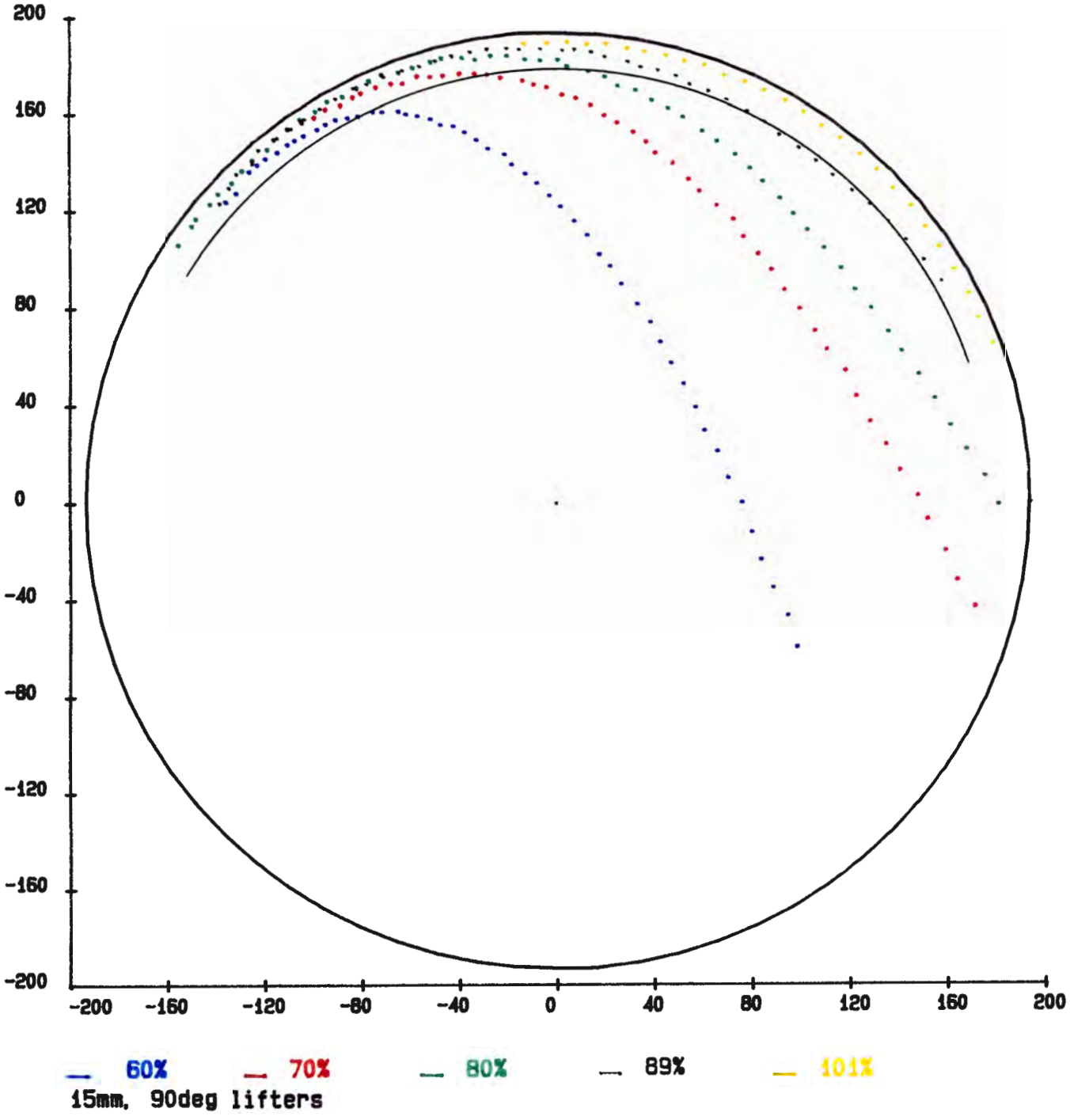

FIGURE 34. Influence of mill speed upon charge trajectories

the lift and impact point of the outer charge. The degree of lift can be ascertained by noting where the rods cross over the solid black line that traces the tip of the lifter-bar.

Figure 35 is a further composite plot, in which the height of the lifter-bars are varied.

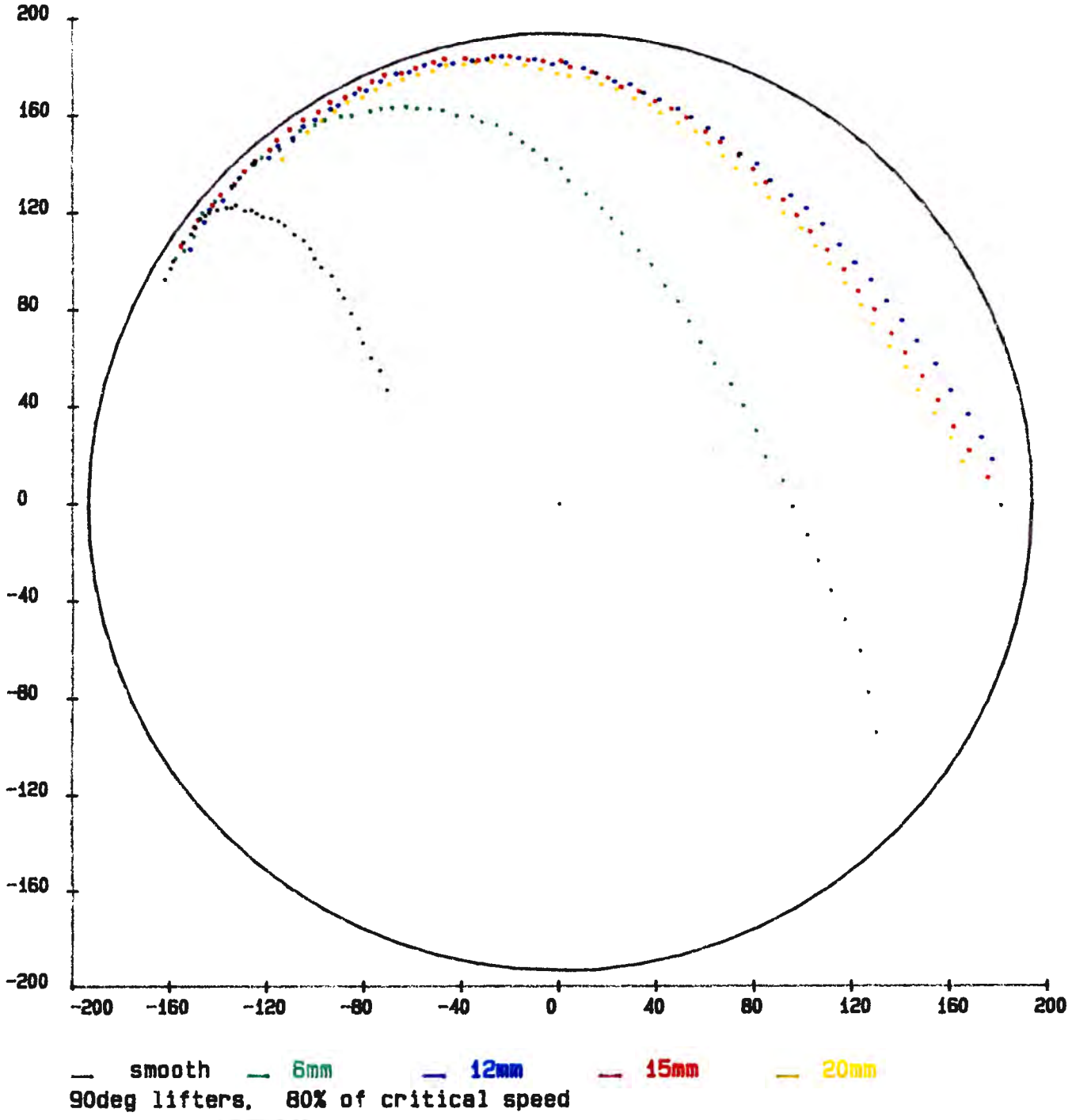

FIGURE 35. Influence of lifter-bar height upon charge trajectories

dramatic increase in both the lift and impact point as the height of the lifter-bar increases from 0 up to a rod radius of 6mm. Both these factors display a similar increase up to the 12mm high lifter-bar, but it is shown later that this further increase takes place principally in the range of lifter heights just greater than the radius of a rod. Secondly, from a lifter height of 12mm up to 20mm there is a decrease in the impact angle. This is contrary to normal expectations, and a factor of great practical importance, that is hitherto unreported. It is discussed in detail at a later stage.

Because of the problem of rods slipping off the sloping lifter-bars in clusters, it was difficult to locate isolated rods moving down the face of the lifter-bars. Figure 36 shows some of the few such plots that were obtained. This composite plot shows the large effect that the face-angle of the lifter-bars has upon the trajectory of the charge.

This effect of the rods acting as a group can be seen in figure 37. In this instance the rods resting against the lifter-bar are pushed to the tip of the bar, by the rods that are resting against them, and are projected off the bar prior to the other rods. This arises because the rod resting upon another rod has a higher angle of departure, than one resting against the sloping face of the lifter-bar. The low resultant trajectories of the outer layer of rods show that a sloping face can be utilised to suppress the lifting and projecting actions of the lifter-bar. This is of particular practical importance in high-speed mills.

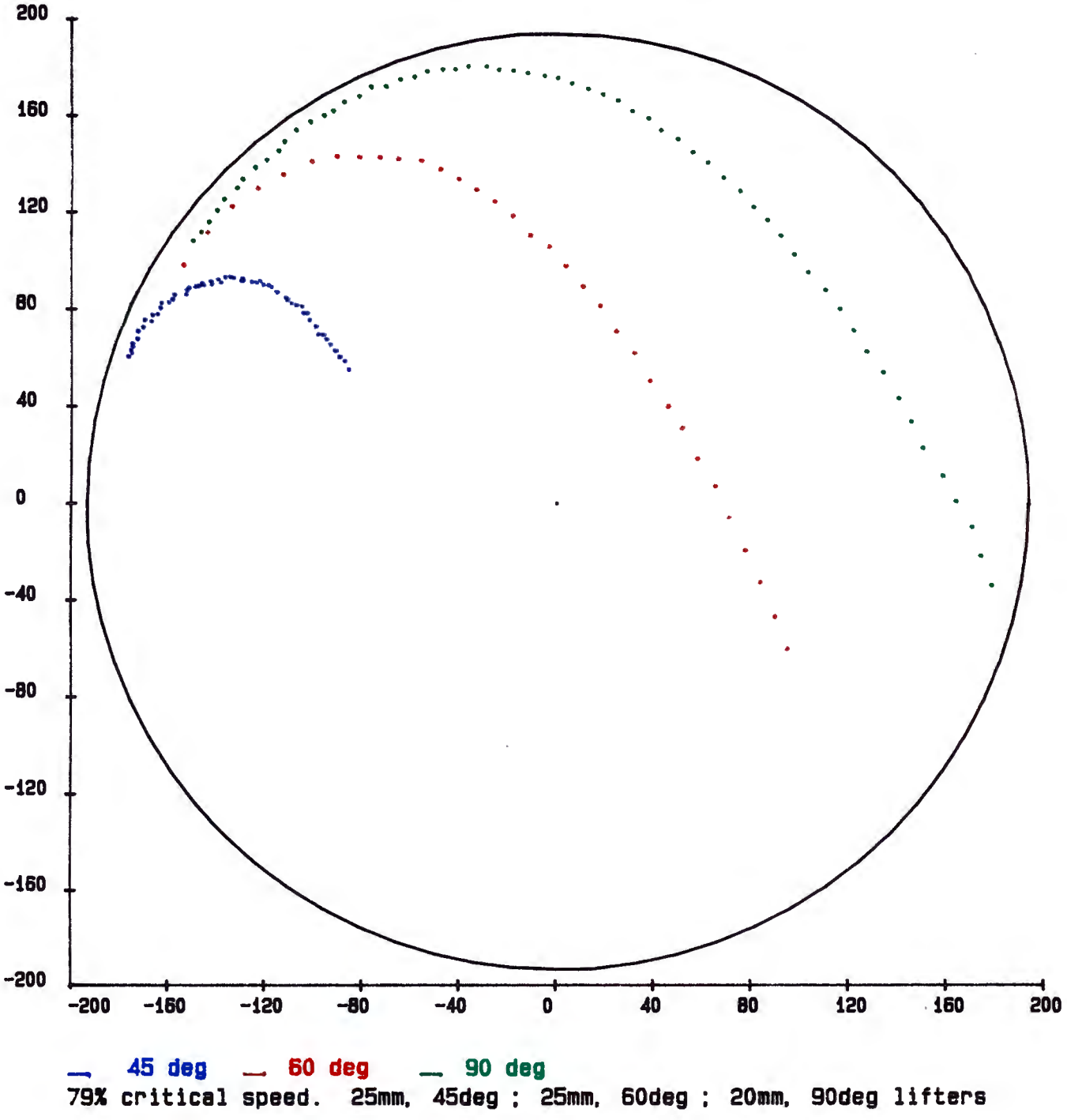

FIGURE 36. Influence of lifter-bar face-angle upon charge trajectories

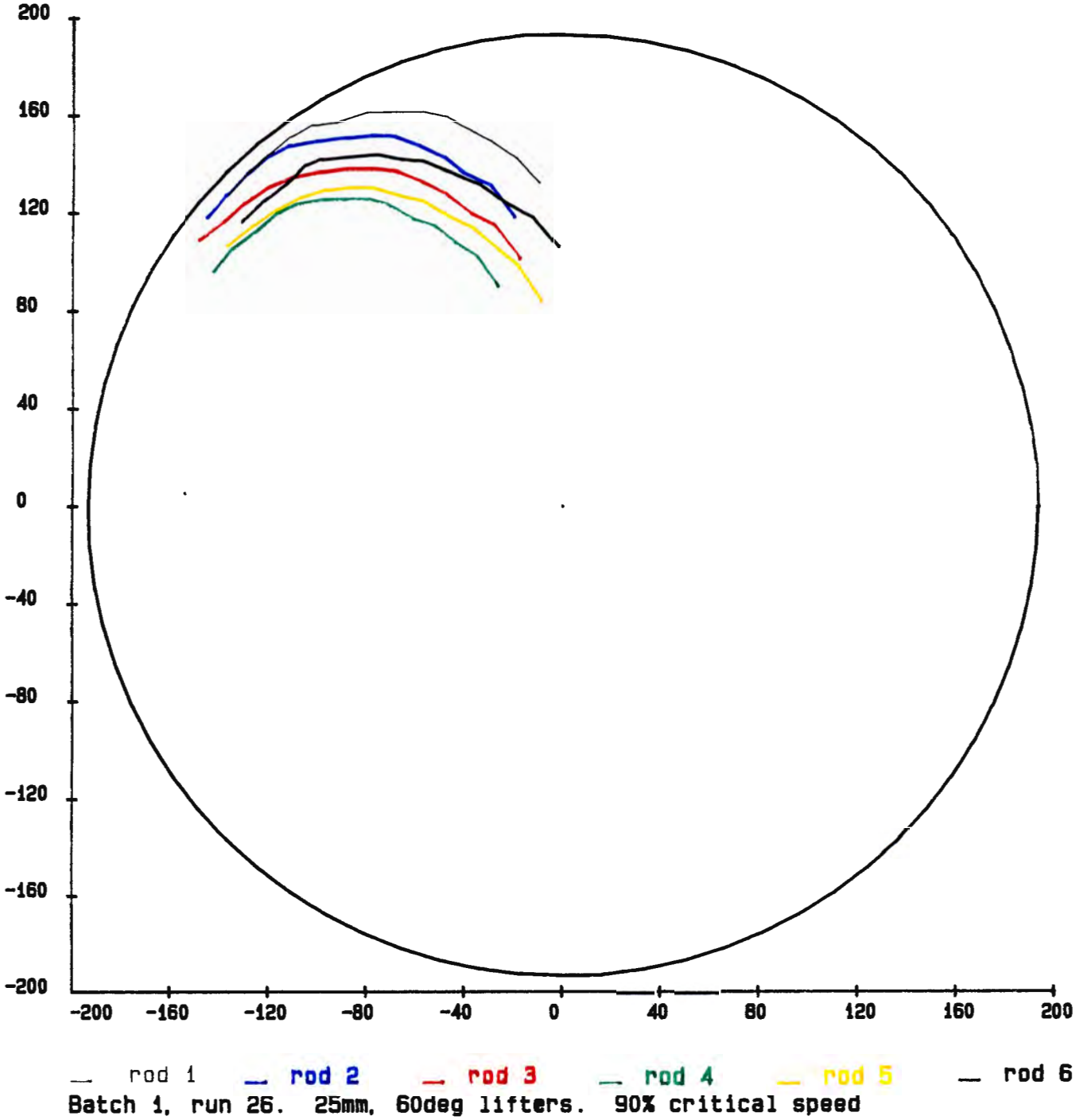

FIGURE 37. Group interaction of rods on a sloping-faced lifter-bar

7.2. Comparison of the theory with experimental results

Using the rod motion calculation method given in appendix VI, a computer programme was written to enable the rapid calculation of rod trajectories under varying conditions. As this programme was central to the comparison of theoretically predicted and experimentally derived results, it is listed in appendix XI. A full calculation was carried out by hand to check that the programme was computing correctly.

In comparing the theory with the experimental results, the following experimentally determined factors were used:

Radius of mill, $R \equiv 193{,}5mm$

Radius of rod, $a \equiv 6mm$

Width of lifter-bar, $2y \equiv 25mm$

Static coefficient of friction, $\mu_s \equiv 0$

Kinetic coefficient of friction, $\mu_k \equiv 0{,}19$

The following factors varied in the experiments; lifter-bar face angle, ρ; lifter-bar height, h'; mill speed, in revolutions per minute(rpm) or percentage of critical speed.

From the calculation method it can be seen that there are no adjustable variables, all variables are either experimentally determined, or fixed by given experimental conditions. Therefore the theory cannot be adjusted to fit the results.

It was considered that the best method of comparison is to plot predicted and experimentally determined rod trajectories together. Figure 38 shows a theoretical plot with two experimental plots of different rods in the same run. This indicates that although a theoretical line may not fully coincide with an experimental trajectory, they can correspond within the range of experimental uncertainty.

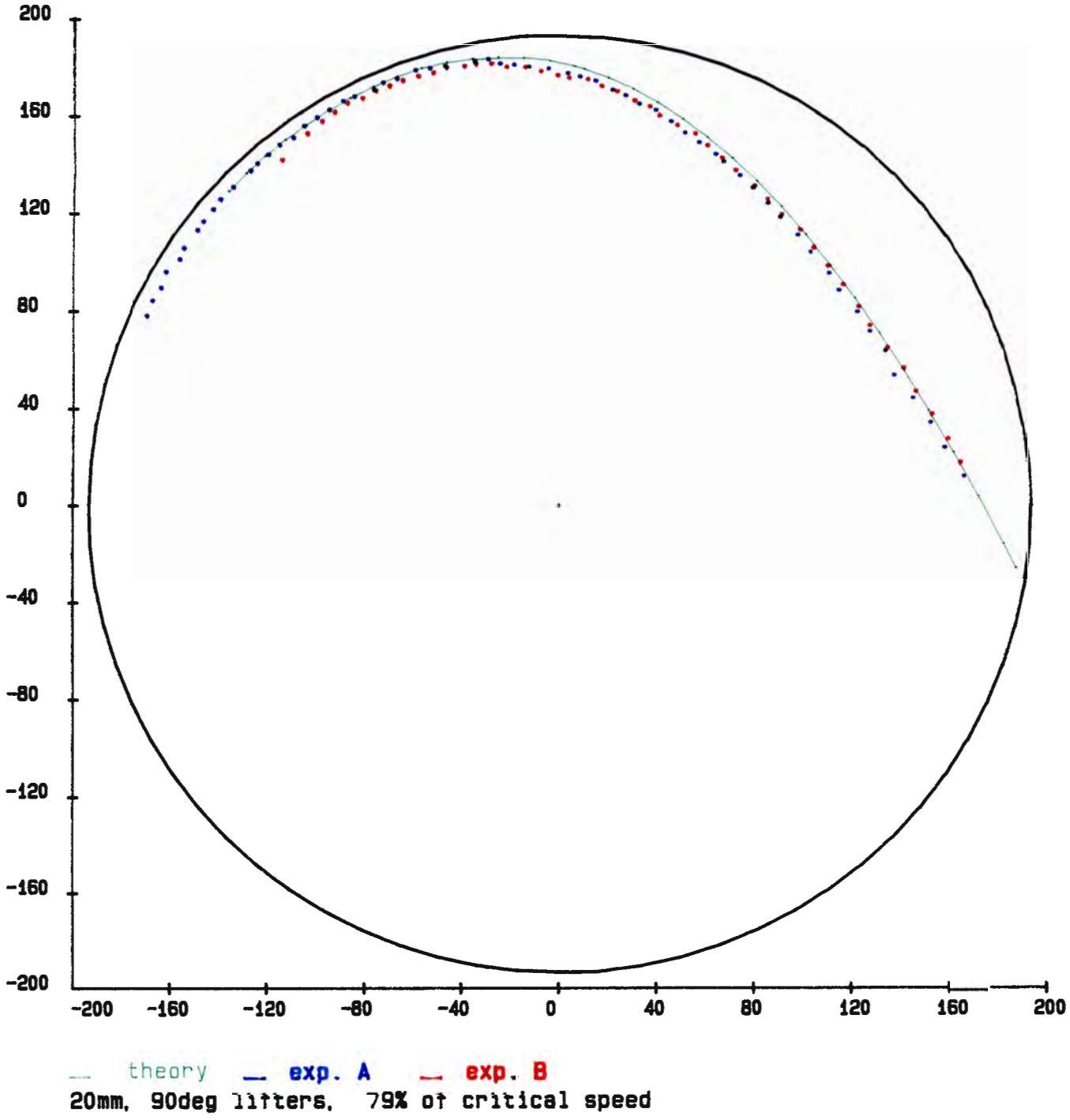

FIGURE 38. A theoretical plot falling within the range of uncertainty of experimental plots

To illustrate the range of applicability of the theory, a plot of the theoretical and experimental trajectories over a wide range of speeds is given in figure 39. On the whole the correlation is excellent. The plot at 60,6% critical speed can be considered to be within the experimental uncertainties.

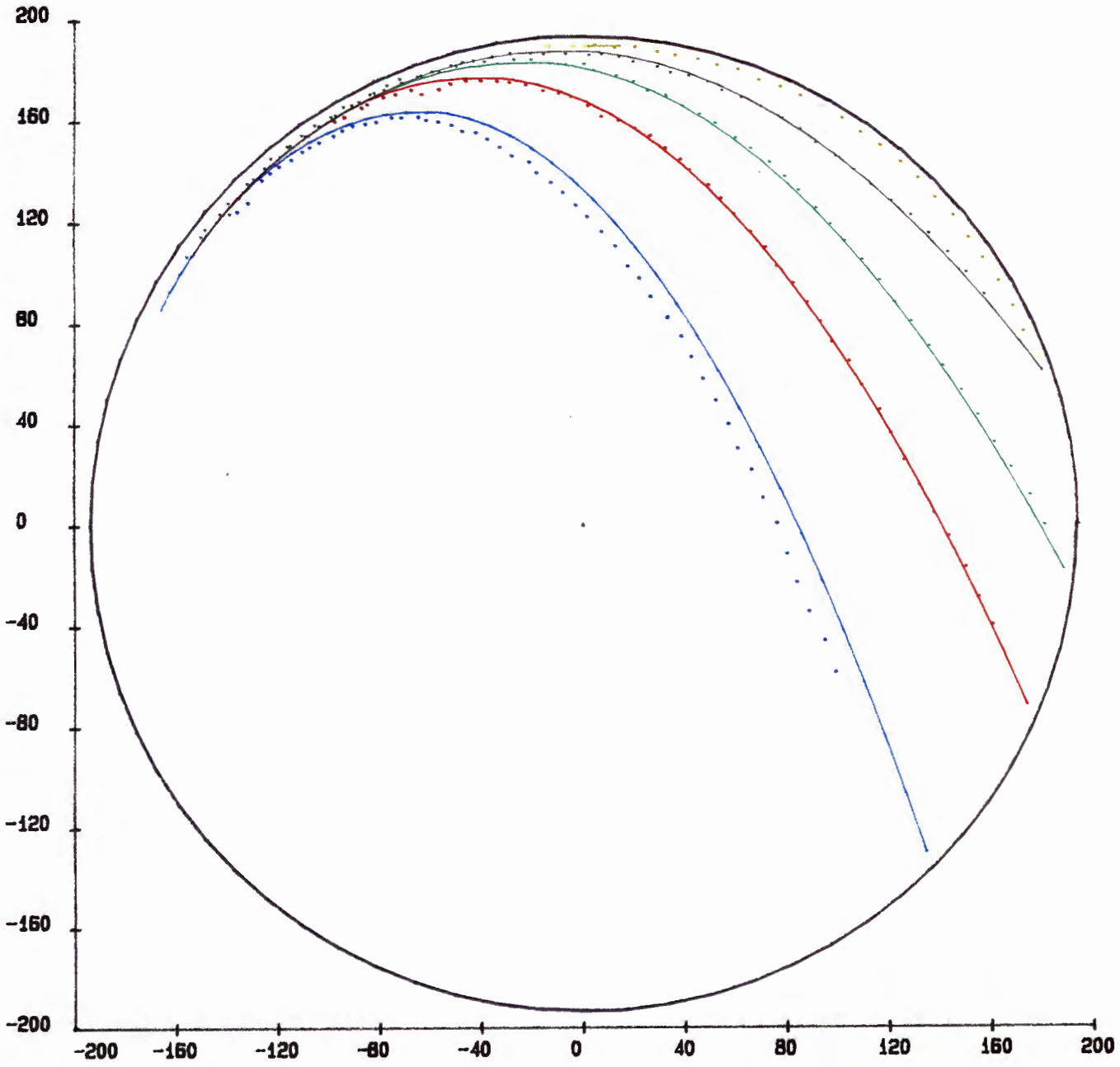

FIGURE 39. Comparison of theoretical and experimental plots over a wide range of speeds

A further comparative plot is given of the range of trajectories resulting from increasing the height of the lifter-bars. The theory predicts the same surprising result as the experimental work, that the higher lifter-bars do not project the rods as high as the lower lifter-bars.

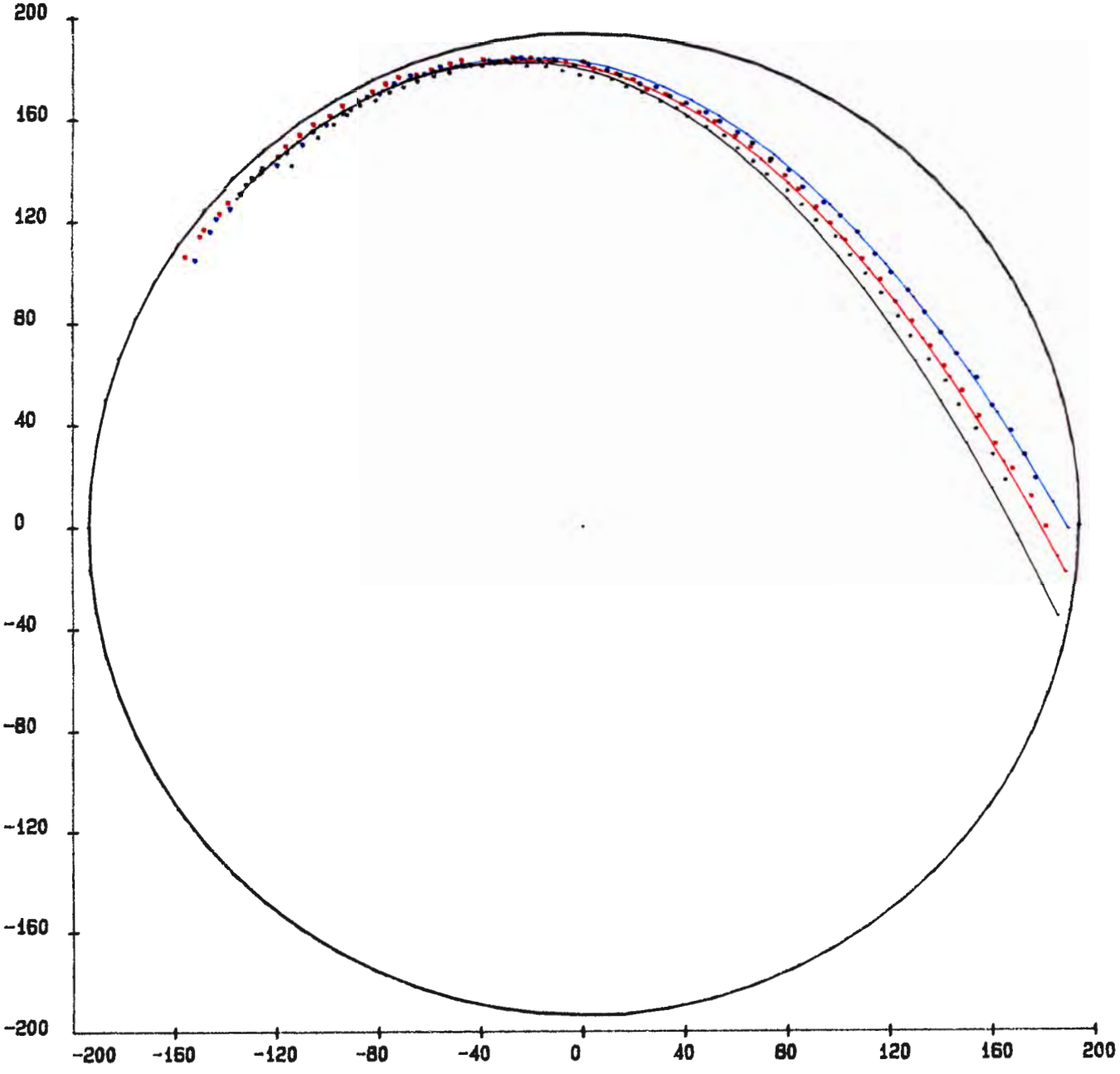

FIGURE 40. Comparison of theoretical and experimental plots for a range of lifter-bar heights

7.3. Analysis of the theory

Now that it has been established that the theory provides a good prediction of the influence of lifter-bars and mill speed upon the rod trajectories, the theory can be analysed to provide a deeper insight into the observed effects.

7.3.1. Influence of mill speed

A plot of mill speed versus impact angle yields a surprising result, as shown in figure 41, there are two linear regions. A linear regression carried out on the principle region, from 60 to 84% of critical speed, yields a coefficient of correlation of 0,9999 , so is truely linear. There is a distinct inflection of the line at a value of 85% of critical speed, followed by a second minor linear region. This inflection occurs because, under these particular conditions, at above 84% critical speed the rod is projected off the lifter-bar prior to reaching the tip of the bar, so a new set of controlling conditions apply.

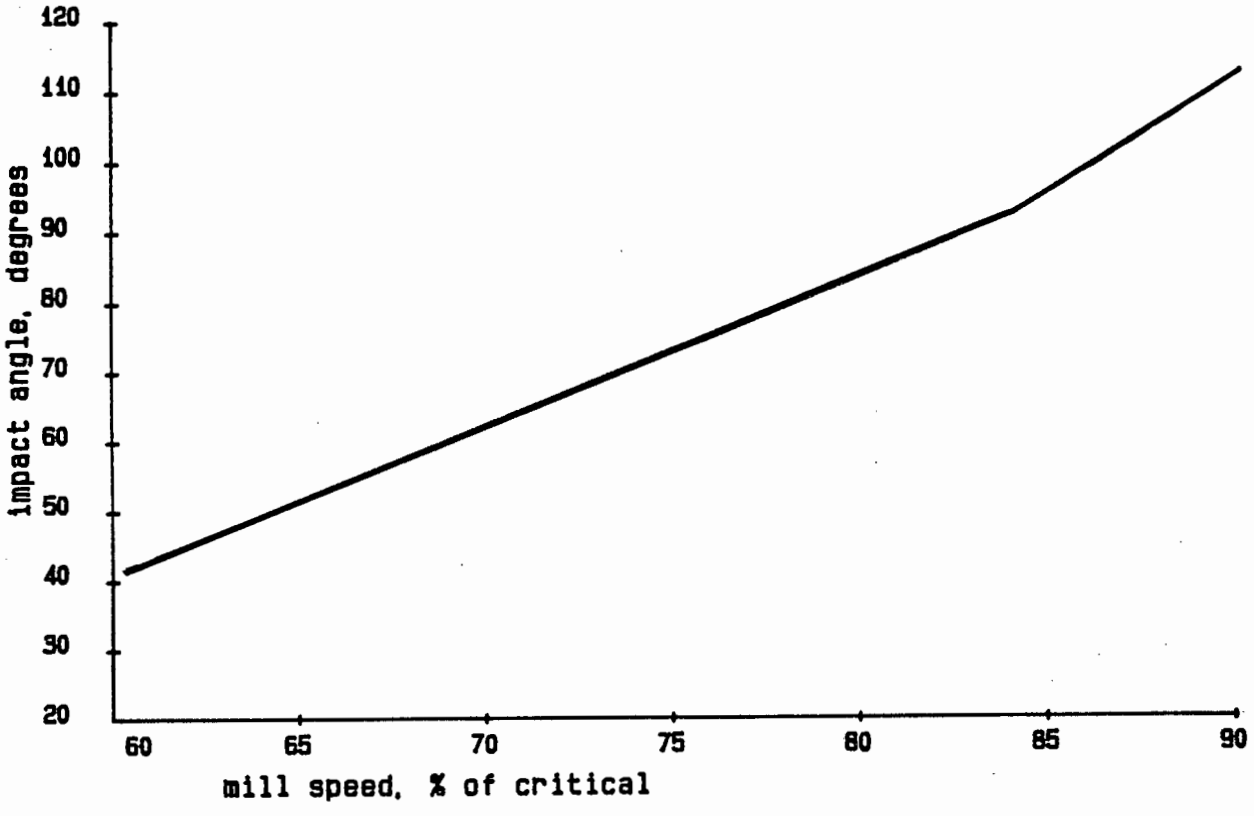

FIGURE 41. The relationship between mill speed and the impact angle. 12mm, 90° lifter-bar

The second linear region has a steeper gradient than the major region. This is because the factors, discussed in the following section, that lower the trajectory of the rod no longer apply, as the rod is not rolling any further along the lifter-bar with the increasing mill speed, as is the case at below 85% critical speed.

7.3.2. Influence of lifter-bar height

Once the height of a lifter-bar is greater than the rod radius, it has only a small effect upon the trajectory of the rods, as seen in figure 42. There is a peak in the projected impact angle for a lifter-bar height about equal to a rod diameter, thereafter the impact angle drops off slightly.

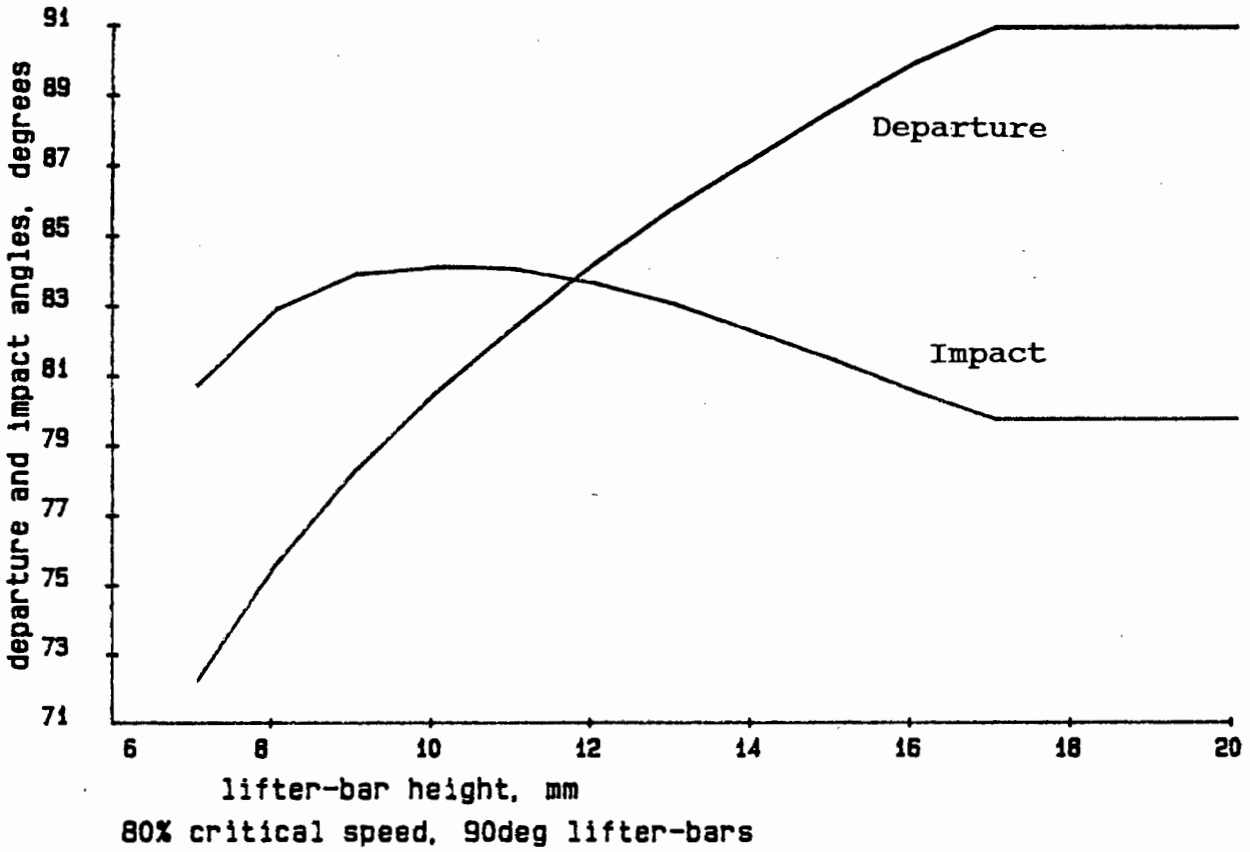

FIGURE 42. The relationship between lifter-bar height and the angles of departure and impact

The underlying cause of this drop-off in the height of the trajectory is the radial acceleration of the rod. As the rod slides along the face of the lifter-bar the radial velocity

increases relative to the tangential component of the velocity. In addition the face of the lifter-bar becomes progressively more vertical as it lifts the rod higher, so it projects the rod off at a more horizontal angle. Thus although the net velocity at the moment of projection off the lifter-bar increases with increasing height of the lifter-bar, the initial velocity vector of the free-flight trajectory is directed progressively further downwards. The direction factor gradually dominates the velocity factor and leads to a shallower trajectory.

The departure angle increases steadily with increasing lifter-bar height, as is to be expected, for most lifter-bar heights. However above a critical lifter-bar height, dependent upon the speed of the mill and face-angle of the lifter-bar, the rods follow identical trajectories, independent of the height of the lifter-bar. This occurs because the rod is projected off the face of the lifter-bar prior to reaching its tip, as shown by the constant departure angle above a lifter-bar height of 17mm, in figure 42. This condition arises when the face of the lifter-bar is close to perpendicular, and so the gravitational acceleration acting on the rod is directed away from the lifter-bar face, thus accelerating the rod away from the face. The escape of the rod from the face of the lifter-bar is facilitated by the fact that in moving towards the tip of the lifter-bar the tangential velocity of the face decreases, due to its decreasing radius of rotation. With the tangential component of the rods velocity increasing due to the gravitational acceleration, the rod moves free of the lifter-bar face. The horizontal region on the impact-angle curve corresponds with this region of constant trajectories.

The influence of lifter-bar height upon impact angle is dependent upon the speed of the mill. This is clearly shown by figure 43, which shows trajectories in a mill running at 60% of the critical speed. In this instance the impact angle gradually increases and then levels out, without passing through a maximum. This is corroborated by the experimental results given in figure 31.

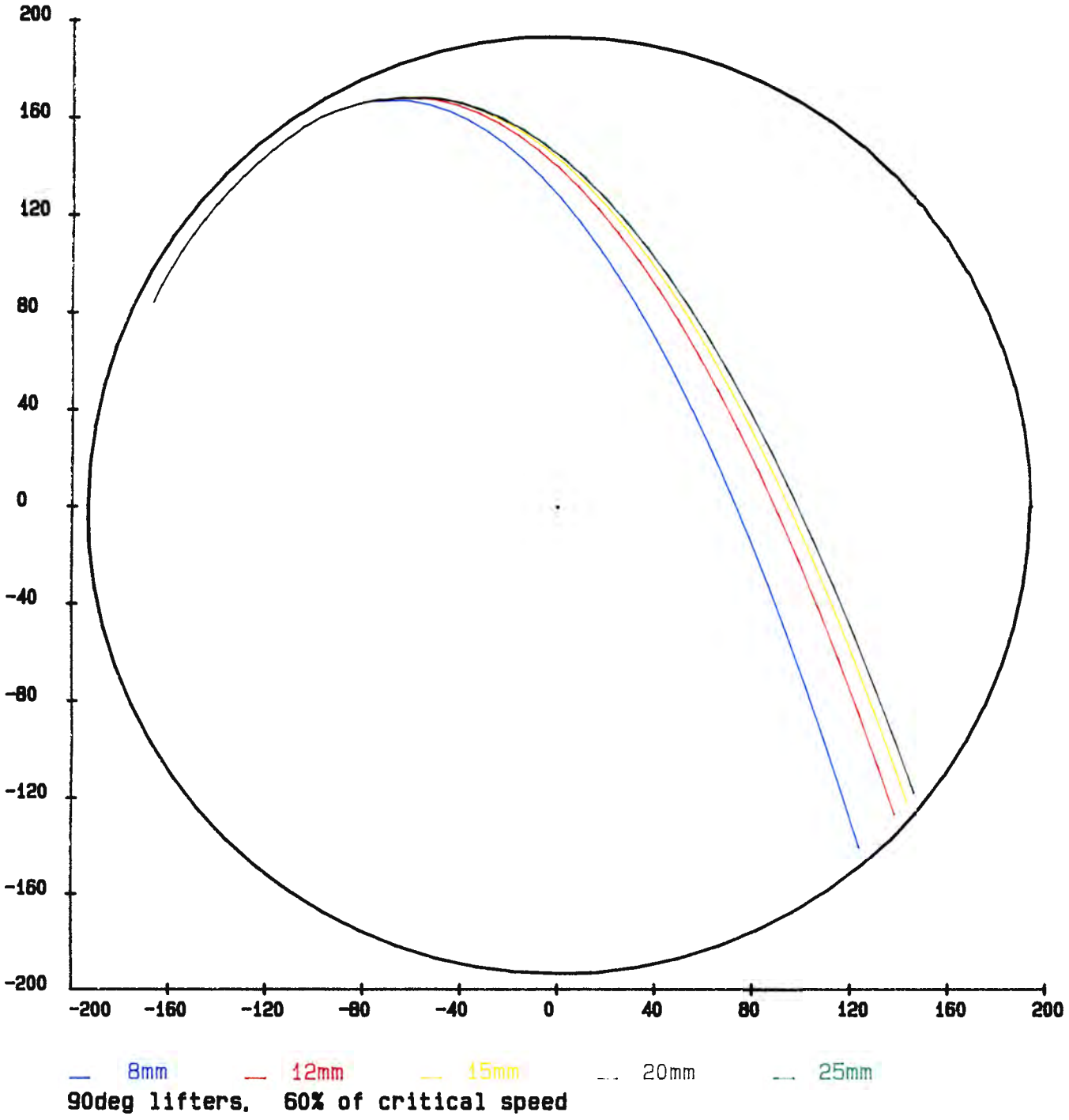

FIGURE 43. Increasing height of rod trajectories with increasing lifter-bar height, for a mill running at 60% critical speed

7.3.3. Influence of lifter-bar face-angle

The large effect that changing the lifter-bar face-angle has upon the outermost rod trajectories is shown in figure 44. For this high-speed mill, running at 90% critical, a perpendicular lifter-bar projects the outer layer of charge high up onto the opposing face of the mill.

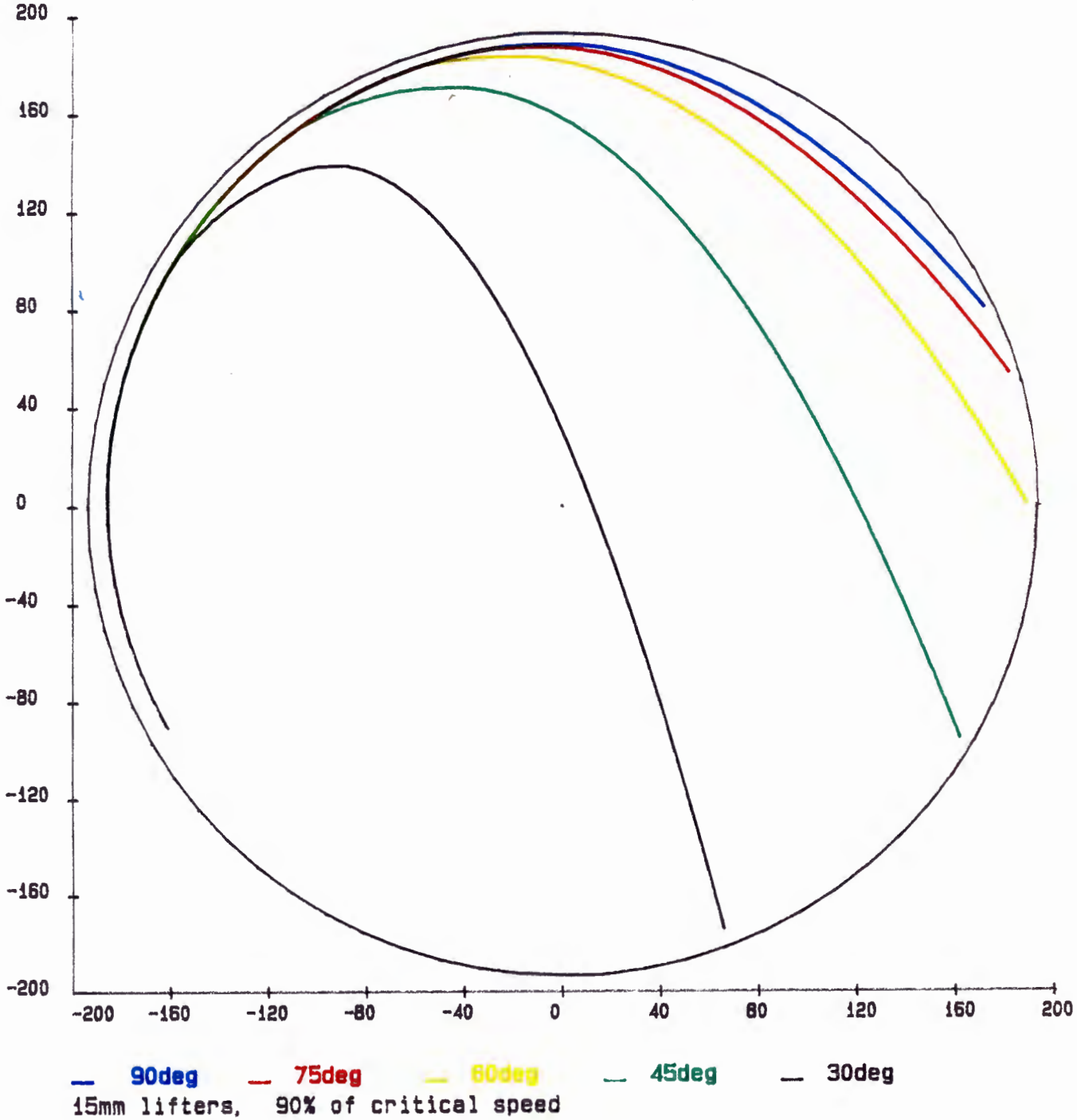

FIGURE 44. Theoretical plots of the rod trajectories for lifter-bars of various face angles.

The angle of the lifter-bars can be tuned to project this outer layer onto the toe of the charge. In this instance a 45^0 lifter-bar would be ideal. Using this technique, lifter-bars can be used to key in the bulk of the charge, without projecting the outer layers onto the mill shell.

7.4. Power draw of the mill

As this is an aside to the main thrust of the work, and the experimental results are not accurate enough to warrant a quantitative treatment, this is discussed in a qualitative manner.

The raw data of the current draw of the mill and of the phase-lag between current and voltage, need to be converted into figures reflecting the relative power draw of the mill. The maximum power is delivered when the current and voltage are in phase. When an electric motor is run under load the voltage tends to lag the current, and the effective power supplied is decreased.

For: $P \equiv$ Power draw
$V \equiv$ Voltage
$I \equiv$ Current
$\phi \equiv$ Phase-lag between current and voltage

We have:
$$P = \vec{V}.\vec{I}$$
$$\equiv V.I.\cos\phi \quad \ldots\ldots \text{ if there is a phase-lag}$$
$$\equiv R.I.I.\cos\phi$$

so:
$$P \propto I^2.\cos\phi \tag{56}$$

Now $\cos\phi$ is a function of the current I, this relationship is given in by the equation of the linear fit given in figure 25.

$$\cos\phi = 0{,}323I - 1{,}327 \tag{57}$$

so:
$$P \propto 0{,}32I^3 - 1{,}33I^2 \tag{58}$$

Thus by substituting the measured current draws into equation

(58) the relative power draws can be derived. These are derived from the data given in table VIII-4, and are given in table 3.

TABLE 3

Power draw for a range of lifter-bar heights and mill speeds

MILL SPEED % CRITICAL	LIFTER-BAR HEIGHTS					
	25	20	12	6	20&12	smooth
60	5,73	6,04	6,45	9,17	8,57	8,92
65	6,04	5,94	7,42	10,0	8,92	9,91
70	6,56	9,91	7,76	11,5	9,78	10,8
75	6,98	10,4	9,53	12,2	10,7	12,0
80	10,9	10,8	10,6	14,0	11,1	13,2
85	11,5	11,1	11,3	15,1	11,9	15,4
90	11,8	11,5	12,0	15,3	11,8	18,2
95	-	11,9	13,5	15,0	12,3	20,9
100	-	12,3	13,6	13,7	11,9	23,9
105	-	-	15,3	13,6	12,2	27,5
110	-	-	15,1	12,6	12,7	31,9
115	-	-	15,3	12,6	-	35,6
120	-	-	13,9	10,3	12,3	-

Figure 45 shows how the relative power draw of the mill varies with increasing speed, for a range of lifter-bar heights. There is a very distinct difference in power draw between a smooth-lined mill and one with lifter-bars. The curve for the smooth-lined mill shows no sign of a levelling off in the power draw, even with the mill rotating at 120% of the critical speed. This corresponds with the observed high degree of slip, for although the mill is rotating at well above 100% of the critical speed, the charge is not close to centrifuging.

The low 6mm lifter-bars, equivalent to a rod radius in height, lead to a distinct peak in the power draw, at 90% of the critical speed, with a greatly decreased power draw at higher speeds. A somewhat flatter peak is found in production mills, indicating a slightly lower level of keying-in of the charge. The 12mm, one rod diameter, lifter-bar also has a peak in power draw, but this is shifted relative to the peak for the low lifter-bars, This is discussed at a later stage.

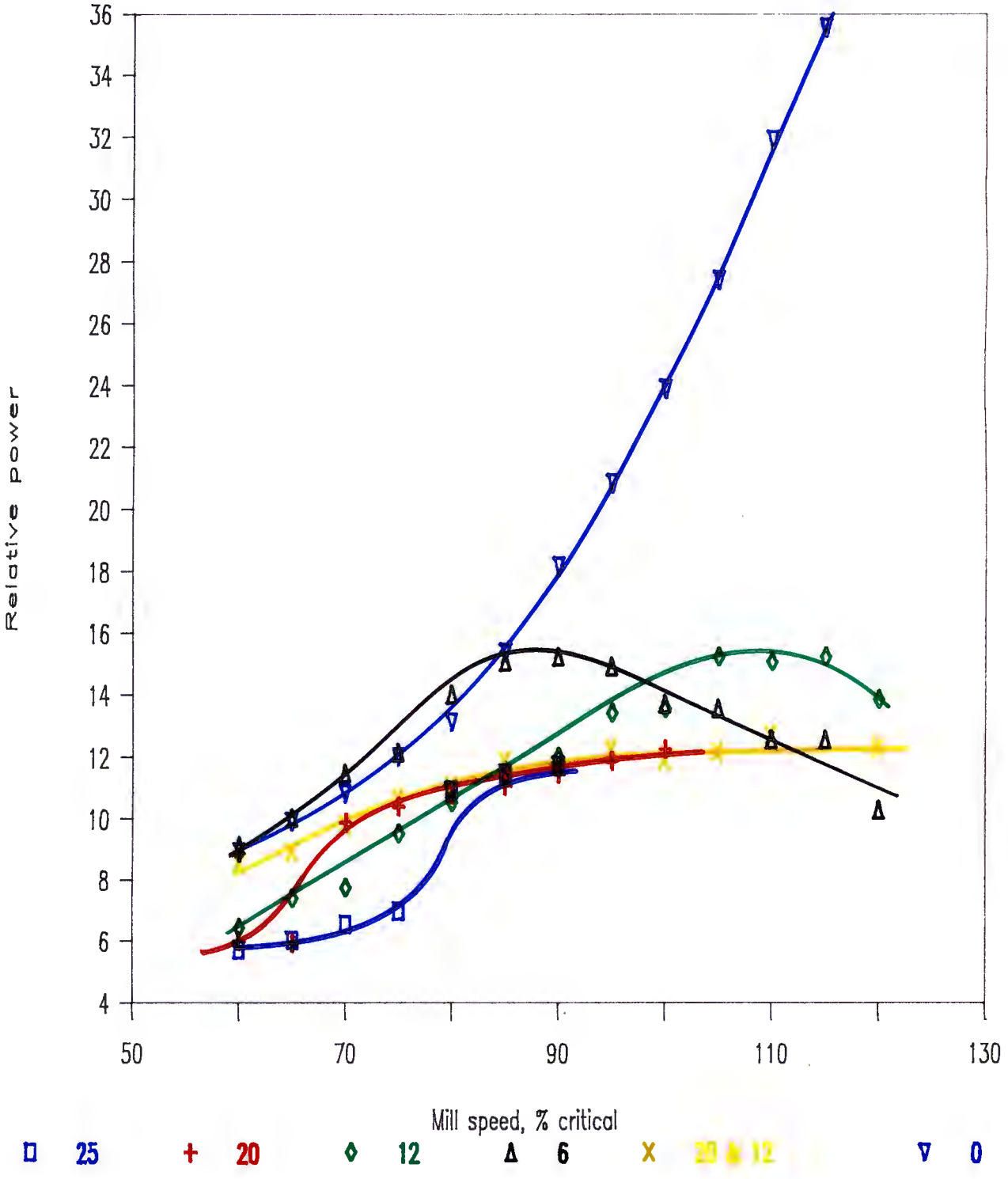

FIGURE 45. Relative mill power draw, for a 45% mill filling, and with various lifter-bars

The low lifter-bars draw approximately the same power as the smooth-lined mill, up to about 85% of the critical speed. All higher lifter- bars cause the mill to draw far less power at equivalent speeds, despite the fact that the charge is being lifted higher and projected further by the lifter-bars.

The 20 and 25mm lifter-bars cause a sudden increase in power draw at around 70% and 80% of critical speed respectively, thereafter evening off to a constant level. The liner configuration with alternating rows of 12 and 20mm lifter-bars provides an interesting power curve. The power-draw increases gradually as the mill speed increases up to 90% of the critical speed, and then levels out. This may be an indication of a stable and favourable milling action.

An interesting point to note, is that at 80% of the critical speed all the liner configurations, with lifter-bars higher than one rod radius, provide about the same power draw. This can be explained by the observation that the rod trajectories are almost independent of lifter-bar height at that speed. This emphasises that the height of a lifter-bar is not of great importance, once it is above a rod radius in height.

The only anomalous curve is that for the 12mm lifter-bars, this anomaly arises out of the simplified experimental conditions present in the mill. It was noted (table VIII-1) that at high mill speeds the outer layer centrifuged, effectively forming a new mill shell within which the remainder of the charge tumbled. Thus the resultant power curve is a superposition of the curve for a smooth liner and one for lifter-bars, hence the power peak is at a supercritical speed. This is the type of effect that Hukki[21] based his prediction on of mills running more efficiently at supercritical speeds. It should be noted however, that in a real mill such an effect is unlikely to arise, because of the size distribution of the charge within the mill. An ideal smooth layer of charge trapped between lifter-bars, of the same height as the diameter of the top-size of the charge, is not going to form. If any radial segregation according to the size of the

charge takes place in the mill, it would favour the smaller particles centrifuging first and migrating to the mill perimeter, as discussed earlier.

Figure 46 presents the relative power draw curves of a range of mill speeds, for increasing height of lifter-bars. This is only presented for mill speeds up to 90% critical, as this is the normal limit in practical milling.

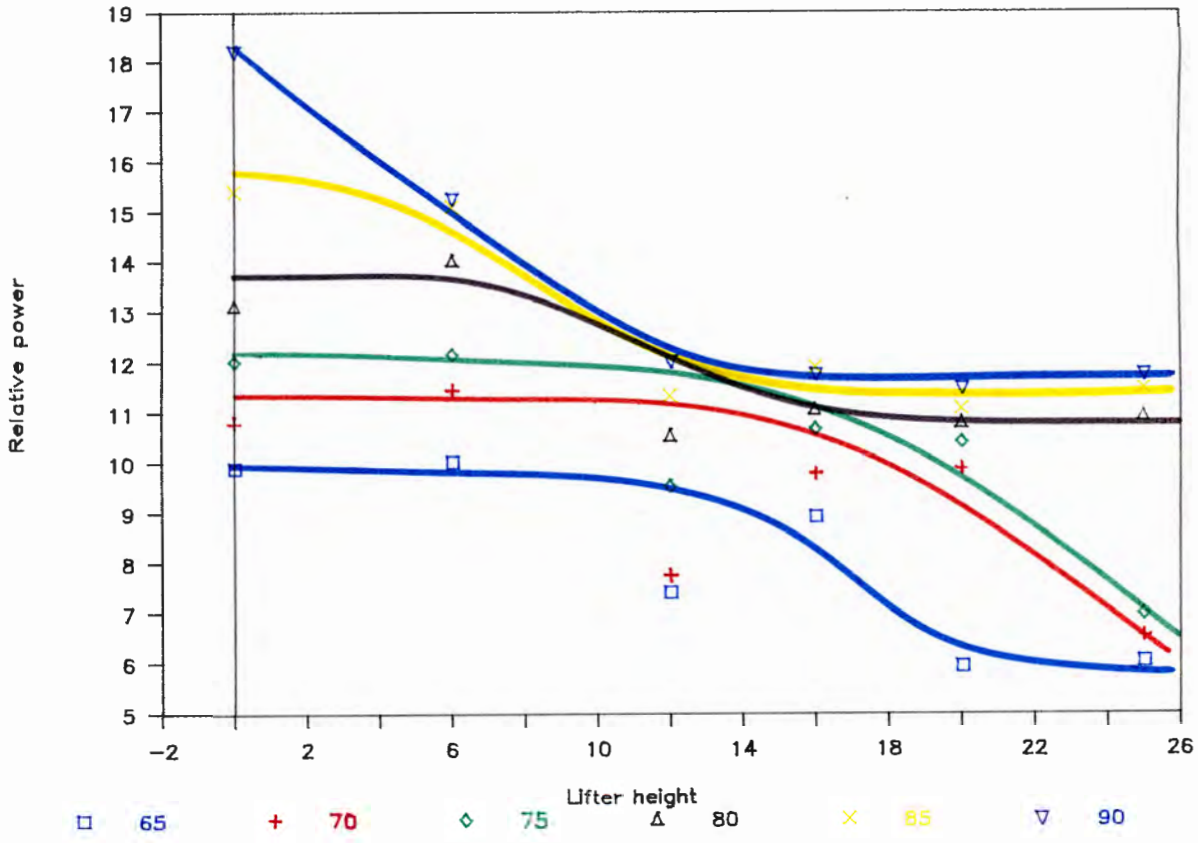

FIGURE 46. Relative mill power draw curves, for a range of mill speeds

For the sake of convenience the liner having alternating rows of 12 and 20mm lifter-bars is classified as having a 16mm lifter-bar height.

The general trend is that of a decreasing power draw with increasing lifter-bar height. With mill speeds of 80% upwards the

power draw levels off for all lifter heights greater than a rod radius. Ignoring the anomalous values for the 12mm lifter-bars, it is seen that the power draws decrease greatly for higher lifter-bars, at speeds below 80% critical. This coincides with two layers of rods becoming fully keyed-in by these high lifter-bars.

It is clear that the effect of lifter-bars upon the mill power draw, and charge motion within the mill, is dependent upon the speed of the mill. Therefore any installation of lifter-bars in a mill must be related to the speed of the mill, expressed as a per centage of its critical speed.

CHAPTER 8

CONCLUSIONS

8.1. Scope and validity of the work

A theoretical model, based upon the fundamental laws of motion, was developed to describe the motion of an isolated rod or ball in a rotary mill, as affected by the geometry of the mill lining. This model takes account of both the static and kinetic coefficients of friction acting between the grinding element and the lifter-bar, and allowance is made for rolling and slipping of the element. The model considers flat-faced lifter-bars of any face-angle and of any height. Only the very outer layer of charge is considered, however this is an important indicator of the charge motion as it yields the outermost limits of the bulk charge motion. The model needs to be slightly refined to allow for the interaction of the element with the tip of the lifter-bar, for low lifter-bars. In its present form the model underestimates the lifting action of lifter-bars that have a heights from zero to just greater than a grinding element radius.

In general the correlation between the theoretical model and the experimental results is good, and indicates that the model gives the correct predictions of charge motion. The predictions are however limited by the uncertainty in the measurement of the kinetic coefficient of friction, arising out of limitations in the experimental apparatus. This limitation has been shown to cast some uncertainty upon the predicted lifting action of the angled lifter-bars. From a rough comparison with experimental data (the data not being suitable for a proper comparison), it appears that the theory is predicting higher trajectories than those found for angled lifter-bars, indicating that the actual value of the kinetic coefficient of friction is lower than that used.

Bearing in mind the limitations of the theoretically predicted

trajectories, they will on the whole give good predictions of the outer charge motion, and all the predicted trends will be correct.

8.2. Theoretical and experimental Predictions

In previous work that studied the effect of lifter-bars upon the charge motion only the point to which the charge is lifted was commented upon, however the full trajectory and especially the impact point of the charge are of great importance. In milling it is desirable to key-in the charge to the rotary motion of the mill, but in doing so the charge should not be projected onto the mill shell. If the grinding element impacts directly onto the lining then accelerated wear of the lining and rapid degradation of the grinding media take place, without any milling of the ore being achieved. So it is important that the grinding elements are projected onto the toe of the charge. Taking this into consideration, the impact point is emphasised in this work.

8.2.1. Influence of lifter-bar height

It was shown that for a smooth lining extensive slip of the charge takes place. This results in the wasting of energy, accelerated liner wear, and inefficient charge motion. There is a tremendous increase in the height of the charge trajectories, as the height of the lifter-bars is increased from zero to just greater than a grinding-element radius. To prevent slipping of the charge on the liner, the lifter-bar should be at least as high as a grinding-element radius.

Once the lifter-bar height is greater than the grinding element radius, then increasing height leads to an increase in the degree of lift, up to a critical lifter-bar height. Once the lifter-bar is higher than the critical height the grinding element is projected off the lifter-bar prior to reaching the tip, so has a constant angle of lift.

Increasing the height of the lifter-bar, beyond that of a

grinding-element radius, results in a slight increase in the height of the impact angle, followed by a decrease and then a levelling out (figure 47). This effect has not been noted before, and is of considerable practical importance. This shows that a higher lifter-bar is not going to project the charge to a point higher up the side of the mill, so high lifter-bars can confidently be installed in mills.

8.2.2. Influence of lifter-bar face-angle

Increasing the face-angle of a lifter-bar from a shallow angle up to 90° (a rectangular profile), results in a greatly increased lift and impact angle of the grinding elements, as illustrated in figure 48. By making use of this effect the face-angle can be tuned to make the lifter-bar drop the charge onto any desired point. This is especially important in high-speed mills, such as are found on the South African gold mines, as lifter-bars can be installed to key-in the charge without projecting it onto the mill shell.

8.2.3. Influence of mill speed

There is a linear relationship between the speed of the mill and the impact angle (figure 49). This linearity holds provided the lifter-bar is below the critical height, beyond that height a new linear region is entered into. Mill speed has a large effect on the height of the trajectories, and on the motion of the bulk of the charge.

8.2.4. Relative importance of the variables

To obtain a direct comparison of the relative effects of the above-mentioned variables, they are all plotted against the impact angle, for a 100° range (figures 47 to 49). The range of each variable is given according to how that variable may reasonably be changed in a production mill.

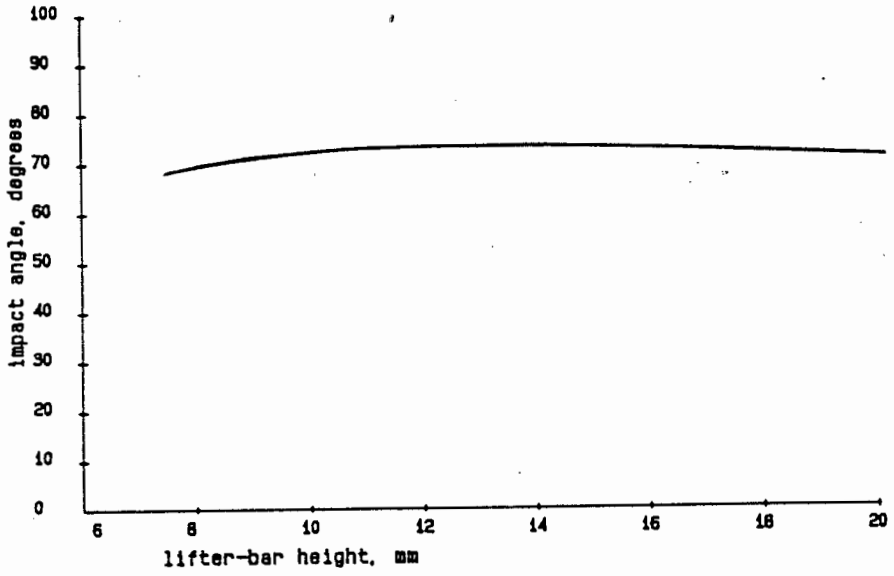

FIGURE 47. Influence of varying lifter-bar height

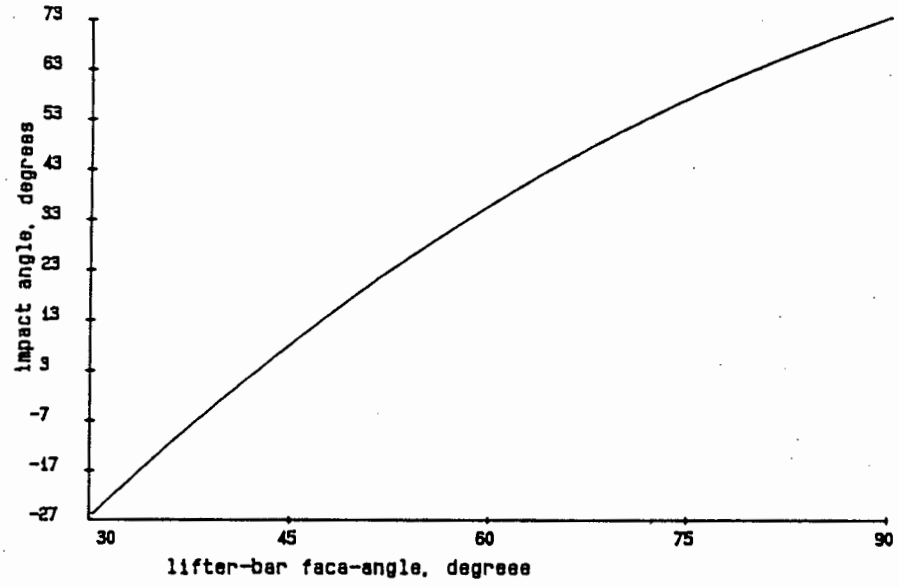

FIGURE 48. Influence of varying lifter-bar face-angle

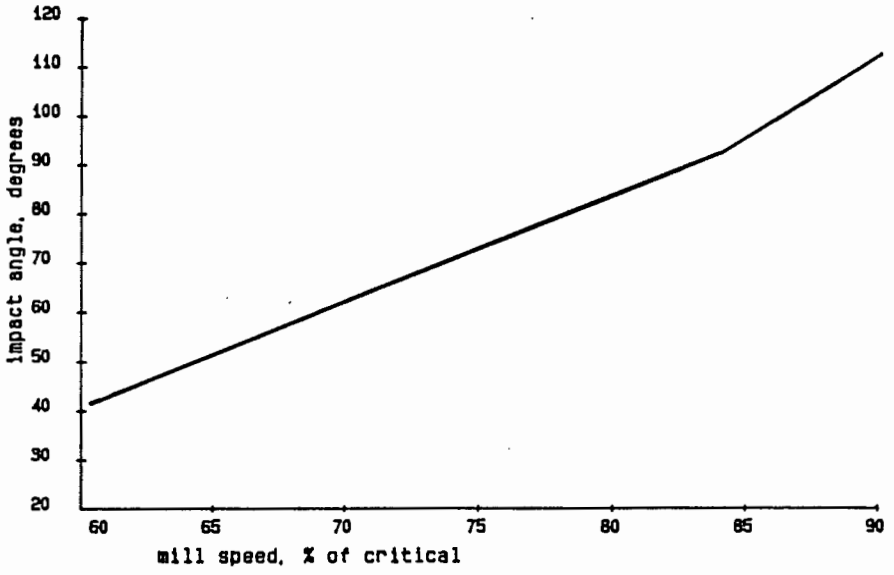

FIGURE 49. Influence of varying the mill speed

8.3. Relationship to production mills

Because the theoretical model is based upon the fundamental laws of motion, it can be applied to any size of mill. All trajectories and angles of departure and impact are independent of the size, so can be directly scaled up. It must be borne in mind however, that the pressures in the charge and the forces of impact increase with increasing size of mill. So for identical charge motions different grinding characteristics apply for different sized mills.

To give more accurate predictions of the charge motion in a production mill, the static and kinetic coefficients of friction for balls, rods, or rocks resting upon a lifter-bar covered with slurry, need to be measured. In a pebble mill the rocks rapidly round off to smooth oval shapes (as is easily observed by looking at the charge in such a mill), so can be approximated by spheres. Therefore the theoretical model can be directly applied to predict the motion of the charge in a production mill.

8.4. Recommended future work

The static and kinetic coefficients of friction should be measured under vibrating conditions at much higher frequencies than those used, preferably up to 15kHz. They should also be measured for real grinding elements resting upon lifter-bar materials that are covered with the slurry from a mill.

To facilitate the location of isolated rods on sloping-faced lifter-bars, in the analysis of the films, the experimental mill should be run with a very low load of just a few rods. The motion of the rods within the bulk of the charge should also be analysed, in the hope of relating this to the milling action that takes place. The mill should also be run with a mixed charge consisting of rods having a range of sizes. This should show what influence the size distribution of the charge in a mill has upon the charge motion.

Following on from the testwork on experimental mills, the effect of the lifter-bar height and geometry upon the liner life, milling efficiency, and power consumption in production mills, should be assesed. Having improved the life of the liner by improving the liner design, the materials of liner construction can than be tested to find the most cost-effective materials.

8.5. Summary

Some important effects of lifter-bar geometry upon the charge motion have been discovered. The interaction of the three principle variables is summarised in the three-dimensional plots given in figures 50 to 52. The predictions of the theoretical model are applicable to production mills, and can be improved upon by extending some of the experimental work. There is a wide scope for continued work in this field, and it has been shown to have consequences of particular benefit to production milling.

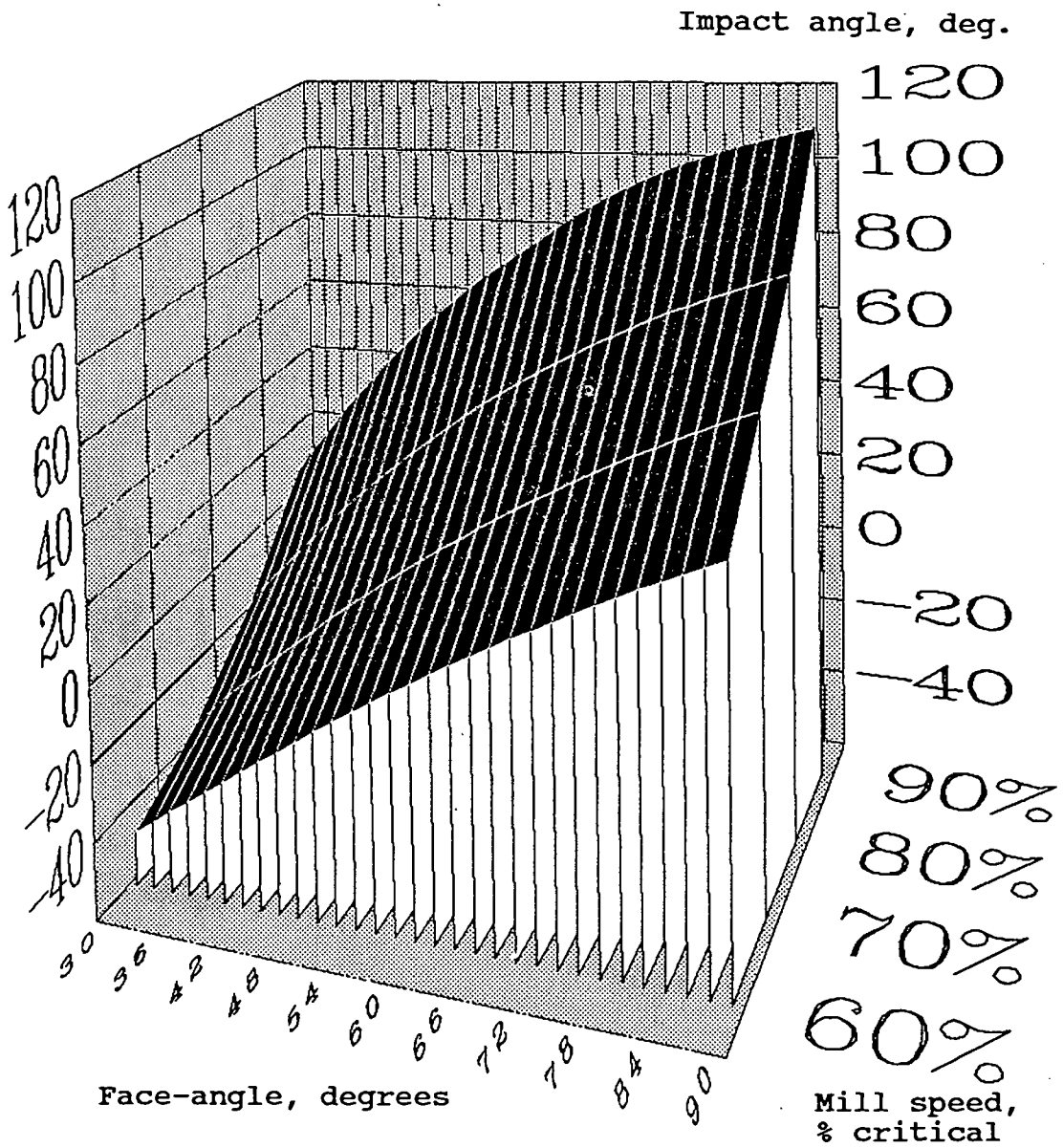

FIGURE 50. The combined influence of lifter-bar face-angle and mill speed upon the impact angle

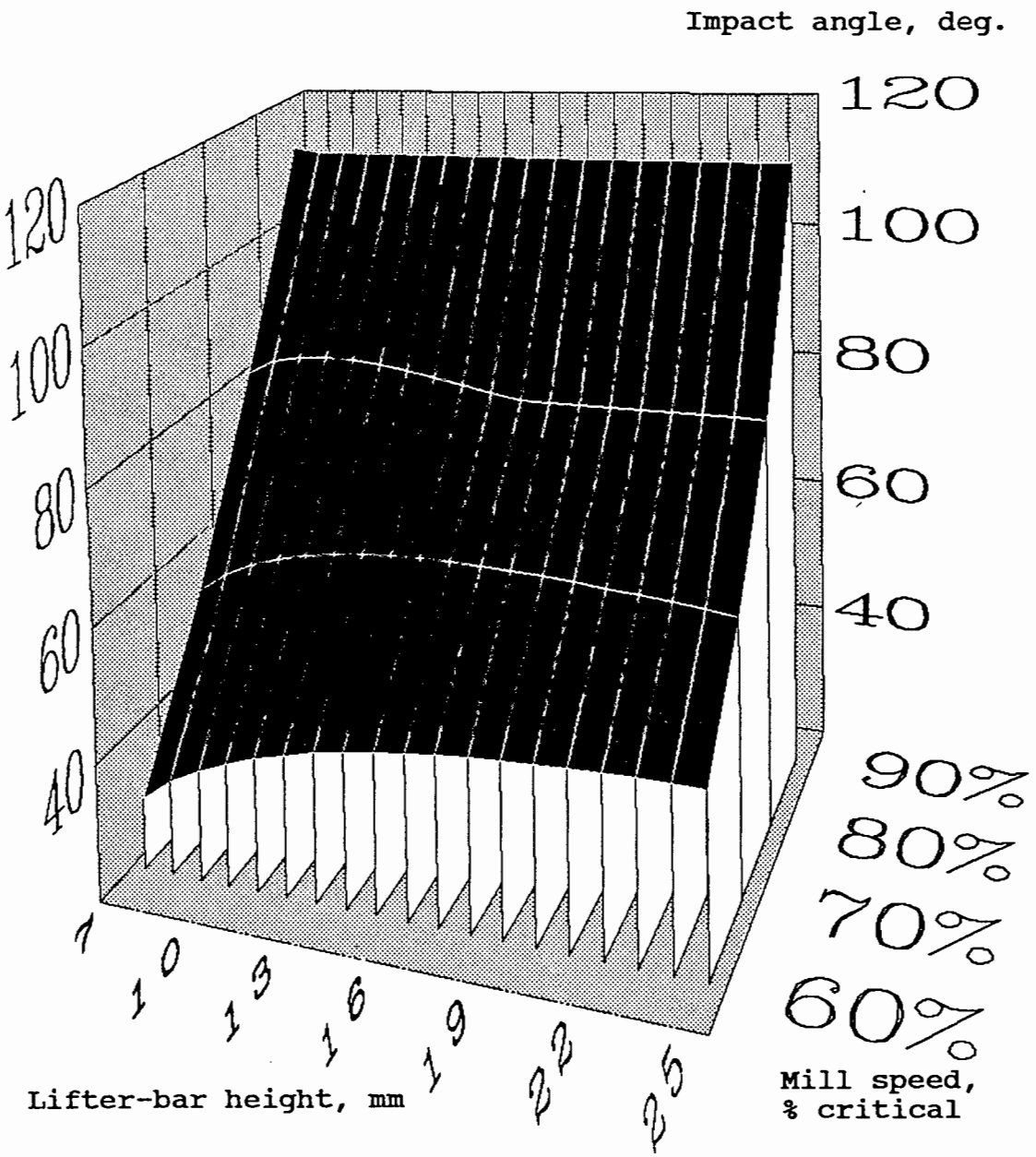

FIGURE 51. The combined influence of lifter-bar height and mill speed upon the impact angle

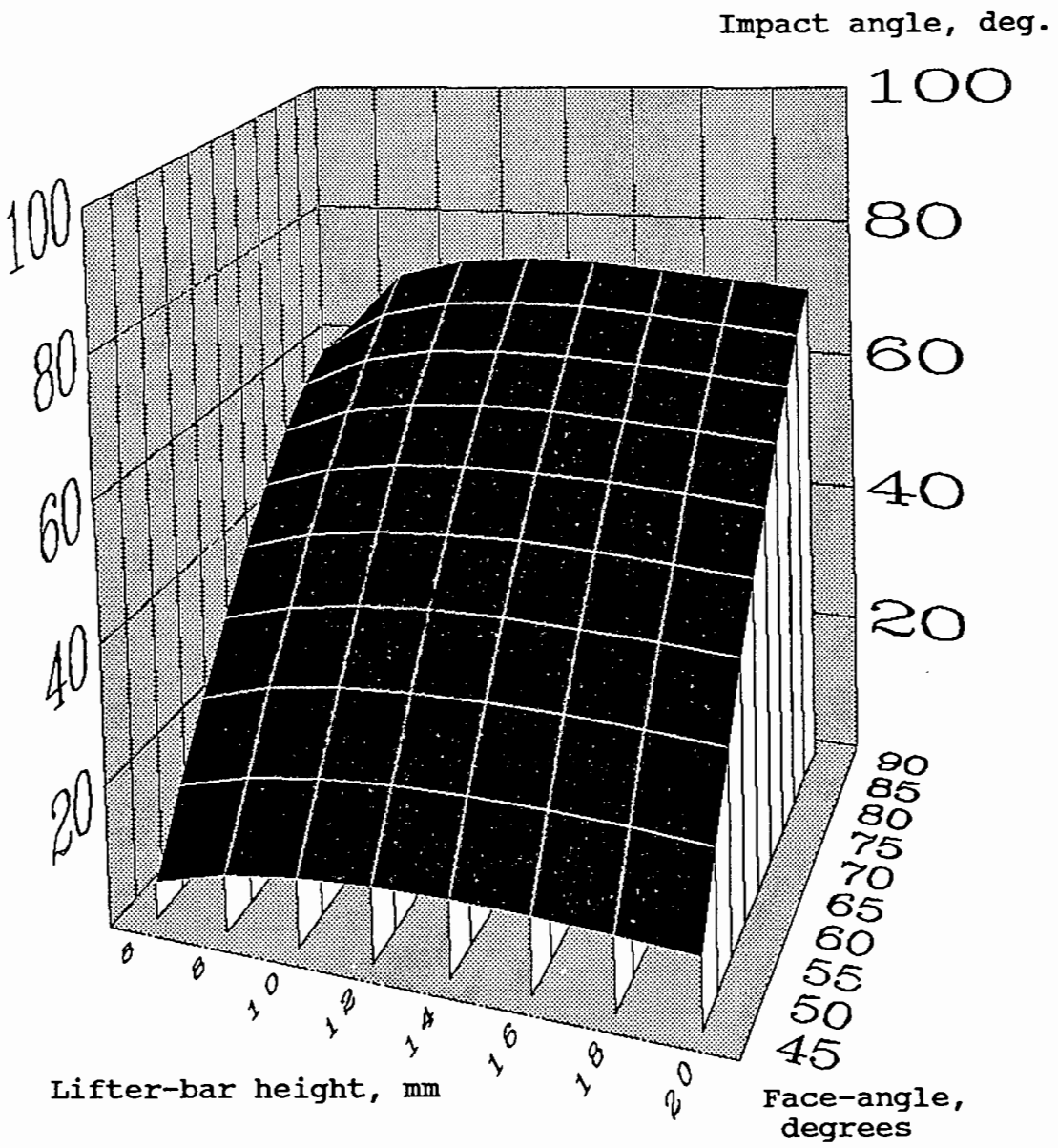

FIGURE 52. The combined influence of lifter-bar height and face-angle upon the impact angle

REFERENCES

1. WHITE, H.A. The theory of the tube mill. *The Journal of The Chemical, Metallurgical and Mining Society of South Africa.* May, 1905. pp. 290-305.
2. DAVIS, E.W. Fine crushing in ball-mills. AIME Trans., vol. 61. 1919. pp. 250-296.
3. HAULTAIN, H.E.T., and DYER, F.C. Ball paths in tube mills. CIM Trans., vol. 25. 1922. pp. 276-291.
4. GOW, A.M., CAMPBELL, A.B., and COGHILL, W.H. AIME Trans., Milling Methods, 1930. pp. 51-81.
5. FAHRENWALD, A.W., and LEE, H.E. Ball mill studies. AIME Technical Publication no. 375. 1931.
6. MEADERS, R.C., and MacPHERSON, A.R. Technical design of autogenous mills. *Mining Engineering*, vol. 16. 1964. pp. 81-83.
7. MARECHAL, B. Contribution to a study of dry quasi-autogenous milling. Third part: Internal mechanics of the aerofall mill. Mintek Translation TR-1199. (Contribution a l'etude de la fragmentation quasi-autogene en voie seche. Presented at the Faculty of Sciences, Nancy, 17th May, 1968.)
8. VERMEULEN, L.A., and HOWAT, D.D. Fluctuations in the slip of the grinding charge in rotary mills with smooth liners. *International J. of Mineral Processing*, vol. 16, 1986. pp. 153-188.
9. McIVOR, R.E. Effects of speed and liner configuration on ball mill performance. *Mining Engineering*, Jun. 1983. pp. 617-622.
10. VERMEULEN, L.A. The lifting action of lifter bars in rotary mills. *J. of The S.A. Inst. of Min. and Metall.*, vol. 85, no. 2. 1985. pp. 51-63.
11. VERMEULEN, L.A., OHLSON DE FINE, M.J., and SCHAKOWSKI, F. Physical information from the inside of a rotary mill. *J. S.Afr. Inst. Min. Metall., vol. 84, no. 8. 1984. pp. 247-253.*

12. VERMEULEN, L.A. Estimation of milling parameters by use of a conductivity bolt. *Mintek TM. no. 19048*, Mintek, Randburg. July, 1985.

13. ROSE, M.E., and SULLIVAN, R.M.E. A Treatise on the internal mechanics of ball, tube and rod mills. *Constable, London. 1958.*

14. SPIEGEL, M.R. Mathematical handbook of formulas and tables. *McGraw-Hill inc., 1978.*

15. HOWAT, D.D. Reduction in metal consumption by the use of alternating lines of higher and lower lifter bars in a rod mill. *Mintek report M97*, Mintek, Randburg. 1983.

16. POWELL, M.S. The use of lifter bars in rotary mills. *Mintek reoprt M310*, Mintek, Randburg. 1987.

17. POWELL, M.S. Survey of milling and mill lining practice on the South African gold mines. *Mintek Report* M350, Mintek, Randburg. 1987

18. BRADLEY, A.A., HINDE, A.L., and LLOYD, P.J. The determination of the efficiency of the milling process. *J. S.Afr. Inst. Min. Metall.*, June 1972, pp. 277-281.

19. JOWETT, A. An introduction to the assessment of energy requirements and product size in comminution. *Minerals Sci. Energy*, vol. 3, 1971. pp. 33-43

20. POWELL, M.S. The selection of materials for, and the design of liners for rotary mills. ANTIWEAR '88, preprints of the conference, 20-22 Sept. 1988. The Royal Society, London. The Institute of Metals, London.

21. HUKKI, R.T. Grinding at supercritical speeds in rod and ball mills. *Sventsa Gruvföreningen and Jernkontoret.* Progress in mineral dressing, Trans. Tenth Int. Miner. process. congr., Stockholm 1957. Almqvist and Wiksell, Stockholm, pp. 85-109

22. NITYANAND, N., MANLEY, B., and HENEIN, H. An analysis of radial segregation for different sized spherical solids in rotary cylinders. *Metallurgical trans.*, vol. 17B, Jun. 1986, pp. 247-257

BIBLIOGRAPHY

BRADLEY, A.A., HINDE, A.L., and LLOYD, P.J. The determination of the efficiency of the milling process. *J. S.Afr. Inst. Min. Metall.*, June 1972, pp. 277-281.

DAVIS, E.W. Fine crushing in ball-mills. AIME Trans., vol. 61. 1919. pp. 250-296.

FAHRENWALD, A.W., and LEE, H.E. Ball mill studies. AIME Technical Publication no. 375. 1931.

GOW, A.M., CAMPBELL, A.B., and COGHILL, W.H. AIME Trans., Milling Methods, 1930. pp. 51-81.

HAULTAIN, H.E.T., and DYER, F.C. Ball paths in tube mills. CIM Trans., vol. 25. 1922. pp. 276-291.

HOWAT, D.D. Reduction in metal consumption by the use of alternating lines of higher and lower lifter bars in a rod mill. *Mintek report M97*, Mintek, Randburg. 1983.

HUKKI, R.T. Grinding at supercritical speeds in rod and ball mills. *Sventsa Gruvföreningen and Jernkontoret.* Progress in mineral dressing, Trans. Tenth Int. Miner. process. congr., Stockholm 1957. Almqvist and Wiksell, Stockholm, pp. 85-109

JOWETT, A. An introduction to the assessment of energy requirements and product size in comminution. *Minerals Sci. Energy*, vol. 3, 1971. pp. 33-43

MARECHAL, B. Contribution to a study of dry quasi-autogenous milling. Third part: Internal mechanics of the aerofall mill. Mintek Translation TR-1199. (Contribution a l'etude de la fragmentation quasi-autogene en voie seche. Presented at the Faculty of Sciences, Nancy, 17th May, 1968.)

McIVOR, R.E. Effects of speed and liner configuration on ball mill performance. *Mining Engineering*, Jun. 1983. pp. 617-622.

MEADERS, R.C., and MacPHERSON, A.R. Technical design of autogenous mills. *Mining Engineering*, vol. 16. 1964. pp. 81-83.

NITYANAND, N., MANLEY, B., and HENEIN, H. An analysis of radial segregation for different sized spherical solids in rotary cylinders. *Metallurgical trans.*, vol. 17B, Jun. 1986, pp. 247-257

POWELL, M.S. The use of lifter bars in rotary mills. *Mintek reoprt M310*, Mintek, Randburg. March 1987.

POWELL, M.S. Survey of milling and mill lining practice on the South African gold mines. *Mintek Report* M350, Mintek, Randburg. June 1988

POWELL, M.S. The selection of materials for, and the design of liners for rotary mills. ANTIWEAR '88, preprints of the conference, 20-22 Sept. 1988. The Royal Society, London. The Institute of Metals, London.

ROSE, M.E., and SULLIVAN, R.M.E. A Treatise on the internal mechanics of ball, tube and rod mills. *Constable, London. 1958.*

SPIEGEL, M.R. Mathematical handbook of formulas and tables. *McGraw-Hill inc., 1978.*

VERMEULEN, L.A., OHLSON DE FINE, M.J., and SCHAKOWSKI, F. Physical information from the inside of a rotary mill. *J. S.Afr. Inst. Min. Metall., vol. 84, no. 8. 1984. pp. 247-253.*

VERMEULEN, L.A. The lifting action of lifter bars in rotary mills. *J. of The S.A. Inst. of Min. and Metall.*, vol. 85, no. 2. 1985. pp. 51-63.

VERMEULEN, L.A. Estimation of milling parameters by use of a conductivity bolt. *Mintek TM. no. 19048*, Mintek, Randburg. July, 1985.

VERMEULEN, L.A., and HOWAT, D.D. Fluctuations in the slip of the grinding charge in rotary mills with smooth liners. *International J. of Mineral Processing*, vol. 16, 1986. pp. 153-188.

WHITE, H.A. The theory of the tube mill. *The Journal of The Chemical, Metallurgical and Mining Society of South Africa.* May, 1905. pp. 290-305.

APPENDIX I

DIAGRAMS

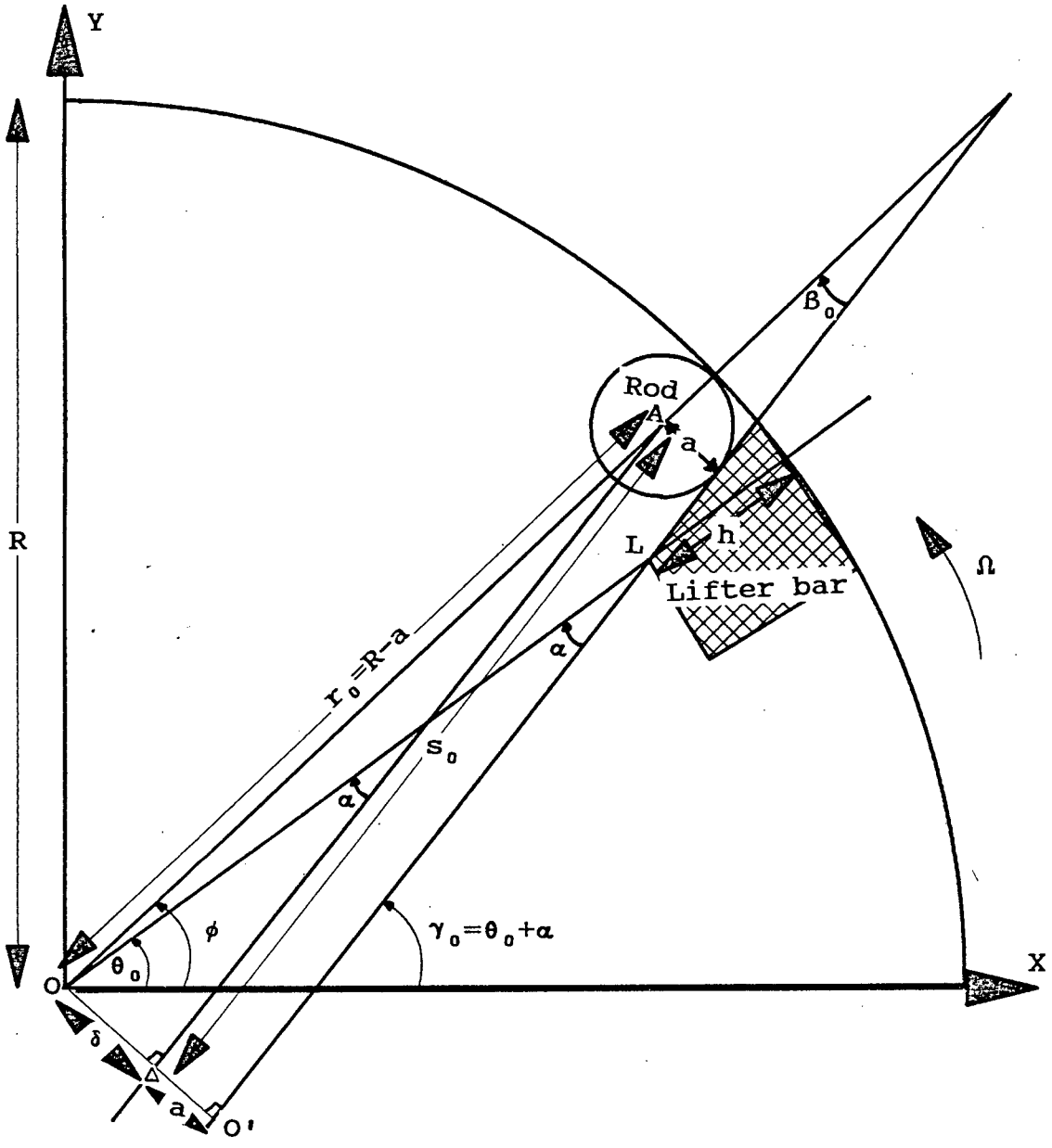

FIGURE I-1. Rod on a lifter-bar in a rotary mill

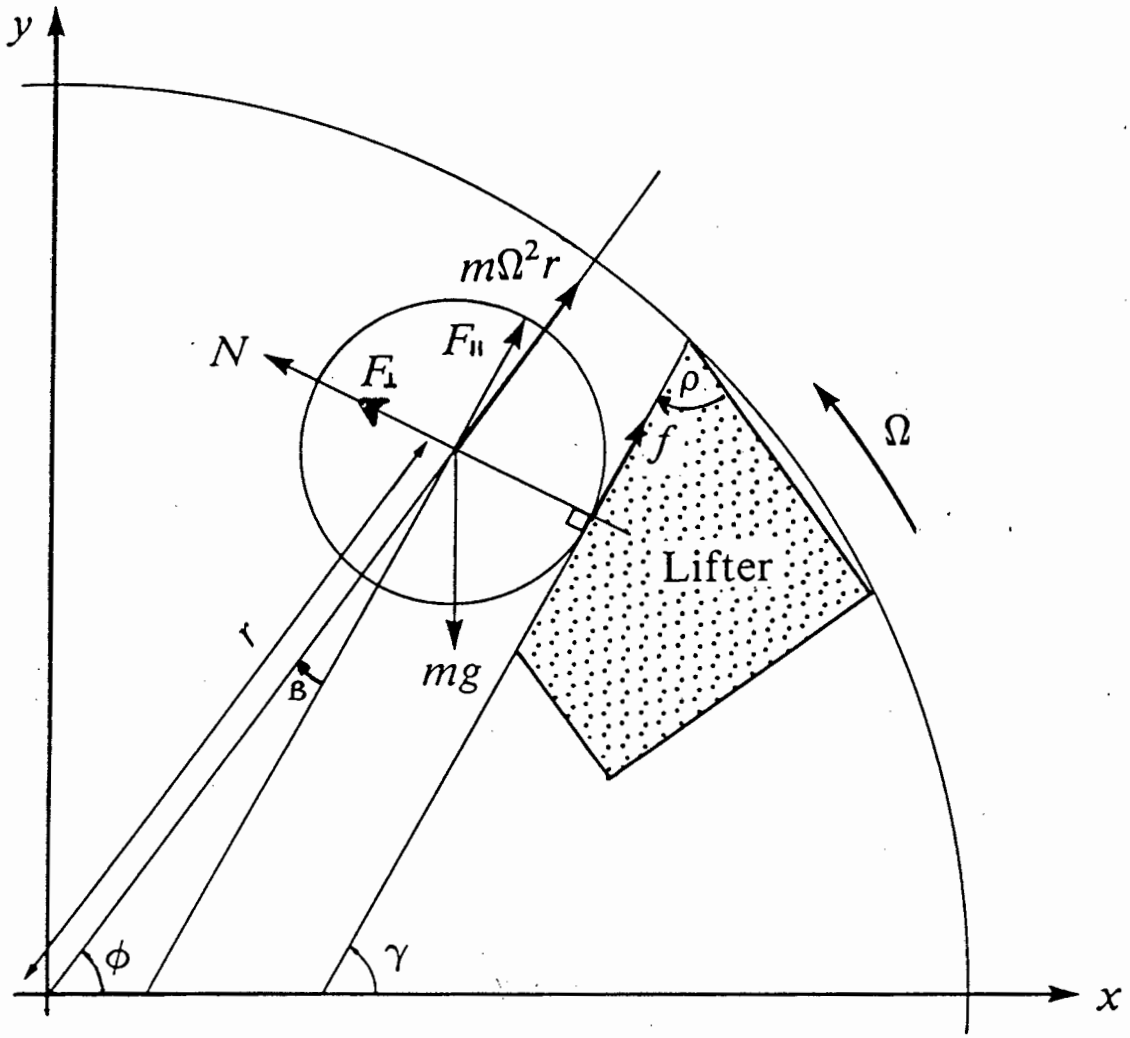

FIGURE I-2. Forces on a rod in contact with a lifter-bar

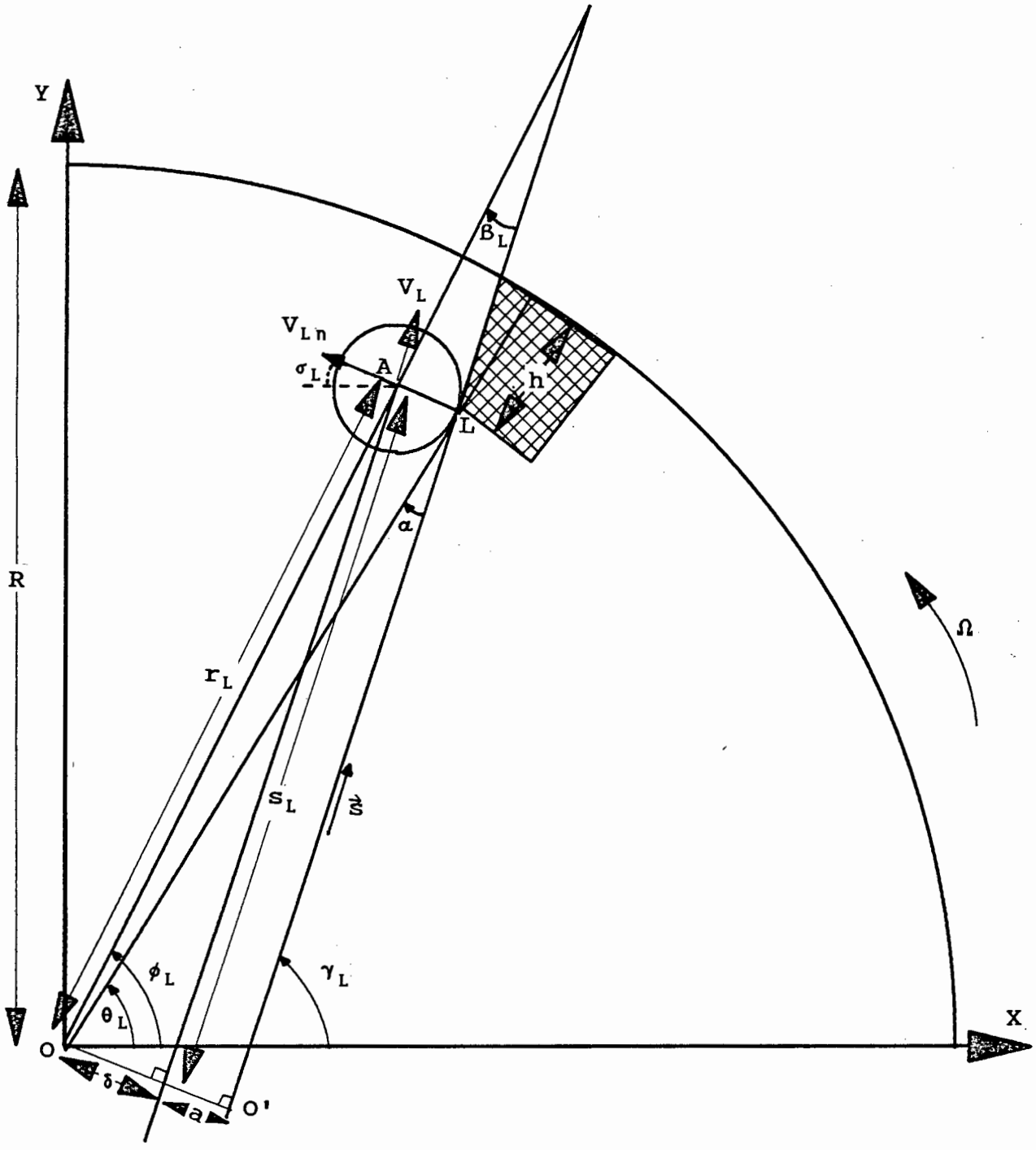

FIGURE I-3. Rod at the point of departure from the lifter-bar

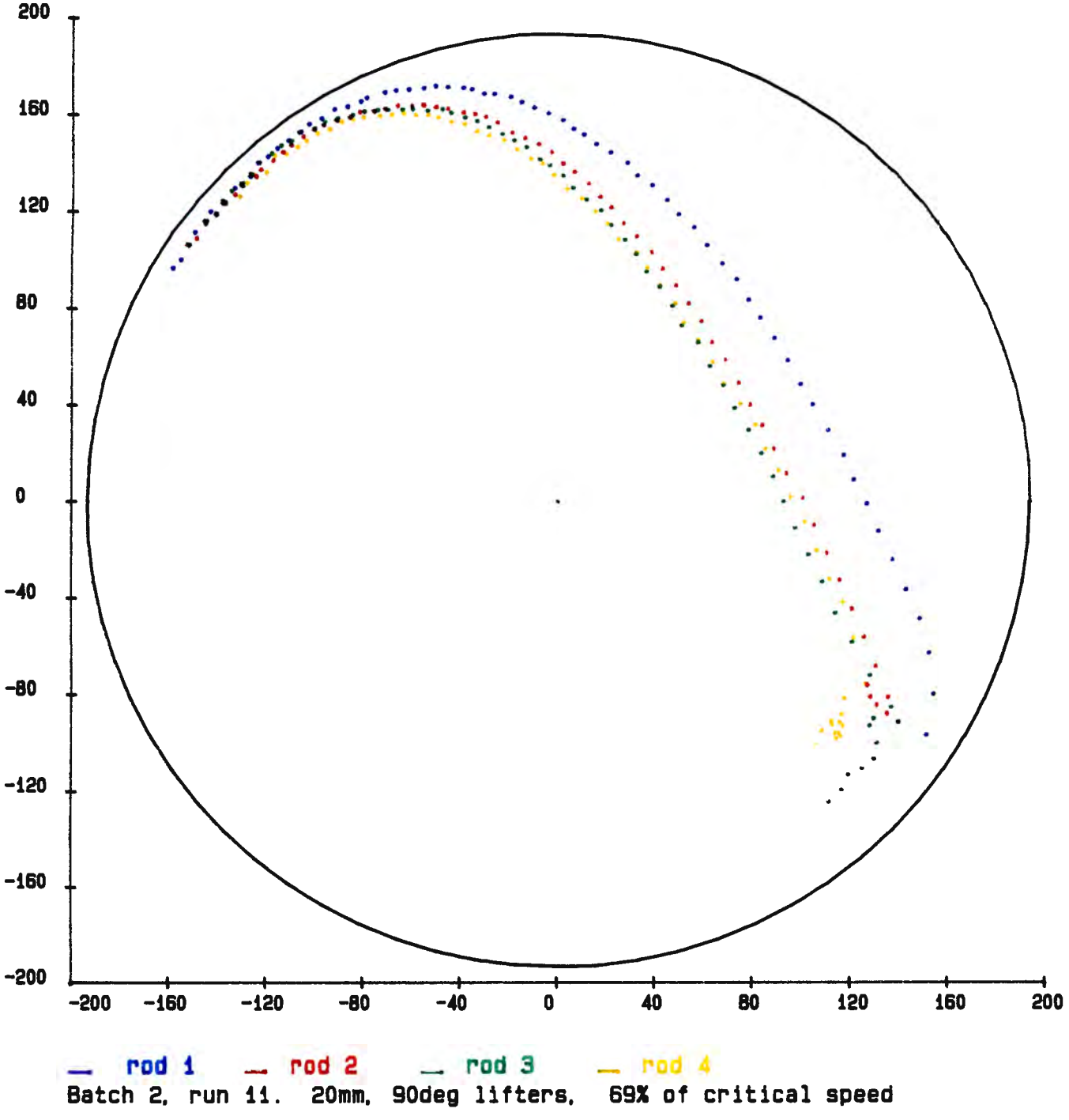

FIGURE I-4. Trajectories of a group of four rods at near 70% of critical speed

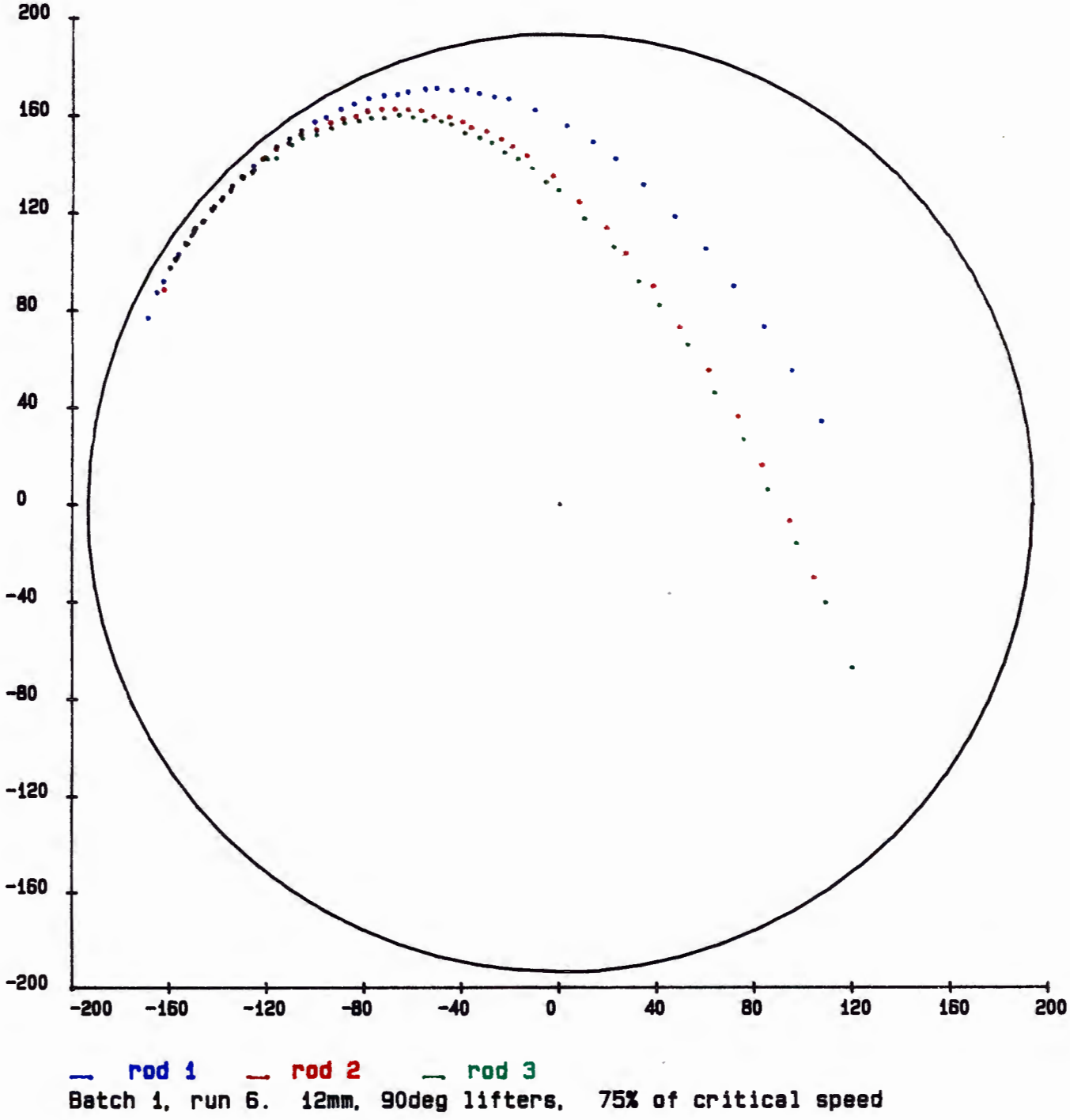

FIGURE I-5. Clustered trajectories of the outer two rods at 75% of critical speed

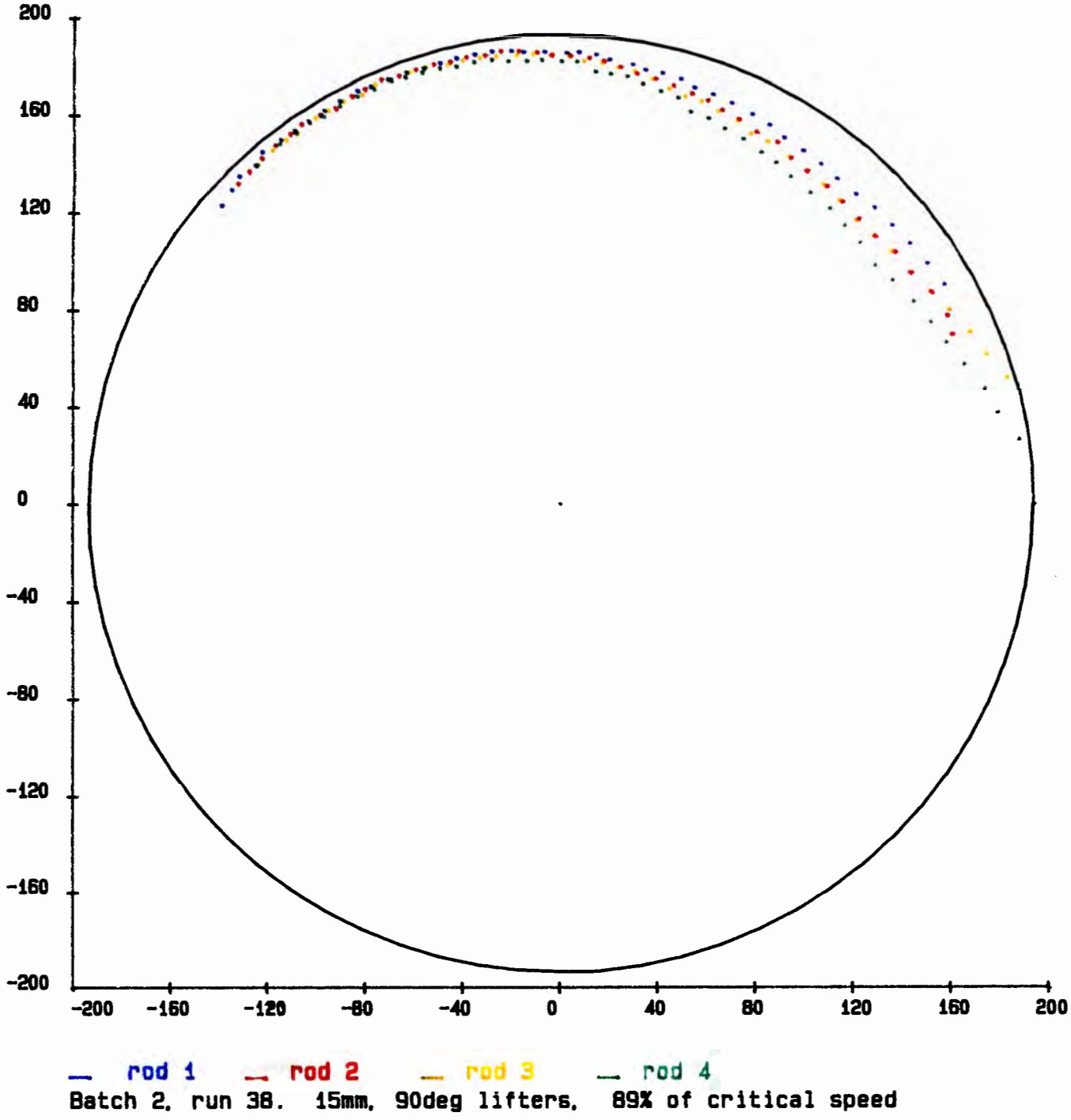

FIGURE I-6. The high flight-paths of rods at nearly 90% of critical speed

APPENDIX II

RELATIONSHIP BETWEEN β_0 AND α

Referring to figure I-1, In triangle $OA\Delta$:

$$\sin\beta_0 = \frac{\delta}{r_0} \qquad \text{(IIa)}$$

$$= \frac{\delta}{R - a} \qquad \text{where} \quad r_0 = R-a$$

In triangle $\Delta(OLO')$:

$$\frac{\delta+a}{R-h} = \sin\alpha \rightarrow \delta = (R-h).\sin\alpha - a \qquad \text{(IIb)}$$

$$\rightarrow \sin\beta_0 = \frac{(R-h).\sin\alpha - a}{r_0} \qquad \text{(IIc)}$$

APPENDIX III

SOLUTION OF THE DIFFERENTIAL EQUATION (15)

We have

$$\ddot{s} - \frac{2}{3}\Omega^2 s = -\frac{2}{3}g.\sin\gamma \qquad \text{(IIIa)}$$

$$\left(\ddot{s} - \frac{5}{7}\Omega^2 s = -\frac{5}{7}g.\sin\gamma \quad \text{for a sphere} \right)$$

where $\gamma = \gamma_0 + \Omega t$

This is a linear non-homogeneous second order differential equation of the form:

$$\frac{d^2s}{dt^2} + a.\frac{ds}{dt} + b.s = R(t)$$

where : $a = 0$

$$b = -\frac{2}{3}\Omega^2 \qquad \left(b = -\frac{5}{7}\Omega^2 \text{ for a sphere} \right)$$

$$R(t) = -\frac{2}{3}g.\sin\gamma \qquad \left(R(t) = -\frac{5}{7}g.\sin\gamma \right)$$

for m_1 and m_2 the roots of $m^2 + am + b = 0$

i.e. $m^2 - \frac{2}{3}\Omega^2 = 0$

We get $m_1 = \sqrt{\frac{2}{3}}\,\Omega, \qquad m_2 = -\sqrt{\frac{2}{3}}\,\Omega \qquad \left(\pm\sqrt{\frac{5}{7}}\Omega \text{ for a sphere} \right)$

These are real and distinct, so the solution is of the form[14]:

$$s = c_1 e^{m_1 t} + c_2 e^{m_2 t} + \frac{e^{m_1 t}}{m_1 - m_2}\int e^{-m_1 t} R(t)\, dt + \frac{e^{m_2 t}}{m_2 - m_1}\int e^{-m_2 t} R(t)\, dt$$

$$= c_1 e^{\sqrt{2/3}\Omega t} + c_2 e^{-\sqrt{2/3}\Omega t} + \frac{e^{\sqrt{2/3}\Omega t}}{2\sqrt{2/3}\Omega}\int e^{-\sqrt{2/3}\Omega t}\left(-\frac{2}{3}g\right)\sin\gamma\, dt + \frac{e^{-\sqrt{2/3}\Omega t}}{-2\sqrt{2/3}\Omega}\int e^{\sqrt{2/3}\Omega t}\left(-\frac{2}{3}g\right)\sin\gamma\, dt$$

now: $\int e^{at}.\sin(bt)dt = \dfrac{e^{at}(a.\sin(bt) - b.\cos(bt))}{a^2 + b^2}$

(the constant is incorporated into the differential equation).

$a = \pm \sqrt{2/3}.\Omega \quad ; \quad b = \Omega$

So:

$$S(t)=c_1e^{\sqrt{2/3}\Omega t} + c_2e^{\sqrt{2/3}\Omega t} - \frac{2ge^{\sqrt{2/3}\Omega t}}{3x2\sqrt{2/3}\Omega}\left[\frac{e^{-\sqrt{2/3}\Omega t}(-\sqrt{2/3}\Omega\sin\gamma-\Omega\cos\gamma)}{2/3\Omega^2 + \Omega^2}\right]$$

$$+ \frac{2g.e^{-\sqrt{2/3}\Omega t}}{3x2\ \sqrt{2/3}\Omega}\left[\frac{e^{\sqrt{2/3}\Omega t}(\sqrt{2/3}\Omega.\sin\gamma - \Omega.\cos\gamma)}{2/3\Omega^2 + \Omega^2}\right]$$

$$S(t) = c_1e^{\sqrt{2/3}\Omega t} + c_2e^{-\sqrt{2/3}\Omega t} - \frac{g\ \Omega}{\sqrt{2/3}\Omega 5\Omega^2}\ (-\sqrt{2/3}.\sin\gamma - \cos\gamma)$$

$$+ \frac{g\ \Omega}{\sqrt{2/3}\Omega 5\Omega^2}\ (\sqrt{2/3}.\sin\gamma - \cos\gamma)$$

$$= c_1e^{\sqrt{2/3}\Omega t} + c_2e^{-\sqrt{2/3}\Omega t} + \frac{g}{5\sqrt{2/3}\Omega^2}\ (\sqrt{2/3}.\sin\gamma+\cos\gamma+\sqrt{2/3}.\sin\gamma-\cos\gamma)$$

$$S(t) = c_1e^{\sqrt{2/3}\Omega t} + c_2e^{-\sqrt{2/3}\Omega t} + \frac{2}{5}.\frac{g}{\Omega^2}.\sin\gamma \qquad \text{(IIIb)}$$

$$\left(S(t) = c_1e^{\sqrt{5/7}\Omega t} + c_2e^{-\sqrt{5/7}\Omega t} + \frac{5g}{12\Omega^2}.\sin\gamma \quad \text{for a sphere} \right)$$

From the boundary conditions, at t = 0 at the point of equilibrium :

$S(0) = S_0$ which is known.

$\left(\dfrac{ds}{dt}\right)_{t=0} = 0$, rod has not started rolling yet.

For $t = 0$, $S_0 = S(0) = c_1 + c_2 + \dfrac{2}{5}.\dfrac{g}{\Omega^2}.\sin\gamma_0$ (IIIc)

$$\frac{ds}{dt} = \sqrt{2/3}\Omega c_1 . e^{\sqrt{2/3}\Omega t} - \sqrt{2/3}\Omega c_2 . e^{-\sqrt{2/3}\Omega t} + \frac{2\Omega g}{5\ \Omega^2} . \cos\gamma$$

$$\left(\frac{ds}{dt}\right)_{t=0} = 0 = \sqrt{2/3}\Omega c_1 - \sqrt{2/3}\Omega c_2 + \frac{2g}{5\Omega} . \cos\gamma_0$$

$$\rightarrow \quad c_2 = c_1 + \frac{2}{5}\sqrt{3/2}\frac{g}{\Omega^2} . \cos\gamma_0 .$$

Substituting back into (IIIc)

$$S_0 = c_1 + c_1 + \frac{2}{5}\sqrt{3/2}\frac{g}{\Omega^2} . \cos\gamma_0 + \frac{2g}{5\Omega^2} . \sin\gamma_0$$

$$\rightarrow c_1 = \frac{S_0}{2} - \sqrt{3/2}\frac{g}{5\Omega^2} . \cos\gamma_0 - \frac{g}{5\Omega^2} . \sin\gamma_0$$

and $$c_2 = \frac{S_0}{2} - \sqrt{3/2}\frac{g}{5\Omega^2} . \cos\gamma_0 - \frac{g}{5\Omega^2} . \sin\gamma_0 + \sqrt{3/2}\frac{2g}{5\Omega^2} . \cos\gamma_0 .$$

$$c_2 = \frac{S_0}{2} - \frac{g}{5\Omega^2} . \sin\gamma_0 + \sqrt{3/2}\frac{g}{5\Omega^2} . \cos\gamma_0$$

So:

$$S(t) = \frac{S_0}{2} e^{\sqrt{2/3}\Omega t} - \sqrt{3/2}\frac{g}{5\Omega^2} . e^{\sqrt{2/3}\Omega t} \cos\gamma_0 - \frac{g}{5\Omega^2} . e^{\sqrt{2/3}\Omega t} \sin\gamma_0$$

$$+ \frac{S_0}{2} . e^{-\sqrt{2/3}\Omega t} - \frac{g}{5\Omega^2} . e^{-\sqrt{2/3}\Omega t} \sin\gamma_0 + \sqrt{3/2}\frac{g}{5\Omega^2} . e^{-\sqrt{2/3}\Omega t} \cos\gamma_0$$

$$+ \frac{2g}{5\Omega^2} . \sin\gamma$$

$$S(t) = S_0 \left(\frac{e^{\sqrt{2/3}\Omega t} + e^{-\sqrt{2/3}\Omega t}}{2} \right) - \sqrt{3/2} . \frac{2g}{5\Omega^2} . \cos\gamma_0 \left(\frac{e^{\sqrt{2/3}\Omega t} - e^{-\sqrt{2/3}\Omega t}}{2} \right)$$

$$- \frac{2g}{5\Omega^2} . \sin\gamma_0 \left(\frac{e^{\sqrt{2/3}\Omega t} + e^{-\sqrt{2/3}\Omega t}}{2} \right) + \frac{2g}{5\Omega^2} . \sin\gamma$$

$$S(t) = S_0 \cosh\sqrt{2/3}\Omega t - \sqrt{3/2}.\frac{2g}{5\Omega^2}.\cos\gamma_0.\sinh\sqrt{2/3}\Omega t$$

$$- \frac{2g}{5\Omega^2}.\sin\gamma_0.\cosh\sqrt{2/3}\Omega t + \frac{2g}{5\Omega^2}.\sin\gamma$$

$$\boxed{S(t) = \left(S_0 - \frac{2g}{5\Omega^2}.\sin\gamma_0 \right)\cosh\sqrt{2/3}\Omega t - \frac{\sqrt{6}g}{5\Omega^2}.\cos\gamma_0.\sinh\sqrt{2/3}\Omega t + \frac{2g}{5\Omega^2}.\sin\gamma} \qquad \text{(IIId)}$$

$$\left(S(t) = \left[S_0 - \frac{5g}{12\Omega^2}.\sin\gamma_0 \right]\cosh\sqrt{5/7}\Omega t - \frac{\sqrt{35}g}{12\Omega^2}.\cos\gamma_0.\sinh\sqrt{5/7}\Omega t + \frac{5g}{12\Omega^2}.\sin\gamma \quad \text{for a sphere} \right)$$

$$\boxed{\frac{ds}{dt} = \sqrt{2/3}\Omega\left(S_0 - \frac{2g}{5\Omega^2}.\sin\gamma_0\right).\sinh\sqrt{2/3}\Omega t - \frac{2g}{5\Omega}\left(\cos\gamma_0.\cosh\sqrt{2/3}\Omega t - \cos\gamma\right)} \qquad \text{(IIIe)}$$

$$\left(\frac{ds}{dt} = \sqrt{5/7}\Omega\left[S_0 - \frac{5g}{12\Omega^2}.\sin\gamma_0 \right]\sinh\sqrt{5/7}\Omega t - \frac{5g}{12\Omega}(\cos\gamma_0.\cosh\sqrt{5/7}\Omega t - \cos\gamma) \quad \text{for a sphere} \right)$$

APPENDIX IV

SOLUTION OF THE DIFFERENTIAL EQUATION (25)

We have:

$$\frac{d^2s}{dt^2} - \Omega^2 s = g[\mu_K.\cos(\gamma_0 + \Omega t) - \sin(\gamma_0 + \Omega t)] + \Omega^2 \delta\mu_K \qquad \text{(IVa)}$$

This is a linear non-homogeneous second order differential equation of the form:

$$\frac{d^2s}{dt^2} + a\frac{ds}{dt} + bs = R(t)$$

where: $a = 0$

$b = -\Omega^2$

$R(t)$= right hand side

for m_1 amd m_2 the roots of $m^2 + am + b = 0$.
We get $m_1 = \Omega$, $m_2 = -\Omega$.
These are real and distinct, so the solution is of the form[14]:

$$S = c_1 e^{\Omega t} + c_2 e^{-\Omega t} + \frac{e^{\Omega t}}{2\Omega}\int e^{-\Omega t}\{g[\mu_K\cos(\gamma_0+\Omega t) - \sin(\gamma_0+\Omega t)] + \Omega^2\delta\mu_k\}dt$$

$$+ \frac{e^{-\Omega t}}{-2\Omega}\int e^{\Omega t}\{g[\mu_K\cos(\gamma_0+\Omega t) - \sin(\gamma_0+\Omega t)] + \Omega^2\delta\mu_k\}dt \qquad \text{(IVb)}$$

for standard integrals:

$$\int e^{at}.\sin(bt)dt = e^{at}.\frac{\{a.\sin(bt) - b.\cos(bt)\}}{a^2 + b^2}$$

and $$\int e^{at}.\cos(bt)dt = e^{at}.\frac{\{a.\cos(bt) + b.\sin(bt)\}}{a^2 + b^2}$$

The constants being incorporated into the differential equation. Dividing each integral in equation (IVb) into sin, cos and $\Omega^2\delta\mu_K$ components, the first integral becomes:

$$g\int e^{-\Omega t}\mu_K.\cos(\gamma_0+\Omega t)dt - g\int e^{-\Omega t}.\sin(\gamma_0+\Omega t)dt + \int e^{-\Omega t}\Omega^2\delta\mu_K dt =$$

$$ge^{-\Omega t}\mu_K\left(\frac{-\Omega\cos(\gamma_0+\Omega t)+\Omega\sin(\gamma_0+\Omega t)}{2\Omega^2}\right) - ge^{-\Omega t}\left(\frac{-\Omega\sin(\gamma_0+\Omega t)-\Omega\cos(\gamma_0+\Omega t)}{2\Omega^2}\right)$$

$$- \frac{\Omega^2\delta e^{-\Omega t}\mu_k}{\Omega}$$

The second integral becomes:

$$g\mu_K e^{\Omega t}\,\frac{(\Omega\cos\gamma + \Omega\sin\gamma)}{2\Omega^2} - \frac{g.e^{\Omega t}}{2\Omega^2}(\Omega\sin\gamma - \Omega\cos\gamma) + \frac{\Omega^2\delta.e^{\Omega t}\mu_K}{\Omega}$$

using $\gamma = \gamma_0 + \Omega t$ for simplicity of writing.
This yields:

$$S \doteq c_1e^{\Omega t} + c_2e^{-\Omega t} + \frac{e^{\Omega t}ge^{-\Omega t}\mu_K}{2\Omega.2\Omega^2}\,(-\Omega\cos\gamma + \Omega\sin\gamma)$$

$$+ \frac{e^{\Omega t}\Omega.\sin\gamma.g.e^{-\Omega t}}{2\Omega.2\Omega^2} + \frac{e^{\Omega t}.\cos\gamma.\Omega g.e^{-\Omega t}}{2\Omega.2\Omega^2} - \frac{\Omega\delta.e^{-\Omega t}e^{\Omega t}\mu_K}{2\Omega.\Omega}$$

$$- \frac{e^{-\Omega t}g\mu_K.e^{\Omega t}.\Omega.\cos\gamma}{2\Omega.2\Omega^2} - \frac{g\mu_K.e^{\Omega t}.e^{-\Omega t}\Omega.\sin\gamma}{2\Omega.2\Omega^2}$$

$$+ \frac{e^{-\Omega t}g.e^{\Omega t}.\Omega.\sin\gamma}{2\Omega.2\Omega^2} - \frac{e^{-\Omega t}g.e^{\Omega t}.\Omega.\cos\gamma}{2\Omega.2\Omega^2} - \frac{\Omega^2\delta.e^{\Omega t}.e^{-\Omega t}.\mu_K}{2\Omega.\Omega}$$

$$S = c_1e^{\Omega t} + c_2e^{-\Omega t} - \frac{\mu_K g.\cos\gamma}{4\Omega^2} + \frac{\mu_K g.\sin\gamma}{4\Omega^2} + \frac{g.\sin\gamma}{4\Omega^2} + \frac{g.\cos\gamma}{4\Omega^2}$$

$$- \frac{g\mu_K.\cos\gamma}{4\Omega^2} - \frac{g\mu_K.\sin\gamma}{4\Omega^2} + \frac{g.\sin\gamma}{4\Omega^2} - \frac{g.\cos\gamma}{4\Omega^2} - \frac{\delta\mu_K}{2} - \frac{\delta\mu_K}{2}$$

$$S = c_1e^{\Omega t} + c_2e^{-\Omega t} - \frac{\mu_K g.\cos\gamma}{2\Omega^2} + \frac{g.\sin\gamma}{2\Omega^2} - \delta\mu_K \qquad \text{(IVc)}$$

The boundary conditions are $S(0) = S_I$, $\left(\frac{ds}{dt}\right)_{t=0} = v_I$

for consistency: $\gamma_{t=0} = \gamma_I$

$$S(0) = c_1 + c_2 - \frac{\mu_K g.\cos\gamma_I}{2\Omega^2} + \frac{g.\sin\gamma_I}{2\Omega^2} - \delta\mu_K = S_I$$

$$c_1 = S_I - c_2 + \frac{g}{2\Omega^2}(\mu_K.\cos\gamma_I - \sin\gamma_I) + \delta\mu_K \qquad \text{(IVd)}$$

$$\frac{ds}{dt} = \Omega c_1 e^{\Omega t} - \Omega c_2 e^{-\Omega t} + \frac{\mu_K g.\sin\gamma}{2\Omega} + \frac{g.\cos\gamma}{2\Omega}$$

$$\left(\frac{ds}{dt}\right)_{t=0} = v_I = \Omega c_1 - \Omega c_2 + \frac{g}{2\Omega}(\mu_K.\sin\gamma_I + \cos\gamma_I)$$

$$c_2 = c_1 - \frac{v_I}{\Omega} + \frac{g}{2\Omega^2}(\mu_K.\sin\gamma_I + \cos\gamma_I) \qquad \text{(IVe)}$$

Substituting (IVe) into (IVd) yields:

$$c_1 = S_I - c_1 + \frac{v_I}{\Omega} - \frac{g}{2\Omega^2}(\mu_K.\sin\gamma_I + \cos\gamma_I) + \frac{g}{2\Omega^2}(\mu_K.\cos\gamma_I - \sin\gamma_I)$$

$$+\delta\mu_k$$

$$c_1 = \frac{S_I}{2} + \frac{v_I}{2\Omega} - \frac{g}{4\Omega^2}(\mu_K.\sin\gamma_I + \cos\gamma_I) + \frac{\delta}{2}\mu_K + \frac{g}{4\Omega^2}(\mu_K.\cos\gamma_I - \sin\gamma_I)$$

So by equation (IVe)

$$c_2 = \frac{S_I}{2} + \frac{v_I}{2\Omega} - \frac{g}{4\Omega^2}(\mu_K.\sin\gamma_I + \cos\gamma_I) + \frac{\delta\mu_K}{2} + \frac{g}{4\Omega^2}(\mu_K.\cos\gamma_I - \sin\gamma_I)$$

$$- \frac{v_I}{\Omega} + \frac{g}{2\Omega^2}(\mu_K.\sin\gamma_I + \cos\gamma_I)$$

$$c_2 = \frac{S_I}{2} - \frac{v_I}{2\Omega} + \frac{g}{4\Omega^2}(\mu_K.\sin\gamma_I + \cos\gamma_I) + \frac{g}{4\Omega^2}(\mu_K.\cos\gamma_I - \sin\gamma_I) + \frac{\delta\mu_K}{2}$$

Substituting c_1 and c_2 into equation (IVc) yields:

$$S = \frac{S_I}{2}e^{\Omega t} + \frac{v_I}{2\Omega}e^{\Omega t} - \frac{g}{4\Omega^2}(\mu_K.\sin\gamma_I + \cos\gamma_I)e^{\Omega t} + \frac{\delta e^{\Omega t}}{2}\mu_K$$

$$+ \frac{g}{4\Omega^2}(\mu_K.\cos\gamma_I - \sin\gamma_I)e^{\Omega t} + \frac{S_I}{2}e^{-\Omega t} - \frac{v_I}{2\Omega}e^{-\Omega t}$$

$$+ \frac{g}{4\Omega^2}(\mu_K.\sin\gamma_I + \cos\gamma_I)e^{-\Omega t} + \frac{g}{4\Omega^2}(\mu_K.\cos\gamma_I - \sin\gamma_I)e^{-\Omega t}$$

$$+ \frac{\delta e^{-\Omega t}}{2}\mu_K - \frac{\mu_K g.\cos\gamma}{2\Omega^2} + \frac{g.\sin\gamma}{2\Omega^2} - \delta\mu_K$$

$$S = S_I\left(\frac{e^{\Omega t} + e^{-\Omega t}}{2}\right) + \frac{v_I}{\Omega}\left(\frac{e^{\Omega t} - e^{-\Omega t}}{2}\right) - \frac{g}{2\Omega^2}(\mu_K \sin\gamma_I + \cos\gamma_I)\left(\frac{e^{\Omega t} - e^{-\Omega t}}{2}\right)$$

$$+ \frac{g}{2\Omega^2}(\mu_K.\cos\gamma_I - \sin\gamma_I)\left(\frac{e^{\Omega t} + e^{-\Omega t}}{2}\right) + \frac{g}{2\Omega^2}(\sin\gamma - \mu_K.\cos\gamma)$$

$$+ \delta\left(\frac{e^{\Omega t} + e^{-\Omega t}}{2}\right)\mu_K - \delta\mu_K$$

$$S = S_I.\cosh\Omega t + \frac{v_I}{\Omega}.\sinh\Omega t - \frac{g}{2\Omega^2}(\mu_k.\sin\gamma_I + \cos\gamma_I)\sinh\Omega t$$

$$+ \frac{g}{2\Omega^2}(\mu_K.\cos\gamma_I - \sin\gamma_I)\cosh\Omega t + \frac{g}{2\Omega^2}(\sin\gamma - \mu_K.\cos\gamma)$$

$$+ \delta.\cosh\Omega t.\mu_K - \delta\mu_K$$

$$S = \left[S_I + \delta\mu_K + \frac{g}{2\Omega^2}(\mu_K.\cos\gamma_I - \sin\gamma_I)\right]\cosh\Omega t +$$

$$\left[\frac{v_I}{\Omega} - \frac{g}{2\Omega^2}\left\{\mu_K.\sin\gamma_I + \cos\gamma_I\right\}\right]\sinh\Omega t - \frac{g}{2\Omega^2}\left[\mu_K.\cos\gamma - \sin\gamma\right] - \delta\mu_K$$

(IVf)

$$\frac{ds}{dt} = \Omega\left[S_I + \delta\mu_K + \frac{g}{2\Omega^2}(\mu_K.\cos\gamma_I - \sin\gamma_I)\right]\sinh\Omega t +$$

$$\left[v_I - \frac{g}{2\Omega}\left\{\mu_K\sin\gamma_I + \cos\gamma_I\right\}\right]\cosh\Omega t - \frac{g}{2\Omega}\left[-\mu_K.\sin(\gamma_I+\Omega t) - \cos(\gamma_I+\Omega t)\right]$$

(IVg)

APPENDIX V

RELATIONSHIP BETWEEN SOME VARIABLES

V.1. Relationship between α and ρ

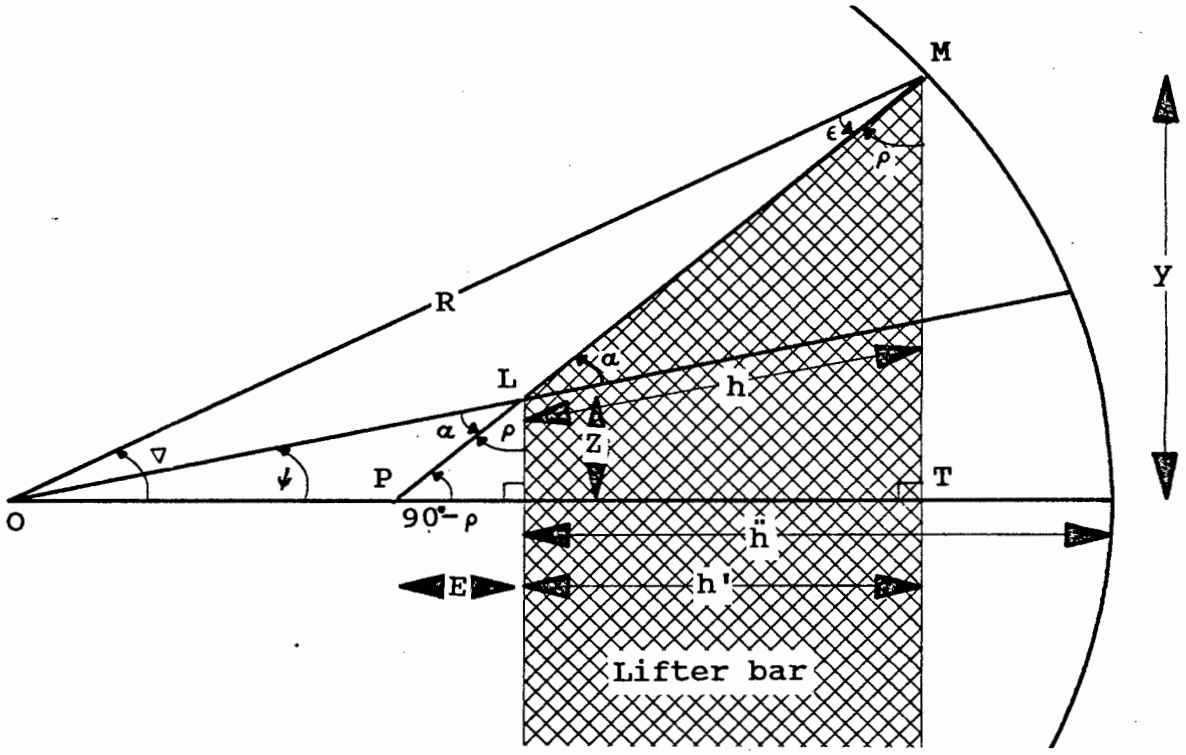

FIGURE V-1. Detail of a lifter bar

h' ≡ height of lifter bar

y ≡ ½ width of lifter bar

R ≡ radius of mill

ρ ≡ face angle of lifter

α ≡ angle between lifter face and radius vector

The variables h', y, R, and ρ are all known.

Referring to figure V-1, in triangle MTP, it can be seen that:

$$\tan\rho = \frac{E+h'}{y} \quad \rightarrow \quad E = y.\tan\rho - h'$$

In triangle LPQ :

$$\tan\rho = \frac{E}{Z} \quad \rightarrow \quad Z = \frac{E}{\tan\rho}$$

In triangle OQL :

$$\tan\psi = \frac{Z}{R-h''}$$

From triangle OMT :

$$R - h'' = \sqrt{R^2 - y^2} - h'$$

$$\tan\psi = \frac{E}{\left(\sqrt{R^2 - y^2} - h'\right)\tan\rho}$$

$$\tan\psi = \frac{y.\tan\rho - h'}{\left(\sqrt{R^2 - y^2} - h'\right).\tan\rho}$$

$$\boxed{\psi = \arctan\left[\frac{y\tan\rho - h'}{\left(\sqrt{R^2 - y^2} - h'\right)\tan\rho}\right]} \qquad (Va)$$

But if $\rho = 90^0$ $\qquad \psi = \arctan\dfrac{y}{\sqrt{R^2 - y^2} - h'}$ $\qquad (Va_1)$

By the external angle to triangle OPL

$$90^0 - \rho = \psi + \alpha$$

$$\alpha = 90^0 - \rho - \psi \qquad (Vb)$$

$$\boxed{\alpha = 90^0 - \rho - \arctan\left[\frac{y.\tan\rho - h'}{\left(\sqrt{R^2 - y^2} - h'\right)\tan\rho}\right]} \qquad (Vc)$$

This relationship is important for specifying the manufacture of a lifter-bar, as the face angle ρ must be given, whereas angle α

is used in the calculations.

As α will be derived from the calculations of desired charge motions, it is also useful to have ρ in terms of α.

V.2. ρ in terms of α

From triangle OLM, and using the sine rule :

$$\frac{\sin(180 - \alpha)}{R} = \frac{\sin \epsilon}{(R - h)}$$

but: $\sin(180 - \alpha) = \sin\alpha$.

So: $\epsilon = \arcsin\left[\sin\alpha\left(\frac{R-h}{R}\right)\right]$

From Δ OTM :

$$\cos(\epsilon + \rho) = \frac{y}{R}$$

$$\rightarrow \quad \epsilon + \rho = \arccos\left(\frac{y}{R}\right)$$

Therefore:

$$\boxed{\rho = \arccos\left(\frac{y}{R}\right) - \arcsin\left[\sin\alpha\left(\frac{R-h}{R}\right)\right]} \qquad \text{(Vd)}$$

$$\psi = 90 - \alpha - \rho \qquad \text{(Ve)}$$

V.3. Relationship between h and h'

In the calculations h is used, but h' is the specified design height of the lifter, so it is necessary to determine the relationship between them. Referring to figure VI, it can be seen that:

$$h = R - \overline{OL} \qquad h'' = R - \overline{OQ}$$

$$h - h'' = R - R + \overline{OQ} - \overline{OL}$$

$$\rightarrow \quad h = h'' + \overline{OQ} - \overline{OL} \qquad \text{(Vf)}$$

but:

$$\overline{OL} = \frac{\overline{OQ}}{\cos\psi} \qquad \text{and} \qquad \overline{OQ} = R - h''$$

So: $h = h'' + \overline{OQ}\left(1 - \frac{1}{\cos\psi}\right)$

$$= h'' + R - h'' - \frac{(R - h'')}{\cos\psi}$$

$$= R - \frac{R - h''}{\cos\psi}$$

we have $R - h'' = \sqrt{R^2 - y^2} - h'$

So $$\boxed{h = R - \frac{\sqrt{R^2 - y^2} - h'}{\cos\psi}} \qquad \text{(Vg)}$$

where ψ is given by equation (Va).

and $$\boxed{h' = \sqrt{R^2 - y^2} + (h-R).\cos\psi} \qquad \text{(Vh)}$$

Where ψ given by equation (Ve).

APPENDIX VI

SAMPLE CALCULATION OF ROD MOTION IN A ROTARY MILL

The following variables are required:

Static coefficient of friction; μ_s
Kinetic coefficient of friction; μ_k
Internal radius of mill; R
Rod radius; a
Lifter-bar face-angle; ρ
Lifter height; h'
Lifter width; 2y (y = ½ Lifter width)
Mill speed in rpm, or % of critical => Ω rad.s^{-1}

Certain factors used throughout the calculations can then be calculated:

$r_0 = R - a$

$$\psi = \arctan\left[\frac{y.\tan\rho - h'}{(\sqrt{R^2 - y^2} - h')\tan\rho}\right] \qquad \text{equation (Va) (VIa)}$$

If $\rho = 90^\circ$, $$\psi = \arctan\left[\frac{y}{\sqrt{R^2 - y^2} - h'}\right] \qquad (VIa_1)$$

$$\alpha = 90^\circ - \rho - \psi \qquad \text{equation (Vb) (VIb)}$$

$$\Omega = 2\Pi \times \frac{rpm}{60} \quad \text{or} \quad \Omega = \frac{1{,}88 \times \%\text{critical speed}}{\sqrt{R}}$$

$$h = R - \frac{\sqrt{R^2 - y^2} - h'}{\cos\psi} = \text{radial Lifter height} \qquad \text{equation (Vg) (VIc)}$$

$$\delta = \sin\alpha(R - h) - a \qquad (VId)$$

$$\beta_0 = \arcsin\left(\frac{\delta}{r_0}\right) \qquad \left(\equiv \arctan\frac{\delta}{\sqrt{r_\delta^2 - \delta^2}}\right) \qquad \begin{matrix}\text{If no arcsin}\\ \text{or arccos}\\ \text{fn. available}\end{matrix} \qquad (VIe)$$

equation (IIc)

$$S_0 = r_0.\cos\beta_0 \qquad \text{(VIf)}$$

$$S_L = (R-h).\cos\alpha \qquad \text{(VIg)}$$

$$\beta_L = \arctan\left(\frac{\delta}{S_L}\right) \qquad \text{(VIh)}$$

$$r_L = \frac{S_L}{\cos\beta_L} \qquad \text{(VIi)}$$

VI.1. Calculating the point of equilibrium

This is the point at which the forces on the rod are in equilibrium, so it will move away from the shell of the mill and start to roll down the Lifter face.

Using equation (5)

Sliding + Rolling

$$\sin\gamma_0 - \mu_s \cos\gamma_0 = \frac{\Omega^2}{g}\left[r_0\sqrt{1 - \left(\frac{\delta}{r_0}\right)^2} - \mu_s\delta \right] \qquad \text{(VIj)}$$

For the condition of the static coefficient of friction being zero, refer to section VI.7.

Here an iterative process of substituting values for γ_0 is used to solve equation (VIj). Starting with small γ_0 and increasing it until the left hand side of the equation is greater than the right hand side, then returning to the second last γ_0 used and increasing it by smaller intervals. This is repeated until a solution of the desired degree of accuracy is obtained.

Then $\phi_0 = \gamma_0 - \beta_0$ (VIk)

The point of equilibrium is then defined by ϕ_0, r_0.

VI.2. Maximum slope for pure rolling

The rod will start off by rolling, but once a certain critical angle of slope of the lifter-bar is passed, the rod will start to slip.

The minimum value of γ_m can initially be calculated by using equation (20) with $S = S_L$.

$$\mathrm{Sin}\gamma_{m(min)} - 3\,\mu_s \cos\gamma_{m(min)} = \frac{\Omega^2}{g}(3\delta\mu_s + S_L) \qquad \text{(VIl)}$$

The iterative method is again used to derive $\gamma_{m(min)}$.

VI.3. Pure rolling until $\delta_{m(min)}$ or S_L

Equation (16) is solved for t, using $S = S_L$

$$S_L = \left(S_0 - \frac{2g}{5\Omega^2}.\mathrm{Sin}\gamma_0\right).\cosh\sqrt{\frac{2}{3}}\Omega t$$

$$- \frac{\sqrt{6}g}{5\Omega^2}\cos\gamma_0.\sinh\sqrt{\frac{2}{3}}\Omega t + \frac{2g}{5\Omega^2}\sin(\gamma_0 + \Omega t) \qquad \text{(VIm)}$$

Naturally angles in radians must be used in this equation. The maximum value of t for $\gamma \leq \gamma_{m(min)}$, is given by $\gamma_0 + \Omega t \leq \gamma_{m(min)}$, ie. $t_{min} = (\gamma_{m(min)} - \gamma_0)/\Omega$.
Equation (VIl) is solved for this t_{min}. If $S_{min} \leq S_L$ then the rod rolls until the tip of the lifter is reached and equation (VIm) must be solved iteratively. If $S_{min} > S_L$ then this S_{min} is carried directly to 'pure rolling until γ_m'.

VI.4. Pure rolling until γ_m

The constraints given by equation (20) are used, which allows for pure rolling up to γ_m, while obeying the limit given by equation (21).

$$0{,}6\,\sin(\gamma_0 + \Omega t) - 3\mu_s.\cos(\gamma_0 + \Omega t) \leq$$

$$\frac{\Omega^2\delta 3\mu_s}{g} + \left(\frac{S_0\Omega^2}{g} - 0{,}4\,\sin\gamma_0\right).\cosh\sqrt{\frac{2}{3}}\Omega t - \frac{\sqrt{6}}{5}\cos\gamma_0.\sinh\sqrt{\frac{2}{3}}\Omega t \qquad \text{(VIn)}$$

This is solved iteratively for t_I at the equality, t_I then yields S_I by equation (16).

$$S_I = S(t_I) = \left(So - \frac{2g}{5\Omega^2}.\sin\gamma_0\right).\cosh\sqrt{\frac{2}{3}}\,\Omega t_I$$

$$- \frac{\sqrt{6}g}{5\Omega^2}\cos\gamma_0.\sinh\sqrt{\frac{2}{3}}\,\Omega t + \frac{2g}{5\Omega^2}.\sin(\gamma_0 + \Omega t_I) \qquad \text{(VIo)}$$

V_I is derived from equation (17)

$$\left(\frac{ds}{dt}\right)_{t=t_I} = V_I = \frac{\sqrt{2}\Omega}{\sqrt{3}}\left(S_o - \frac{2g}{5\Omega^2}\sin\gamma_o\right).\sinh\frac{\sqrt{2}\Omega t_I}{\sqrt{3}}$$

$$- \frac{2g}{5\Omega}\left(\cos\gamma_o\cosh\frac{\sqrt{2}\Omega t_I}{\sqrt{3}} - \cos(\gamma_o + \Omega t_I)\right) \qquad \text{(VIp)}$$

$$\gamma_m = \gamma_o + \Omega t_I \qquad \text{(VIq)}$$

$$\gamma_I = \gamma_m$$

The possibility of N being negative is also tested for constantly, using equation (28).

$$g.\cos\gamma + \Omega^2\delta < 0 \qquad \text{(VIr)}$$

VI.5. Sliding after rolling

Equation (26) is solved, again using iterative methods, with $S(t) = S_L$

For the condition of the static coefficient of friction being zero and the kinetic coefficient of friction being greater than zero, refer to section VI.7.

$$S_L = \left[S_I + \delta\mu_k + \frac{g}{2\Omega^2}.(\mu_k.\cos\gamma_I - \sin\gamma_I)\right].\cosh\Omega t$$

$$+ \left[\frac{V_I}{\Omega} - \frac{g}{2\Omega^2}(\mu_k.\sin\gamma_I + \cos\gamma_I)\right].\sinh\Omega t$$

$$- \frac{g}{2\Omega^2}\left[\mu_k.\cos(\gamma_I + \Omega t) - \sin(\gamma_I + \Omega t)\right] - \delta\mu_k \qquad \text{(VIs)}$$

This yields t_L, which gives:

$$\gamma_L = \gamma_I + \Omega t_L \qquad \text{(VIt)}$$

$$\phi_L = \gamma_L - \beta_L \qquad \text{(VIu)}$$

$$V_L = \Omega\left[S_I + \delta\mu_k + \frac{g}{2\Omega^2}.(\mu_k.\cos\gamma_I - \sin\gamma_I)\right].\sinh\Omega t_L$$

$$+ \left[V_I - \frac{g}{2\Omega}(\mu_k.\sin\gamma_I + \cos\gamma_I)\right].\cosh\Omega t_L$$

$$- \frac{g}{2\Omega}\left[-\mu_k.\sin\gamma_L - \cos\gamma_L\right] \qquad \text{equation (27)}$$

(VIv)

VI.6. Free-flight trajectory

The coordinates are changed to cartesian (x, y) coordinates

$$(X_L,\ Y_L) = (r_L.\cos\phi_L\ ,\ r_L.\sin\phi_L) \qquad \text{(VIw)}$$

Now V_L is the velocity along the face of the lifter, to this the velocity due to the rotation of the mill must be added to obtain the net velocity of the rod. This additional velocity component is tangential, and equals $r_L\Omega$:

$$\rightarrow\ (V_{XL};\ V_{YL}) = (V_L.\cos\gamma_L - \Omega r_L.\sin\phi_L\ ;\ V_L.\sin\gamma_L + \Omega r_L.\cos\phi_L) \qquad \text{(VIx)}$$

$$\text{Net velocity } V_{Ln} = \sqrt{V_{xL}^2 + V_{yL}^2} \qquad \text{(VIy)}$$

$$\text{angle of departure } \sigma_L = \arctan\left(-\frac{V_{YL}}{V_{XL}}\right) \text{ to horizontal} \qquad \text{(VIz)}$$

$$\text{In flight } x = x_L + V_{xL}t \qquad \text{(VIaa)}$$

$$y = y_L + V_{yL}t - \tfrac{1}{2}gt^2 \qquad \text{(VIab)}$$

This can be set within the limit :

$x^2 + y^2 \leq r_0^2$, at which point the rod strikes the mill shell. (VIac)

$$\text{ie. } {}^1/_4 g^2t^4 - V_{y1}gt^3 + (V_{y1}^2 - Y_{Lg})t^2 + 2(X_LV_{xL} + Y_LV_{yL})t + (X_L^2 + Y_L^2 - r_0^2) = 0 \qquad \text{(VIad)}$$

$$\text{The impact point is given by } (X_E\ ,\ Y_E) \text{ or } (r_0\ ,\ \phi_E) \qquad \text{(VIae)}$$

$$\text{where } \phi_E = \arctan\left(\frac{Y_E}{X_E}\right) + 180^\circ \qquad \text{(VIaf)}$$

$$\text{Then } V_{xE} = V_{xL} \qquad \text{(VIag)}$$

$$V_{yE} = V_{yL} - gt \qquad \text{(VIah)}$$

$$V_E = \sqrt{V_{yE}^2 + V_{xE}^2} \qquad \text{(VIai)}$$

$$\text{at angle } \sigma_E = \arctan\left(\frac{V_{yE}}{V_{xE}}\right) \text{ to horizontal} \qquad \text{(VIaj)}$$

VI.7. Static coefficient of friction zero and kinetic coefficient of friction greater than zero

Equation VIj can be simplified in this case to:

$$\sin\gamma_0 = \frac{\Omega^2}{g}\left(r_0\sqrt{1-\left(\frac{\delta}{r_0}\right)^2}\right)$$

$$\gamma_0 = \arcsin\left(\frac{\Omega^2}{g}r_0\sqrt{1-\left(\frac{\delta}{r_0}\right)^2}\right)$$

$$\gamma_0 = \arcsin\left(\frac{\Omega^2}{g}r_0.\cos\beta_0\right) \qquad \text{(VIj')}$$

This gives the point of equilibrium. Because the static coefficient of friction is zero, the rod immediately starts to slip. So we move on to equation (VIs).

$$S_L = \left[S_0 + \delta\mu_k + \frac{g}{2\Omega^2}(\mu_k.\cos\gamma_0 - \sin\gamma_0)\right].\cosh\Omega t$$

$$- \frac{g}{2\Omega^2}\left[(\mu_k.\sin\gamma_0+\cos\gamma_0)\sinh\Omega t + \mu_k.\cos(\gamma_0 + \Omega t) - \sin(\gamma_0 + \Omega t)\right]$$

$$-\delta\mu_k \qquad \text{(VIs')}$$

$$\gamma_L = \gamma_0 + \Omega t \qquad \text{(VIt')}$$

$$V_L = \Omega\left[S_0 + \delta\mu_k + \frac{g}{2\Omega^2}.(\mu_k.\cos\gamma_0 - \sin\gamma_0)\right].\sinh\Omega t_L$$

$$- \frac{g}{2\Omega}(\mu_k.\sin\gamma_0 + \cos\gamma_0)\cosh\Omega t_L - \frac{g}{2\Omega}(-\mu_k.\sin\gamma_L - \cos\gamma_L) \qquad \text{(VIv')}$$

This gives the velocity at the tip of the lifter-bar, as the rod is projected into flight. The same equations apply from here on as in the standard calculation.

VI.8. Summary

This set of equations supply the logical sequence for calculating the motion of an isolated rod in a rotary mill with flat-faced lifter-bars of any face-angle and of any height.

APPENDIX VII

LIST OF APPARATUS

VII.1. Filming of the charge motion

1) Cylindrical test mill
   - 387mm diameter by 300mm long (internally)
   - 2 of 25mm thick armourplate glass ends
   - 2 of rubber rims fitted to the glass
   - 2 of 280mm diameter steel flanges, with an 86mm flange width
   - 16 of 10mm bolts to fasten the flanges
   - 48 of 8mm allen head screws to fasten the lifter bars
   - disk of ½mm thick steel sheet
2) Mounting-rig for the mill
   - 100mm diameter rubber wheels
   - AC electric motor, 0,75hp, 1460rpm
   - Stone Wallworth continuously variable mechanical gearbox
3) Cine' film, 16mm, 7 of 122m reels, Ektachrome high speed daylight film, 7251, colour
4) Hycam, rotating prism, 16mm, high speed motion picture camera
5) Flood lights, 2 of 2000W
6) Strobe
7) Steel rods, 425 of 12mm diameter and 295mm long
8) Lifter-bars, 300mm long with a 25mm wide base. Three by 8mm screwholes each 8mm deep in the base, two holes 25mm from either end, one hole 126mm from the front end of the lifter. 16 of each shape
   - 90° lifters :6mm, 12mm, 14,4mm, 20mm, and 25mm high
   - 75° lifters 25mm high
   - 60° lifters 25mm high
   - 45° lifters 25mm high
   - 30° lifters 14,4mm high
   - 90° for 12mm and 60° for 13mm, total height 25mm lifters

VII.2. Analysis of the films

1) Eiki 16mm projector with 25mm, wide angle lens
2) Summagraphics MM101 graphics tablet

3) Four-function mouse
4) Sperry personal computer
5) HP7475A plotter
6) Printer

VII.3. Lifter bar vibration

1) Accelerometer
2) Shielded cable, 20m
3) Charge amplifier
4) Storage oscilloscope
5) Camera, 35mm, with oscillascope mounting bracket

VII.4. Measurement of the coefficients of friction

1) Sliding rack
2) Sliding sheet
3) Sliding sample
4) Vibrator, maximum thrust 196N
5) Foam sheets, 60mm thick
6) Video camera
7) Video equipment capable of frame-by-frame advancement of the video

VII.5. Power draw of the mill

1) Multimeter, AC current range up to 10A
2) Switch
3) Oscilloscope, dual input

APPENDIX VIII

RESULTS

VIII.1. Filming of charge motion

The following table VIII-1 is a full summary of the conditions of each run that was filmed.

TABLE VIII-1

Summary of the runs that were filmed

F	RUN	LIFTER BAR ANGLE	LIFTER BAR HEIGHT	% FILLING	SPEED %CRIT	COMMENTS
BATCH 1						
1	1	smooth		45	90	stop watch not running
	2	"		45	75	
	3	"		15	75	scrapped, as too much slip at this low load
	4	"		15	90	
	5	90	12	15	90	problem with 4 rods jamming between lifters
	6	"	"	15	75	
	7	"	"	45	90	charge centrifuged
	8	"	"	45	75	almost centrifuge,speed unsure
2	17	30	14,5	45	75	
	18	"	"	45	90	speed unsure
	19	"	"	15	90	
	20	"	'	15	75	speed unsure
	21	45	25	15	75	violent,bouncing rod motion, not good for motion analysis
	22	"	"	15	90	
	23	"	"	45	90	Tendency to centrifuge,due to fluctuations in mill speed. If power draw drops,speed goes up
	24_A	"	"	45	75?	speed incorrect
	24_B	"	"	"	75	repeated run at correct speed
3	25	60	25	45	75	
	26	"	"	45	90	
	27_A	"	"	15	90	centrifuged for both runs, speed unsure
	27_B	"	"	15	90	
	28	"	"	15	75	
	29	75	25	15	75	speed most likely higher
	32	"	"	45	75	
	16_A	90&60	12&13	45	75	lamps not on full power
	16_B	" "	" "	"	"	
	13	" "	" "	"	"	
	1	smooth		45	90	repeated run 1,with the watch

F ≡ film number

TABLE VIII-1 (continued)

F	RUN	LIFTER BAR ANGLE	LIFTER BAR HEIGHT	% FILLING	SPEED %CRIT	COMMENTS
BATCH 2						
4	1	90	25	40	63	camera at exposure f=2.0
	1_A	"	"	"	"	camera at exposure f=1.4
	2	"	"	"	70	
	3	"	"	"	75	
	4	45	25	"	60	
	5	"	"	"	70	tangled as stopped the mill
	6	"	"	"	75	tangles as stop,fine during the run
	7	"	"	"	80	
	8	"	"	"	85	apparent surging in speed
	9	"	"	"	90	filmed till mill stopped, but rods did not tangle
5	10	90	20	"	60	all following runs at exposure f = 2.0
	11	"	"	"	70	
	12	"	"	"	75	
	13	"	"	"	80	
	14	"	"	"	90	
	15	"	"	"	100	two layers centrifuged
	16	90	20&12	"	60	alternate rows of 20 and 12mm lifters
	17	"	"	"	70	
	18	"	"	"	75	
	19	"	"	"	80	18/2 card on information board
	20	"	"	"	90	
6	21	"	"	"	100	
	22	90	12	"	60	
	23	"	"	"	70	
	24	"	"	"	75	
	25	"	"	"	80	
	26	"	"	"	90	close to centrifuging
	27	"	"	"	100	outer charge layer centrifuged forming a shell within which the rest didn't centrifuge
	28	90	6	"	60	
	29	"	"	"	70	
	30	"	"	"	75	
	31	"	"	"	80	
7	32_A	"	"	"	90	one lifter loosens & falls off
	32_B	"	"	"	"	repeat
	33	"	"	"	100	does not centrifuge
	34	smooth		"	80	
	35	"		"	90	
	36	"		"	100	does not centrifuge
	37	90	15	"	100	outer layer centrifuges,second just off centrifuging
	38	"	"	"	90	
	39	"	"	"	80	
	40	"	"	"	70	
	41	"	"	"	60	

APPENDIX IX

RODPLOT PROGRAMME

As part of the experimental technique involved the efficient gathering of large quantities of data, recording the progressive rod locations, this computer programme is included. It is written in basic, for use on an IBM personal computer.

```
10 '############    FILING ROD READINGS FROM MM1201 GRAPHICS TABLET   ############

20 PI=3.141593
30 DEF SEG=0 :POKE &H417 ,(PEEK(&H417) OR &H40)   'set to upper case
40 DIM XY(100,12) , RA(100,12)
50 CLS :PRINT TAB(20);"ROD POSITIONS PROJECTED ONTO MM1201 DIGITISER" :PRINT :PR
INT
60 PRINT "THIS PROGRAM SETS UP ARRAYS OF X,Y COORDINATES RELATIVE TO THE MILL CE
NTRE" :PRINT
70 PRINT "THE FILM SHOULD BE PROJECTED PERPENDICULARLY ONTO THE GRAPHICS TABLET
, FILLING MOST OF MARKED-OFF WORKING AREA"
80 PRINT "A SHEET OF PAPER SHOULD BE TAPED ONTO THE TABLET , WITH AN APPROPRIATE
 SIZED    CIRCLE AND ITS CENTRE DRAWN ON . THIS ASSISTS IN LOCATING THE PROJECTE
D FILM"
90 PRINT "THE CENTRE OF THE MILL IS THEN CAREFULLY DOTTED . THIS IS IMPORTANT AS
 ALL      FURTHER READINGS ARE BASED ON THIS CENTRAL COORDINATE"
100 PRINT "THE HORIZONTAL AND VERTICAL AXES OF THE MILL ARE THEN MARKED FROM AN
INITIAL    FRAME"
110 PRINT "A SELECTION OF POINTS ON THE INTERNAL MILL RADIUS ARE THEN MARKED , S
O AS TO SETTHE SCALE"
120 PRINT "THE PATH OF A NUMBER OF RODS CAN THEN BE SIMULTANEOUSLY FOLLOWED AND
RECORDED , BY SUCCESIVELY DOTTING THE CENTRE OF EACH ROD IN EACH PROJECTED FRAME
"
130 LOCATE 25,1 :COLOR 1,14:PRINT TAB(27);"PRESS RETRN TO CONTINUE";TAB(79)
140 INPUT "",G :LOCATE 25,1 :COLOR 7,0 :PRINT TAB(79)
150 CLS :PRINT "REMOVE DISK FROM DRIVE A , AND PLACE STORAGE DISK IN ITS PLACE"
:INPUT "PRESS RETURN WHEN READY",G
160 GOSUB 1840
170 GET #2,1 :PRINT A$;",";B$;",";C$
180 SCALE = CVS(AA$) :CX%=CVI(AB$) :CY%=CVI(AC$) :CLOSE #2
190 PRINT "THE PRESENT SCALE IS ";SCALE;" AND THE MILL CENTRE IS ";CX%;",";CY% :
PRINT "TO CHANGE THESE ENTER THE `SET UP TABLET ROUTINE' , OTHERWISE GO DIRECTLY
 TO THE `ROD ENTRY' ROUTINE"
200 PRINT :PRINT :INPUT "PRESS RETURN TO CONTINUE",G
210 '------------   MAIN MENUE   --------------
220 CLS :PRINT "TO SET UP TABLET PRESS 1" :PRINT :PRINT "TO ENTER ROD POSITIONS
 PRESS 2" :PRINT :PRINT "TO DISPLAY CURRENT DATA PRESS 3" :PRINT :PRINT "TO RETR
IEVE DATA ON FILE PRESS 4" :PRINT :PRINT "TO MANIPULATE DATA PRESS 5" :PRINT
230 PRINT "TO ADD TO AN EXISTING ARRAY PRESS 6" :PRINT :PRINT "TO END PRESS 0"
240 K$=INKEY$ :IF K$="" GOTO 240 ELSE K=VAL(K$)
250 ON K GOTO 280 ,680 ,1300 ,1180 ,1880 ,2300
260 CLOSE :END
270 '--------------  SETTING UP TABLET  -------------
280 CLS :PRINT TAB(31);"SETTING UP TABLET":PRINT :PRINT
290 PRINT "PLACE SHEET OF PAPER WITH CIRCLE , CENTRE , HORIZONTAL , AND VERTICAL
 AXES MAKED ON IT , ONTO TABLET":PRINT
300 PRINT "NOW PLACE MOUSE ONTO TABLET. PRESS BUTTON  1  TO OBTAIN READINGS. USE
 THESE TO  ALIGN THE CIRCLE AXES WITH THOSE OF THE TABLET" :PRINT :PRINT TAB(20)
;:COLOR 1,14 :PRINT "PRESS BUTTON  4  TO RETURN TO PROGRAM" :COLOR 7,0
310 PRINT :PRINT :PRINT TAB(20);"PRESS RETRN TO PROCEED" :INPUT "",G
320 PRINT :PRINT :PRINT "YOU ARE NOW IN THE TABLET MODE. THE KEYBOARD IS NON-FUN
CTIONAL"
```

```
330 FOR T%=1 TO 4000 :NEXT
340 CLS :LOCATE 25,1 :PRINT TAB(20):COLOR 1,14 :PRINT "PRESS BUTTON  4  ON MOUSE
 TO RETURN TO PROGRAM";:COLOR 7,0
350 LOCATE 1,1 :PRINT "  X";TAB(12);"Y"
360 GOSUB 1060 :PRINT XX%;TAB(10);YY%
370 IF FF%<>4 GOTO 360
380 LOCATE 25,1 :PRINT TAB(79)
390 PRINT "TAPE THE SHEET SECURELY DOWN" :PRINT :PRINT "PROJECT FILM PERPENDICUL
ARLY ONTO TABLET , AND ALIGN WITH CIRCLE.":PRINT "INNER EDGES OF CIRCLE AND MILL
 SHOULD COINCIDE , AS SHOULD VERTICAL & HORIZONTAL AXES"
400 PRINT "DOT THE CENTRE OF THE CIRCLE. DO THIS A FEW TIMES TO GET CONSISTENT R
EADINGS ,  THE MOUSE BEING LIFTED BETWEEN EACH READING. THE LAST THREE , PRIOR T
O PRESSING BUTTON 4 , SHALL BE USED TO GIVE AN AVERAGE."
410 PRINT :PRINT :PRINT TAB(20);:COLOR 1,14 :PRINT "PRESS BUTTON  4  ON MOUSE TO
 FINISH";:COLOR 7,0
420 PRINT :PRINT " CX";TAB(11);"CY"
430 GOSUB 1060 :IF CX3>0 AND FF%=4 THEN GOTO 470 ELSE CX1=XX% :CY1=YY% :PRINT CX
1;TAB(10);CY1
440 GOSUB 1060 :IF CX3>0 AND FF%=4 THEN GOTO 470 ELSE CX2=XX% :CY2=YY% :PRINT CX
2;TAB(10);CY2
450 GOSUB 1060 :IF CX3>0 AND FF%=4 THEN GOTO 470 ELSE CX3=XX% :CY3=YY% :PRINT CX
3;TAB(10);CY3
460 GOTO 430
470 CX%=(CX1+CX2+CX3)/3 :CY%=(CY1+CY2+CY3)/3 :PRINT "AVERAGE CENTRE IS (";CX%;",
";CY%;")"
480 PRINT :PRINT "NOW DOT THE INNER EDGE OF MILL SHELL IN AT LEAST FIVE WELL SEP
ARATED POINTS":PRINT "THIS CHECKS THE CIRCULARITY OF THE MILL AND SETS THE SCALE
"
490 PRINT :PRINT :PRINT TAB(20);:COLOR 1,14 :PRINT "   PRESS BUTTON  4  ON MOUSE
 TO FINISH , THIS READING ISN'T USED.";:COLOR 7,0 :PRINT :PRINT :PRINT " EX";TAB
(11);"EY";TAB(21);"R"
500 FOR I = 1 TO 5
510 GOSUB 1060 :IF FF%=4 AND EX%(5)>0 THEN I = 5 :GOTO 520 ELSE EX%(I)=XX% :EY%(
I)=YY% :R(I)=((EX%(I)-CX%)^2+(EY%(I)-CY%)^2)^.5 :PRINT EX%(I);TAB(10);EY%(I);TAB
(20);R(I)
520 NEXT
530 IF FF%<>4 GOTO 500
540 R=0
550 FOR I = 1 TO 5
560 R=R+R(I) :NEXT
570 R=R/5
580 PRINT "R = ";R :PRINT :PRINT
590 INPUT "ENTER MILL RADIUS IN mm ";MR%
600 PRINT :SCALE = MR%/R :PRINT "SCALE = ";SCALE
610 GOSUB 1840
620 LSET AA$=MKS$(SCALE) :LSET AB$=MKI$(CX%) :LSET AC$=MKI$(CY%)
630 PUT #2,1 :CLOSE #2
640 PRINT :PRINT :PRINT "YOU ARE NOW READY TO ENTER ROD POSITIONS"
650 INPUT "PRESS RETURN TO CONTINUE",G
660 GOTO 220
670 '------------------  FOLLOWING ROD POSITIONS  -------------
680 CLS :PRINT TAB(20);"FOLLOWING ROD POSITIONS" :PRINT :PRINT
690 FILES:PRINT"ENTER THE TITLE OF THIS RUN, NOT MORE THAN 7 CHARACTERS, AND NOT
 TO END WITH `R'":COLOR 1,14:PRINT"DO NOT REPEAT A LISTED NAME , OTHERWISE THE F
ILED RESULTS ARE REPLACED BY THE   NEW ONES":COLOR 7,0:INPUT "TITLE ";TL$:TL$=LE
FT$(TL$,7)
700 PRINT :PRINT "ENTER THE NUMBER OF RODS TO BE FOLLOWED , UP TO 6 " :INPUT "NO
 OF RODS ";NR% :IF NR%>6 THEN BEEP:GOTO 700
710 NF%=0
720 PRINT :PRINT "CONTROL SHALL NOW GO OVER TO THE MOUSE" :PRINT :PRINT "THE BUT
TONS HAVE THE FOLLOWING FUNCTIONS :";:PRINT " 1   ROD POSITION" :PRINT TAB(44);"
2   NO ROD LOCATION FOR THAT FRAME"
730 PRINT TAB(44);"3   ERASE LAST READING AND":PRINT TAB(48);"THEN REENTER" :PRI
NT TAB(44);"4   END"
740 PRINT :PRINT "RODS MUST ALWAYS BE ENTERED IN THE SAME SEQUENCE FOR EACH SUCC
ESIVE FRAME"
750 PRINT :PRINT "THERE IS A `BEEP' AFTER EACH ENTRY . REENTER IF NO BEEP IS HEA
RD."
760 INPUT "PRESS RETURN TO CONTINUE",G
```

```
770 CLS :LOCATE 25,1 :COLOR 1,14 :PRINT "   1 = ROD POSITION.    2 = NO ROD.
3 = REDO READING    4 = FINISHED";TAB(80); :COLOR 7,0 :LOCATE 1,1
780 PRINT "  ";
790 FOR I%=1 TO NR% :I$=RIGHT$(STR$(I%),1) :PRINT"   X";I$;"    Y";I$;"  "; :NEX
T
800 IF ZAP%=4 THEN PRINT :GOSUB 2330
810 PRINT :L%=NF%+1 :T%=NR%*2-1
820 L$=RIGHT$(STR$(L%),2) :PRINT L$;
830 FOR I%=1 TO T% STEP 2
840 GOSUB 1060 :IF FF%=4 THEN I%=T% :GOTO 880
850 IF FF%=3 THEN GOSUB 960
860 XY(L%,I%)=(XX%-CX%)*SCALE :XY(L%,I%+1)=(YY%-CY%)*SCALE :IF FF%=2 THEN XY(L%,
I%)=999 :XY(L%,I%+1)=999
870 X=XY(L%,I%):Y=XY(L%,I%+1) :PRINT USING "+###.#";X,Y;:PRINT " ";
880 NEXT
890 GOSUB 990
900 PRINT "" :L%=L%+1 :IF L%=101 GOTO 920
910 IF FF%<>4 GOTO 820 ELSE GOTO 930
920 PRINT "MAX OF 100 FRAMES ALLOWED , START A NEW SET OF READINGS ,UNDER A NEW
NAME"
930 L%=L%-1 :NF%=L% :PRINT "THE RESULTS ARE NOW STORED UNDER ";TL$
940 INPUT "TO COMPILE MORE RESULTS ENTER 1 , OTHERWISE JUST PRESS RETURN  ",G :I
F G=1 GOTO 690 ELSE GOTO 220
950 'replacing entries
960 IF I%>1 THEN I% = I%-2 :LOCATE ,POS(1)-13 :RETURN 840
970 L%=L%-1 :I%=T% :LOCATE CSRLIN-1,NR%*13-10 :RETURN 840
980 'storage subroutine
990 OPEN "R",#2,TL$,48
1000 FIELD #2,4 AS X$(1),4 AS Y$(1),4 AS X$(2),4 AS Y$(2),4 AS X$(3),4 AS Y$(3),
4 AS X$(4),4 AS Y$(4),4 AS X$(5),4 AS Y$(5),4 AS X$(6),4 AS Y$(6)
1010 FOR I%=1 TO 6 :LSET X$(I%)=MKS$(XY(L%,I%*2-1)):LSET Y$(I%)=MKS$(XY(L%,I%*2)
)
1020 NEXT
1030 PUT #2,L%
1040 CLOSE #2 :RETURN
1050 '--------------  DRIVER SUBROUTINE  ------------------
1060 COUNT%=15
1070 ON ERROR GOTO 1140
1080 OPEN "COM1:9600,N,8,1,CS,DS" AS #1
1090 PRINT #1,"B";"i"
1100 IF LOC(1) <13 GOTO 1100
1110 INPUT#1,X$ :INPUT#1,Y$ :INPUT#1,F$
1120 XX%=VAL(X$) :YY%=VAL(Y$) :FF%=VAL(F$)
1130 CLOSE #1 :BEEP:RETURN
1140 COUNT%=COUNT%-1 :IF COUNT%=0 GOTO 1160
1150 RESUME
1160 ON ERROR GOTO 0 :RESUME
1170 '------------  RETRIEVING DATA  ------------
1180 CLS :FILES :INPUT "ENTER NAME OF FILE TO BE RETRIEVED  ";TL$
1190 PRINT :PRINT :PRINT "FILE BEING LOADED"
1200 OPEN "R",#2,TL$,48
1210 IF RIGHT$(TL$,1)="R" GOTO 1500
1220 FIELD #2,4 AS X$(1),4 AS Y$(1),4 AS X$(2),4 AS Y$(2),4 AS X$(3),4 AS Y$(3),
4 AS X$(4),4 AS Y$(4),4 AS X$(5),4 AS Y$(5),4 AS X$(6),4 AS Y$(6)
1230 L%=1
1240 WHILE L%>0
1250 GET #2,L%
1260 FOR I%=1 TO 6 :XY(L%,I%*2-1) =CVS(X$(I%)) :XY(L%,I%*2) =CVS(Y$(I%)) :NEXT
1270 IF XY(L%,1)=0 GOTO 1290 ELSE L%=L%+1
1280 WEND
1290 CLOSE #2
1300 NF%=L%-1
1310 NR%=6 :I%=1
1320 WHILE I%<=NR%
1330 IF XY(1,I%*2-1)=0 AND XY(1,I%*2)=0 THEN NR%=I%-1
1340 I%=I%+1 :WEND
1350 IF ZAP%=4 THEN RETURN 2310
1360 PRINT :GOSUB 1760   'print or display
```

```
1370 PRINT#3, "RUN ";TL$ :PRINT#3,
1380 PRINT#3, "  ";
1390 FOR I%=1 TO NR% :I$=RIGHT$(STR$(I%),1) :PRINT#3,"   X";I$;"    Y";I$;"  ";
:NEXT
1400 IF NR%<6 THEN PRINT#3,""
1410 FOR L%=1 TO NF%
1420 L$=RIGHT$(STR$(L%),2) :PRINT#3,L$;
1430 FOR I%=1 TO NR%
1440 X=XY(L%,I%*2-1):Y=XY(L%,I%*2) :PRINT#3,USING "+###.#";X,Y;:PRINT#3," "; :NE
XT
1450 IF NR%<6 THEN PRINT#3, ""
1460 NEXT
1470 CLOSE#3 :COLOR 1,14 :PRINT "PRESS RETURN TO CONTINUE" :COLOR 7,0
1480 INPUT "",G
1490 GOTO 220
1500 FIELD #2,4 AS R$(1),4 AS A$(1),4 AS R$(2),4 AS A$(2),4 AS R$(3),4 AS A$(3),
4 AS R$(4),4 AS A$(4),4 AS R$(5),4 AS A$(5),4 AS R$(6),4 AS A$(6)
1510 L%=1
1520 WHILE L%>0
1530 GET #2,L%
1540 FOR I%=1 TO 6 :RA(L%,I%*2-1) =CVS(R$(I%)) :RA(L%,I%*2) =CVS(A$(I%)) :NEXT
1550 IF RA(L%,1)=0 GOTO 1570 ELSE L%=L%+1
1560 WEND
1570 CLOSE #2 :NF%=L%-1
1580 NR%=6 :I%=1
1590 WHILE I%<=NR%
1600 IF RA(1,I%*2-1)=0 AND RA(1,I%*2)=0 THEN NR%=I%-1
1610 I%=I%+1 :WEND
1620 PRINT :GOSUB 1760   'print or display
1630 PRINT#3, "RUN ";TL$;" IN RADIAL COORDINATES" :PRINT#3, :PRINT#3, "  ";
1640 FOR I%=1 TO NR% :I$=RIGHT$(STR$(I%),1) :PRINT#3,"   R";I$;"    A";I$;CHR$(2
48);" "; :NEXT
1650 PRINT#3,""
1660 FOR L%=1 TO NF%
1670 L$=RIGHT$(STR$(L%),2) :PRINT#3,L$;
1680 FOR I%=1 TO NR%
1690 R=RA(L%,I%*2-1):A=RA(L%,I%*2) :PRINT#3,USING " ###.#";R,A;:PRINT#3," "; :NE
XT
1700 IF NR%<6 THEN PRINT#3,""
1710 NEXT
1720 CLOSE#3 :COLOR 1,14 :PRINT "PRESS RETURN TO CONTINUE" :COLOR 7,0
1730 INPUT "",G
1740 GOTO 220
1750 '------------  PRINT OR DISPLAY  ------------
1760 PRINT :PRINT "TO DISPLAY ON SCREEN PRESS  0" :PRINT "TO PRINT PRESS  1"
1770 K$ = INKEY$ :IF LEN(K$)=0 GOTO 1770 ELSE K%=ASC(K$)
1780 IF K%=48 THEN OPEN "SCRN:" FOR OUTPUT AS #3 :PP%=0 :RETURN
1790 IF K%=49 THEN OPEN "LPT1:" FOR OUTPUT AS #3 :PP%=1
1800 IF K%<>49 THEN BEEP :GOTO 1760
1810 INPUT "ONCE PRINTER IS TURNED ON AND READY , PRESS RETURN",G
1820 RETURN
1830 '-------------SCALE & CENTRE STORAGE  ------------
1840 OPEN "R",#2,"SETUP.DAT",8
1850 FIELD #2,4 AS AA$,2 AS AB$,2 AS AC$
1860 RETURN
1870 '-----------  MANIPULATING DATA  -----------------
1880 CLS :PRINT "THIS CONVERTS THE READINGS IN THE PRESENT ARRAY OF DATA TO RADI
AL COORDINATES."
1890 TL$=TL$+"R" :IF LEN(TL$)>8 THEN TL$=RIGHT$(TL$,8)
1900 FOR L% = 1 TO NF%
1910 FOR I%=1 TO NR% :X=XY(L%,I%*2-1) : Y=XY(L%,I%*2)
1920 RA(L%,I%*2-1)=(X*X + Y*Y)^.5
1930 IF X<0 AND Y>0 THEN RA(L%,I%*2)= -ATN(Y/X)*180/PI :GOTO 2010
1940 IF X>0 AND Y>0 THEN RA(L%,I%*2)= 180-ATN(Y/X)*180/PI :GOTO 2010
1950 IF X>0 AND Y<0 THEN RA(L%,I%*2)= 180-ATN(Y/X)*180/PI :GOTO 2010
1960 IF X<0 AND Y<0 THEN RA(L%,I%*2)= 360-ATN(Y/X)*180/PI :GOTO 2010
1970 IF X=0 AND Y<0 THEN RA(L%,I%*2)=270 :GOTO 2010
1980 IF X=0 AND Y>=0 THEN RA(L%,I%*2)=90
```

```
1990 IF Y=0 AND X>0 THEN RA(L%,I%*2)=180
2000 IF Y=0 AND X<=0 THEN RA(L%,I%*2)=0
2010 NEXT I%
2020 NEXT L%
2030 GOSUB 1760
2040 PRINT#3, "RUN ";TL$;". RADIAL COORDINATES" :PRINT#3, "  ";
2050 FOR I%=1 TO NR% :I$=RIGHT$(STR$(I%),1) :PRINT#3,"   R";I$;"    A";I$;CHR$(2
48);" "; :NEXT
2060 PRINT#3,""
2070 FOR L%=1 TO NF%
2080 L$=RIGHT$(STR$(L%),2) :PRINT#3,L$;
2090 FOR I%=1 TO NR%
2100 R=RA(L%,I%*2-1):A=RA(L%,I%*2) :PRINT#3,USING " ###.#";R,A;:PRINT#3," "; :NE
XT
2110 IF NR%<6 THEN PRINT#3,""
2120 NEXT
2130 CLOSE#3 :COLOR 1,14 :PRINT "PRESS RETURN TO CONTINUE" :COLOR 7,0
2140 INPUT "",G
2150 CLS :PRINT "TO REDISPLAY OR PRINT ENTER 1" :PRINT :PRINT "TO SAVE ENTER 2"
:PRINT :PRINT "TO RETURN TO MAIN MENUE ENTER 0"
2160 INPUT ;K
2170 ON K GOTO 2030 ,2190
2180 GOTO 220
2190 PRINT :PRINT "THIS SHALL BE STORED UNDER THE SAME NAME AS THE X,Y COORDINAT
ES , BUT WITH AN   `R' ON THE END"
2200 PRINT "ARRAY BEING STORED UNDER ";TL$
2210 OPEN "R",#2,TL$,48
2220 FIELD #2,4 AS R$(1),4 AS A$(1),4 AS R$(2),4 AS A$(2),4 AS R$(3),4 AS A$(3),
4 AS R$(4),4 AS A$(4),4 AS R$(5),4 AS A$(5),4 AS R$(6),4 AS A$(6)
2230 FOR L%= 1 TO NF%
2240 FOR I% = 1 TO 6 :LSET R$(I%)=MKS$(RA(L%,I%*2-1)) :LSET A$(I%)=MKS$(RA(L%,I%
*2))
2250 NEXT I%
2260 PUT #2,L%
2270 NEXT
2280 CLOSE #2 :GOTO 220
2290 '------------ADDING TO AN ARRAY  ---------------
2300 ZAP%=4 :GOSUB 1180
2310 PRINT :PRINT "NUMBER OF RODS BEING FOLLOWED IS ";NR% :PRINT :PRINT "THERE A
RE ";NF%;" ENTRIES SO FAR"
2320 GOTO 720
2330 FOR L%=NF%-3 TO NF%
2340 L$=RIGHT$(STR$(L%),2) :PRINT L$;
2350 FOR I%=1 TO NR%
2360 X=XY(L%,I%*2-1):Y=XY(L%,I%*2) :PRINT USING "+###.#";X,Y;:PRINT " "; :NEXT
2370 PRINT ""
2380 NEXT
2390 ZAP%=0 :RETURN
```

APPENDIX X

COEFFICIENTS OF FRICTION

The kinetic coefficient of friction can be calculated from the time taken for a sample to slide down an inclined plane.

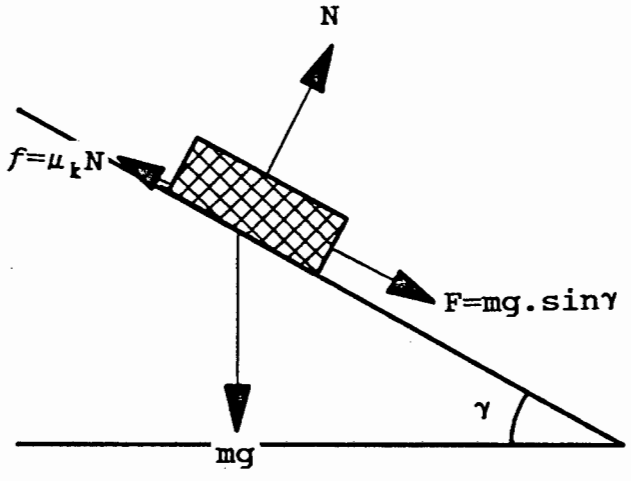

FIGURE X-1. Sample sliding down an inclined plane

The acceleration of the sample is given by the net force acting down the plane.

$$a = \frac{F_{net}}{m}$$

$$= \frac{F - f}{m}$$

$$= \frac{mg.\sin\gamma - \mu_k.mg.\cos\gamma}{m}$$

$$= g(\sin\gamma - \mu_k.\cos\gamma)$$

$$\rightarrow \mu_k = \frac{\sin\gamma - a/g}{\cos\gamma} \qquad \text{(Xa)}$$

Now if the sample is timed from the moment it is released from being held on a surface, with a slope having γ greater than $\arctan\mu_s$, then its acceleration can be calculated from the time it takes to slide a known distance, d.

$$d = \tfrac{1}{2}at^2$$

$$\rightarrow \quad a = \frac{2d}{t^2} \qquad \text{(Xb)}$$

equations Xa and Xb yield:

$$\mu_k = \frac{\sin\gamma - 2d/gt^2}{\cos\gamma} \qquad \text{(Xc)}$$

APPENDIX XI

COMPUTER PROGRAMME FOR CALCULATING ROD MOTION

This programme is written in Turbo basic, for use on an IBM personal computer. A full listing of the programme is given below. It uses the same variables as the main theory, but written out when greek letters are used.

```
10 'PROGRAM TO CALCULATE ROD MOTION IN A ROTARY MILL
12 '
14 '  JULY 1988  ,  M.S. POWELL
15 CLEAR
16 DIM X(200) ,Y(200) ,AA(50) ,XP(200) ,YP(200)
17 DEF FNCOSH(X)=.5*(EXP(X)+EXP(-X))
18 DEF FNSINH(X)=.5*(EXP(X)-EXP(-X))
19 ON ERROR GOTO 5000
20 DEF FNASIN(X)= ATN(X/SQR(1-X*X))
21 DEF FNACOS(X)= 1.570796 - ATN(X/SQR(1-X*X))
22 NB% = 1
23 CLS
24 '-----------------    INPUT   --------------
25 PRINT "   ENTER ANGLES IN DEGREES AND DIMENSIONS IN mm":PRINT
30 INPUT "STATIC COEFFICIENT OF FRICTION ,u ";U!
35 INPUT "KINETIC COEFFICIENT OF FRICTION ,uk ";UK!
40 INPUT "INTERNAL RADIUS OF MILL ,R ";R!
50 INPUT "ROD RADIUS ,a ";A!
60 INPUT "LIFTER ANGLE ,p ";P! :INPUT "LIFTER HEIGHT ,h' ";H! :
   INPUT "LIFTER BASE WIDTH ,2Y ";Y!
70 INPUT "MILL SPEED ,% Critical ";MSP!
72 'INPUT "FILMING SPEED , frames/second ";FS!
75 '------------------  CALCULATING INITIAL DATA  -----------
80 PI = 3.141593 :G!=9800   'G! in mm/s-2
85 R0! = R!-A! :Y!=Y!/2 :RPM!=MSP!/SQR(R!*2/1000)/100*42.3
90 IF P!=90 THEN P!=P!*PI/180 :V!=ATN(Y!/(SQR(R!*R!-Y!*Y!)-H!)) :GOTO 105
100 P!=P!*PI/180 :V! =(Y!*TAN(P!)-H!)/((SQR(R!*R! - Y!*Y!)-H!)*TAN(P!))
    :V!=ATN(V!)
105 ALPHA!=PI/2-P!-V!
110 W!=RPM!*PI/30 :HR!=R!-((SQR(R!*R!-Y!*Y!)-H!)/COS(V!)) : AP!=A! :GOTO 115
111 PRINT "S0 < SL" : RR!=R!-HR!
112 ETA! = FNACOS((A!*A!+RR!*RR!-R0!*R0!)/(2*A!*RR!))
113 LAMBDA! = PI-ETA!-ALPHA!
114 IF LAMBDA! > PI/2 THEN AP! = A!*SIN(ETA!+ALPHA!) ELSE AP!=A!
115 DELTA!=SIN(ALPHA!)*(R!-HR!)-AP!
117 B0!=ATN(DELTA!/SQR(R0!*R0!-DELTA!*DELTA!)) :S0!=R0!*COS(B0!)
118 HC!=(SQR(R!*R!-(DELTA!+A!)^2)-S0!)*SIN(P!): IF H!<HC! AND AP!=A! GOTO 111
119 PRINT "B0 = ";B0!;"  S0 = ";S0!
120 PRINT "MILL RADIUS =";R!;"mm , MILL SPEED =";RPM!;"rpm ,or";MSP!;"%crit
    , ROD RADIUS =";A!;" mm "
130 PRINT "COEFFICIENTS OF FRICTION : STATIC = ";U!;" , KINETIC = ";UK!
140 PRINT "LIFTER BAR SPECS :LEADING ANGLE =";P!*180/PI;CHR$(248);",
    HEIGHT =";H!;"mm , BASE WIDTH =";Y!*2;"mm"
209 '--------------    CALCULATING  POINT OF EQUILIBRIUM    -----------
210 IF AP!<A! GOTO 6000
212 IF U!=0 THEN GM0!=FNASIN(W!*W!*R0!*COS(B0!)/G!) :GOTO 290
215 X!=(W!*W!/G!)*(R0!*SQR(1-(DELTA!/R0!)^2)-U!*DELTA!)
```

```
220 GM0! =0 :Z! =.1
230 WHILE 1
240 GM0! = GM0!+Z!
250 DMY!=SIN(GM0!)-U!*COS(GM0!)
260 IF DMY!>X! THEN GM0!=GM0!-Z! :Z!=Z!/10 :IF Z!<.000001 THEN EXIT LOOP
270 WEND
290 PHI0!=GM0!-B0!
300 PRINT "GAMMA 0 = ";GM0!*180/PI;CHR$(248);"  ,  PHI 0 = ";PHI0!*180/PI
305 XP(1)=COS(PHI0!)*R0! :YP(1)=SIN(PHI0!)*R0!    '=======XP , YP=======
310 SL!=COS(ALPHA!)*(R!-HR!) :BL!=ATN(DELTA!/SL!)
315 PRINT "S0 = ";S0!;"   SL = ";SL!
320 IF U!=0 GOTO 490
349 '--------------    MAX SLOPE FOR PURE ROLLING    ---------------
350 X! = (W!*W!/G!)*(DELTA!*3*U! + SL!)
360 GMM! =0 :Z!=.1
370 WHILE 1
380 GMM! = GMM!+Z!
390 DMY!=-3*U!*COS(GMM!) + SIN(GMM!)
400 IF DMY!>X! THEN GMM!=GMM!-Z! :Z!=Z!/10 :IF Z!<.000001 THEN EXIT LOOP
410 WEND
489 '-----------------  MAIN CONTROL ROUTINE  ----------------
490 IF U!=0 THEN GOSUB 1100 :GOTO 540  ' for U static =0, but UK! >0
520 ZZ%=1 :GOSUB 1000 :IF ZZ% =2 GOTO 540   'find gamma max
530 GOSUB 1400   'sliding after rolling
540 GOSUB 1600  'trajectory across mill
545 GOSUB 3000
547 PRINT : INPUT "DO YOU WISH TO VIEW THE FILE Y/N  ",LOOK$
548 IF LOOK$ = "Y" THEN GOSUB 4000 ELSE 550
550 PRINT :PRINT "PRESS  'P'  FOR A PRINT OUT (ENSURE PRINTER IS ON) ,
    ANY OTHER KEY TO CONTINUE"
560 K$=INKEY$ :IF K$="" GOTO 560
580 IF K$="P" OR K$="p" THEN GOSUB 1900
585 PRINT :INPUT "ENTER 'R' TO RETRIEVE A FILE FOR VIEWING  ",K$
587 IF K$="R" OR K$="r" THEN GOSUB 4100
590 PRINT :PRINT"PRESS SPACER BAR FOR MORE CALCULATIONS , OR 'E' TO END"
600 K$=INKEY$ :IF K$="" GOTO 600 ELSE K%=ASC(K$)
610 IF K%=32 GOTO 15
620 IF K%=69 OR 101 THEN END
630 BEEP :GOTO 590
999 '--------   PURE ROLLING   -------------  from 520
1000 WP!=SQR(2/3)*W!
1005 AA!=(S0!-.4*G!*SIN(GM0!)/W!^2)
1006 BB!=(6^.5*G!/(5*W!^2))*COS(GM0!)
1010 T!=0 :Z!=.01 :NB%=1
1020 WHILE 1
1030 T!=T!+Z! :IF Z!=.01 THEN NB%=NB%+1   'only add to XP,YP for large
     interval
1040 DMY!=AA!*FNCOSH(WP!*T!) - BB!*FNSINH(WP!*T!) + .4*G!*SIN(GM0!+W!*T!)
     /W!^2
1045 R1=SQR(DMY!*DMY!+DELTA!*DELTA!) :PHI1=(GM0!+W!*T!)-ATN(DELTA!/DMY!)
1046 XP(NB%)=R1*COS(PHI1)  :  YP(NB%)=R1*SIN(PHI1)  '========XP , YP=======
1050 IF DMY!<SL! THEN T!=T!-Z! :Z!=Z!/10 :IF Z!<.000001 THEN EXIT LOOP
1055 IF (GM0!+W!*T!)>GMM! THEN T!=T!-Z! :Z!=Z!/10 :GOSUB 1200 :GOTO 1090
1057 IF W!*W!*DELTA! + G!*COS(GM0!+W!*T!) <0 THEN T!=T!-Z! :Z!=Z!/10
     :IF Z!<.000001 THEN PRINT "N  IS NEGATIVE , ROD ROLLS TILL PROJECTED
     INTO FLIGHT":RETURN 2000
1060 WEND
1070 GML!=GM0!+W!*T! :PHIL!=GML!-BL!
1080 PRINT "TIME TO ROLL TO END = ";T!;"  ,  GAMMA L = ";GML!*180/PI;"  ,
     PHI L = ";PHIL!*180/PI
1085 ZZ% =2 :GOSUB 1800
1090 RETURN
1099 '---------   PURE SLIDING   ----------- from 490
1100 CC!=G!/(2*W!*W!) :DD!=(S0!+UK!*DELTA!+CC!*(UK!*COS(GM0!)-SIN(GM0!)))
     :EE!=(UK!*SIN(GM0!)+COS(GM0!))
1110 T!=0 :Z!=.01 :NB%=1
1120 WHILE 1
```

```
1130 T!=T!+Z! :IF Z!>.001 THEN NB%=NB%+1
1140 DMY!=DD!*FNCOSH(W!*T!) - CC!*(EE!*FNSINH(W!*T!) + UK!*COS(GM0!+W!*T!)
     -SIN(GM0!+W!*T!)) - UK!*DELTA!
1142 PHI1 = (GM0!+W!*T!)-ATN(DELTA!/DMY!) :R1 = SQR(DMY!*DMY!+DELTA!*DELTA!)
1143 IF R1>R0! THEN R1=R0!
1146 XP(NB%) = R1*COS(PHI1) :YP(NB%) = R1*SIN(PHI1)  '=====XP , YP======
1150 IF DMY!<SL! THEN T!=T!-Z! :Z!=Z!/10 :IF Z!<.000001 GOTO 1170
1155 IF W!*W!*DELTA! + G!*COS(GM0!+W!*T!) <0 THEN T!=T!-Z! :Z!=Z!/10
     :IF Z!<.000001 THEN PRINT "N  IS NEGATIVE , ROD SLIDES TILL PROJECTED
     INTO FLIGHT, PRIOR TO REACHING LIFTER TIP":RETURN 2000
1160 WEND
1170 GML!=GM0!+W!*T! :PHIL!=GML!-BL! :TL!=T!
1180 PRINT "TIME TO SLIDE TO END = ";TL!;"  ,  GAMMA L = ";GML!*180/PI;"  ,
     PHI L = ";PHIL!*180/PI
1185 VL! = W!*(DD!*FNSINH(W!*TL!) - CC!*(EE!*FNCOSH(W!*TL!)-UK!*SIN(GML!)
     -COS(GML!)))
1186 IF TL! = 0 THEN VL! = 0
1187 PRINT"VL ALONG LIFTER FACE ONLY = ";VL!
1190 RETURN
1199 '------------   ROLLING TO GAMMA MAX , FOLLOWED BY SLIDING   --from 1055
1200 FF!=W!*W!*DELTA!*3*U!/G! :GG!=W!*W!*S0!/G!-.4*SIN(GM0!) :HH!=SQR(6)
     *COS(GM0!)/5
1210 TI!=T!
1220 WHILE 1
1230 TI!=TI!+Z!
1240 DMY!=FF!+GG!*FNcosh(WP!*TI!) - HH!*FNsinh(WP!*TI!)
1250 IF (.6*SIN(GM0!+W!*TI!)-3*U!*COS(GM0!+W!*TI!)) > DMY! THEN TI!=TI!-Z!
     :Z!=Z!/10 :IF Z!<1E-08 GOTO 1270
1255 IF W!*W!*DELTA! + G!*COS(GM0!+W!*TI!) <0 THEN TI!=TI!-Z! :Z!=Z!/10
     :IF Z!<.000001 THEN PRINT "N  IS NEGATIVE , ROD ROLLS TILL PROJECTED INT
1260 WEND
1265 DMY!=AA!*FNcosh(WP!*TI!) - BB!*FNsinh(WP!*TI!) + .4*G!*SIN(GM0!+W!*TI!)
     /W!^2 :T!=TI!:RETURN 2000
1270 SI!=AA!*FNcosh(WP!*TI!) - BB!*FNsinh(WP!*TI!) + .4*G!*SIN(GM0!+W!*TI!)
     /W!^2
1280 GMM!=GM0!+W!*TI!
1290 VI! = WP!*(S0!-.4*G!*SIN(GM0!)/W!^2)*FNsinh(WP!*TI!) - (.4*G!/W!)
     *(COS(GM0!)*FNcosh(WP!*TI!) - COS(GM0!+W!*TI!))
1300 PRINT "AT TRANSITION FROM PURE ROLLING TO ROLLING & SLIPPING
     SI = ";SI!;" , GAMMA MAX = ";GMM!*180/PI;" , TI = ";TI!;" , VI = ";VI!
1305 R1=SQR(SI!*SI!+DELTA!*DELTA!) :PHI1=GMM! - ATN(DELTA!/DMY!)
1306 XP(NB%)=R1*COS(PHI1)  :  YP(NB%)=R1*SIN(PHI1)  '========XP , YP=======
1310 RETURN
1399 '---------------   SLIDING AFTER ROLLING   -----------from 530
1400 II!=(SI!+DELTA!*UK!+.5*G!*(UK!*COS(GMM!)-SIN(GMM!))/W!^2) :JJ!=VI!/W!
     -.5*G!*(UK!*SIN(GMM!)+COS(GMM!))/W!^2 :CC!=G!/(2*W!^2)
1410 T!=0 :Z!=.001
1420 WHILE 1
1430 T!=T!+Z! :IF Z!=.001 THEN NB%=NB%+1
1440 DMY!=II!*FNcosh(W!*T!) + JJ!*FNsinh(W!*T!) - CC!*(UK!*COS(GMM!+W!*T!)
     -SIN(GMM!+W!*T!)) - DELTA!*UK!
1450 IF DMY!<SL! THEN T!=T!-Z! :Z!=Z!/10 :IF Z!<.000001 THEN EXIT LOOP
1452 R1=SQR(DMY!*DMY!+DELTA!*DELTA!) :PHI1=(GMM!+W!*T!)-ATN(DELTA!/DMY!)
1453 XP(NB%)=R1*COS(PHI1)  :  YP(NB%)=R1*SIN(PHI1)  '========XP , YP=======
1455 IF W!*W!*DELTA! + G!*COS(GMM!+W!*T!) <0 THEN T!=T!-Z! :Z!=Z!/10
     :IF Z!<.000001 THEN PRINT "N  IS NEGATIVE":RETURN 2005
1460 WEND
1470 GML!=GMM!+W!*T! :PHIL!=GML!-BL! :TL!=T!+TI!
1475 NB%=NB%+1 :RL!=SQR(SL!*SL!+DELTA!*DELTA!)
1476 XP(NB%)=RL!*COS(PHIL!)  :  YP(NB%)=RL!*SIN(PHIL!)  '========XP , YP=====
1477 NB%=NB%+1
1480 VL!=W!*II!*FNSINH(W!*T!) + W!*JJ!*FNCOSH(W!*T!)
     - .5*G!*(-UK!*SIN(GMM!+W!*T!)-COS(GMM!+W!*T!))/W!
1490 PRINT "TIME TO ROLL THEN SLIDE TO END = ";TL!;"  ,  GAMMA L = ";GML!*180
     /PI;"  ,  PHI L = ";PHIL!*180/PI;"  ,  VELOCITY AT TIP ,VL = ";VL!
1500 RETURN
```

```
1599 '--------------------  FREE FLIGHT TRAJECTORY  ----------from 540
1600 IF TL!=0 THEN RL!=R0! : PHIL!=PHI0! :GOTO 1610
1608 RL!=SL!/COS(BL!)
1610 XL!=RL!*COS(PHIL!) :YL!=RL!*SIN(PHIL!) :VXL!=VL!*COS(GML!)-W!*RL!
     *SIN(PHIL!) :VYL!=VL!*SIN(GML!)+W!*RL!*COS(PHIL!) :AVL!=PI+ATN(VYL!/VXL!
      :VTL!=SQR(VXL!*VXL!+VYL!*VYL!)
1620 PRINT "(XL,YL) = (";XL!;",";YL!;")  mm"
1630 PRINT "VTL = ";VTL!;"  (VXL,VYL) = (";VXL!;",";VYL!;")  mm/s , at"
     ;AVL!*180/PI;CHR$(248);"In the reference coordinates"
1640 I%=0 :Z!=.01 :T!=0
1650 WHILE 1
1660 T!=T!+Z! :I%=I%+1 :NB%=NB%+1
1670 X(I%)=XL!+VXL!*T! :Y(I%)=YL!+VYL!*T!-.5*G!*T!*T!
1675 XP(NB%)=X(I%) :YP(NB%)=Y(I%)      '====== XP , YP =======
1680 IF X(I%)^2+Y(I%)^2 > R0!^2 THEN T!=T!-Z! :Z!=Z!/10 :EXIT LOOP
1690 WEND
1700 WHILE 1
1710 T!=T!+Z!
1720 X(I%)=XL!+VXL!*T! :Y(I%)=YL!+VYL!*T!-.5*G!*T!^2
1730 IF X(I%)^2+Y(I%)^2 > R0!^2 THEN T!=T!-Z! :Z!=Z!/10 :IF Z!<.000001 THEN
     EXIT LOOP
1740 WEND
1745 XE=X(I%) :YE=Y(I%) :XP(NB%)=XE :YP(NB%)=YE
IF XE>0 THEN PHIE=ATN(XE/YE) ELSE PHIE = PI/2-ATN(YE/XE)
1750 VXE!=VXL! :VYE!=VYL!-G!*T!  :VE!=SQR(VXE!^2+VYE!^2)
     :AVE!=ATN(VYE!/VXE!)+PI
1760 PRINT "ROD STRIKES MILL SHELL AT (";XE;",";YE;") , WHICH IS AT "
     ;PHIE!*180/PI;CHR$(248)
1770 PRINT "ROD VELOCITY IS  ";VE!;" mm/s , AT ANGLE ,SIGMA E, ";AVE!*180/PI
     ;CHR$(248);"  In reference frame"
1780 RETURN 545
1799 '---------------  ROD DOESN'T SLIDE  ---------from 1085
1800 VL! = WP!*(S0!-.4*G!*SIN(GM0!)/W!^2)*FNsinh(WP!*T!) - (.4*G!/W!)
     *(COS(GM0!)*FNcosh(WP!*T!) - COS(GM0!+W!*T!))
1810 PRINT "THE ROD ONLY UNDERGOES PURE ROLLING , VL = ";VL!;" mm/s"
1820 RETURN
1899 '------------------  PRINTOUT  ---------------
1900 LPRINT "MILL RADIUS =";R!;"mm , MILL SPEED =";CINT(RPM!*100)/100
     ;"rpm or";(CINT(MSP!*10))/10;"%crit , ROD RADIUS =";A!;"mm"
1910 LPRINT "COEFFICIENTS OF FRICTION : STATIC = ";CINT(U!*1000)/1000;"
     , KINETIC = ";CINT(UK!*1000)/1000
1920 LPRINT "LIFTER BAR SPECS :LEADING ANGLE =";CINT(P!*180/PI);CHR$(248);"
     , HEIGHT =";H!;"mm";" , BASE WIDTH =";Y!*2;" mm"
1930 LPRINT "" :LPRINT "POINT OF EQUILIBRIUM , ";CHR$(232);"0 = "
     ;(CINT(PHI0!*1800/PI))/10;CHR$(248)
1940 LPRINT "ROD LEAVES LIFTER AT ";(CINT(PHIL!*1800/PI))/10;CHR$(248);"
     , WITH VELOCITY ";(CINT(VL!*10))/10;" mm/s at ";(CINT(AVL!*1800/PI))
     /10;CHR$(248);"to horizontal"
1950 LPRINT "ROD LOCATION , (XL,YL) = (";CINT(XL!);",";CINT(YL!);")  mm"
1960 LPRINT "ROD VELOCITY , (VXL,VYL) = (";CINT(VXL!);",";CINT(VYL!);") mm/s"
1970 LPRINT "ROD STRIKES MILL SHELL AT (";(CINT(XE*10))/10;",";(CINT(YE*10))
     /10;") , WHICH IS AT ";CINT(PHIE!*1800/PI)/10;CHR$(248)
1980 LPRINT "ROD VELOCITY IS  ";(CINT(VE!*10))/10;" mm/s , AT ANGLE ,SIGMA E,
      ";(CINT(AVE!*1800/PI))/10;CHR$(248);"  TO HORIZONTAL" :LPRINT :LPRINT
       :LPRINT
1981 INPUT "PRESS Y FOR A FULL COORDINATE PRINTOUT, ELSE ANY OTHER KEY  ",K$
1982 IF K$ = "Y" OR K$ = "y" GOTO 1986 ELSE RETURN
1985 LPRINT :LPRINT :LPRINT "X-COOR.";TAB(30);"Y-COOR.":LPRINT "-------"
     ;TAB(30);"-------"
1986 FOR I%=1 TO NB% :LPRINT INT(XP(I%)*1000)/1000;TAB(30);INT(YP(I%)*1000)
     /1000 :NEXT
1987 LPRINT:LPRINT"NUMBER OF COORDINATES IS ";NB%
1990 RETURN
1999 '------------------  SLIPTIME  -------------from 1155 & 1455
2000 GMM! = GM0! :TI!=0 :SI!=S0! :VI!=0
2005 GML!=GMM!+W!*T! :B!=ATN(DELTA!/DMY!):PHIL!=GML!-B!
```

```
2007 II! =(SI!+DELTA!*UK!+.5*G!*(UK!*COS(GMM!)-SIN(GMM!))/(W!*W!))
     :JJ! =VI!/W!-.5*G!*(UK!*SIN(GMM!)+COS(GMM!))/(W!*W!)
2010 VL!=W!*II!*FNsinh(W!*T!) + W!*JJ!*FNcosh(W!*T!) - .5*G!*(-UK!*SIN
     (GMM!+W!*T!)-COS(GMM!+W!*T!))/W!
2020 PRINT "TIME TO ROLL THEN SLIDE TILL FREE FLIGHT = ";T!+TI!;"   ,  GAMMA
     DEP = ";GML!*180/PI;"   ,  PHI DEP = ";PHIL!*180/PI;"   ,  VELOCITY AT
     DEPARTURE ,VL = ";VL!
2030 RL!=DMY!/COS(B!)
2040 GOSUB 1610
2050 GOTO 550
2069 '---------------  ROLLTIME  -------------from 1265
2070 GML!=GM0!+W!*T! : B!=ATN(DELTA!/DMY!) :PHIL!=GML!-B!
2075 VL!=WP!*(S0!-.4*G!*SIN(GM0!)/W!^2)*FNsinh(WP!*TI!) - (.4*G!/W!)
     *(COS(GM0!)*FNcosh(WP!*TI!) - COS(GM0!+W!*TI!))
2080 PRINT "TIME TO ROLL TILL FREE FLIGHT = ";T!;" , GAMMA DEP = "
     ;GML!*180/PI;" , PHI DEP = ";PHIL!*180/PI;" , VELOCITY AT DEPARTURE
     , VL = ";VL!
2085 GOTO 2030
2999 '---------   MOTION COORDINATES TO DISK   ------------------ from 545 -
3000 INPUT "DO YOU WISH TO STORE THESE COORDINATES ON FILE? , Y or N  ",K$
3001 IF K$ <> "Y" AND K$ <> "y" THEN RETURN
3002 CLS: PRINT "THE COORDINATES FOR THE MOTION WILL NOW BE STORED IN A FILE"
     :PRINT
3003 INPUT "DISC DRIVE TO USE, A or B ",DISC1$
3004 IF DISC1$="A" OR DISC1$="a" OR DISC1$="B" OR DISC1$="b" THEN DISC1$
     = DISC1$ + ":" ELSE GOTO 3003
3005 INPUT "FILE NAME (STARTING WITH F ) :";FF$
3010 F$=DISC1$+FF$+".DAT"
3015 GOTO 3200
3020 OPEN F$ AS #3 LEN=8
3030 FIELD #3, 4 AS XX$, 4 AS YY$
3040 FOR I%= 1 TO NB%
3050 LSET XX$ = MKS$(XP(I%))
3060 LSET YY$ = MKS$(YP(I%))
3070 PUT #3,I%
3080 NEXT
3082 CLOSE #3
3084 OPEN DISC1$+FF$+".SIZ" AS #3 LEN = 2
3086 FIELD #3, 2 AS SZ$
3088 LSET SZ$ = MKI$(NB%)
3090 PUT #3,1
3092 CLOSE #3
3100 PRINT
3110 PRINT "FILE INPUT COMPLETED"
3120 RETURN 547
3199 '---------  SEQUENTIAL FILING  ---------------- from 3015 -----
3200 OPEN F$ FOR OUTPUT AS #3
3210 FOR I% = 1 TO NB%
3220 WRITE #3,XP(I%),YP(I%)
3230 NEXT
3235 CLOSE #3
3240 PRINT: PRINT"SEQUENTIAL FILE INPUT COMPLETED"
3250 RETURN 547
3999 '-------------   LOOK AT FILE   ------------------------ from 548 -----
4000 GOTO 4060
4005 OPEN DISC1$+FF$+".SIZ" AS #3 LEN = 2
4010 FIELD #3, 2 AS SZ$
4020 GET #3, 1
4025 CLOSE #3:NB% = CVI(SZ$)
4027 OPEN F$ AS #3 LEN = 8
4028 FIELD #3,4 AS XX$, 4 AS YY$
4030 FOR J%=1 TO NB% :GET #3,J%:PRINT CVS(XX$);TAB(30);CVS(YY$):NEXT
4040 CLOSE #3
4050 RETURN
```

```
4059 '----------SEQUENTIAL RETRIEVAL ----------from 4000 -------
4060 OPEN F$ FOR INPUT AS #3
4065 I%=0
4070 WHILE NOT EOF(3)
4075 I%=I%+1
4080 INPUT #3,XP(I%),YP(I%) :PRINT XP(I%);TAB(30);YP(I%)
4085 WEND
4090 CLOSE #3: NB%=I% :PRINT NB%
4095 RETURN
4099 '------------  VIEW A FILE  ------------- from 587 ---------
4100 IF DISC1$="" GOTO 4110 ELSE GOTO 4130
4110 INPUT "DISC DRIVE TO USE , A or B  ",DISC1$
4120 IF DISC1$="A" OR DISC1$="a" OR DISC1$="B" OR DISC1$="b" THEN DISC1$
     =DISC1$+":"
4130 INPUT "FILE NAME  ",FF$
4140 F$=DISC1$+FF$+".DAT"
4150 GOSUB 4000
4160 RETURN 585
4999 '------------  ERROR TRAPS  -------------
5000 IF ERR = 27 THEN PRINT"RENEW PAPER IN PRINTER":GOTO 5050
5010 IF ERR = 57 THEN PRINT"SWITCH ON PRINTER":GOTO 5050
5020 IF ERR = 61 THEN PRINT" DATA DISK FULL, REPLACE WITH NEW FORMATTED DISK"
     : GOTO 5030
GOTO 5060
5030 INPUT"PRESS ANY KEY TO CONTINUE "K$
RESUME 3200
5050 INPUT"PRESS ANY KEY TO CONTINUE "K$
5055 RESUME
5060 ON ERROR GOTO 0
5999 '--------------------  S0 > SL  --------------- from 210
6000 PRINT "S0 LESS THAN  SL"
6005 IF U! = 0 THEN GM0! = FNASIN(W!*W!*R0!*COS(B0!)/G!) : GOTO 6090
6010 X! = (W!*W!/G!)*(R0!*SQR(1-(DELTA!/R0!)^2) - U!*TAN(PI-LAMBDA!)*DELTA!)
6020 GM0!=0 : Z!=0.1
6030 WHILE 1
6040 GM0! = GM0! + Z!
6050 DMY! = SIN(GM0!)-U!*TAN(PI-LAMBDA!)*COS(GM0!)
6060 IF DMY! > X! THEN GM0! = GM0!-Z!: Z!=Z!/10: IF Z! < 0.000001 THEN EXIT
     LOOP
6070 WEND
6090 PHI0! = GM0! - B0!
6100 PRINT"GAMMA 0  = ";GM0!*180/PI;CHR$(248);"  ,  PHI 0  = ";PHI0!*180/PI
     ;CHR$(248)
6110 XP(1) =COS(PHI0!)*R0! :YP(1) =SIN(PHI0!)*R0!     '===========XP , YP=====
6120 PRINT"ROD PROJECTED DIRECTLY INTO FLIGHT FROM POINT OF EQUILIBRIUM"
6130 GOTO 540
```